l'université nantes angers le mans
PÔLE DE RECHERCHE ET D'ENSEIGNEMENT SUPÉRIEUR

UNIVERSITÉ DE NANTES

Thèse de Doctorat

Abdul HAQ

Mémoire présenté en vue de l'obtention du
grade de Docteur de l'Université de Nantes
sous le label de l'Université de Nantes Angers Le Mans

Discipline : Automatique et Informatique Appliquée
Spécialité : Robotiques
Laboratoire : Institut de Recherche en Communications et Cybernétique de Nantes (IRCCyN)

Soutenue le 04 Juin 2013

École doctorale : 503 (STIM)
Thèse n° : 000000000

Strategies for Energy Storage during a Walking Step of a Bipedal Robot

JURY

Rapporteurs :	**M. Fethi Ben Ouezdou**, Professeur, Université de Versailles St Quentin, LIS Versailles **M. Olivier Stasse**, Chercheur CR1, LAAS-CNRS Université de Toulouse
Examinateurs :	**M. Gabriel Abba**, Titre, Laboratoire de Conception, Fabrication et Commande (LCFC) de Metz **M. Floren Colloud**, Professeur, Université de Poitiers
Directeur de thèse :	**M. Yannick Aoustin**, Maître de Conférence, École Centrale de Nantes, IRCCyN
Co-directrice de thèse :	**Mme Christine Chevallereau**, Directeur de Recherche, École Centrale de Nantes, IRCCyN

dedicated to my loving parents

Acknowledgments

First and foremost I would like to thank my thesis supervisor Mr. Yannick AOUSTIN for giving me the possibility to complete my research work. During my tenure, he contributed to my professional as well as personal development by giving me intellectual freedom in my work, supporting and involving me in new ideas and providing me a friendly research environment.

I would like to express my deepest gratitude to my co-supervisor Mme. Christine CHEVALLEREAU for the continuous support of my Ph.D study and related research, for her patience, motivation, and immense knowledge. Her guidance helped me in all the time of research and writing of this thesis.

I would also like to thank M. Fethi Ben OUEZDOU and M. Olivier STASSE for giving me the honor to be the reviewers of my thesis. Their comments and suggestions helped me a lot to improve my manuscript.

I would also like to thank M. Gabriel ABBA for accepting to be the president of my thesis defense jury and M. Floren COLLOUD for being the member of my thesis committee.

I would like to thank M. Arnaud HAMON for his technical help in programming and being always there as a good friend. I would like to thank all the members of IRCCyN specially the robotic team for their support and friendship during my stay.

I would also like to thank my parents, sisters, and brothers. They were always supporting me and encouraging me with their best wishes.

Finally, I would like to thank my wife, Nudrat HAQ for her support during my study period. She was always there cheering me up and stood by me through the good times and bad. I would also like to thank my baby boy Muhammad Talal ul HAQ for his immense love while coming back to home from work.

Contents

List of Figures

List of Tables

1

General Introduction

Contents

1.1 Motivation

Currently, research on bipedal robots is one of the most exciting and fascinating topic in the field of robotics. The field of application is large both for industrial as well as every day life use, and lots of hard scientific problems are still open. Significant work has been done to generate bipedal walking gait trajectories that are anthropomorphically as close as possible to human walking while energetically efficient and dynamically stable [31, 88, 128]. Researchers in the field of robotics especially humanoid robotic, are inspired by human walking and try to reproduce human walking gait for bipeds. Research in Biomechanics [65, 121, 2] shows that human walking is a process of locomotion in which the erect, moving body is supported by first one leg and then the other. As the moving body passes over the supporting leg, the other leg swings forward in preparation for its next support phase. One foot or the other is always on the ground, and during that period when the support of the body is transferred from the trailing to the leading leg, there is a brief period called "double support phase" when both feet are on the ground [65]. As a person walks faster, these periods of double support become smaller fractions of the walking cycle until, eventually, as a person starts to run, they disappear altogether and are replaced by brief periods called "flight phase" when neither foot is on the ground. The cyclic alternations of the support function of each leg and the existence of a double support phase when both feet are on the ground are essential features of the walking. A cyclic human walking step is composed of two major phases, *stance phase* and *swing phase*.

Generally, robot locomotion is referred to various methods that robots use to geographically move from one place to another. It can be divided into two main categories, *wheeled locomotion* and *legged locomotion*. Wheeled robots are commonly used for payload carrying such as PatrolBot [104] and PowerBot [83] and exploration purposes such as planet Rover [70]. In present, legged robots are generally used for research purpose in laboratories or for entertainment purposes in the entertainment industry. Typical examples of legged robots include HRP series [69, 68], HONDA

Asimo [97], Aldebran robotics NAO [51], Boston dynamics BidDog [15], RiSE [17], and RHex [16] etc.

In terms of energy efficiency on flat surfaces, wheeled robots are the most efficient. This is due to the fact that an ideal rolling (but not slipping) wheel loses no energy (ignoring frictional losses). This is in contrast to legged robots, which suffer an impact with the ground at heel strike and lose energy as a result. Although wheeled robots are typically quite energy efficient and simple to control, legged locomotion may be more appropriate for a number of reasons (e.g. traversing rough terrain, moving and interacting in human environments). Furthermore, studying bipedal robots may beneficially impact on bio-mechanics and improve the design and performance of orthosis and prosthesis. The scope of this study is the generation of energetically efficient walking gaits for a biped. Its scope is limited to planar bipeds because sagittal motion has a dominant contribution to energetic consumption.

Ongoing research on bipedal walking in the past decades resulted in legged robots with impressive versatility. Bipeds such as Asimo [97] (Figure 2.9(a)) or HRP-2 [68] (Figure 2.9(b)) can walk, climb stairs, and even run. Apart from versatility, desirable properties of a humanoid robot are low energy consumption and human-like walking motion. In comparison to human walking, energy efficiency of todays walking robots is mostly inferior. Moreover, walking gaits of most bipedal robots only loosely resemble human gait [99].

In the past two decades, the studies on the passive robots have significantly attracted the attention of researchers to solve the problem of energy optimization and human like walking. A robot is called passive when no external energy (actuator) is required for walking. In 1990 McGeer [80] had first presented his work on passive dynamic walking and demonstrated that it is possible to exploit the mass distribution of the robot to make it walk on a shallow slope without actuation [48].

Based on the McGeer's work on passive walkers, research community of humanoid robots has developed passive dynamic walkers with minimal actuation to make them walk on flat surfaces [31, 32]. These robots are capable of walking on flat surfaces and have energy cost almost equal to that of the human. The three most famous level ground powered walking robots based on the ramp-walking design are the Cornell biped, the Delft biped (Denise) [8, 124] and the MIT learning biped [32]. These powered bipeds have motions close to those of their ramp-walking counterparts [32]. Gini et all [48] extended this idea to fully actuated robots and constructed their robot with joint compliance and special knee design to improve walking efficiency.

Humanoid robots are biologically inspired robots. They look like a human having two legs, a torso, and two hands, although several types of bipedal robots may model only part of the body. For example, most of the active dynamic walking bipeds in research laboratories have only two legs and a torso [100, 107, 44] such as Rabbit [25] having no feet or punctual feet. However, the number of humanoid robots having arms, head and feet are increasing and researchers are concentrating on the energetic effects of arms, feet and compliance in the walking gaits by adding springs to the bipeds. Most of the researchers including [42, 99, 100, 86] are motivated by the hypothesis that bipeds with compliant ankles may be able to exhibit more natural-looking gaits with better energetic efficiency and walking stability as compared to bipeds without compliant joints. Several researchers studied that the design of the knee joint can help to improve the walking efficiency [53, 79] and others concentrated on the addition of passive elastic members in the knee and hip joints. The compliant swinging leg can reduce energetic cost by producing anti-gravity torques that lower the amount of actuator work required for leg swinging [81].

One of the most important and critical issue in the field of robotics especially in the humanoid robot's gait generation is the consumption of energy during walking. Studies show that the legs of the humanoid robots consume more energy in the stance phase than in the swing phase [36]. This difference in energy consumption is because of the demand of high torques to support the robot weight on the ground. Therefore, there is room for significant improvement in optimizing the energy consumption of the support leg. Förg [36] studied that the most inefficient (energy consuming) joint is the support knee joint.

Recently linear elastic members (springs) have been used to recover the lost energy, decrease the energy consumption, and to stabilize the walking gait. In most of the cases, springs are added to the ankle of the biped to store energy and to use it when needed. This stored energy is mainly used during ankle push-off just before heel strike of free leg. Geyer et al. [47] introduced the idea of compliant legs with compression springs for walking and running. They showed that compliant legs are essential to explain walking mechanics. They studied a bipedal spring-mass model, which includes the double support as an essential part of its motion and reproduced the characteristics dynamics of walking. Their model combines the basic dynamics of walking and running in one mechanical system. In another study, compliant controller is used to tune the stiffness of the adaptable compliant actuator to reduce energy consumption of the biped Lucy during walking [119]. Lucy is powered by pleated pneumatic artificial muscles and is able to walk up to a speed of 0.15 m/s.

Another method of reducing energy consumption is to mechanically lock the support knee just before impact and release the lock at the end of double support phase. The knee-lock with active release mechanism is found to be technologically simple and energetically efficient [114]. However, neither the combined effects of knee locking and addition of springs have been explored nor the effects of compliance on energy consumption have been presented as a function of walking speed. Present study will explore both these areas and will preset detailed simulation results and comparison of different techniques to improve walking efficiency.

To have efficient walking gaits, significant work has been done on the recovery of lost energy during each step [80, 73, 31, 76]. However, energetic effects of torsional springs in parallel to the existing actuator, have not been sufficiently explored. The first part of this study concentrates on two different strategies to improve the energetic efficiency of a planar bipedal robot. In the first method torsional springs will be added to different joints of the robot in parallel to the existing actuators, and energetic effects will be studied. Secondly, support knee of the biped will be mechanically locked during the entire swing phase to reduce energy consumption. Both techniques will be applied to different bipedal walking gaits from a most simple to relatively complex and more natural looking gait with finite double support phase for a planar biped.

In the field of humanoid robotics, an other most important and challenging issue is the design and selection of its actuating system. High performances in actuation are required to enhance energetic efficiency and stability of these systems. In the future, humanoid robots are expected to be integrated in human environment to perform human tasks like personal assistance, where they should be able to assist the sick and elderly people, and do dangerous jobs that cannot be done by humans or too risky for them. To integrate robots into human environment, they should be safe and human friendly. For instance, in the field of humanoid robotics, essential and desirable properties for actuators are: (1) high power to mass ratio; (2) ability to produce high torque at low speed; (3) highly integratable (reduction of occupied volume); (4) able to generate smooth joint motions resulting in human-like walking movements.

Robotics systems such as humanoid robots are generally actuated by two main types of actuation Electric and Hydraulic (including pneumatic). Some well know examples of humanoid robots using electric actuators are HONDA ASIMO [58], WABIAN-2 [89], and HRP-2 [68] etc and those using hydraulic actuation are HYDROiD [3], and the University of Tokyo humanoid (UT-Theta 2) [67]. It is worth mentioning that electric actuators have the advantages of reduced cost, ease of use, and are easy to program in the control law. However, a number of disadvantages appear when electric motors are used with mechanical reduction gear box. First of all, due to the quasi-rigid connection between the motor and its payload, it is difficult to produce compliance in the joint required for safety. Secondly, electric actuators have to be sized for the worst case scenario, defined by satisfying the instantaneous highest torque required. This leads to a non-optimal over-sized electric actuator, which will not be used all the time at its full capacity.

Based on the analysis of already existing solutions, and requirements of bipedal robots, a high performance Integrated Electro-Hydraulic Actuator (IEHA) has been developed by S. Alfayad et al. [6, 7], which uses displacement of a micro valve to control hydraulic motor. The newly developed hydraulic actuator is a light weight solution satisfying all the performances needed for actuating a humanoid robot [3]. Advantages of IEHA include, but not limited to, 1) Light weight, 2) complete actuator including micro hydraulic pump, 3) energy storage function, and 4) no central pumping system required. This actuator is capable of storing energy which can be used when needed. The biped HYDROiD equipped with new IEHA actuators is developed under the project called "R2A2" sponsored by the French National Research Agency (ANR). The present study will explore the effects of energy storage on different walking gaits.

1.2 Thesis Organization

The objective of this thesis is to explore different techniques to improve energetic performance of a bipedal robot during walking, and to propose the best option available depending on the type of gait the biped. The energy optimization strategies studied in this manuscript include, mechanical locking of the support knee, addition of springs to different joint of the biped, and integration of hydraulic actuators capable of storing energy. These techniques will be applied on different walking gaits from simple to more and more complex and close to human walking. Parametric optimization algorithms [38] will be used to generate walking gait trajectories for these gaits. Selected optimization criterion will be calculated after applying the above mentioned techniques, and then compared with that of the basic robot without knee locking or adding springs.

This manuscript is composed of six major chapters excluding chapter 1, which gives general introduction of the work and chapter 8, which presents conclusions and perspectives of the present study. In chapter 2, human walking will be explained and different statistics about human walking will be presented. Different phases and events occurring during a complete cycle of human walking gait will be discussed and terminologies used to describe human gait will be presented. The two major phases *stance phase* and *swing phase*, and their sub-phases will be explained in detail. Moreover, robot locomotion will be discussed and then the discussion will be narrowed down to bipedal walking. Human walking will be compared to bipedal walking and relationship between these two will be established. Different characteristics required for a biped to be able to efficiently walk will be enlisted. Furthermore, a criterion to compare energetic efficiency of different machines will be presented. Different energy recovery approaches used to improve energetic efficiency of a biped during walking will be presented and discussed in detail. Effects of springs, knee locking, and knee joint design on energetic efficiency and stability of walking gait will be discussed. Finally, different methods used in present study to improve energetic performance of bipedal walking will be presented and the chapter will be then concluded.

After having an overview of human and bipedal walking, the geometric and inertial parameters of the studied biped will be presented in chapter 3. Three different types of walking gaits studied in this work will be introduced and their different phases during a walking step will be explained. The dynamic model will then be formulated for a seven link planar bipedal robot using the Lagrange formulation for all three walking gaits. The dynamic model in general case, single support, and double support will be developed depending on the type of gait. The impact model for a bipedal robot will be developed, and different possible solutions of foot contact with the ground just after impact will be discussed. Moreover, the dynamic model will be extended to incorporate the effects of springs added in parallel with the existing actuators.

In chapter 4, reference trajectory generation and optimization for a seven link planar biped will be discussed. Moreover, different functions to generate reference walking gait trajectories for a bipedal robot will be presented. Trajectory optimization of all three types of walking gaits presented in previous chapter will be explained and the optimization parameters required for each gait in different cases will be presented. The optimization constraints will be introduced for the cyclic walking gait of the bipedal robot under study. Two different optimization criteria one for electric actuators and other for hydraulic actuators will be presented and different non-linear constrained optimization tools will be explained. Finally, simulation results for optimization functions *fmincon* and *fgoalattain* will be compared.

After presenting the biped under study, developing the dynamic and impact models, and explaining different trajectory generation techniques, simulation results of different types of walking gait trajectories for a bipedal robot will be presented in chapter 5. A number of strategies will be presented to reduce the defined criterion of performance during walking. The objective of this chapter is to compare the performance of these techniques on different walking gaits. For this purpose, three types of walking gaits has been defined in chapter 3 and optimal walking gait trajectories for each gait will be generated and cost of walking will be calculated in chapter 5. Simulation results obtained for each type of gait will be presented for different walking speeds. Effects of springs and knee locking will then be compared on the basis of selected performance criterion of different cyclic walking gaits.

Chapter 6 of this thesis is dedicated to introduction of hydraulic actuators. In this chapter, the working principle of a classical hydraulic actuator will be presented with mathematical expressions. A newly designed high performance Integrated Electro-Hydraulic Actuator (IEHA) [6, 7] will be presented and its advantages over its counterparts will be enlisted. The simplified model of the said actuator will be presented and working of its different parts will be explained in detail. The exploded CAD schematic of the actuator will also be presented to have an overview of different parts of the actuator. Moreover, different working modes of IEHA will be elaborated, and its energy storage function, which is one of the main advantage of this actuator will be presented. Mathematical expressions for energy balance in hydraulic actuators will be developed, and the stored energy and energy available to the actuator during different working stages will be calculated. Finally, different cases of power consumption of an actuator during its working cycle will be explained and generalized storage function will be developed followed by the conclusion of the chapter.

Energetic effects of hydraulic actuators and energy storage will be studied in chapter 7 on different walking gaits of a bipedal robot. A number of methodologies will be presented to improve the energetic efficiency of a humanoid robot during walking. Optimal walking gait trajectories will be generated for two types of walking gaits and the criterion based on the energy consumption of the biped will be defined to compare the performance of different gaits. An Optimization algorithm will be developed, and parameters required to define a reference gait trajectory will also be presented for each gait. Simulation results obtained from optimization algorithm for each type of gait will be presented for different walking speeds. Effects of knee locking and energy storage on consumption of energy during walking of different cyclic walking gaits will then be compared. Similarly, effects of walking speed on step length, time, center of gravity (CoG) of the biped, ground reaction forces, and other parameters will also be discussed.

Finally, the work will be concluded in chapter 8 presenting a number of conclusions drawn from the study. Recommendations for future work in continuity of this work will also be presented.

2

Human Walking vs Bipedal Walking

Contents

2.1 Introduction

In this chapter, human walking will be explained and different statistics about human walking will be presented. The human muscle responsible for walking and other motions will be introduced, and its different parts will be presented. Moreover, different phases during which a human muscle does some work will also be presented. The phases and events occurring during a complete cycle of human walking gait will be discussed and terminologies used to describe human gait will be presented. The two major phases *stance phase* and *swing phase*, and their sub-phases will be explained in detail. Gait timing and foot placement of a standard human walking cycle will be presented.

In the second part of this chapter, robot locomotion will be discussed and then the discussion will be narrowed down to bipedal walking. Humanoid walking will be compared to bipedal walking and relationship between these two will be established. Different bipedal walking gaits will be introduced and events occurring during a gait cycle of each gait will be presented.

Different characteristics required for a biped to be able to efficiently walk will be enlisted. Furthermore, a criterion to compare energetic efficiency of different machines will be explained, and two of the famous humanoid robots will be introduced. Different energy recovery approaches used to improve energetic efficiency of a biped during walking will be presented and discussed in detail. Effects of springs, knee locking, and knee joint design on energetic efficiency and stability of walking gait will be discussed. Finally, different methods used in present study to improve energetic performance of bipedal walking will be presented and the chapter will be then concluded.

2.2 Human Walking

There are two main means of locomotion in humans, walking and running. Walking is one of the main gaits of human locomotion and is typically slower than running. Generally, in bio-mechanics and humanoid robotics, walking is defined by an 'inverted pendulum' gait in which the body vaults over the stiff limb with each step [78]. Walking is generally distinguished from running in that only one foot at a time leaves contact with the ground and there is a period of double-support. In contrast, running begins when there exist a flight phase during which both feet are off the ground during each step. The present study will focus on walking gaits only, and different phases of human walking gait are presented in 2.3.

The most effective method to distinguish walking from running is to measure the height of a person's center of mass using motion capture or a force plate at mid-stance. During walking, the center of mass reaches a maximum altitude at mid-stance while during running, it is at minimum. Definitions based on the percent of the stride, during which a foot is in contact with the ground for greater than 50% contact are indicative of walking for animals with any number of limbs [13]. However, running humans and animals may have contact periods greater than 50% of a gait cycle when rounding corners, running uphill or carrying loads.

Although walking speeds can vary greatly depending on factors such as height, weight, age, terrain, surface, load, culture, effort, and fitness, the average human walking speed is about 5.0 kilometers per hour (km/h). Specific studies have found pedestrian walking speeds ranging from 4.51 km/h to 4.75 km/h for older individuals, and from 5.32 km/h to 5.43 km/h for younger individuals [72, 34]. These are the average comfortable walking speeds at which metabolic cost [52] is minimum; a brisk walking speed can be around 6.5 km/h.

2.2.1 Human Muscle

A driving force is required to take a walking step or undergo and activity, and this force is produced by different muscles. The human muscular system is comprised of three different types of muscle tissue: cardiac, smooth and skeletal muscle. Together these three types of muscle make up about half of the body's mass, and skeletal muscle alone makes up about 80% of the muscular system [41]. Skeletal muscle falls under the categories of striated and voluntary muscle. The principal driving element in human walking is skeletal muscle, which is a form of striated muscle tissue existing throughout the human body [13]. As their name suggests, most skeletal muscles are attached to bones by bundles of collagen fibers known as tendons. Most of the space within muscle fibers is generally occupied by myofibrils (see Figure 2.1), which are composed of protein elements a few millimeters long, lined up parallel to each other and to the long axis of the fiber [2]. Certain unicellular organisms also use protein similar to those found in skeletal muscle of humans as motors to alter their shape and move.

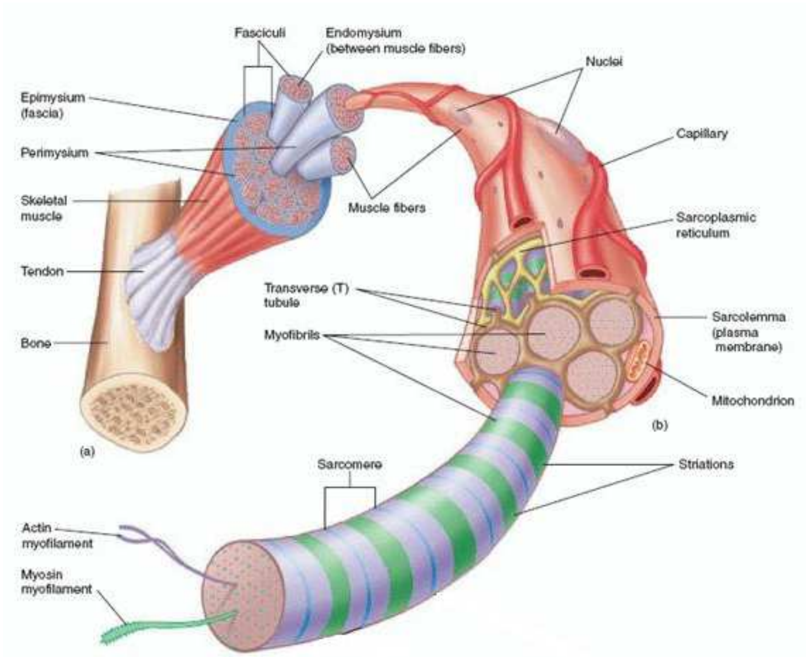

Figure 2.1 – Skeletal muscle anatomy

In general muscle generate energy for movement by doing work in order to function as biological motor. Therefore, it can be said that human muscles are biological equivalents of robotic actuators. Muscles produce energy by exerting force F while contracting, and this phenomenon is called muscle contraction. Work done W by a muscle during contraction can be obtained from the product of force applied F and change in length ΔL. By definition muscles produce positive work when they shorten. However, muscles may also function to generate force with little or no change in length [13]. In this case, the contraction is referred to as being *isometric*. During ideal isometric contraction the joint velocity is null, which results in zero energy and power.

Based on the isometric phase of human muscle, the present study will introduce this phase in bipedal walking using an integrated electro-hydraulic actuator. Energy produced during this phase will be stored and then reused when needed. The working of these actuators will be explained in chapter 6 and the simulation results will be presented in chapter 7.

2.3 Phases of Human Walking Gait

Before proceeding to describe different phases of the human walking, it is important to explain the anatomical terms use in bio-mechanics to study human walking. The anatomical terms describing the relationships between different parts of the body are based on the anatomical position, in which a person is standing upright, with the feet together and the arms by the sides of the body, with the palms forward. This position, together with the reference planes and the terms describing relationships between different parts of the body, is illustrated in Figure 2.2. Six terms are used to describe directions, with relation to the center of the body. These are best defined by:

1. The umbilicus is *anterior*
2. The buttocks are *posterior*
3. The head is *superior*
4. The feet are *inferior*
5. *Left* is left of the subject
6. *Right* is right of the subject

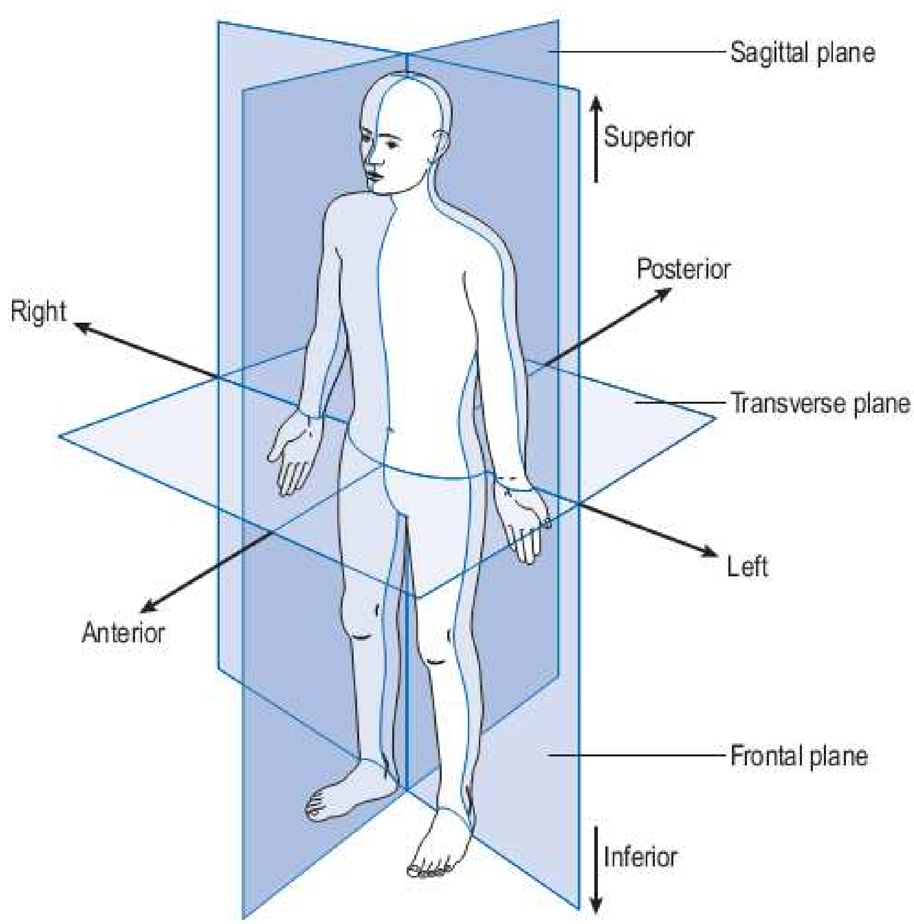

Figure 2.2 – The anatomical position, with three reference planes and six fundamental directions [121]

The anterior surface of the body is *ventral* and the posterior surface is *dorsal*. The word *dorsum* is used for both the back of the hand and the upper surface of the foot. The terms *cephalad* (towards the head) and *caudad* (towards the "tail") are sometimes used in place of superior and inferior. Further details about different representations used to study human walking can be found in [121].

To study walking gait, the motion of the limbs is described using reference planes:

— A *sagittal* plane is any plane which divides part of the body into right and left portions; the *median* plane is the midline sagittal plane, which divides the whole body into right and left halves.
— A *frontal* plane divides a body part into front and back portions
— A *transverse* plane divides a body part into upper and lower portions.

Human walking is a process of locomotion in which the body's center of gravity moves forward in sagittal plane, osculates left-right in transversal plane, moves up-down in frontal plane. These cyclic pattern of body movements are repeated over and over, step after step. The moving body is supported by first one leg and then the other, and as it passes over the supporting leg, the other leg swings forward in preparation for its next support phase. At all times, at least one foot remains on the ground [18]. There is a brief period called double support phase" when both feet are on the ground. As a person walks faster, these periods of double support become smaller fractions of the walking cycle until, eventually, as a person starts to run, they disappear altogether and are replaced by brief periods called "flight phase" when neither foot is on the ground [65]. In the act of walking there are two basic requisites: first the continuing ground reaction forces that support the body, and second the periodic movement of each foot from one position of support to the next in the direction of progression. A cyclic human walking is composed of two major phases, *stance phase* and *swing phase* (single support phase).

The *gait cycle* (walking cycle) is defined as the time interval between two successive occurrences of one of the repetitive events of walking. Although any event could be chosen to define the gait cycle, it is generally convenient to use the instant at which one foot contacts the ground (initial contact or heel strike). If it is decided to start with initial contact of the right foot, as shown in Figure 2.3, then the cycle will continue until the right foot contacts the ground again. The left foot, of course, goes through exactly the same series of events as the right, but displaced in time by half a cycle.

The following terms are used to identify major events during the gait cycle:

1. Initial contact
2. Opposite toe off
3. Heel rise
4. Opposite initial contact
5. Toe off
6. Feet adjacent
7. Tibia vertical

The above seven events subdivide the gait cycle (see Figure 2.3) into seven periods, four of which occur in the stance phase, and three in the swing phase.

2.3.1 Stance Phase

The stance phase of a foot starts with its contact on the ground and ends when it takes off the ground. It is also called the *support phase* or *contact phase*. It lasts from initial contact to toe off. Stance phase also contains a brief period called *double support phase* during which both feet are in contact on the ground. Following are the sub-phases of stance phase as shown in Figure 2.3.

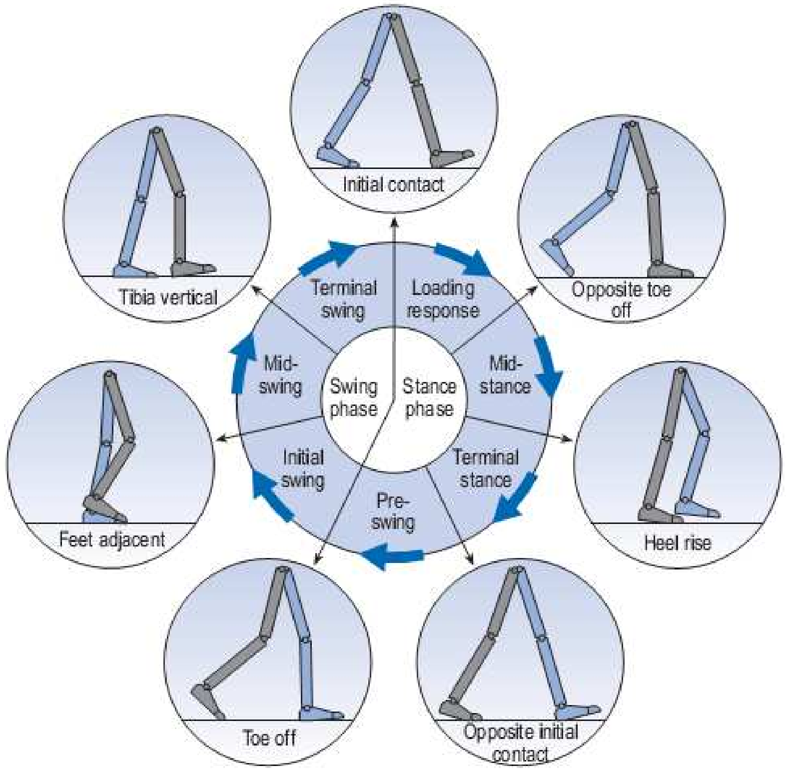

Figure 2.3 – Positions of the legs during a single gait cycle by the right leg (gray) [121].

Loading response: starts when the foot comes in contact with the ground for the first time. It lasts from initial contact (heel strike) to flat foot contact or opposite toe off. This phase is also called double support phase (or "Initial double limb support") during which both feet are in contact on the ground. It is characterized by a very rapid loading onto the forward limb with shock absorption and slowing of the body's forward momentum. The foot usually progresses to foot flat, and the knee acts as a shock absorber (see [65] for more discussion).

Mid-stance: starts when toe of the stance foot touches the ground and that of opposite foot takes off the ground. Mid-stance ends when heel of the stance foot rises and it starts rotating on its toe. The start of the Mid-stance is also the start of single support phase where only one foot is in contact on the ground. During this phase, the body passes over the fixed foot (stance foot), the center of mass rises to its peak while both forward and vertical velocity decrease. Forward shear then reverses to aft shear, the center of mass falls, and forward and vertical velocity increase.

Terminal stance: is also called "Mid-stance through Heel off". This sub-phase starts at heel rise and ends at opposite initial contact. At the end of this phase, single support phase ends and second double support phase of the gait cycle starts. Once the peak in elevation of the center of mass is achieved in previous phase, the center of mass falls until the end of single limb stance (single support phase) at opposite foot strike.

Pre-swing: lasts from opposite initial contact to toe off. At the end of this phase, second double support phase ends and second single support starts. At this instance, the initial support leg becomes swing leg and vice versa. During pre-swing, the foot rotates on its toe and prepares for take off. As weight is transferred rapidly to the forward limb, the trailing limb is ending its extension movement in preparation to swing forward in front of the body.

2.3.2 Swing Phase

During the swing phase, only one foot is in contact on the ground. It lasts from toe off to the next initial contact. There are two single support phases one for each leg during a complete gait cycle. The critical event of foot clearance occurs around 75% of the gait cycle [65] when the swinging limb passes the standing limb (feet adjustment). The swing phase is subdivided into:

Initial swing: starts at toe off and ends at foot adjustment. As discussed before, the second single support phase starts at toe off which is also the start of initial swing. This phase is also called acceleration phase during which the swing foot accelerates. The instance of feet adjustment is almost the middle of single support phase.

Mid-swing: lasts from feet adjustment to tibia vertical. During this phase, the foot decelerates and prepares for initial contact on the ground.

Terminal swing: is the phase between tibia vertical and initial contact. At the end of this phase, single support phase ends and double support phase of a new gait cycle starts.

The duration of a complete gait cycle is known as the *cycle time*, which is divided into *stance time* and *swing time*. The average cycle consists of 62% stance phase and 38% swing phase [65, 121]. In some other studies, the cycle time is divided into single support time and double support time. In normal human walking, the double support time is about 20% of the cycle time.

2.4 Gait Cycle Timing

Unfortunately, the nomenclature used to describe the gait cycle varies considerably from one publication to another. The present text uses the terminology used in [121] which will be understood by most people working in the field. Moreover, alternative terminology is given where appropriate. Significant work has been done by the researchers of International Society of Biomechanics (ISB) for the standardization and homogenization of body landmarks, local frames positions and orientations [125, 11, 126].

Figure 2.4 shows the timings of initial contact and toe off for both feet during a little more than one gait cycle. The walking cycle starts when right initial contact (at 0% of cycle time) occurs while the left foot is still on the ground. At this instance, a period of double support (also known as double limb stance) starts and lasts from initial contact on the right to toe off on the left. At left toe off (12% of cycle time), swing phase of the left leg begins. During the swing phase on the left side, only the right foot is on the ground, giving a period of right single support (or single limb stance), which ends with initial contact by the left foot (50% of cycle time). There is then another period of double support, until toe off on the right side (62% of cycle time). Left single support corresponds to the right swing phase and the cycle ends with the next initial contact on the right (100% of cycle time). For a cyclic walking, the step is supposed to be repeated for any number of times.

The distance between two successive placements of the same foot is called "*stride length*". Different terminologies used to describe the placement of the feet on the ground are shown in Figure 2.5. The stride length consists of two step lengths, left and right, each of which is the

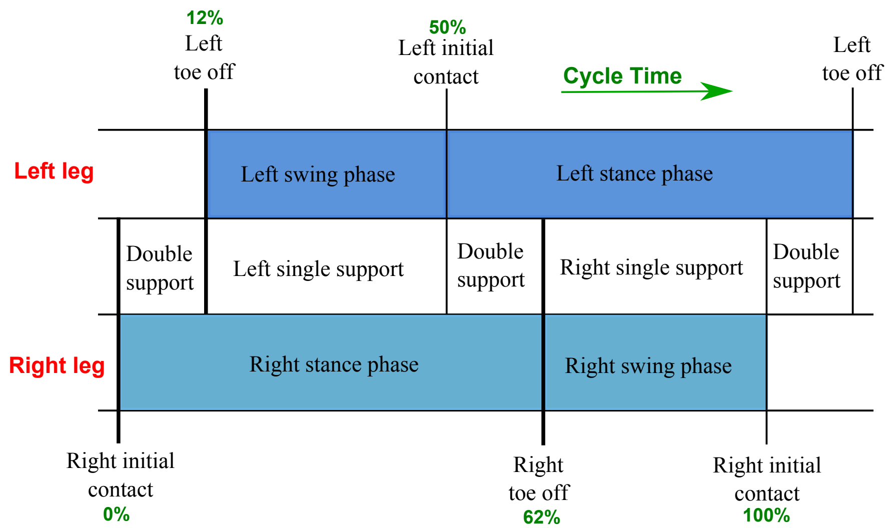

Figure 2.4 – Timing of single and double support during a little more than one gait cycle, starting with right initial contact [121].

distance by which the named foot moves forward in front of the other one. During walking in a straight line, the stride length, measured between successive positions of the left foot, must always be the same as the stride length measured between successive positions of the right foot. If the left foot is moved forward to take a step and the right one is brought up beside it, rather than in front of it, the right step length will be zero. It is even possible for the step length on one side to be negative, if that foot never catches up with the other one.

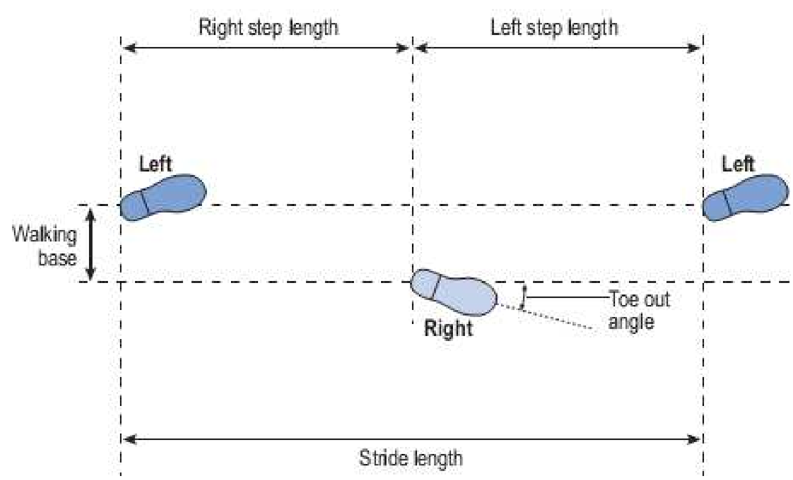

Figure 2.5 – Terms used to describe foot placement on the ground [121].

The side-to-side distance between the line of the two feet is called the *walking base* [121] (also known as the "stride width" [65] or "base of support"). It is usually measured at the midpoint of the back of the heel but sometimes below the center of the ankle joint. The preferred units for stride length and step length are meters and for the walking base, millimeters. The *toe out* (or, less commonly, toe in) is the angle in degrees between the direction of progression and a reference line on the sole of the foot. The reference line varies from one study to another; it may be defined anatomically but is commonly the mid-line of the foot.

2.5 Robot Locomotion

Before establishing relationship between human walking and bipedal walking, it is worthy to understand robotics locomotion. The various method that robots use to geographically move from one place to another are called *robot locomotion*. It can be divided into two main categories, *wheeled locomotion* and *legged locomotion*. Legged locomotion mechanisms are often inspired by biological systems, which are very successful in moving through a wide area of harsh environments.

In terms of energy efficiency on flat surfaces, wheeled robots are the most efficient. This is due to the fact that an ideal rolling (but not slipping) wheel loses no energy (ignoring frictional losses). Therefore, wheel rolling at a given velocity needs negligible input to maintain its motion. This is in contrast to legged robots, which suffer an impact with the ground at heel strike and lose energy as a result. Although wheeled robots are typically quite energy efficient and simple to control, legged locomotion may be more appropriate for a number of reasons (e.g. traversing rough terrain, cross gaps which are as large as its stride, moving and interacting in human environments). Furthermore, studying bipedal robots may beneficially impact on bio-mechanics and improve the design and performance of orthosis and prosthesis.

2.6 Bipedal Walking

The bipeds are mimicking the human walking and other motions like running, dancing, gestures and face expressions. For this purpose, some humanoid robots may also have a 'face', with 'eyes' and 'mouth' like HRP-4C [82, 69], however the main objective is to generate balanced cyclic walking patterns. The primary objective of the recent research is to develop effective locomotion systems, capable of walking and or running that are energetically efficient in addition to stability and robustness to disturbances [61]. The bipeds are generally designed in such a way to fulfill the stable motion (walking) requirements as well as light weight to consume less energy [61, 90, 48]. These have to be dynamically and statically balanced to avoid falling while walking or standing or even climbing and descending stairs.

In common with other gaits, walking involves progression by alternating periods of loading and unloading. In walking, as distinct from running, at least one foot is always in contact with the ground. In bipedal locomotion, this results in periods of single support in which only one foot is in contact on the ground and periods of double support, in which both feet make contact for some time during the gait cycle. The present study only deals with 2D bipedal walking gaits. Different types of walking gaits will be studied and their performance criteria will be calculated, and then compared with that calculated after using different techniques to improve energetic performance during walking.

The number of humanoid robots having feet has significantly increased in recent years and is still increasing very rapidly. Figure 2.9 presents two of the most popular humanoid robots Asimo 2.9(a) and HRP-2 2.9(b), Asimo is a child size while HRP-2 is an adult size biped. A biped having at least two feet, two knees and a torso will be assumed to establish relationship of bipedal walking and present different events occurring during a walking step.

The number of events during a gait cycle depends upon the type of walking gait the biped is following. One of the most commonly used type is the one having only single support phases

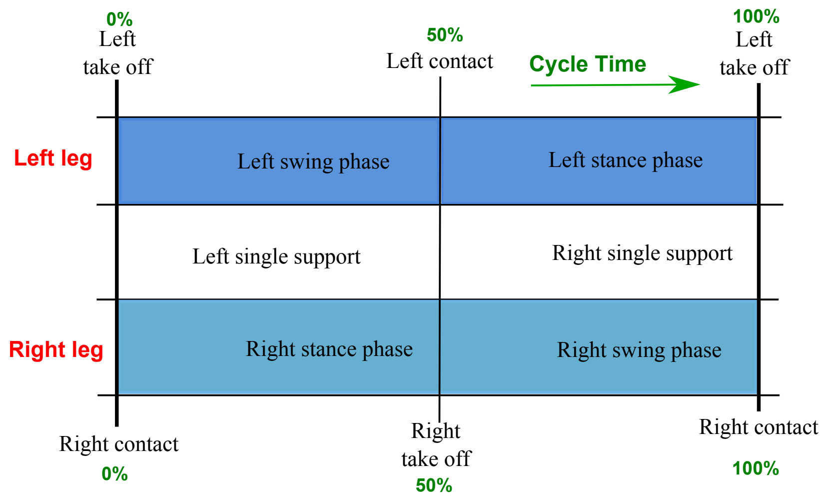

Figure 2.6 – Timing of gait type 2 during a walking cycle, starting with right contact

separated by impulsive impacts, and having flat foot contact on the ground at the time of impact. In present study, this gait is named "gait type 2" and is explained in detail in 3.3.2. Different events occurring during a walking cycle are graphically represented in Figure 2.6. Gait type 1 is similar to type 2 but has no impact. The swing foot touches the ground with zero velocity.

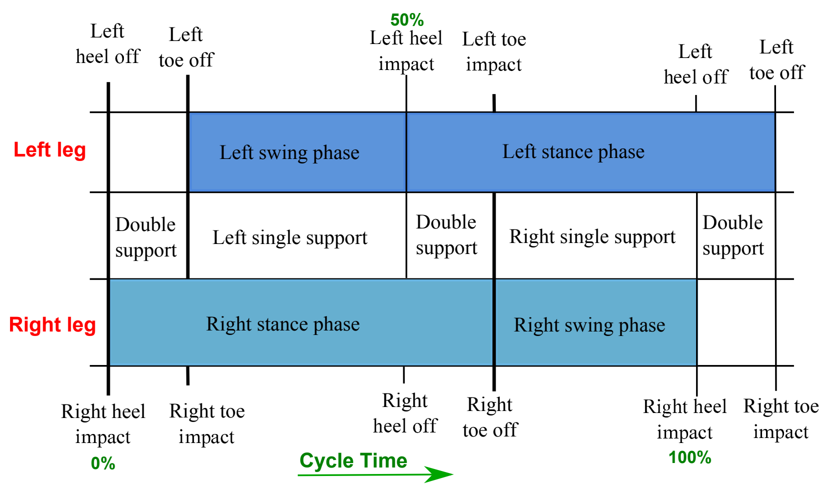

Figure 2.7 – Timing of gait type 3 during a walking cycle, starting with right contact

The third type of studied gait has finite double support phase with feet rotation, and has two impacts. It will be called gait type 3 and is presented in 3.3.3. Different events of gait type 3 are detailed in Figure 2.7. While it is not possible for the studied robot to have flat foot impact on the ground with the foot already in contact to remain in flat contact on the ground, it is possible to have flat foot impact with the foot already in contact to remain in contact but with rotation on its toe as the heel takes off at impact. Walking gait type 3 is more close to human walking and will be studied in section 4.6 for a biped with electric actuators and in section 7.4 for a biped with hydraulic actuators.

The fourth type of bipedal walking gait is the most complex and closest to human walking having all the phases of a human walk presented in 2.3. During a walking cycle of this gait, the stance foot starts rotating on its toe (heel off or heel rise) a little before the end of single support phase [113, 111] as shown in Figure 2.8. This type of gait is not very common in bipedal walking due to the limitation of mechanical structure of the biped particularly because of the design of feet without toes. Study of this gait is beyond the scope of the present work, and is only presented for the purpose of explaining different events during a cycle.

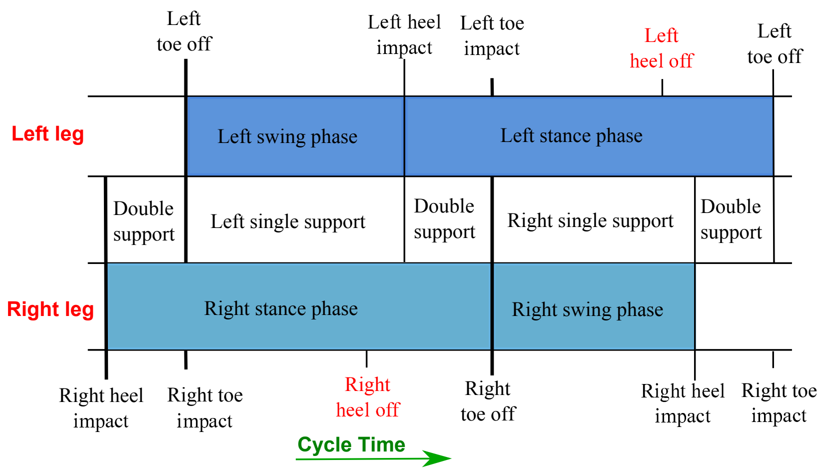

Figure 2.8 – Timing of gait type 4 during a walking cycle, starting with right contact

2.7 Energy Optimization

The focus of the today's work is to develop a low consumption high mobility biped robot with suitable utilization of actuators and control techniques [90, 48]. In order to have efficient, dynamically balanced and human like gait characteristics, for the purpose to manufacture a biped walking robot, one should constraint itself to a system, which should have more or less the following characteristics.

— Light weight
— Statically and dynamically balanced
— Smooth and cyclic walking
— Robust and efficient mechanical design
— Redundant structure etc.

These characteristics put limitations on the researchers and constrain them to a defined path in order to achieve the desired bio-mimetic results. Thus on one hand due to its wide spread application areas, these types of robots have greatly grasped the attention of the researchers in the field of walking robotics. However, on the other hand they have put a great challenge in front of the researchers to well design and control the dynamics of its human like walking [100, 42].

2.8 Energy Recovery Approaches

One of the most important and critical issue in the field of robotics especially in humanoid robots gait generation, is the consumption of energy during walking. Research is being done to generate dynamically stable and energetically efficient bipedal gaits as close as possible to human walk [31, 88, 128].

Ongoing research on bipedal walking in the past decades resulted in legged robots with impressive versatility. Bipeds such as Asimo [97] (Figure 2.9(a)) or HRP-2 [68] (Figure 2.9(b)) can walk, climb stairs, and even run. A multi-degree of freedom biped prototype with flexible feet called ROBIAN (Figure 2.9(c)) has been developed to provide a test-bed of active/passive prosthesis devices enhancing research on the human being locomotion apparatus [105, 102]. Apart from versatility, desirable properties of a humanoid robot are low energy consumption and human-like walking motion. In comparison to human walking, energy efficiency of todays walking robots is mostly inferior. Moreover, walking gaits of most bipedal robots only loosely resemble human gait [99].

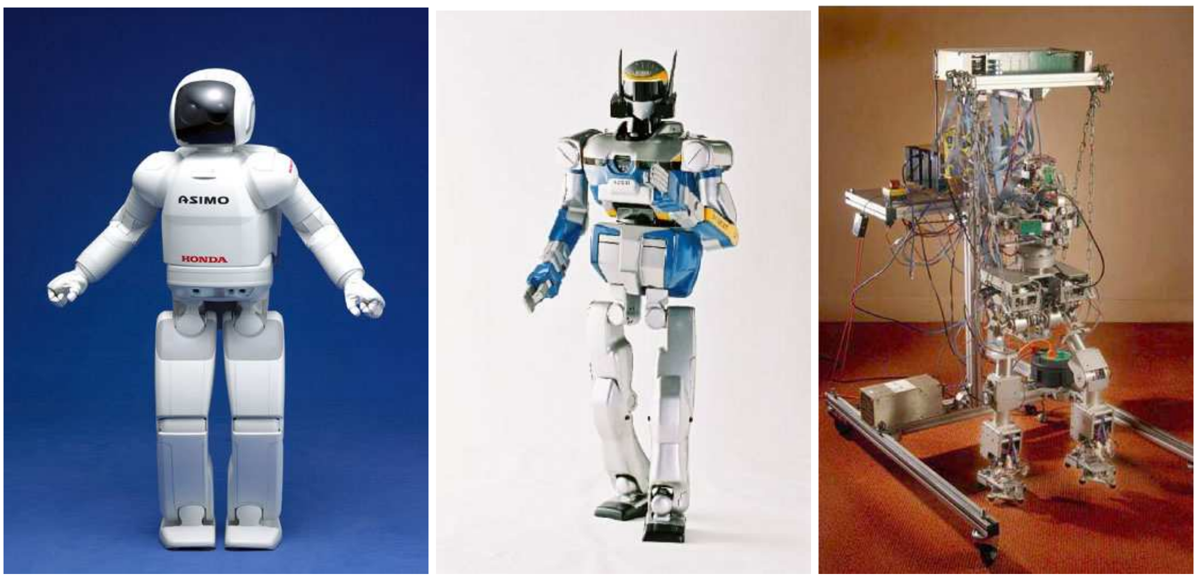

(a) ASIMO (b) HRP-2 (c) ROBIAN

Figure 2.9 – Humanoid Robots

In the recent years, significant improvements have been made in the mechanical design, actuators and control strategies of the bipedal robots to achieve the basic goal of energetically efficient, dynamically stable and robust human like walking gaits. The key issue in locomotion is the consumption of energy. To recover and minimize the energy, it is essential to measure the energy efficiency of locomotion. The energy efficiency of level locomotion is usually measured by the specific cost of transport C_{et}, which is the total energy consumed by the system, and is generally used to compare different walkers or locomotive machines [45, 36]. A related measure to C_{et} is the mechanical energy efficiency C_{mt}, which only considers the positive mechanical work of the actuators [31, 32]. Table 2.1 presents C_{et} and C_{mt} values for different robots and machines. In present, C_{et} for the biped HYDROiD could not be calculated due to unavailability of the biped and a number of technical details of the motors and actuators.

$$C_{et} = \frac{\text{energy used}}{\text{weight} \times \text{ distance traveled}} \tag{2.1}$$

To have efficient walking gaits, significant work has been done on the recovery of lost energy during each step. However energetic effects of torsional springs in parallel to the existing actuator, and that of hydraulic actuators have not been sufficiently explored. The mechanical energy consumption of such a mechanism is due primarily to the energy lost as the swing leg impacts with ground at heel strike [73, 31]. In case of level ground walking, this loss may be compensated by two general methods of actuation [80]. One is to apply an impulsive push along the trailing leg (toe-off impulse method), preferably immediately before heel strike for minimal energetic cost. The second method is to apply a hip torque against the stance leg, using the torso as a base [73, 76].

Table 2.1 – Estimated Specific Cost of Transport C_{et} and Mechanical Energy Efficiency C_{mt} of Several Locomotive Devices [31]

Robot/Machine		C_{et}	C_{mt}
Walking Robots	Honda's ASIMO	3.2	1.6
	TU Delf's Denise	5.3	0.08
	MIT's Spring Flamingo	2.8	0.07
	Collin's Cornell	0.20	0.055
	McGeer's Dynamite	-	0.04
Humans	Walking	0.20	0.05
Flying Machines	Modern Helicopter	1.6	0.4
	Wright Flyer	0.72	0.18
	Boing 747	0.12	0.05
	Modern Glider	-	0.02
Other	Efficient Auto	0.06	0.015
	Cyclist	0.04	0.01
	Freight Train	0.012	0.003
	Freighter	0.004	0.001

The second reason for lost energy is the actuation of the swing leg during swing phase, which is obvious from the passive nature of leg swing in McGeer's [80] model. However, studies on human walking show that leg swing is not a passive movement and require actuation for stable walking [116, 122]. Following are some of the approaches that have been successfully implemented to minimize the energy consumption of a biped during walking:

— Passive dynamic walking
— Addition of springs
— Design of knee joint
— Introducing compliance in the gait

2.8.1 Passive Dynamic Bipedal Walking

Passive dynamics is an approach to robotic movement control (especially walking), based on utilizing the momentum of swinging limbs for greater efficiency. This method is based on using the morphology of a mechanical system as a basis for necessary controls. Passive dynamics are used to create robotic and prosthetic limbs that move more efficiently by conserving momentum and reducing the number of actuators required for motion.

In 1990 McGeer [80] has first presented his work on passive dynamic walking and demonstrated the possibility to exploit the mass distribution of the robot to make it walk on a shallow slope without actuation. The prototype was exploiting the gravity force to swing the leg forward, exactly as a double pendulum would do. The only power needed was the one necessary to shorten the leg in order to create foot clearance during the swinging motion [48]. Tehrani Safa [110] extended this work by replacing the ramp with stairs to show the similarities and differences between these two kinds of passive walking to specify the role of surface profile in walking stability.

A number of passive dynamic walking bipeds has been developed based on the McGeer's work on passive walkers. These bipeds have minimal actuation to walk on flat surfaces [31, 32]. These bipedal robots are capable of walking on flat surfaces, and have energy cost almost equal to that of the human. Figure 2.10 shows the three most famous level ground powered walking robots based on the ramp-walking designs,the Cornell biped (Figure 2.10(a)), the Delft biped (Figure 2.10(b)), and the MIT learning biped (Figure 2.10(c)). These powered robots have motions close to those of their ramp-walking counterparts [32]. However, these bipeds are less adaptable to different walking gaits, less robust, and less adaptable to transportation of objects and performing assistance jobs.

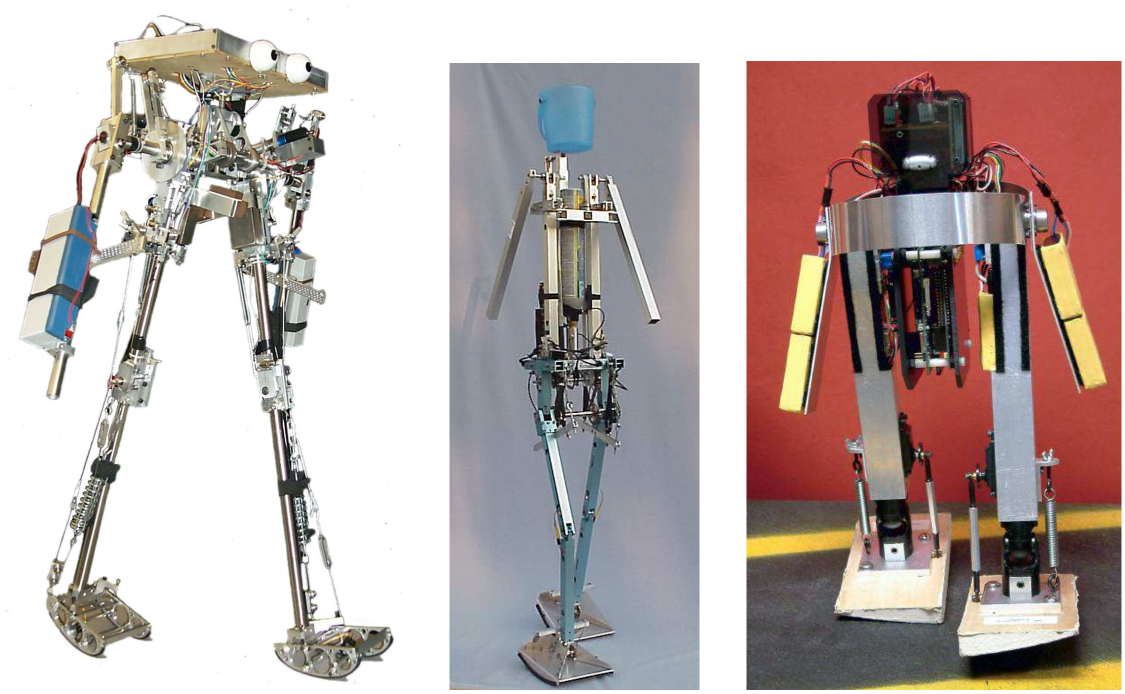

(a) Cornell biped (b) Delft biped (c) MIT learning biped

Figure 2.10 – Passive Dynamic Walkers

2.8.2 Addition of Springs

Springs have been recently used in the field of humanoid robotics for a number of reasons, which include, 1) to recover the lost energy, 2) to decrease the energy consumption, 3) to stabilize the walking gait. Generally, springs are added to the ankle joint of the biped to store energy and use it when needed mainly during the ankle push-off just before heel strike. Studies indicate that there is a direct trade-off between the toe-off impulse from the trailing leg and the rotational torque between the legs [76]. Using the toe-off impulse alone to power gait is four times less energetically expensive then using the hip torque alone [73, 76].

Studies also show that humanoid robots consume more energy during the stance phase than during the swing phase of the leg [36]. This difference in energy consumption is because of the demand of high torques to support the robot weight on the ground. Therefore, there is a room for energy optimization in the support leg. Forg [36] studied that the most inefficient (energy consuming) is the support knee joint, and linear springs can be introduced to reduce the energy consumption.

Energetic effects of springs

Farrell et all [42] have studied the energetic effects of adding springs at the passive ankle of a biped. After arbitrarily choosing the spring stiffness, and optimizing the motion, they found that the cost of standing with springs is more efficient while walking is more costly as compared to that of the same action without springs. However, the combined energetic effect of standing and walking with springs was more efficient than exhibiting the same motion without springs. Numerical results obtained by [42] are reproduced here in table 2.2.

Table 2.2 – Optimized motion with arbitrarily chosen springs for an average velocity of 1.25 m/s [42].

Stiffness -	- -	Walking Cost	Standing Cost	Cost Change Walking 2m	Cost Change Standing 2s	Cost Change Walking 2m and Standing 2s
K Nm/rad	q_o rad	C_w J/m	C_s J/s	δC J	δC J	δC J
0	-	184	563	-	-	-
25	3.3	187	460	6	-205	-199
50	3.3	223	359	78	-407	-329
75	3.3	257	278	145	-570	-425
50	3.2	295	307	223	-511	-288
50	3.3	223	359	78	-407	-329
50	3.4	208	409	48	-308	-261

Collins [31] has added springs at the ankle of their well know walking robot called Cornell (see Figure 2.10(a)) to study the energetic effects of spring addition. Specific cost of transport and mechanical energy efficiency values for Cornell robot in comparison with other locomotive machines are given in table 2.1. Schematic of the ankle spring mechanism along with working procedure is shown in Figure 2.11. In powered walking, adding energy with a “push-off” impulse from the stance leg just before heel strike is four times as effective as restoring energy after the collision has occurred [31, 73] because it simultaneously restores energy and reduces the subsequent collision.

Daniela Forg [36] has investigated the influence of linear elastic elements on technical bipedal locomotion, with a special emphasis on energy consumption. The experiments were conducted on the humanoid robot called JOHNNIE. They have studies 12 joints (six joints per leg) of the robot and then selected the one consuming more energy compared to the other joints/actuators. The energy comparison was based on the current drawn by the actuator. The support knee joint was found to be the most energy consuming joint and so was assumed to be the one having great potential for energy saving, hence selected for further study and experiments. They found that current drawn by the knee joint actuator is negligible during the swing phase and significantly high during the support phase. After carefully selecting the support knee joint for further analysis,

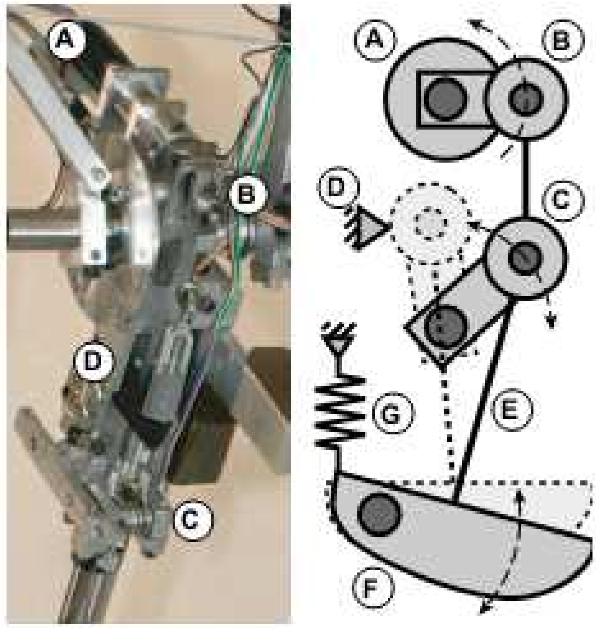

Figure 2.11 – Ankle Spring Drive Train of Cornell Robot [31]: Just after push-off, a DC motor (A), in series with a one-way rotary clutch, drives a motor crank (B). A cable attached to the end of the motor crank via a bearing pulls up an over-center latch (C) until it locks in place against an adjustable stop (D). A cable (E) running from the over-center latch through the knee and to the foot (F) pulls the foot into ready position,stretching a large spring, (G). At push-off, a solenoid at (D) moves the over-center latch back past its equilibrium point and the ankle extends, torqued by the spring. The motor crank is pulled along passively as the one-way clutch is rotated in its free direction.

a torsional spring parallel to the knee actuator was introduced and then cost of transport was calculated at different values of spring stiffness. They found that up to 29% of energy can be saved by introducing identical torsional springs in parallel to the existing actuator at both knees joint with a stiffness of 21.5 Nm/rad.

Another study conducted by Migliore and colleagues [81] shows, that the energetic cost of leg swinging in dynamic robots can be reduced without significantly affecting the stability by emulating the physiological use of passive joint stiffness. They suggest that similar efficiency improvements could be realized in dynamic walking robots. The study was conducted on an experimental model of two segment robotic swinging leg with hip and knee joint. They have studied their model for fixed and variable spring stiffness and found that same results as that of variable stiffness can be achieved while using fixed stiffness spring. The results shows that energetic cost reduction of about 25% can be achieved using hip stiffness and energetic cost reduction of approximately 66% can be achieved using knee stiffness alone.

Stability effects of springs

Wisse [124] has successfully used ankle springs to replace the rigid arc feet by flat feet while having the same stability. The authors conclude that "*The rigid arc feet, well known from passive dynamic walking literature, can equally well be replaced by flat feet mounted on ankles with a torsional spring. The arc radius has a positive effect on the disturbance behavior, and the spring stiffness has a similar effect*". Sensitivity to disturbances is decreased with increasing spring constant k so as with foot radius.

2.8.3 Design of Knee Joint

Addition of knee joint plays an important role in human like gait generation as well as energy consumption. Using stiff legs could actually simplify the motion and robot structure but in practice, it has several important functions in the walking dynamics [48]. In case of a robot with straight legs, the foot clearance have to be created by an additional pelvic tilt. This means a reduced step length and a bigger energy consumption because the pelvis is the heaviest part of the body while knee stretching just lift the foot [48].

Human gait studies show that during swing phase of the leg, the knee joint is unlocked and can swing freely, and during stance phase the knee joint has very small angular velocity and the variation in joint angle is very small. Therefore, it is possible to lock the support knee joint without significantly affecting the gait trajectory. Based on this assumption, knee joints have been designed with locking mechanism that could be engaged and disengaged when needed. Cornell robot (see fig: 2.10(a)) has a knee joint, which can rotate freely when not locked. When the knee reaches full extension midway through swig, so called "knee-strike”, the locking mechanism engages, and the knee remains locked in full extension throughout the remainder of the swing and during stance. Thus the knee motion is largely unactuated [31].

Many studies were conducted on legged robot in order to improve their efficiency and stability. Several modern robots are designed to walk and behave like humans (Figure 2.9), but until now the efficiency of the human gait is still far from being reached (see Table 2.1 for comparison). However, some robots based on the passive dynamic walking as shown in figure 2.10 have comparable energy efficiency to the human gait. In this sense, the work of McGeer [80] can be considered exemplar. His passive dynamic walker made a stable gait without close loop control, considering the walking motion as a natural oscillation of a double pendulum; and this is actually how humans seem to walk [48]. The comparison of specific cost of transport for different robots and machines is given in table 2.1.

Gini [48] manufactured the robot called LARP (Light Adaptive-Reactive biPed), a humanoid legged system with anthropomorphic feet, knees and a mass distribution similar to the human limb. It has twelve active degrees of freedom and the range of motion of each joint is similar to that of the humans during walking. They have designed a special knee joint composed of two circular surfaces rolling on each other as shown in figure 2.12. They found that energetic efficiency of the biped is improved by implementing rolling contact knee joint. A comprehensive study on rolling contact knee joint has been done by Mathieu Hobon in [79]. He compared a selected performance criteria during walking of a biped having classical knee joints with that of rolling contact joints using different optimization techniques.

To obtain the rolling motion of one link on another of the knee joint, Hamon and Aoustin [53, 54] have studied a new cross four-bar linkage mechanism for the knee joint, which replaces the traditional revolute joint. Significant reduction in knee torque and hence energy consumption has been presented by the authors.

Advantages of rolling contact knee joint

This kind of joint for the knee articulation has several advantages respect to a pin joint.

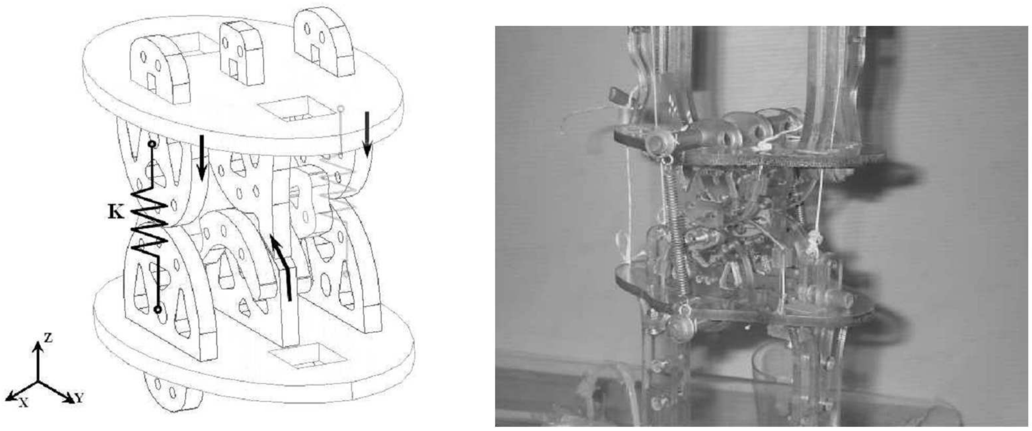

Figure 2.12 – The Joint Design (left) and Prototype (Right) of LARP [48]

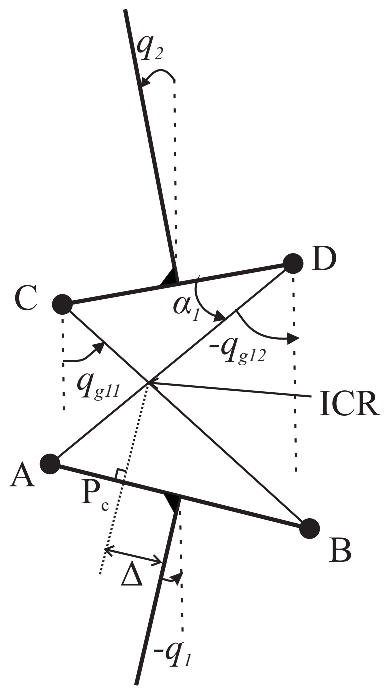

Figure 2.13 – Representation of cross four bar knee joint [54]

1. It is energy efficient because of reduced friction of the joint.
2. Using elastic actuators or even a passive knee, the leg can be bent exploiting inertial forces due to hip actuation. In this sense, an efficient knee joint is fundamental to reduce the demand of high hip torque.
3. The center of rotation (*cr*) is not fixed, as in a pin joint, but moves upward and backward during rotation (Fig. 2.14). This motion increases the foot clearance necessary to swing the leg, and the shank active rotation can thus be reduced.
4. The knee could be passive during swing phase in some robots and will reduce energy consumption.

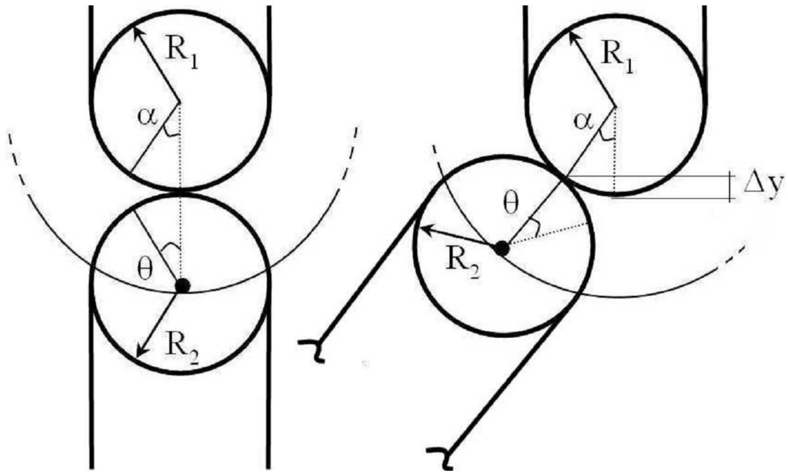

Figure 2.14 – Schematic of rolling contact knee joint [48]

2.8.4 Introducing Compliance in the Gait

Compliance is the inverse of stiffness. Therefore, something with more compliance will be less stiff and will act like a spring. Compliance could be in bending, compression or torsion. In the field of bipedal robotics, compliance is introduced in the gait to restore the lost energy and to have the damping effect to minimize the impulsive losses of heel strike. For this purpose a large number of researchers have installed springs at the ankle [87, 42] and they call it the compliant ankle [99, 73]. To add compliance to the gait Gini [48] have designed a compliant human-like knee instead of a classical pin-joint.

Apart from using ankle or knee springs, Nakano [86] proposed a dynamic biped walking robot with flexible beams. This robot has two legs, which is a pair of flexible beams instead of a pair of rigid crura and femurs. The flexible beams are expected to bring a light weight robot, and also act as joints at knees, which have been operated by electrical or hydraulic motors. The flexible beams robot and its walking cycle at the stance phase is shown in figure 2.15. Figure 2.15(b) shows that the percentage of body weight force on the stance leg during walking cycle, resembles the human walk cycle with some differences during knee flexion.

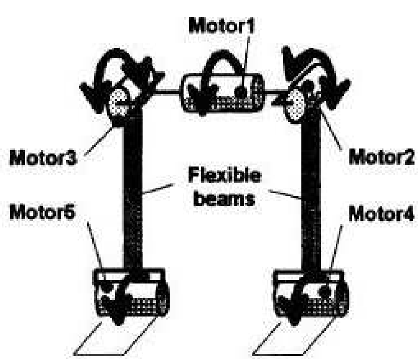

(a) Flexible Beams Robot

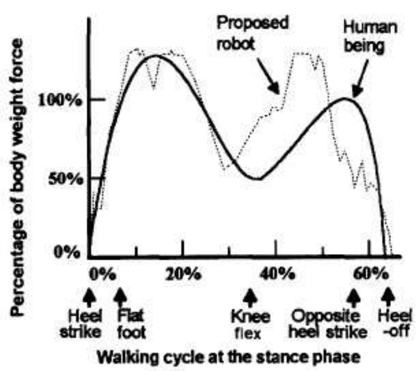

(b) Percentage of body weight force on the stance leg

Figure 2.15 – Flexible Beams Robot and its Walking Cycle [86]

As a result from the flexible beams robot, following features have been found. (1) The weight of the proposed robot can be reduced to half as compared with conventional rigid body robots. (2) Rapid and stable walking can be attained by the milt movement of the flexible legs.(3) Energy consumption for dynamic walking is reduced to 70% as compared with rigid body robots [86].

2.8.5 Other Methods of Energy Recovery

Instead of using springs, artificial muscle actuators are used to have compliance in articulations and reduce weight and energy consumption of the robot [96]. A number of studies have been carried out to study behavior of Pneumatic Artificial Muscle (PAM) for humanoid applications [123] and rehabilitation applications [94]. Vanderborght [117, 118] developed the bipedal walking robot called Lucy shown in figure 2.16(a). Special about it is that the biped is not actuated with the classical electrical drives but with pleated pneumatic artificial muscles (Fig: 2.16(b)). In an antagonistic setup of such muscles, both the torque and the compliance are controllable. From human walking there is evidence that joint compliance plays an important role in energy efficient walking and running. Moreover pneumatic artificial muscles have a high power to weight ratio and can be coupled directly without complex gearing mechanism, which can be beneficial towards legged mechanisms. Additionally, they have the capability of absorbing impact shocks, and store or release motion energy.

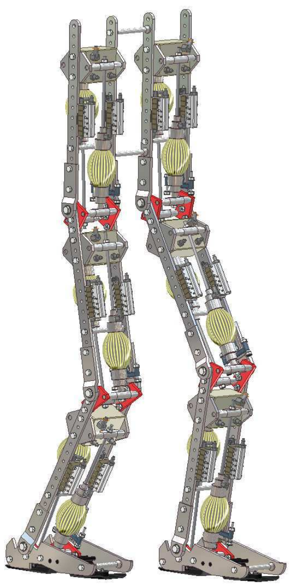

(a) CAD drawing of robot Lucky

(b) Three contraction levels of Pneumatic Muscle

Figure 2.16 – CAD drawing and pneumatic muscle of the biped Lucy [118]

Recently, the use of hydraulic actuators has significantly increased in field of robotics particularly humanoid robotic systems. These actuators have exceptional performance and high power to weight ratio. A central pumping or pressure unit called "central hydraulic block" is used to provide required pressure to each actuator to produce desired motion. One huge motor-pump is usually used to produce the pressure and the flow necessary to actuate several joints. This solution was able to demonstrate high performances, for large output forces as well as for generation of smooth movements. Based on the characteristics of hydraulic actuators, a high performance

Integrated Electro-Hydraulic Actuator (IEHA) is developed by S. Alfayad et al. [6, 7]. The newly developed hydraulic actuator is a light weight solution satisfying all the performances needed for actuating a humanoid robot [3]. Advantages of IEHA include, but not limited to, 1) Light weight, 2) complete actuator including micro hydraulic pump, 3) energy storage function, and 4) no central pumping system is required.

The new Integrated Electro-Hydraulic Actuator (IEHA) has an integrated reservoir in which energy can be stored in the form of hydraulic pressure in order to optimize the power consumption of the joint. It is based on the use of the duty cycle phenomenon to store energy whenever no motion is needed on the joint [6, 7]. This energy will be used when it is needed resulting in a smaller actuating system. Hence, the energy consumption can be considered as optimal during walking or performing manipulating tasks. The scope of the present study is to explore energetic effects of the energy storage capabilities of IEHA on different types walking gaits. This actuator is briefly explained in chapter 6 and simulation results of energy storage on different bipedal walking gaits are presented in chapter 7.

Another important technique to improve energetic efficiency of a bipedal robot during walking is to lock the knee joint of the stance foot. As already discussed, knee joint of the stance leg is one of the most energy consuming, therefore, significant amount of energy can be saved by mechanically locking the knee joint. The knee locking mechanism has to be light weight and less energy consuming. The IEHA can be used to lock knee joint at any desired angle without consuming energy, hence reducing cost of walking. Effects of knee locking on 2D bipedal walking in case of electric actuators are explained in chapter 5, and in case of hydraulic actuators are presented in chapter 7.

2.9 Conclusion

In this chapter, a detailed overview of human walking was presented. Moreover, different phases of human walking were explained and terminologies used to describe human walking were introduced. Anatomy of skeletal muscle, which is responsible of walking and other motions was presented, and expression of work done by a muscle was deduced. Robot locomotion and different types of gaits of bipedal walking were presented and the events occurring during a gait cycle of these gait were explained.

The factors effecting the energetic cost of a biped during walking were discussed. The factors include, mechanical design, mass distribution, actuator selection etc. Moreover, different approaches used to improve energetic efficiency of a biped, and generate an efficient and stable human like gait were presented.

Keeping in mind and benefiting from all the existing methods and techniques for energy efficient bipedal gait generation and searching for new energy recovery and optimization methods. Furthermore, several energy minimization strategies for the bipedal robot HYDROïD were presented, which include:

- Adding torsional springs to different joints in parallel to existing actuators.
- Mechanically locking the support knee during entire stance phase.
- Installing the new integrated hydro-electrical actuator capable of storing energy and release the store energy when needed.

All the techniques presented above will be explored in detail and their effects on bipedal walking will be presented in the following chapters.

3

Presentation and Dynamic Modeling of the Biped

Contents

3.1 Introduction

This chapter is devoted to presentation of the biped, definition of the walking gaits to be studied, and modeling of the biped. A simplified model of the bipedal robot HYDROiD will be presented. The biped is developed under the project called "R2A2" sponsored by the French National

Research Agency (ANR). The geometric and inertial parameters in 2D of the HYDROiD will be presented. Three different types of walking gaits for the studied biped will be explained. The dynamic model will then be formulated for a seven link planar bipedal robot using the Lagrange formulation in general case, in single support phase, and in double support phase depending on the type of gait. The impact model for a bipedal robot will be developed, and different possible solutions of foot contact with the ground just after impact will be discussed.

Dynamic model with torsional springs in parallel to the existing actuators will be developed to calculate the effects of springs on energetic consumption during walking. Moreover, effects of support knee locking on the impact model will be presented. Based on these models, different methods used to generated reference gait trajectories will be presented in chapter 4, and selected performance criteria will be introduced for the comparison of energetic performance during walking. These models will then be used to design bipedal walking gait trajectories with different types of walking gaits to calculate energetic cost of walking in chapter 5 and 7.

3.2 Presentation of the Biped

The planar biped, presented in figure 3.1, is composed of two identical legs and a torso. Each leg consists of a thigh, a shin, and a rigid foot. All joints are revolute, frictionless and can only move in the sagittal plane. Right (foot 1) and left (foot 2) feet are supposed to be the stance and swing foot respectively.

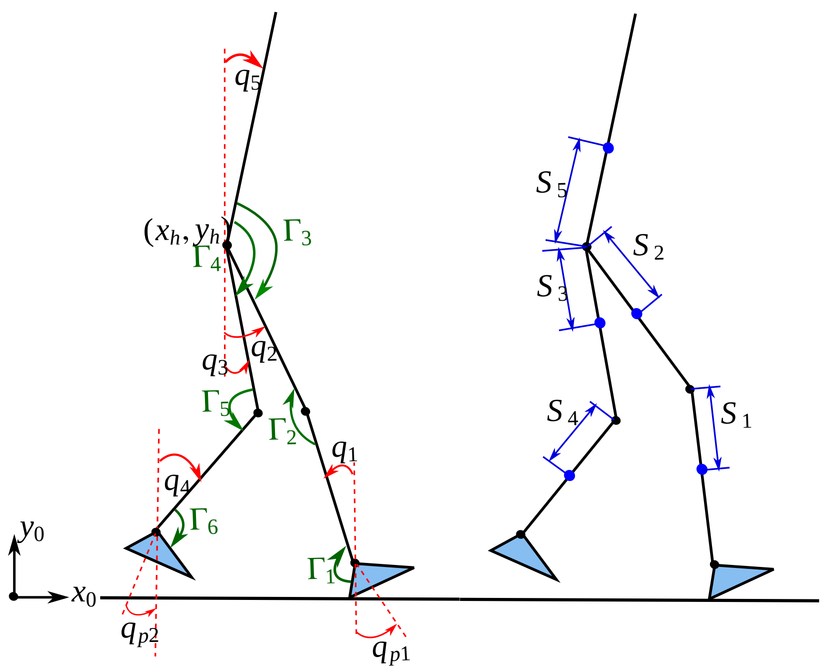

Figure 3.1 – Planar biped, generalized coordinates representation and applied torques

3.2.1 Geometric Parameters of the Biped

The geometric and inertial parameters of the biped are given in table 3.1. These parameters are derived from the humanoid robot named "HYDROiD" [4] having body mass and length similar to those of a human based on geometric human body model designed by Hanavan [57]. The link inertia presented is calculated with respect to the center of mass of the respective link around the axis z perpendicular to the sagittal plane. The HYDROiD robot also has arms but in this study, the mass of arms is merged into the torso mass. The center of gravity and inertia of the torso is recalculated to take into account the effects of arms by considering that the arms are fixed in stretched position along the torso. The geometry of the foot is presented in Figure 3.11 which explains different terms used in table 3.1.

Table 3.1 – Geometric and inertial parameters of the biped

Link	Description	Mass (Kg)	Length (m)	Gravity Center (m)	Inertia ($Kg.m^2$)
0	Foot	0.678	L_p=0.20700 h_p=0.06425	$S\,p_x$= 0.01350 $S\,p_y$= 0.03213	0.00175
1	Shin	2.188	0.392	0.16856	0.02765
2	Thigh	5.025	0.392	0.16856	0.06645
3	Torso	29.27	0.5428	0.192065	0.81496

3.3 Definition of Studied Walking Gaits

Different types of walking gaits can be considered to test the performance of a bipedal robot walking. Optimal walking gait trajectories will be generated for the robot using the algorithm of parametric optimization presented in chapter 4. The goal is to generate walking gait trajectories that closely resemble human walking. In addition, all gait trajectories are assumed to be cyclic. Joint limits and torque constraints of the biped robot HYDROiD are given in table 3.2 below.

Table 3.2 – Joint and Torque Limits of HYDROiD Robot

Joint	Joint angles (deg)		Joint velocities (deg/sec)		Joint torques (Nm)	
q_i	Min	Max	Min	Max	Min	Max
1	-30	30	-245	245	-157	157
2	-90	90	-401	401	-108	108
3	-90	90	-155	155	-150	150
4	-90	90	-155	155	-150	150
5	-90	90	-401	401	-108	108
6	-30	30	-245	245	-157	157

3.3.1 Walking Gait without Impact

In present study, the simplest studied walking gait is the impactless gait having only simple support phases separated by instantaneous impactless transition phases. This walking gait will be called *gait type 1* for simplicity. In gait type 1, the velocity of the swing foot just before touching the ground is null. Foot 1 is the stance and foot 2 is the swing foot. Stance foot is considered as the base link of the biped. The walking step begins with a single support phase and ends with impactless flat foot contact on the ground where the feet exchange their role *i.e.* the stance foot becomes swing foot and vice versa. The stance foot remains in flat contact on the ground during the entire single support phase. At transition phase, relabeling of the joints is done such that the stance foot is always foot 1. This permits one to use the same models for the second step when the swing foot becomes stance foot. There is no change in configuration, velocities and accelerations of the joints during transition phase, only relabeling is done. Figure 3.2 presents walking gait type 1 for a biped. This gait has the minimum number of optimization parameters among all other walking gaits studied in present thesis. Another advantage of this gait is that it has no impact and therefore, the mechanical structure and joints of the biped are preserved.

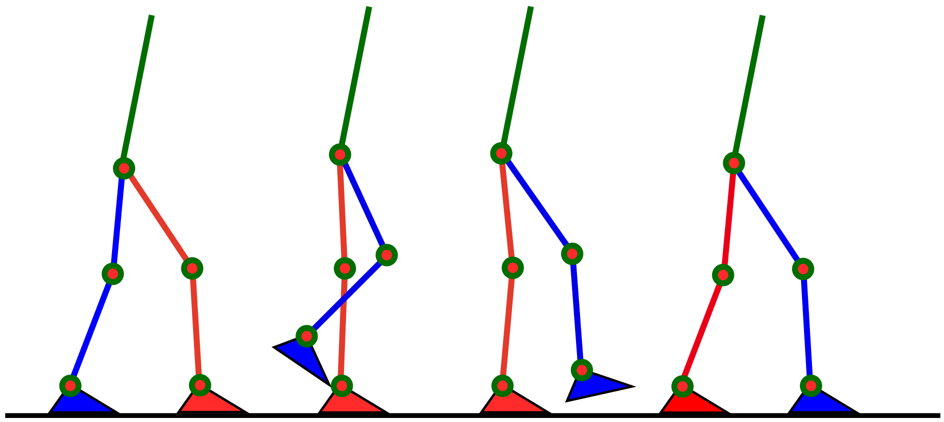

Figure 3.2 – Representation of walking gait type 1

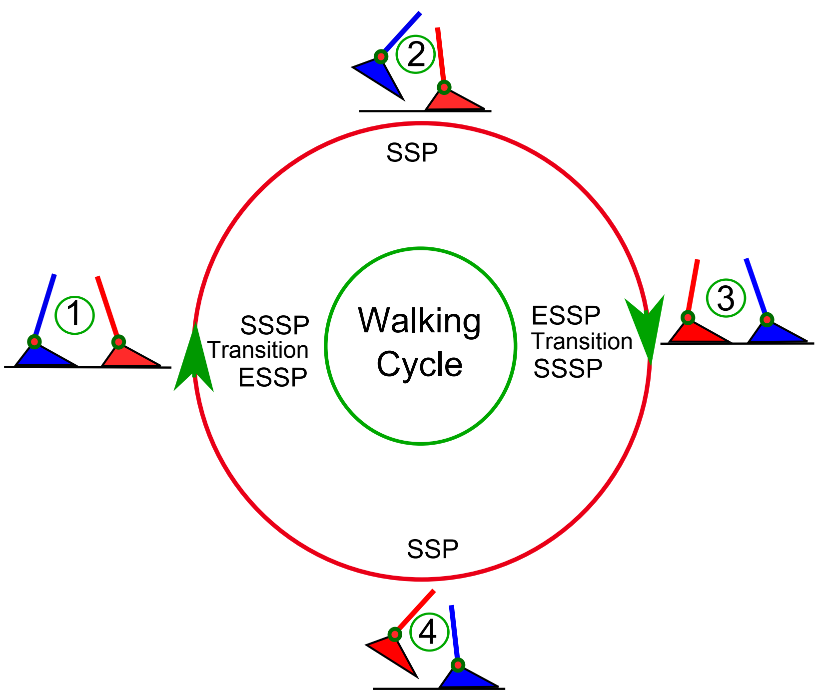

Figure 3.3 – Representation of walking cycle of gait type 1. SSSP: start of single support phase, SSP: single support phase, ESSP: end of single support phase

3.3.2 Walking Gait with Impact

The walking trajectory of this gait is composed of only single support phases separated by impulsive impacts. This gait will be called *gait type 2*. The walking step of gait type 2 begins with a single support phase and ends with an impact on the swing foot. At impact, the feet exchange their role *i.e.* the stance foot becomes the swing foot and vice versa. The impact occurs with flat foot contact on the ground. There is no rotation on the heel or toe of stance foot during the entire single support phase. Stance foot is considered as the base link of the biped. This gait is depicted in Figure 3.4. The advantage of this gait is that it has relatively low number of parameters to optimize resulting in fast convergence and limited calculation cost. Furthermore, it is more energetically efficient than gait type 1.

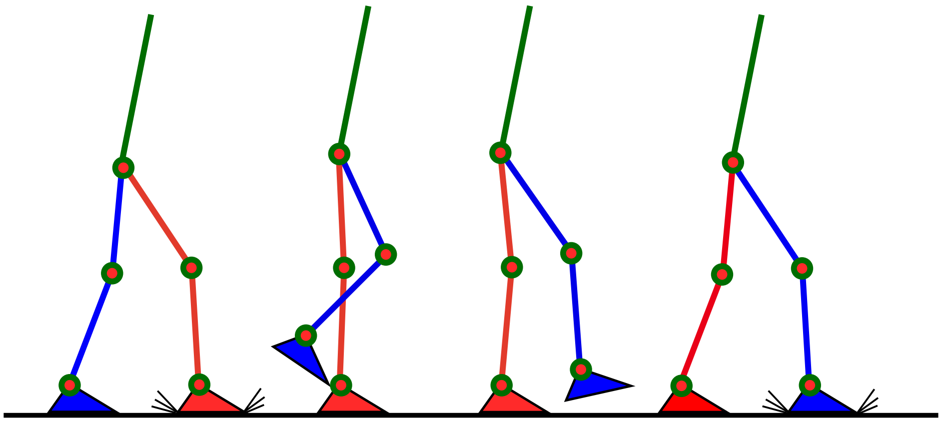

Figure 3.4 – Representaion of walking gait type 2

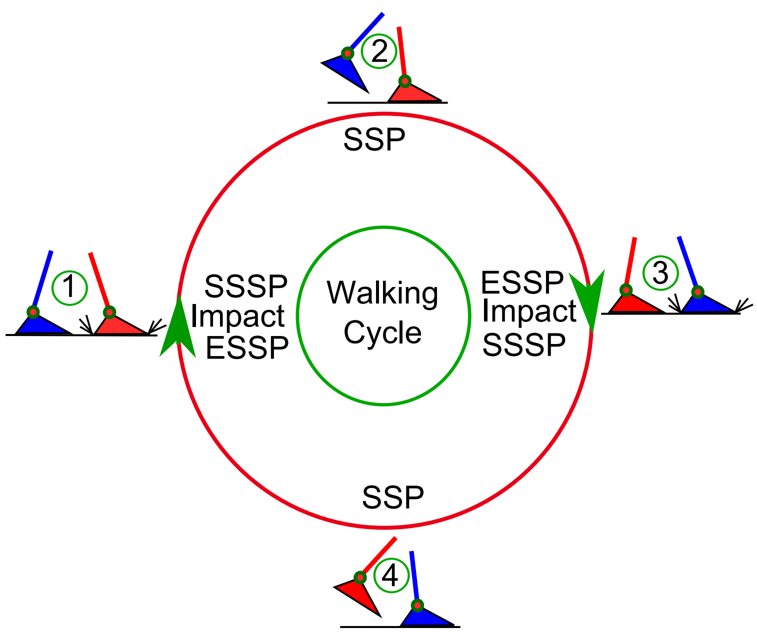

Figure 3.5 – Representation of walking cycle for gait type 2. SSSP: start of single support phase, SSP: single support phase, ESSP: end of single support phase

3.3.3 Walking Gait with Double Support

The introduction of an impact may result in different behaviors after impact. For example, the foot already in contact with the ground can take off or remain on the ground. In the context of obtaining an optimized movement, certain conditions after impact are imposed and it is verified that the constraints associated to these conditions are satisfied. Initially, walking trajectories having double support without take-off of the foot already in contact were studied by Hobon [79] but without success. However, it was found that a walking gait having finite double support phase can be achieved by allowing partial take-off of the heel and rotation around toe of the rear foot and heel of the front foot. In this study, partial take-off of heel of rear foot at impact on heel of front foot is authorized to obtain a gait trajectory close to human walking.

The walking gait with double support phase called *gait type 3* is the more realistic and close to human walking amongst the all studied gaits. It is composed of single support phases and double support phases separated by instantaneous impulsive impacts, as shown in Figure 3.6. There are two impulsive impacts during each walking step, one on the heel strike and second when the toe of the front foot touches the ground. These impacts will be called "heel impact" and "toe impact" respectively. The walking step starts with first impact on heel of the swing foot. At this instance, both feet must stay on the ground to have double support phase. The heel of the front foot and toe of the rear foot remain on the ground while the heel of the rear foot is allowed to take off. This is the beginning of the double support phase and during this phase, the front foot rotates around its heel while the back foot rotates around its toe.

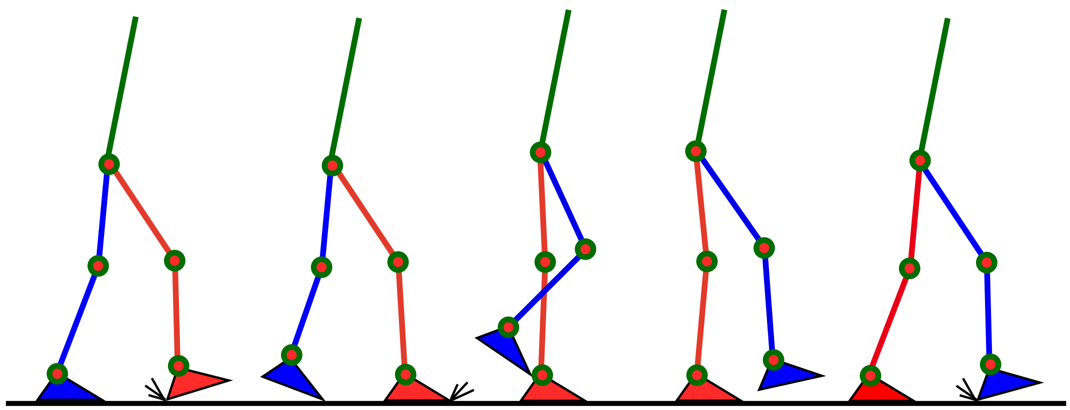

Figure 3.6 – Representation of walking gait type 3

Double support phase ends when the second impact occurs on toe of the front foot. This is the end of double and beginning of single support phase. At this instance, the toe of rear foot takes off the ground and the front foot achieves flat contact on the ground. The front (stance) foot remains in flat contact with the ground during the entire single support phase. For cyclic gaits, this process is repeated every walking step. Figure 3.7 represents the position of feet of the biped during different phase of the walking cycle.

Depending on the type of walking gait, the trajectory optimization problem has a different number of parameters to optimize and constraints to satisfy. In chapter 4, the number of parameters required will be determined to generate walking gait trajectories for each type of walking gait presented.

3.4 Dynamic Modeling of the Biped

The *dynamic model* is used to express and model the behavior of the system over time. In case of a biped, the biped dynamics is concerned with the forces and torques acting on it, and the accelerations they produce. The inverse dynamic model provides the joint torques and forces in

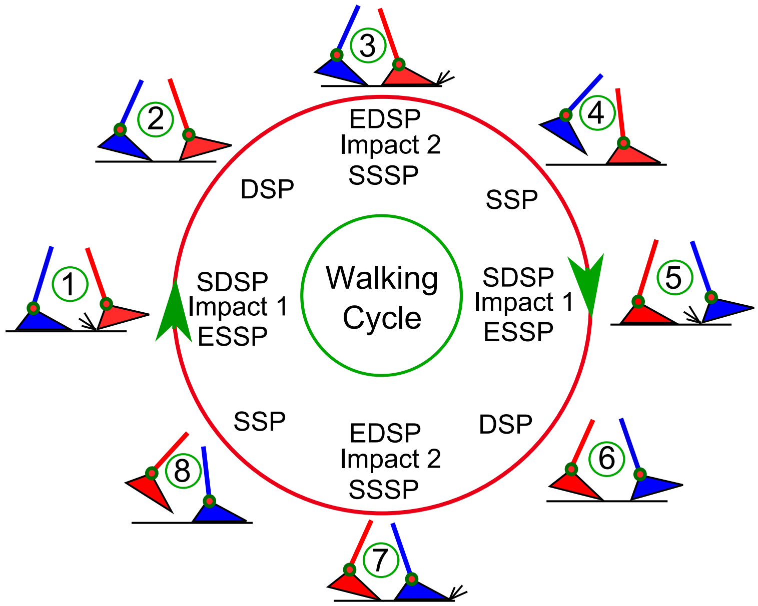

Figure 3.7 – Representation of walking cycle for gait type 3. SDSP: start of double support phase, DSP: double support phase, EDSP: end of double support phase, SSSP: start of single support phase, SSP: single support phase, ESSP: end of single support phase

terms of the joint positions, velocities, and accelerations while the direct dynamic model describes the joint accelerations in terms of the joint positions, velocities and torques [71].

3.4.1 Methods of Formulating Dynamic Model

Several formulations have been used to obtain the dynamic model of robots. However, the following two are commonly used in robotics community for the formulation of the dynamic model:

- The Lagrange formulation
- The Newton-Euler formulation

The Lagrange formulation gives simple results for robots with a small number of degrees of freedom while Newton-Euler formulation is suitable for hyper redundant robots with a large number of degrees of freedom. Since present work is based on a 2D bipedal robot having only six degrees of freedom (dof), therefore, the Lagrange method will be used for the formulation of the dynamic model. The following section briefly describes the formulation of dynamic model using Lagrange method.

3.4.1.1 Lagrange formulation

The Lagrange formulation describes the behavior of a dynamic system in terms of work and energy stored in the system. The Lagrange function is commonly written in the form:

$$L = E - U \tag{3.1}$$

where L is the Lagrangian of the robot defined as the difference between the kinetic energy E and the potential energy U of the system. Finally, in presence of resultant external wrench, the Lagrange equation becomes [71]:

$$\frac{\mathrm{d}}{\mathrm{dt}}\left(\frac{\partial L}{\partial \dot{q}_i}\right) - \frac{\partial L}{\partial q_i} = \mathbf{B}_i\Gamma + \mathbf{J}^{\mathrm{t}}\lambda \qquad \text{for } i = 1 \text{ to } n \tag{3.2}$$

where Γ is the vector of joint torques, $\mathbf{B}_i$ is the i^{th} row of actuation matrix, $\dot{q}_i$ represents the absolute velocity of the link i, and λ is the vector of Lagrange multipliers. The components of vector λ represents a set of forces and moments to be applied to the feet depending on their type of contact on the ground to maintain them in contact position assigned by the constraint equations [29]. For a robot system, the kinetic energy is a quadratic function in the joint velocities is given by [71]:

$$E = \frac{1}{2}\dot{\mathbf{q}}^{\mathrm{t}}\mathbf{A}(\mathbf{q})\dot{\mathbf{q}} \tag{3.3}$$

where $\mathbf{A}(q) \in \mathbb{R}^{n\times n}$ is the symmetric and positive definite inertia matrix of the robot. Its elements are functions of the joint positions. The kinetic energy in equation (3.3) can be re-written as:

$$E = \frac{1}{2}\sum_{i=1}^{n}(m_i V_i^2 + I_i\omega_i^2) \tag{3.4}$$

where m_i is the mass of the link i, V_i is the linear velocity of the center of mass of the link i, ω_i is the angular velocity defined in the center of mass of the link i and I_i is the inertia about center of mass of the link i.

The potential energy of the robot can be calculated as:

$$U = \sum_{i=1}^{n}(m_i g h_i) \tag{3.5}$$

where g is the gravitational acceleration, h_i is the position of the center of mass of the link i along the vertical axis, and n is the number of links of the robot.

3.4.2 Dynamic Model: Double Support Phase with Explicit Contact

To define a planar biped having 6 dof, 9 parameters are required to express the joint motion and the position and orientation of one link in a plane. Thus the generalized coordinate vector for the studied biped is represented by $\mathbf{q} = [q_{p1}\ q_{p2}\ q_1\ q_2\ q_3\ q_4\ q_5\ x_h\ y_h]^{\mathrm{t}}$. The biped in general case is represented in Figure 3.1. The dynamic model is developed by using the equations (3.2) , (3.3) and (3.5) of the Lagrange formulation such as:

$$\mathbf{A}(\mathbf{q})\ddot{\mathbf{q}} + \mathbf{C}(\mathbf{q},\dot{\mathbf{q}})\dot{\mathbf{q}} + \mathbf{G}(\mathbf{q}) = \mathbf{B}\boldsymbol{\Gamma} + \mathbf{J}_1^{\mathrm{t}}\mathbf{R}_1 + \mathbf{J}_2^{\mathrm{t}}\mathbf{R}_2 \tag{3.6}$$

where $\mathbf{A}(\mathbf{q}) \in \mathbb{R}^{9\times 9}$ is the positive definitive inertia matrix, $\mathbf{C}(\mathbf{q},\dot{\mathbf{q}}) \in \mathbb{R}^{9\times 9}$ represents the vector of Coriolis and centrifugal forces, $\mathbf{G}(\mathbf{q}) \in \mathbb{R}^{9\times 1}$ contains the gravity forces, $\mathbf{B} \in \mathbb{R}^{9\times 6}$ is the actuation matrix consisting of zeros and ones, $\mathbf{J}_1^t$ and $\mathbf{J}_2^t$ are the Jacobian matrices of foot 1 and 2 respectively, and $\mathbf{R}_1$ and $\mathbf{R}_2$ are the vectors of ground efforts on foot 1 and 2 respectively.

To ensure contact of feet on the ground, dynamic constraints of contact needs to be added. The constraint equations can be expressed as:

$$\mathbf{J}_1\ddot{\mathbf{q}} + \dot{\mathbf{J}}_1\dot{\mathbf{q}} = 0 \tag{3.7}$$

$$\mathbf{J}_2\ddot{\mathbf{q}} + \dot{\mathbf{J}}_2\dot{\mathbf{q}} = 0 \tag{3.8}$$

The biped's feet can have three types of contacts on the ground, 1) flat foot contact, 2) contact on the heel, and 3) contact on the toe or no contact at all. The dimensions of Jacobian matrix $\mathbf{J}_i$ and ground reactions wrench $\mathbf{R}_i$ depends on the type of contact of the foot i on the ground. If the foot i is in flat foot contact then $\mathbf{J}_i \in \mathbb{R}^{3\times9}$, $\mathbf{R}_i \in \mathbb{R}^{3\times1}$ with $\mathbf{R}_i = [R_{ix}, R_{iy}, M_i]^t$, and the contact equation adds 3 constraints for foot i. Similarly, if the foot i makes contact on the ground with its heel or toe, then $\mathbf{J}_i \in \mathbb{R}^{2\times9}$, $\mathbf{R}_i \in \mathbb{R}^{2\times1}$ with $\mathbf{R}_i = [R_{ix}, R_{iy}]^t$, and the contact equation adds 2 constraints for foot i.

3.4.3 Dynamic Model in Single Support

During single support phase, all the studied walking gaits (type 1, 2, 3) have flat foot contact on the ground. In single support phase, an implicit liaison of the stance foot (foot 1) with the ground is considered (see figure 3.8). The stance foot does not take off or slip during single support phase. The biped configuration can be expressed by a reduced generalized coordinate vector $\mathbf{q}_{ss}$ such that:

$$\mathbf{q}_{ss} = [q_{p2}\ q_1\ q_2\ q_3\ q_4\ q_5]^t$$

Using Lagrange's formulation, the dynamic model can be written:

$$\mathbf{A}_{ss}(\mathbf{q}_{ss})\ddot{\mathbf{q}}_{ss} + \mathbf{C}_{ss}(\mathbf{q}_{ss}, \dot{\mathbf{q}}_{ss})\dot{\mathbf{q}}_{ss} + \mathbf{G}_{ss}(\mathbf{q}_{ss}) = \mathbf{B}_{ss}\mathbf{\Gamma} \tag{3.9}$$

where $\mathbf{A}_{ss}(\mathbf{q}_{ss}) \in \mathbb{R}^{6\times6}$ is the positive definitive inertia matrix, $\mathbf{C}_{ss}(\mathbf{q}_{ss}, \dot{\mathbf{q}}_{ss}) \in \mathbb{R}^{6\times6}$ contains the Coriolis and centrifugal forces, $\mathbf{G}_{ss}(\mathbf{q}_{ss}) \in \mathbb{R}^{6\times1}$ is the vector of gravity forces, $\mathbf{B}_{ss} \in \mathbb{R}^{6\times6}$ is the invertible actuation matrix composed of zeros and ones but differ from identity since absolute joint angles are used, and $\mathbf{\Gamma} \in \mathbb{R}^{6\times1}$ is the joint torques vector.

3.4.3.1 Reaction Forces and Moment

The model presented in equation (3.9) is only valid for the single support phase with flat foot contact on the ground. The ground reaction forces must be calculated to verify if the hypothesis of the contact on the ground is satisfied. It is also important to ensure that the foot does not slip on the ground during walking. It is therefore required to ensure the validity of the following two constraints during the complete single support phase.

$$\begin{cases} R_{1y} > 0 \\ \mu R_{1y} \geq |R_{1x}| \end{cases} \tag{3.10}$$

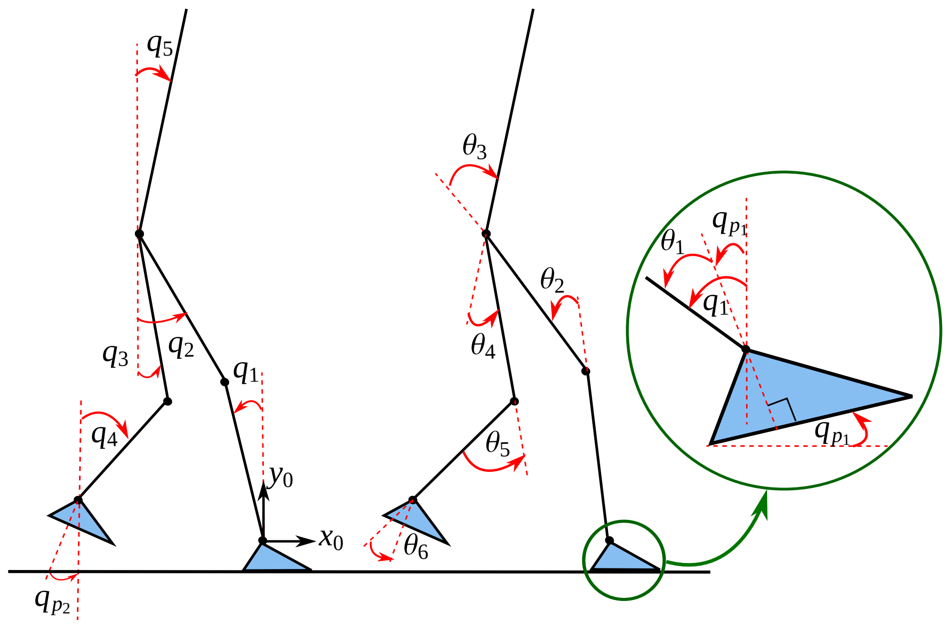

Figure 3.8 – Planar biped, generalized coordinates representation in single support

where R_y and R_x are the vertical and horizontal components respectively of the reaction force of the ground on the support foot, and μ is the coefficient of friction of the foot with the ground.

These ground reaction forces (R_y and R_x) acting on the stance foot can be calculated by the balance equation at the center of mass of the biped. The Subscript 1 will be used for the support foot, and subscript 2 will be used for the swing foot here-forth onward. In single support phase, the ground reaction force R_2 on the swing foot is zero, therefore, the reaction force R_1 on the stance foot can be calculated such that:

$$\begin{bmatrix} R_{1x} \\ R_{1y} \end{bmatrix} = m \begin{bmatrix} \ddot{x}_g \\ \ddot{y}_g \end{bmatrix} + m \begin{bmatrix} 0 \\ g \end{bmatrix} \tag{3.11}$$

Here m is the biped's mass, $\ddot{x}_g$ and $\ddot{y}_g$ are the horizontal and vertical components of the biped's center of mass respectively, R_{1x} and R_{1y} are the horizontal and vertical components respectively of the ground reaction force on foot 1.

Let $S\,(x_s, y_s)$ be the point of application of resultant ground reactions. Thus the dynamic moment γ_g at center of gravity of the biped (see figure 3.9) can be written as:

$$\gamma_g = R_{1x}(y_s + y_g) + R_{1y}(x_s - x_g) + M_1 \tag{3.12}$$

3.4.3.2 The Zero Moment Point

The ZMP criterion is widely accepted as a stability measure for bipedal locomotion. The position of the ZMP is the point on the feet in contact with the ground, such that the sum of all moments due to inertia and active forces equals zero along the transverse axis [106]. To avoid the rotation of the support foot, the Zero Moment Point (ZMP) of the biped must be located in the supporting foot area. The supporting area is defined by the extremities of the feet in contact with the ground,

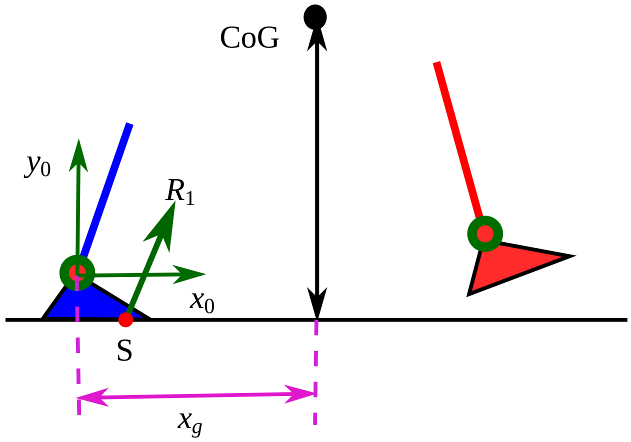

Figure 3.9 – Balance of forces at CoG during single support phase

and is often called the support polygon [109]. During single support phase with flat foot contact on the ground, the support polygon corresponds to the area of convex hull of the support foot. Similarly, during double support phase, it is the convex polygon inscribing the feet [43].

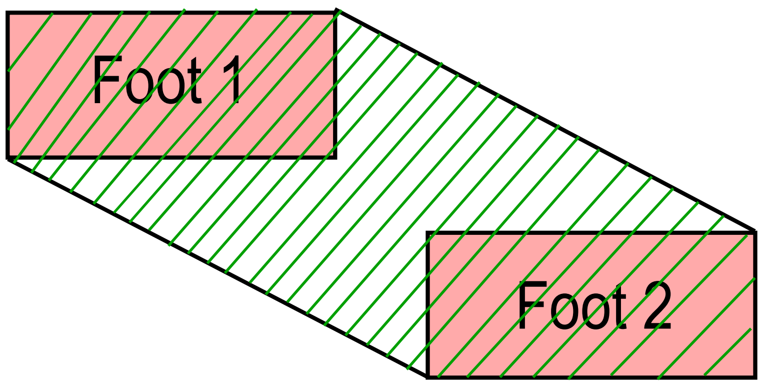

Figure 3.10 – Biped's support polygon

Figure 3.10 is the representation of support polygon for a typical bipedal robot with feet. The filled rectangles represents support polygon during single support phase while the shaded area is the support polygon during double support phase. This representation is valid only when flat contact of the feet on the ground is verified.

The term "ZMP" was first introduced by M. Vukobratovic [120] in 1972. When the biped is in equilibrium on its foot, the ZMP also corresponds to the center of pressure. In case where the ZMP is outside the support polygon, the biped is no more in the equilibrium state, and will rotate around the one extremity of the foot. Therefore, for walking trajectory to be physically possible with the assumed flat foot contact, the ZMP must remain inside the support polygon.

For multi-body systems in the form of kinematic chains, the ZMP can be computed using the D'Alambert's Principle [40, 12]. In our simplified case, the position of ZMP is obtained from the balance of forces on the ankle axis. The foot of the biped is supposed to be an isolated body (figure 3.11) and the effects of rest of the biped on the ankle axis are represented by force vector $\mathbf{f}_O$ and moment vector $\mathbf{m}_O$ applied at point O of ankle of the support foot. The vector of ground reaction forces is represented by $\mathbf{R}$ and moment at point P is represented by $\mathbf{M}$. Let m_p be the

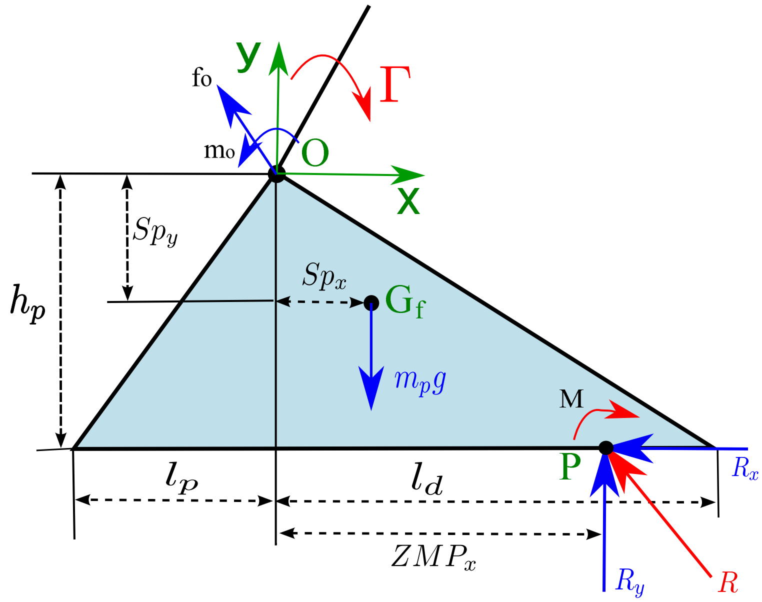

Figure 3.11 – Biped's foot geometry

mass and $\mathbf{G}_f$ be the position vector of center of mas of the foot. The equilibrium equation about the ankle axis can be written as:

$$\mathbf{m}_O + \mathbf{O} \wedge \mathbf{f}_O + \mathbf{OG}_f \wedge m_p\mathbf{g} + \mathbf{OP} \wedge \mathbf{R} + \mathbf{M} = 0 \tag{3.13}$$

where O is the origin of the coordinate system. In case of the planar biped, the coordinates of the ZMP can be obtained by calculating the global equilibrium of the bipedal robot around the vertical axis, which gives:

$$ZMP_x = \frac{\Gamma_1 + Sp_x m_p g - h_p R_x}{R_y} \tag{3.14}$$

where R_x and R_y are the tangential and normal components of the ground reaction force on the stance foot, Γ_1 is the applied torque on the ankle joint, ZMP_x is the position of ZMP, m_p is the foot mass, g is the gravitational force, Sp is the position of center of mass of the foot with respect to ankle and h_p is the height of the foot.

3.4.4 Dynamic Model in Double Support

Walking gait type 3 consist of single and double support phases separated by impulsive impacts. During double support phase, the biped is in contact on the ground with heel of the front foot and toe of the back foot as shown in Figure 3.12. Thus, it is possible to consider perfect pivot contact between heel of the front foot and the ground. The reduced generalized coordinate vector during double support is given by $\mathbf{q}_{ds} = [q_{p1}, q_{p2}, q_1, q_2, q_3, q_4, q_5]^t$. Therefore, the dynamic model in double support phase can be written to take into account the reaction forces applied by ground on the rear foot as:

$$\mathbf{A}_{ds}(\mathbf{q}_{ds})\ddot{\mathbf{q}}_{ds} + \mathbf{C}_{ds}(\mathbf{q}_{ds}, \dot{\mathbf{q}}_{ds})\dot{\mathbf{q}}_{ds} + \mathbf{G}_{ds}(\mathbf{q}_{ds}) = \mathbf{B}_{ds}\boldsymbol{\Gamma} + \mathbf{J}^{t}_{2\,ds}\mathbf{R}_{2\,ds} \tag{3.15}$$

where $\mathbf{A}_{ds}(\mathbf{q}_{ds}) \in \mathbb{R}^{7\times7}$ is the positive definitive inertia matrix, $\mathbf{C}_{ds}(\mathbf{q}_{ds}, \dot{\mathbf{q}}_{ds}) \in \mathbb{R}^{7\times7}$ contains the Coriolis and centrifugal forces, $\mathbf{G}_{ds}(\mathbf{q}_{ds}) \in \mathbb{R}^{7\times1}$ is the vector of gravity forces, $\mathbf{B}_{ds} \in \mathbb{R}^{7\times6}$ is the actuation matrix composed of 1 and 0, and $\boldsymbol{\Gamma} \in \mathbb{R}^{6\times1}$ is the joints torque vector. The ground reaction forces on rear foot $\mathbf{R}_{2\,ds} \in \mathbb{R}^{2\times1}$ are taken into account through the Jacobian matrix $\mathbf{J}_{2\,ds} \in \mathbb{R}^{2\times7}$. The Jacobian matrix at toe of foot 2 is given by (C.7) (see Annex C). The reaction force R_1 has no effect on this dynamic model. Since an implicit pivot contact is assumed on the heel of leg 1 thus this reaction force has no virtual work.

To ensure contact on the ground, following dynamic constraint equations is to be added.

$$\mathbf{J}_{2\,ds}\ddot{\mathbf{q}}_{ds} + \dot{\mathbf{J}}_{2\,ds}\dot{\mathbf{q}}_{ds} = 0 \tag{3.16}$$

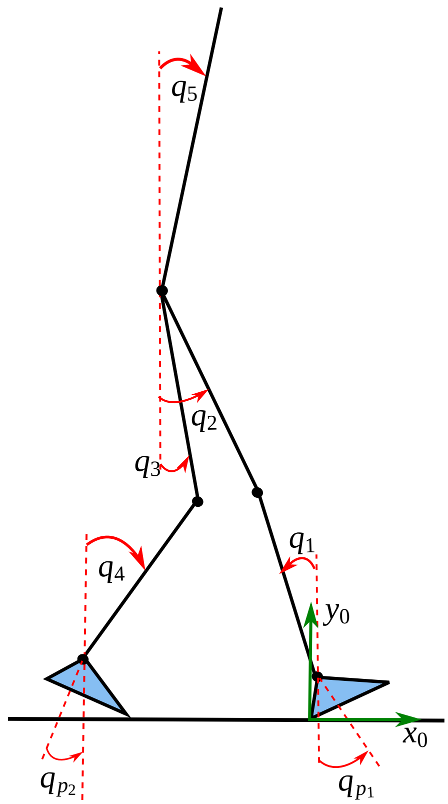

Figure 3.12 – Planar biped, generalized coordinates representation in double support

3.4.4.1 Reaction Forces and Moment

During double support phase, the inverse dynamic model (3.15) has 7 equations and 8 unknowns (6 joint torques and 2 ground reactions). The addition of contact equations of rear foot on the ground add two constraints which leads to 1 degree of over-actuation. Therefore, infinite solutions of this dynamic model exist. Performing the balance of forces on the center of gravity of the biped (see Figure 3.13), following system of equations is obtained:

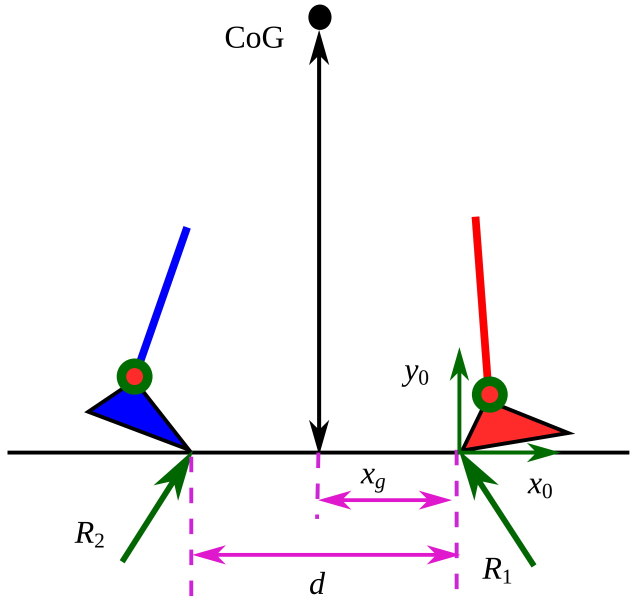

Figure 3.13 – Balance of forces at CoG

$$\begin{cases} \gamma_g = (R_{1x\,ds} + R_{2x\,ds})y_g + R_{2y\,ds}(x_g - d) + R_{1y\,ds}x_g \\ m\ddot{x}_g = R_{1x\,ds} + R_{2x\,ds} \\ m\ddot{y}_g = R_{1y\,ds} + R_{2y\,ds} - mg \end{cases} \tag{3.17}$$

Where, γ_g is the dynamic moment at center of gravity of the biped, $\ddot{x}_g$ and $\ddot{y}_g$ represents tangential and horizontal components of acceleration of CoG of the biped. The system of equations in (3.17) has 3 equations and 4 unknowns. Therefore, to solve this equation one unknown should be calculated or fixed, and after analyzing the system, it is found that only horizontal components of the ground reaction force either on foot 2 ($R_{2x\,ds}$) or on foot 1 ($R_{1x\,ds}$) of the biped can be fixed. In the present study, $R_{2x\,ds}$ is selected to be predefined.

The tangential reaction force on rear foot $R_{2x\,ds}$ during double support phase is calculated depending on the type of criterion used. If the criterion is a function of square of joint torques (see 4.14), $R_{2x\,ds}$ is calculated to minimize the criterion as explained in detail in Annex D. For the criterion based on actuators mechanical energy (see 4.15), $R_{2x\,ds}$ is expressed as a function of time by a third order polynomial during double support phase.

Now, supposing that $R_{2x\,ds}$ is known, joint torques as well as the vertical component of ground reaction force on rear foot can be calculated by decomposing equation (3.15) such that:

$$\begin{bmatrix} \mathbf{\Gamma} \\ R_{2y\,ds} \end{bmatrix} = \begin{bmatrix} \mathbf{B} & \mathbf{J}^{t}_{2y\,ds} \end{bmatrix}^{-1} \begin{bmatrix} \mathbf{A}_{ds}(\mathbf{q}_{ds})\ddot{\mathbf{q}}_{ds} + \mathbf{C}_{ds}(\mathbf{q}_{ds}, \dot{\mathbf{q}}_{ds})\dot{\mathbf{q}}_{ds} + \mathbf{G}_{ds}(\mathbf{q}_{ds}) - \mathbf{J}^{t}_{2x\,ds}R_{2x\,ds} \end{bmatrix} \tag{3.18}$$

The ground reaction forces on front foot can be calculated by writing the force balance equations on center of mass of the biped as:

$$\begin{cases} R_{1x\,ds} = m\ddot{x}_g - R_{2x\,ds} \\ R_{1y\,ds} = m\ddot{y}_g - R_{2y\,ds} + mg \end{cases} \tag{3.19}$$

Thus, after solving the dynamic equation (3.18) and calculating R_{2y}, components of the ground reaction forces can easily be calculated by (3.19). These reaction forces will be used to calculate and impose constraints of no-slipping and no-take-off.

3.4.4.2 The Zero Moment Point

The Zero Moment Point (ZMP) in double support phase can be written through the center of pressure of each foot such that:

$$ZMP_{ds} = \frac{l_{cp1} R_{1y\,ds} + l_{cp2} R_{2y\,ds}}{R_{1y\,ds} + R_{2y\,ds}} \tag{3.20}$$

Where, l_{cp1} and l_{cp2} are the center of pressure (CoP) of foot 1 and 2 respectively. For gait type 3 during double support phase, the center of pressure of foot 1 is located in its heel while that of foot 2 is in its toe. If the biped is dynamically stable and ZMP is inside the support polygon, CoP coincides with ZMP [98]. The position of CoP can be calculated using equations of ZMP for example equation (3.14) in case of flat foot contact on the ground.

3.4.5 Dynamic Model with Springs

Addition of springs in parallel to an actuator or in series on a link, allows one to store certain amount of energy and release the stored energy when required by the system. The goal of present study is to improve the energetic efficiency of the bipedal robot under study. For this purpose, torsional springs are added to the biped structure in parallel with the existing actuators. To incorporate the effects of springs on the dynamics of the bipedal robot, modification of the dynamic model of the biped is needed. The inverse dynamic model from equation (3.6) of the bipedal robot having torsional spring in parallel of the actuator can be written [100]:

$$\mathbf{A}(\mathbf{q})\ddot{\mathbf{q}} + \mathbf{C}(\mathbf{q}, \dot{\mathbf{q}})\dot{\mathbf{q}} + \mathbf{G}(\mathbf{q}) + \mathbf{\Gamma}_s = \mathbf{B}\mathbf{\Gamma} + \mathbf{J}_1^t \mathbf{R}_1 + \mathbf{J}_2^t \mathbf{R}_2 \tag{3.21}$$

Where $\mathbf{\Gamma}_s$ is the vector of spring torque and is obtained from equation:

$$\mathbf{\Gamma}_s = \sum_{j=1}^{m} \mathbf{\Gamma}_{sj} \tag{3.22}$$

Where j is the joint on which spring is installed, m is the total number of joints having springs in parallel with the existing actuator, and $\mathbf{\Gamma}_{sj}$ is the spring torque provided by joint j.

The spring torque is obtained from derivative of the spring potential energy. The potential energy of the spring is given by:

$$U_j = \frac{1}{2} K_j (\theta_j - \theta_0)^2 \tag{3.23}$$

Where U_j and K_j are the spring potential energy and spring stiffness respectively at joint j, θ_j is the angle between link j and $j-1$ (see figure 3.8) and θ_0 is the spring offset or bias angle at joint j.

According to Lagrange formulation, the spring torque vector $\mathbf{\Gamma}_{sj}$ on j^{th} joint can be calculated as:

$$\mathbf{\Gamma}_{sj} = \frac{\delta U_j}{\delta \mathbf{q}} \tag{3.24}$$

3.5 Calculation of matrices A, B, C and G

The elements of matrix **A** are functions of the joint positions. An (i, j) element of **A** is denoted by $\mathbf{A}_{ij}$. To compute the elements of matrix **A**, the symbolic expression of kinetic energy of all the joints of the robot is calculated. Then the derivative of expression of total kinetic energy of the robot gives the inertia matrix **A**:

$$\mathbf{A} = \frac{\partial^2 E}{\partial \dot{\mathbf{q}}^2} \tag{3.25}$$

The matrix **B** is obtained from the concept of virtual work of actuator's torque. The virtual work δW_i $(i = 1, ..., n)$ of each torque Γ_i, applied to the corresponding joint variable $\delta\theta_i$, can be written as:

$$\begin{aligned} \delta W_i &= \delta\theta_i \Gamma_i \\ &= \mathbf{B}_i^{\mathrm{t}} \delta \mathbf{q} \Gamma_i \end{aligned} \tag{3.26}$$

Then the matrix of torques is $\mathbf{B} = [\mathbf{B}_1, ..., \mathbf{B}_1, ..., \mathbf{B}_n]$ with [71]:

$$\mathbf{B}_i = \frac{\partial}{\partial \mathbf{\Gamma}_i}\left(\frac{\partial \delta W}{\partial \delta \mathbf{q}}\right) \tag{3.27}$$

Here, θ_i is the i^{th} joint variable and W is the virtual work associated to actuation. The actuated joint angles θ_i for each joint in double support phase can be calculated as:

$$\begin{cases} \delta\theta_1 = \delta q_1 - \delta q_{p_1} \\ \delta\theta_2 = \delta q_2 - \delta q_1 \\ \delta\theta_3 = \delta q_5 - \delta q_2 \\ \delta\theta_4 = \delta q_3 - \delta q_5 \\ \delta\theta_5 = \delta q_4 - \delta q_3 \\ \delta\theta_6 = \delta q_{p_2} - \delta q_4 \end{cases} \tag{3.28}$$

Thus, the actuation matrix $\mathbf{B}_{ds}$ is obtained from equation (3.28) and is presented below:

$$\mathbf{B}_{ds} = \begin{bmatrix} -1 & 0 & 0 & 0 & 0 & 0 \\ 0 & 0 & 0 & 0 & 0 & 1 \\ 1 & -1 & 0 & 0 & 0 & 0 \\ 0 & 1 & -1 & 0 & 0 & 0 \\ 0 & 0 & 0 & 1 & -1 & 0 \\ 0 & 0 & 0 & 0 & 1 & -1 \\ 0 & 0 & 1 & -1 & 0 & 0 \end{bmatrix} \tag{3.29}$$

Similarly, during single support phase where $\delta q_{p_1} = 0$, the actuation matrix $\mathbf{B}_{ss}$ is the last six rows of $\mathbf{B}_{ds}$.

The matrix $\mathbf{C}(\mathbf{q}, \dot{\mathbf{q}})$ can be calculated by using the *Christoffell symbols* $c_{i,jk}$. An (i, j) element of the matrix $\mathbf{C}(\mathbf{q}, \dot{\mathbf{q}})$ is calculated from equation (3.30), where i is the row and j is the column of the matrix $\mathbf{C}(\mathbf{q}, \dot{\mathbf{q}})$.

$$\begin{cases} C_{ij} = \sum_{k=1}^{n} c_{i,jk}\dot{q}_k \\ c_{i,jk} = \frac{1}{2}\left[\frac{\delta A_{ij}}{\delta q_k} + \frac{\delta A_{ik}}{\delta q_j} - \frac{\delta A_{jk}}{\delta q_i}\right] \end{cases} \tag{3.30}$$

Finally, the elements of gravity vector $\mathbf{G}$ are calculated by derivation of the potential energy of the robot. Here, G_i represents the i^{th} element of the matrix $\mathbf{G}$.

$$G_i = \frac{\partial U}{\partial q_i} \tag{3.31}$$

3.6 The Impact Model

The ground and foot of the biped is supposed to be rigid, therefore, the impact is modeled between two rigid bodies which can produce discontinuities in velocities. The discontinuities produced as a result of impulsive impact could be problematic especially in case of gait type 3 where both feet are supposed to remain on the ground after impact. The impact is modeled through algebraic equations of the passive impact [9]. The word ”passive” means that no impulsive torques are applied during this impact. In following sections, impact model for gait type 2 and 3 will be developed.

3.6.1 Different Possible Solutions of Impulsive Impact

During impact, the biped has an abrupt change in instantaneous velocity. The accelerations and reaction forces are therefore considered to be infinite for an infinitesimally small period of time. A number of hypotheses can be applied to the biped behavior just after impact. For the swing foot (foot coming in contact with the ground), the possibilities are, contact on the ground, bouncing back, slipping and rotation of the foot [112]. The behavioral possibilities for support foot (foot on the ground) are, take-off, stay on the ground, slipping and rotation. For every hypothesis applied, there are a number of constraints to be satisfied on the contact forces [112]. The swing foot will be named "foot 2", and parameters relative to it will be represented by a subscript 2, while that of support foot will be represented by a subscript 1. Following are some of the possible behaviors of the biped just after impact:

— The swing foot (foot 2), bounce back just after having impact. In this case, an impulsive force will apply on the stance foot (foot 1), which is already in contact on the ground. This case has no utility for bipedal walking. Since single support on the new foot is not possible, therefore, a number of kinematic constraints will be imposed to ensure that foot 2 will remain in contact on the ground.

— Supposing that foot 2 remains on the ground after the impact, and foot 1 takes off just after the impact. In this case, an impulsive force is observed at foot 2. The validity of this kind of impact must be verified by ensuring the unilateral constraints on foot 2 which remains on the ground. It is also important to verify that the behavior of foot 1, which leaves the ground is physically possible. It should be ensured that all corners of foot 1 take-off just after impact. During the impact phase, no finite duration double support exist, the feet change their role, and the stance foot becomes the swing foot.

— Finally, both feet remain in contact on the ground just after impact. In this case, an impulsive force exerted by the ground on both feet is observed. The normal component of ground reaction forces must be unilateral to verify that the feet will not take-off the ground. Similarly, the no-slipping constraint must be verified to ensure that the contact foot will not slip. A double support phase is achieved when both feet remain on the ground just after impact at least partially. For example at heel impact of gait type 3, heel of the front foot and toe of the rear foot remain on the ground while heel of the rear foot is allowed to take off.

3.6.2 Resolving Impulsive Impact

3.6.2.1 Assumptions of impact

Following assumptions are made to develop the impact model:

— The impact is absolutely inelastic and instantaneous
— The biped configuration is constant during impact
— The velocities, accelerations and torques are discontinuous at impact
— The foot does not slip during impact

3.6.2.2 Impact model for gait type 2

For a walking gait with instantaneous double support phase (gait type 2), when foot 2 (swing foot) comes in contact on the ground, foot 1 (support foot) immediately leaves the ground. The duration of the double support phase is infinitesimally small, and the walking gait can be treated as walking without double support phase.

The impact model is deduced from the dynamic model by assuming that the acceleration and the reaction forces are Dirac delta-functions. The impact model is obtained by integrating the dynamic model presented in (3.6) with respect to infinitesimally small interval of time T^- to T^+. The joint torques $\mathbf{\Gamma}$, Coriolis forces $\mathbf{C}(\mathbf{q}, \dot{\mathbf{q}})$, and gravity forces $\mathbf{G}(\mathbf{q})$ have finite values, and therefore, do not appear in the impact model. Thus, the impact model can be written as:

$$\mathbf{A}(\mathbf{q}(T))(\dot{\mathbf{q}}^{+} - \dot{\mathbf{q}}^{-}) = \mathbf{J}_2^t \mathbf{I}_2 \tag{3.32}$$

Here $\mathbf{q}(T)$ denotes the configuration of the biped at instant $t = T$, $\dot{\mathbf{q}}^{-}$ and $\dot{\mathbf{q}}^{+}$ are the joint velocity vectors just before and after impact respectively. Vector $\mathbf{I}_2 \in \mathbb{R}^{3\times1}$ represents the impulsive ground reaction forces and moment on the support foot.

The velocity of the support foot ($j = 1$) just before impact is zero. This kinematic constraint of velocity is expressed as:

$$\mathbf{J}_1\dot{\mathbf{q}}^{-} = 0 \tag{3.33}$$

To ensure flat foot contact on the ground, the velocity of the swing foot ($j = 2$) just after impact must be zero. This constraint is expressed as:

$$\mathbf{J}_2\dot{\mathbf{q}}^{+} = 0 \tag{3.34}$$

Assuming that the stance foot lifts off the ground just after impact, the vertical component of velocity of the taking-off foot must be directed upwards. This constraint is ensured by adding a constraint (see (4.20)) in the optimization algorithm.

The matrix equations (3.32) and (3.34) are simultaneously solved to find the velocity vector $\dot{\mathbf{q}}^{+}$ just after impact, and the impact impulsive forces and moment vector $\mathbf{I}_2 \in \mathbb{R}^{3\times1}$. The solution of the matrix equation (3.35) depends on the velocity vector $\dot{\mathbf{q}}^{-}$ just before impact.

$$\begin{bmatrix} \mathbf{A} & -\mathbf{J}_2^t \\ \mathbf{J}_2 & 0 \end{bmatrix} \begin{bmatrix} \dot{\mathbf{q}}^{+} \\ \mathbf{I}_2 \end{bmatrix} = \begin{bmatrix} \mathbf{A}\dot{\mathbf{q}}^{-} \\ 0 \end{bmatrix} \tag{3.35}$$

3.6.2.3 Impact model for gait type 3

The walking gait type 3 is composed of single support phases separated by double support phases and two impacts. One at the start of double support phase called "heel impact" and second at the end of double support phase called "toe impact" (see Figure 3.7). After the first impact at heel of the front foot, double support phase starts, and at this instance, heel of front foot and toe of rear foot must remain on the ground. To ensure that the above condition is satisfied, the impact model can be written as:

$$\mathbf{A}(\mathbf{q})(\dot{\mathbf{q}}^{+} - \dot{\mathbf{q}}^{-}) = \mathbf{J}_{2\,toe}^t \mathbf{I}_{2\,toe} + \mathbf{J}_{1\,heel}^t \mathbf{I}_{1\,heel} \tag{3.36}$$

Here $\mathbf{q}$ denotes the configuration of the biped at the end of the single support phase, $\dot{\mathbf{q}}^{-}$ and $\dot{\mathbf{q}}^{+}$ are the joint velocity vectors just before and after heel impact respectively. Vector $\mathbf{I}_{2\,toe} \in \mathbb{R}^{2\times1}$ and $\mathbf{I}_{1heel} \in \mathbb{R}^{2\times1}$ represents the impulsive ground reaction forces on toe of rear foot and heel of front foot respectively.

The velocity of heel of front foot and toe of rear foot must be zero just after impact. These constraints can be written as:

$$\mathbf{J}_{1heel}\dot{\mathbf{q}}^+ = 0 \tag{3.37}$$

$$\mathbf{J}_{2\,toe}\dot{\mathbf{q}}^+ = 0 \tag{3.38}$$

By simultaneously solving equations (3.36), (3.37) and (3.38), we have:

$$\begin{bmatrix} \mathbf{A} & -\mathbf{J}^t_{1\,heel} & \mathbf{J}^t_{2\,toe} \\ \mathbf{J}_{1\,heel} & 0 & 0 \\ \mathbf{J}_{2\,toe} & 0 & 0 \end{bmatrix} \begin{bmatrix} \dot{\mathbf{q}}^+ \\ \mathbf{I}_{1\,heel} \\ \mathbf{I}_{2\,toe} \end{bmatrix} = \begin{bmatrix} \mathbf{A}\dot{\mathbf{q}}^- \\ 0 \\ 0 \end{bmatrix} \tag{3.39}$$

Where the Jacobian matrices $\mathbf{J}_{1heel} \in \mathbb{R}^{2\times9}$ at heel of the front foot and $\mathbf{J}_{2toe} \in \mathbb{R}^{2\times9}$ at toe of the rear foot are given by (C.10) and (C.11) respectively in section C.3 of Annex C.

The second impact occurs when toe of the front foot touches the ground. At this instance, double support phase ends and single support phase starts. The front foot is in flat contact on the ground and must remain on the ground. The velocity of the foot just after impact must be zero and the foot must not rotate. The impact model is given by (3.35) and can be re-written for foot 1 such that:

$$\mathbf{A}(\mathbf{q})(\dot{\mathbf{q}}^+ - \dot{\mathbf{q}}^-) = \mathbf{J}^t_1\mathbf{I}_1 \tag{3.40}$$

Here $\mathbf{q}$ denotes the configuration of the biped at the end of double support phase, $\dot{\mathbf{q}}^-$ and $\dot{\mathbf{q}}^+$ are the joint velocity vectors just before and after impact respectively. Vector $\mathbf{I}_1 \in \mathbb{R}^{3\times1}$ represents the impulsive ground reaction wrench on the stance foot at toe impact, and $\mathbf{J}_1 \in \mathbb{R}^{3\times9}$ is the Jacobian at the point on the ground just below the ankle of stance foot is given by (C.13).

To ensure flat foot contact on the ground, the velocity of front foot just after impact must be zero and there should be no rotation. This constraint is expressed as:

$$\mathbf{J}_1\dot{\mathbf{q}}^+ = 0 \tag{3.41}$$

Finally, to calculate joint velocities just after impact and impulsive wrench on front foot, we have:

$$\begin{bmatrix} \mathbf{A} & -\mathbf{J}^t_1 \\ \mathbf{J}_1 & 0 \end{bmatrix} \begin{bmatrix} \dot{\mathbf{q}}^+ \\ \mathbf{I}_1 \end{bmatrix} = \begin{bmatrix} \mathbf{A}\dot{\mathbf{q}}^- \\ 0 \end{bmatrix} \tag{3.42}$$

3.6.3 Impact Model with Knee Locked

To express impact model with knee locked, the support knee of the biped is assumed to be locked mechanically at any desired or pre-selected position. The knee locking mechanism is assumed to be weightless, and its energy consumption is negligible. The locking is bilateral and the torque at knee joint is provided by the mechanical lock. The knee is locked at the instance of impact, and remains locked until the other foot (swing) comes in contact with the ground. At this point, the previously locked knee is released and the new support knee is locked. The knee locking at impact modifies the impact model in equation (3.32), and can be written as:

$$\mathbf{A}(\mathbf{q}(T))(\dot{\mathbf{q}}^+ - \dot{\mathbf{q}}^-) = \mathbf{J}_2^t\mathbf{I}_2 + \mathbf{J}_k^t\mathbf{I}_k \tag{3.43}$$

where $\mathbf{I}_k$ is the impulsive reaction on the locked knee, and $\mathbf{J}_k \in \mathbb{R}^{1\times 9}$ represents the Jacobian of the locked knee and contains ones and zeros. The velocity of the knee joint after impact must be zero, and to satisfy this constraint, following equation is to be imposed:

$$\mathbf{J}_k\dot{\mathbf{q}}^+ = 0 \tag{3.44}$$

The matrix equations (3.34), (3.43) and (3.44) are simultaneously solved to find the velocity vector $\dot{\mathbf{q}}^+$ just after impact, the impulsive impact forces, and moment vector $\mathbf{I}_2 \in \mathbb{R}^{3\times 1}$ of the support foot and the knee impulse I_k. For example for gait type 1 and 2, the system of equation can be written as:

$$\begin{bmatrix} \mathbf{A} & -\mathbf{J}_2^t & -\mathbf{J}_k^t \\ \mathbf{J}_2 & 0 & 0 \\ \mathbf{J}_k & 0 & 0 \end{bmatrix} \begin{bmatrix} \dot{\mathbf{q}}^+ \\ \mathbf{I}_2 \\ \mathbf{I}_k \end{bmatrix} = \begin{bmatrix} \mathbf{A}\dot{\mathbf{q}}^- \\ 0 \\ 0 \end{bmatrix} \tag{3.45}$$

In case of walking gait with double support phase (gait type 3), the stance knee joint is locked at second impact (toe impact). The knee stays locked during entire single support phase, and is unlocked at heel impact of the next step. During double support phase, the knee joint is not locked and can move freely. The impact model with knee locked at toe impact can be written as:

$$\begin{bmatrix} \mathbf{A} & -\mathbf{J}_1^t & -\mathbf{J}_k^t \\ \mathbf{J}_1 & 0 & 0 \\ \mathbf{J}_k & 0 & 0 \end{bmatrix} \begin{bmatrix} \dot{\mathbf{q}}^+ \\ \mathbf{I}_1 \\ \mathbf{I}_k \end{bmatrix} = \begin{bmatrix} \mathbf{A}\dot{\mathbf{q}}^- \\ 0 \\ 0 \end{bmatrix} \tag{3.46}$$

3.6.4 Exchange of Feet Role

When the swing phase is completed and the velocity vector after impact $\dot{\mathbf{q}}^+$ (initial velocity of next step) of the biped has been calculated, the change of reference frame R_0 needs to be done. At this point the previous stance foot takes off the ground and the swing foot becomes the stance foot. Therefore, the geometric parameters of the biped need to be redefined with respect to foot 2 fixed to the ground. The new stance foot need to the base link R_0.

The redefinition of the geometric parameters is a drawback of the implicit liaison and is a complex task. To avoid the redefinition of geometric parameters and use a unique model for each single support phase, it is assumed that foot 1 is always the stance foot. The position and velocity vectors of the feet are exchanged at impact, which means that the position and velocity of the stance foot becomes the position and velocity of the swing foot and vice versa.

To accomplish the task of exchanging position and velocity of the legs, a permutation matrix $\mathbf{E}$ is defined. Let $\mathbf{q}$ and $\dot{\mathbf{q}}^+$ be the final position and velocity after impact of the biped respectively and $\mathbf{q}_{ini}$ and $\dot{\mathbf{q}}_{ini}$ be the initial position and velocity of the biped for the next step. Thus using symmetry of the legs and the predefined matrix $\mathbf{E}$, we have:

$$\mathbf{q}_{ini} = \mathbf{E}\mathbf{q} \tag{3.47}$$

$$\dot{\mathbf{q}}_{ini} = \mathbf{E}\dot{\mathbf{q}}^{+} \tag{3.48}$$

Where $\mathbf{q}_{ini}$ and $\dot{\mathbf{q}}_{ini}$ are the new position and velocity vectors. The permutation matrix $\mathbf{E}$ is defined depending on the robot structure and walking gait type. In present study, the robot structure does not change but the gait type changes. The matrix $\mathbf{E}$ depends on generalized coordinate vector and is given for gait types 1 and 2 in (4.5) and for gait type 3 in (4.13).

3.7 Conclusion

In this chapter, a seven link planar bipedal robot was presented. The geometric and inertial parameters derived from the actual biped called HYDROiD were also detailed. The body mass and link lengths of the biped HYDROiD are based on Hanavan model. Different walking gaits to be studied were presented with the schematics of foot placement during different phases of the walking cycle. The dynamic model of the bipedal robot was developed for different walking phases. The impulsive impact model for the bipedal robot was also deduced from the dynamic model. Moreover, different possible solutions of the foot contact on the ground just after impulsive impact were discussed.

Finally, the possibility of adding springs in parallel to the existing joint actuator was explored, and the dynamic model was modified accordingly to take into account the effects of springs. The option of mechanically locking the support knee was also explored, and the change was incorporated in the impact model. Moreover, ZMP was explained with the help of the foot geometry and expressions to calculated ZMP during single support as well as double support phase were developed. In following chapters, optimal walking gait trajectories will be generated for different types of walking gaits using parametric optimization method. The effects of spring addition and knee locking on consumption of energy during walking will be studied using different models presented in this chapter.

4

Optimal Walking Gait Trajectory Generation

Contents

4.1 Introduction

The design of walking cyclic gaits for legged robots particularly the bipeds has attracted the interest of many researchers for several decades. Significant work has been done on the trajectory planning of planer bipedal robots [77, 27, 37] and these days extensive work is in progress on 3D bipedal robots [28, 39]. Apart from the walking gait trajectory generation, researchers are also working on generating stable running trajectories for humanoid robots [62, 66]. The scope of our work is to generate optimal walking gait trajectories for planar biped for different types of walking gaits.

Walking is a periodical phenomenon, and the objective of this chapter is to design a cyclic walking gait for the studied biped. The cyclic walking gaits, which are presented in section 3.3, consists of a single support phase, finite or instantaneous double support phase, and passive impact. For the biped under study, optimal reference trajectories for different types of walking gaits having instantaneous and finite double support phase will be generated. Moreover, different functions to generate reference walking gait trajectories for a bipedal robot will be defined. Dynamic and impact model of each gait will be recalled from chapter 3 and additional information required to solve the model will be explained. Moreover, optimization parameters required to generate an optimal walking gait trajectory will be enlisted for each gait with and without stance knee locked.

Furthermore, two different optimization criteria, one for electric actuators and second for hydraulic actuators will be presented and the optimization problem will be formulated. A set of optimization constraints required to generate a valid bipedal gait trajectory will be introduced for a cyclic walking gait. Different non-linear constrained optimization tools will be enlisted and two of them used in present study will be detailed. Finally, simulation results for selected optimization functions will be compared, and then the conclusion of the chapter will be provided.

4.2 Reference Trajectory

In the past couple of decades, a lot of work has been done on the human like trajectory generation and optimization. A number of different optimization techniques are used in the field of robotics to generate reference gait trajectories. The aim is to obtain optimal and stable bipedal walking trajectories as close as possible to human walking. Shih [106] work is based on generating biped's trajectory by optimizing ZMP position, Hao Chen [23] worked on on-line walking pattern generation using ZMP criterion for optimization and Tsu-Tian Lee [75] concentrated on the path planing with minimum energy consumption of a planar biped. Recently, Genetic Algorithms (GAs) are also widely used for the optimization of walking gait trajectories. Cardenas Maciel Selene L. [21] used GAs to formulated a constrained optimization problem of periodic motion generation by minimizing the energy criterion and incorporating the ZMP as an indicator of stability.

One of the prerequisite condition for bipedal walking is that the reference trajectory must satisfy the constraint of ZMP. For stable walking, the conditions of contact with the ground have to be satisfied. Therefore, the zero moment point (ZMP), must be located inside the support polygon of the stance foot [115, 1]. Two different ZMP based methods are used to define reference trajectory. In the first method, the ZMP of the robot is predefined and kept inside the support polygon of the stance foot during the step. The robot's center of mass (CoM) trajectory is then calculated from this predefined ZMP [109]. Finally, the robot joint's motion is calculated to follow CoM trajectory with the help of Linear Inverted Pendulum Model (LIMP) [74, 109]. Second method is to generate joints motion as a function of times from its initial and final conditions using polynomial or spline function. In the second method, ZMP is calculated from robot's dynamics and then verified to keep it inside the support polygon [55, 112]. The gait trajectory is accepted if

ZMP is inside the supporting area and rejected if its outside the support polygon.

For bipedal walking gait trajectory generation, polynomial and spline functions are commonly used to approximate the motion of the joints as a function of time [112, 20]. The definition of the reference trajectory is important for the design of the walking robot, the choice of the actuators and the definition of the control law. This work is carried out on a French bipedal robot called HYDROiD and is based on the second method (calculate ZMP from robot's dynamics) of trajectory generation for the studied biped. Cubic spline [75] functions are used to define the reference trajectory for the biped under study. Walking gait trajectories are generated using joint variables. Compared to Cartesian variables, joint variables require reduce cost of calculations by avoiding the solution of inverse geometric model at every point of the trajectory. It also avoid singularities, which may arise if Cartesian variables are used.

Parametric optimization techniques are commonly used to generate optimal gait trajectories. The pre-requisite for these techniques is the definition of reference trajectory by parametric functions. These functions depend on the choice of optimization parameters. These parameters could be the joint variables as in [84, 60] or could be the Cartesian coordinates like in [26, 85]. In present study, joint variables are used as optimization parameters.

4.3 The Cubic Spline Function

Cubic spline functions [14, 101] are commonly used to define the trajectory of each joint of the biped from an initial to a final configuration as a function of time [24]. To generate walking gait trajectories of type 1, a cubic spline function of time with known end points and only one passage point is used. The end and passage points are part of the optimization parameters and are selected by the optimization algorithm to minimize the criterion. A general expression of cubic spline function can be written as:

$$q_i = \varphi_i(t) = \begin{cases} \varphi_{i,1}(t) & \text{if} \quad t_0 \le t \le t_1 \\ \varphi_{i,2}(t) & \text{if} \quad t_1 \le t \le t_2 \\ & \vdots \\ \varphi_{i,n}(t) & \text{if} \quad t_{n-1} \le t \le t_n \end{cases} \tag{4.1}$$

Here, n is the number of selected knots and $\varphi_{i,1}(t), \ldots, \varphi_{i,n}(t)$ are time functions of third order such that:

$$\varphi_{i,k}(t) = \sum_{j=0}^{3} a_{i,k}^{j}(t - t_k)^j \quad \text{for} \quad k = 1, ..., n \tag{4.2}$$

where the coefficients $a_{i,k}^{j}$ are calculated such that the joint's configuration, velocity and acceleration are continuous in $t_1, ..., t_n$. The cubic spline functions are defined by specifying an initial configuration $q_i(0)$, an initial angular velocity $\dot{q}_i(0)$, a final configuration $q_i(T)$, and a final velocity $\dot{q}_i(T)$, with $n-2$ intermediate configurations and T the duration of the phase. In present study, t_i is uniformly distributed over the duration of the step time T. Since present study has only two knots during single support phase, thus the passage point is selected at the middle of the duration of single support.

4.4 Optimization of Walking Gait without Impact

The walking gait without impact (gait type 1) has only single support phases separated by transition phases. At transition, the feet exchange their role. To generate walking gait trajectories of type 1, the evolution of different articulations are described as a function of time by a single function between the beginning and the end of single support phase. To avoid the problem of oscillation, which arises by using a higher order function for trajectory generation, cubic spline functions are used, which allow to select one or several intermediate passage points on the trajectory while keeping the order of the function low. Selecting passage points on the trajectory improves the convergence of the optimization algorithm. The continuity of joints velocity is ensured by piecewise polynomials of third order. Figure 3.3 represents the position of feet of the biped during different phase of the walking cycle of gait type 1.

4.4.1 Model of the Biped

The dynamic model in single support phase, presented in equation (3.9) and with springs given in chapter 3 are valid for gait type 1. The walking gait type 1 consists of only swing phases, and there are no impacts. The velocities and configuration are constant during impactless phase. During this phase, the feet exchange their role and the swing foot become stance foot. The vector of joint configurations and velocities after the exchange of feet role can be found by:

$$\mathbf{q}_{ini\,ss} = \mathbf{E}\mathbf{q}_{fin\,ss} \tag{4.3}$$

$$\dot{\mathbf{q}}_{ini\,ss} = \mathbf{E}\dot{\mathbf{q}}_{fin\,ss} \tag{4.4}$$

Where $\mathbf{q}_{ini\,ss}$ and $\mathbf{q}_{fin\,ss}$ are the position vectors before and after the exchange of feet role, $\dot{\mathbf{q}}_{ini\,ss}$ and $\dot{\mathbf{q}}_{fin\,ss}$ represents the velocity vectors before and after the exchange of feet role, $\mathbf{q}_{ss} = [q_{p2}\ q_1\ q_2\ q_3\ q_4\ q_5]^{\mathrm{t}}$ is the reduced generalized coordinate vector. The exchange of feet allows that the joints of the support foot are always q_1, q_2 and q_3, and therefore a single dynamic model can be used for both single support phases. The permutation matrix $\mathbf{E}$ for gait type 1 can be written as:

$$\mathbf{E} = \begin{bmatrix} 1 & 0 & 0 & 0 & 0 & 0 \\ 0 & 0 & 0 & 0 & 1 & 0 \\ 0 & 0 & 0 & 1 & 0 & 0 \\ 0 & 0 & 1 & 0 & 0 & 0 \\ 0 & 1 & 0 & 0 & 0 & 0 \\ 0 & 0 & 0 & 0 & 0 & 1 \end{bmatrix} \tag{4.5}$$

In the case where trajectory optimization is carried out with knee locked, the impact model is used to calculate the joints velocity vector just after impact. This is because the knee joint velocity is not zero just before impact, and as a result of this non-zero velocity, impact occurs on the knee joint. This produces discontinuities in all the joint velocities, and the velocity vector resulting from the knee impact can be calculated from (3.45).

To generate walking gait trajectory during single support phase, it is required to find the coefficients of cubic spline functions defined in section 4.3. To determine these coefficients, five boundary conditions are required, which are the initial joint configuration $\mathbf{q}_{ini\,ss}$, velocities $\dot{\mathbf{q}}_{ini\,ss}$ at $t = 0$, the intermediate configuration $\mathbf{q}_{int\,ss}$ at $t = T/2$, the final joint configuration $\mathbf{q}_{fin\,ss}$, and velocities $\dot{\mathbf{q}}_{fin\,ss}$ at $t = T$.

The joint configuration during double support phase with flat foot contact on the ground is calculated as a function of hip position (h_x, h_y), orientation of the torso, and step length d. The step length d is the distance between axis of ankles of the feet. The joint angles of both legs are calculated by solving the IGM (see Annex B), which ensures flat foot contact on the ground during double support phase. This configuration represents joint angles at the end of the single support phase as well as at the start of the next single support phase.

In the case, where the knee is locked, the two legs are in knee looked configuration at double support. The joint configuration is calculated from three independent variables, which are the knee locking angle β, angle of the torso and step length d. Thus, 4 parameters are needed to calculate the biped configuration in double support phase with flat foot contact and 3 parameters are required in case the knee is locked.

The cyclic nature and impaclessness of gait trajectories allow to reduce the number of optimization parameters. If there is no impact, the joint velocities do not change at transition and the joint velocities $\dot{\mathbf{q}}_{ini\,ss}(t = 0)$ at the beginning of single support phase can be calculated by multiplying the joint velocities $\dot{\mathbf{q}}_{fin\,ss}(t = T)$ at the end of single support phase with permutation matrix $\mathbf{E}$ explained in section 4.4.1. In case the support knee is locked, there is an impact at the knee joint and the velocities after impact are calculated using the impact model (3.45). For both case, joints configuration vector $\mathbf{q}_{ini\,ss}(t = 0)$ at the beginning of single support phase can be obtained from joints position $\mathbf{q}_{fin\,ss}(t = T)$ at the end of single support phase by solving the equation (4.3). The permutation matrix $\mathbf{E}$ for gait type 1 is presented in equation (4.5).

Another characteristic of impactless walking gait is that landing velocity of the swing foot $\mathbf{V}_2$ just before transition is null. Final velocities of one leg (say swing leg) can be calculated as a function of final velocities of the other leg (say stance leg) by solving $\mathbf{V}_2 = 0$ such that:

$$\begin{cases} V_{2x} = h_p\cos(q_{p2})\dot{q}_{p2} - L_1\cos(q_1)\dot{q}_1 - L_2\cos(q_2)\dot{q}_2 + L_3\cos(q_3)\dot{q}_3 + L_4\cos(q_4)\dot{q}_4 \\ V_{2y} = h_p\sin(q_{p2})\dot{q}_{p2} - L_1\sin(q_1)\dot{q}_1 - L_2\sin(q_2)\dot{q}_2 + L_3\sin(q_3)\dot{q}_3 + L_4\sin(q_4)\dot{q}_4 \end{cases} \tag{4.6}$$

Since, for impactless walking gait, the linear velocity $\mathbf{V}$ and angular velocity $\dot{q}_{p2}$ of the swing foot is null just before touching the ground, therefore, this condition can be applied to equation (4.6) to obtain:

$$\begin{cases} 0 = -L_1\cos(q_1)\dot{q}_1 - L_2\cos(q_2)\dot{q}_2 + L_3\cos(q_3)\dot{q}_3 + L_4\cos(q_4)\dot{q}_4 \\ 0 = -L_1\sin(q_1)\dot{q}_1 - L_2\sin(q_2)\dot{q}_2 + L_3\sin(q_3)\dot{q}_3 + L_4\sin(q_4)\dot{q}_4 \end{cases} \tag{4.7}$$

By re-arranging and separating the know terms, we have:

$$\begin{cases} L_3\cos(q_3)\dot{q}_3 + L_4\cos(q_4)\dot{q}_4 = L_1\cos(q_1)\dot{q}_1 + L_2\cos(q_2)\dot{q}_2 \\ L_3\sin(q_3)\dot{q}_3 + L_4\sin(q_4)\dot{q}_4 = L_1\sin(q_1)\dot{q}_1 + L_2\sin(q_2)\dot{q}_2 \end{cases} \tag{4.8}$$

For gait type 1, joint velocities of swing leg $(\dot{q}_3, \dot{q}_4)$ are calculated as a function of joint velocities of stance leg. The above system of equations can be written in matrix form and solved for swing leg joint velocities as under:

$$\begin{bmatrix} L_3\cos(q_3) & L_4\cos(q_4) \\ L_3\sin(q_3) & L_4\sin(q_4) \end{bmatrix} \begin{bmatrix} \dot{q}_3 \\ \dot{q}_4 \end{bmatrix} = \begin{bmatrix} L_1\cos(q_1)\dot{q}_1 + L_2\cos(q_2)\dot{q}_2 \\ L_1\sin(q_1)\dot{q}_1 + L_2\sin(q_2)\dot{q}_2 \end{bmatrix} \tag{4.9}$$

Thus the number of variables of joint velocities is reduced and we have only three independent variables, which are torso velocity $\dot{q}_5$ and velocities of stance leg ($\dot{q}_1$ and $\dot{q}_2$). To avoid singularities, a constraint imposing $q_3 \neq q_4$ is added in the optimization algorithm.

4.4.1.1 Optimization parameters

The optimization parameters are optimized using the parametric optimization procedure to find the optimal walking gait trajectories by minimizing the predefined criterion presented in equation (4.14). The set of optimization parameters used in present study for gait type 1 is:

— 4 parameters at the end of the step just before impact i.e. hip configuration (h_x, h_y), torso orientation, and step length d.
— 3 parameters of final velocities at the end of the step.
— 6 parameters of intermediate configuration.

Thus, 13 optimization variables are required to generate walking gait trajectory of type 1. The walking speed is manually selected and the step time T is calculated from distance traveled d (step length) and selected speed.

Optimization parameters with knee locked

The number of optimization parameters to generate a walking gait trajectory of type 1, are further reduced to 10 or 9 when knee is locked depending on whether β is an optimization variable or not. These parameters are:

— 3 or 2 (β optimized or constant) parameters at the end of the step just before impact i.e. knee locking angle β, torso orientation, and step length d.
— 2 parameters of final velocities at the end of the step just before impact.
— 5 parameters of intermediate configuration of the biped.

In the case, where spring is added to the biped structure, an additional parameter of spring constant K is required to be optimized.

4.5 Optimization of Walking Gait with Impact

As explained in section 3.3, the walking gait with impact (type 2) is composed of single support phases separated by impulsive impacts. It is identical to gait type 1 except that there is an impulsive impact at the end of single support phase when the swing foot touches the ground. At each impact, three different events occur, which are 1) end of double support phase, 2) exchange of feet role, and 3) start of single support phase.

4.5.1 Model and Gait Trajectory Optimization

Due to the presence of impact, discontinuities in joint velocities exist. Therefore, joint velocities just after impact $\dot{\mathbf{q}}^+$ must be calculated by solving the impact model (3.35), which also gives the impulsive wrench on foot 2. Feet role is exchange at impact so that stance foot is always foot 1 and a unique model during single support phase can be used. The vector of joints velocity at the beginning of the single support phase $\dot{\mathbf{q}}_{ini}$ can be deduced from joint velocities just after impact $\dot{\mathbf{q}}^+$ by equation (4.10). The permutation matrix $\mathbf{E}$ is given by equation (4.5).

$$\dot{\mathbf{q}}_{ini} = \mathbf{E}\dot{\mathbf{q}}^+ \tag{4.10}$$

In the case of knee locked, the joints velocity vector just after impact $\dot{\mathbf{q}}^+$ is calculated by solving the impact model presented in equation (3.45). The impulsive wrench $\mathbf{I}_2$ on foot 2 and impulsive reaction I_k on the knee of leg 2 is also calculated by the same impact model. The Jacobian matrices of foot 2 and knee 2 are given by equation (C.3) and (C.5) respectively.

Similar to gait type 1, cubic spline function is used to express evolution of joint variables as a function of time. General expression for cubic spline functions is presented in (4.1). Feet position during double and single support phase is shown in Figure 3.5, which represents a complete gait cycle (two walking steps).

Procedure to find coefficients of the cubic spline and joint configuration during double support phase with or without knee locking is the same as explained for gait type 1 in section 4.4.1. In case of gait type 2, we have 6 independent variables of joint velocities while these were 3 for gait type 1. Similarly, the joints position vector $\mathbf{q}_{ini}(t = 0)$ at the start of the single support phase can be found by (4.4).

4.5.1.1 Optimization Parameters

The optimization parameters used in present study for gait type 2 are:

- 4 parameters at the end of the step just before impact i.e. hip configuration (h_x, h_y), torso orientation, and step length d.
- 6 parameters of final velocities at the end of the step just before impact.
- 6 parameters of intermediate configuration of the biped.

Therefore, 16 parameters are required to generate and optimize walking gait trajectory of type 2. The biped's walking speed is a preselected parameter and the step time T is calculated from distance traveled d (step length) and the selected walking speed.

Optimization parameters with knee locked

The number of optimization parameters to generate a walking gait trajectory of type 2, are further reduced to 13 or 12 when knee is locked depending on whether β is an optimization variable or not. These parameters are:

- 3 or 2 (β optimized or constant) parameters at the end of the step just before impact i.e. knee locking angle, torso orientation, and step length d.
- 5 parameters of final velocities at the end of the step just before impact.
- 5 parameters of intermediate configuration of the biped.

In case where spring is added to the biped structure, an additional parameter of spring constant K is required to be optimized.

4.6 Optimization of Walking Gait with Double Support

The third type of studied walking gait (type 3) explained in section 3.3, is graphically represented in Figure 3.7 showing different phases of the gait cycle during a walking step. To generate walking gait trajectory for optimization process, the gait is divided into double support phase and single support phase. Evolution of different articulations for these two phases are defined as a function of time by two different functions. During double support phase, the joint trajectory is defined by a spline function without intermediate point. Similar to gait type 1 and 2, the gait trajectory during single support phase is generated using a cubic spline function with one intermediate passage point.

Feet position during double and single support phase is shown in Figure 3.7, which represents a complete walking cycle of gait type 3. At heel impact (impact 1), single support phase ends, feet exchange their role, and double support phase begins. Similarly, at toe impact (impact 2), double support phase ends and single support phase begins.

Considering that the biped is connected to the ground at the heel of the front foot by a perfect pivot joint. The generalized coordinate vector is expressed by $\mathbf{q}_{ds} = [q_{p1}, q_{p2}, q_1, q_2, q_3, q_4, q_5]^t$ during double support phase, and the dynamic model of the biped is given in (3.15). The dynamic model in double support has 7 equations while 8 unknowns (6 joint torques and 2 reaction forces on foot 2). To solve the dynamic model, R_{2x} is selected to be predefined as explained in section 3.4.4 of chapter 3.

4.6.1 Calculating Ground Reaction Force $\mathbf{R_{2x\,ds}}$ on Rear Foot

To solve the dynamic model in double support phase, and calculate joint torques as well as ground reactions on both feet, it is required that horizontal component of ground reaction $R_{2x\,ds}$ on foot 2 is to be known. The ground reaction $R_{2x\,ds}$ can be calculated either by locally minimize the criterion based on joint torques (4.14) or by expressing it using a polynomial function of time. If the criterion optimized is a function of the square of the torque, it is also function of the square of $R_{2x\,ds}$, thus an explicit solution can be found easily. Detailed calculations of $R_{2x\,ds}$ are provided in annex D. On the other hand, if the criterion is based on the mechanical energy product of torque and velocity the optimal reaction force is not so easy to calculate. In this case the horizontal reaction $R_{2x\,ds}$ is expressed as a third order polynomial function of time. In this case, the number of optimization parameters are increase depending on the order of polynomial function (4 coefficients in our case). After calculating $R_{2x\,ds}$, equation (3.18) and (3.19) can be used to calculate $R_{2y\,ds}$ and $\mathbf{R_1}$ respectively.

4.6.2 Gait Trajectory Optimization

The walking gait trajectory for gait type 3 is generated and optimized in two part. In first part, reference joint trajectory during double support phase is generated by a spline function with two nodes.

To define the walking gait trajectory during double support phase, four boundary conditions are needed, which are:

— Initial joint configuration $\mathbf{q}_{ds\,ini}$ at time $t = 0$
— Final joint configuration $\mathbf{q}_{ds\,fin}$ at time $t = T_{ds}$

- Initial joint velocities $\dot{\mathbf{q}}_{ds\,ini}$ at time $t = 0$
- Final joint velocities $\dot{\mathbf{q}}_{ds\,fin}$ at time $t = T_{ds}$

During single support phase with flat foot contact on the ground, the biped has six degrees of freedom. The single support phase of gait type 3 corresponds exactly to that of gait type 1 and 2. A cubic spline with one passage point is used to generate gait trajectory during single support phase. To determine the coefficients of the spline, five boundary conditions are needed:

- Initial joint positions $\mathbf{q}_{ss\,ini}$ at time $t = T_{ds}$
- Final joint positions $\mathbf{q}_{ss\,fin}$ at time $t = T_{ds} + T_{ss}$
- Intermediate joint positions $\mathbf{q}_{ss\,int}$ at time $t = T_{ds} + \frac{T_{ss}}{2}$
- Initial joint velocities $\dot{\mathbf{q}}_{ss\,ini}$ at time $t = T_{ds}$
- Final joint velocities $\dot{\mathbf{q}}_{ss\,fin}$ at time $t = T_{ds} + T_{ss}$

Where $\mathbf{q_{ss}}$ and $\mathbf{q}_{ds}$ are the generalized coordinate vectors during singles and double support phases respectively. T_{ds} and T_{ss} are the durations of double and single support phases. Here $q_{p1} = 0$ as foot 1 remains in flat contact on the ground during the entire swing phase.

The continuity between double support phase and single support phase has to be ensured. From this condition of continuity, joint positions $\mathbf{q}_{ss\,ini}(T_{ds})$ at the beginning of single support phase are deduced from joint positions $\mathbf{q}_{ds\,fin}(T_{ds})$ at the end of double support phase as:

$$\mathbf{q}_{ss\,ini}(T_{ds}) = \mathbf{q}_{ds\,fin\,(1:6)}(T_{ds}) \tag{4.11}$$

Similarly, joint velocities at the beginning of single support phase can be determined from velocities at the end of double support phase (see Figure 3.7 impact 2) by applying the impact model presented in equation (3.35).

The cyclic nature of gait trajectories allows to calculate joint velocities at the beginning of double support phase ($t = 0$) from joint velocities at the end of single support phase ($t = T_{ds} + T_{ss}$) by solving the heel impact equation (3.39) see Figure 3.7 (impact 1). Similarly, the joints position vector $\mathbf{q}_{ds\,ini}(t = 0)$ at the beginning of double support phase can be found from the position vector at the end of single support phase $\mathbf{q}_{ss\,fin}(t = T_{ds} + T_{ss})$ as:

$$\mathbf{q}_{ds\,ini}(0) = \mathbf{E}[0, \mathbf{q}_{ss\,fin}(T_{ds} + T_{ss})] \tag{4.12}$$

Where $\mathbf{E}$ is the permutation matrix for walking gait type 3, such that:

$$\mathbf{E} = \begin{bmatrix} 0 & 1 & 0 & 0 & 0 & 0 & 0 \\ 1 & 0 & 0 & 0 & 0 & 0 & 0 \\ 0 & 0 & 0 & 0 & 0 & 1 & 0 \\ 0 & 0 & 0 & 0 & 1 & 0 & 0 \\ 0 & 0 & 0 & 1 & 0 & 0 & 0 \\ 0 & 0 & 1 & 0 & 0 & 0 & 0 \\ 0 & 0 & 0 & 0 & 0 & 0 & 1 \end{bmatrix} \tag{4.13}$$

During double support phase, the biped is in contact on the ground with heel of the front foot and toe of the back foot with a distance d between the feet. In this configuration $\mathbf{q}_{ds\,ini}(0)$ (beginning of the double support phase at heel impact), the biped has 5 independent variables. Thus, it is possible to calculate two joint angles as a function of others variables (see Annex B, section B.2). The joint configuration at the end of single support phase is also the joint configuration at the start of double support phase after permutation.

Similarly, two angles of the joint configuration $\mathbf{q}_{ds\,fin}(T_{ds})$ at the end of double support phase can also be calculated from other joint angles. In present study, the angles of shin (q_3) and thigh (q_4) of the swing foot is calculated as a function of other joint angles and step length.

4.6.2.1 Optimization Parameters

To improve the convergence of optimization algorithm, the intermediate passage point during single support is fixed except the orientation of the torso. A suitable value of the intermediate point $q_{int} = [q_{p2},\, q_1,\, q_2,\, q_3,\, q_4]$ was found after carrying out a number of optimization, and optimizing q_{int} along with the gait at different walking speeds. The optimal values found are:

$$\mathbf{q}_{int} = [-0.2749,\ 0.0060,\ 0.0302,\ 0.3103,\ -0.4163]$$

Thus, the optimization parameters for gait type 3 for the criterion based on square of the joint torques (used in chapter 5) are:

- 4 joint positions at the end of double support phase
- 5 joint velocities at the end of double support phase
- 4 joint positions at the end of single support phase
- 6 joint velocities at the end of single support phase
- 1 orientation of torso at intermediate point of single support phase
- 1 step length d
- 1 duration of double support phase T_{dsp} in percentage of total step time T

Thus, 22 parameters are required to generate optimal gait trajectories with double support phase. In case, criterion based on product of torque and joint velocity is used (used in chapter 7), 4 additional parameters of coefficients of polynomial to express tangential reaction on rear foot during double support phase are required to be optimized.

Parameters with knee locked

For walking gait type 3, knee of the stance foot is locked at toe impact (end of double support phase) and released at heel impact (end of single support phase). The stance knee remain locked during entire single support phase. The number of optimization parameters to generate a walking gait trajectory of type 3, while knee is locked are:

- 3 joint positions at the end of double support phase
- 4 joint velocities at the end of double support phase
- 3 joint positions at the end of single support phase
- 5 joint velocities at the end of single support phase
- 1 orientation of torso at intermediate point of single support phase
- 1 step length d
- 1 duration of double support phase T_{dsp} in percentage of total step time T
- 1 knee locking angle β

Therefore, 19 or 18 (β optimized or constant) optimization variables are needed to generate walking gait trajectories of type 3 with stance knee locked. Moreover, in case where spring is added to the biped structure, an additional parameter of spring constant K is required to be optimized. Similar to previous case, 4 additional parameters are required if criterion based on mechanical work of actuators is used.

NOTE: By optimizing the walking gait trajectory of gait type 3, it was found that the optimal trajectory has negligible impulsive reactions at heel impact and that the heel of the front foot touches the ground with zero velocity. It is therefore concluded that the only possible optimal trajectory for gait type 3 is the one without heel impact (first impact). Therefore, to improve the convergence of the optimization algorithm, the gait is modeled with null velocity of heel of the front foot at first impact.

4.7 Optimization Tools

To enable numerical computation methods, a family of trajectories is specified in terms of a parameter space as discussed in section 4.2. The optimization can then be viewed as an incremental search in the parameter space while satisfying all constraints. The direction of search of the optimal parameters in each step is determined by computing the gradient of a cost functional with respect to the parameters while constrained to move in a direction tangent to the constraints. Hence, much of nonlinear programming can be considered as an application of Newton's method or gradient descent. As in standard optimization, second-order derivatives of the cost functional can be used to indicate when the search should terminate. The numerical issues associated with these methods are quite involved. Following are some of the popular optimization techniques available in Matlab:

- *ga* and *gamultiobj*: Single and multi-objective Genetic Algorithms
- *fminsearch*: unconstrained nonlinear optimization
- *patternsearch*: Pattern search
- *simulannealbnd*: Simulated annealing algorithm
- *fmincon*: constrained nonlinear optimization
- *fgoalattain*: Multi-objective goal attainment

In case of local minimization tools, one of the main difficulties with trajectory optimization methods is that they can become stuck in a local minimum in the space of trajectories. This means that their behavior depends strongly on the initial guess. It is generally impossible for them to find a trajectory that does not belongs to the family of initial trajectory, and cannot recover from a bad initial guess. Thus it is required to initialize the optimization multiple times with different initial variables to find possible global minimum. On the other hand, although global optimization tools can find global minimum but the calculation cost is high and are difficult to implement. In present thesis, *fmincon* and *fgoalattain* will be used for their simplicity and fast convergence.

The optimization variables presented in respective sections of each gait will be optimized using the parametric optimization procedure to find the optimal solution by minimizing the predefined optimization criterion given by equation (4.14). The Matlab function "*fmincon*" and "*fgoalattain*" will be used to optimize the selected criterion. These two functions will be alternately used when one fail to find a solutions the other one will be used to see if there exist a better solution than that already found by the first function.

4.8 Optimization Criterion

The choice of the optimization criterion is important in the design of optimal trajectory, in this section, two different types of criteria commonly used for bipedal gait optimization will be discussed. The first criterion presented in (4.14), is a quantity proportional to the loss of energy in the actuators. It is minimized for a motion on a half cycle of duration T. The general form of minimal energy performance represents the losses by Joule effects for the electric motors for the traveled distance d.

$$C_\Gamma = \frac{1}{d}\int_0^T \boldsymbol{\Gamma}^{\mathrm{t}}\boldsymbol{\Gamma}\,\mathrm{d}t \tag{4.14}$$

Where C_Γ is the objective function to be minimized, d is the length of half step T represents the duration of half step and $\boldsymbol{\Gamma}$ is the vector of the applied joint torques.

The second criterion used in the optimization algorithm is based on the actuators energy. This criterion is used to minimizes the actuators effort to take one step *i.e.* cover a distance d for a motion on a half cycle of duration T. It is to be noted that energy must be provided in both phases of acceleration and braking (deceleration) that can not be recovered, which justifies the presence of the absolute values.

$$C_E = \frac{1}{d}\int_0^T |\boldsymbol{\Gamma}(t)|^{\mathrm{t}}|\dot{\mathbf{q}}(t)|\mathrm{d}t \tag{4.15}$$

Where C_E is the objective function to minimize and $\dot{\mathbf{q}}$ represents the joint velocity matrix.

The letter C without a subscript to represents both optimization criteria. The objective is to minimize the criterion C by finding the optimal values of optimization parameters under non-linear constraints and cubic spline functions as the basis of motion. The optimization problem can formally be stated as follows.

$$\begin{cases} \text{Minimize} & C(P_0) \\ \text{Subject to} & g_i(P_0) \leq 0 \qquad \text{for} \quad j = 1, 2, \ldots, l \end{cases} \tag{4.16}$$

Where $C(P_0)$ is the objective function to minimize with l constraints $g_i(P_0) \leq 0$ to satisfy. These constraints will be defined in the following section.

4.9 Optimization Constraints

To ensure that the biped will successfully walk, and the trajectory is possible, a number of constraints must be satisfied during walking step. These constraints are imposed in the optimization algorithm to calculate optimal and realistic gait trajectories. Generally, two types of constraints are applied to ensure walking on level ground.

4.9.1 Dynamic Constraints

These constraints are required for successful walking of the biped and are imposed to ensure that the optimized generated trajectory is valid. The dynamic constraints are based on the biped's feet contact with the ground.

The vertical component of the Ground Reaction Forces (GRF) on stance foot must always be positive so that the biped's foot remains on the ground all the time during a walking step. This constraint is also referred to "no-take-off" constraint. It must also be ensured that during different phases of the walking step, the support foot must not slip. To satisfy no-slipping, a suitable value of the coefficient of friction μ between the foot and the ground is defined. The no-take-off and no-slipping constraints are:

$$\begin{cases} R_{1y} > 0 \\ \mu R_{1y} \geq |R_{1x}| \end{cases} \tag{4.17}$$

here R_{1y} and R_{1x} are the vertical and horizontal components respectively of the ground reaction force on stance foot.

During single support phase, flat contact of the foot on the ground is assumed, which ensures that the entire surface of the sol of the foot is in contact with the ground. It is therefore necessary to ensure that there is no rotation of the foot during single support phase. ZMP constraint is defined to ensure no rotation of the foot. The ZMP of the biped must be inside the support polygon (see section 3.4.3.2). This constraint is defined as:

$$l_p \leq ZMP_x \leq l_d \tag{4.18}$$

here l_p is the foot length between heel and ankle and l_d is the length from toe to ankle (see figure 3.11).

During double support phase, both feet rest on the ground. Therefore, the constraints of no-take-off and no slipping on foot 2 must be verified such as:

$$\begin{cases} R_{2y} > 0 \\ \mu R_{2y} \geq |R_{2x}| \end{cases} \tag{4.19}$$

here R_{2y} and R_{2x} are the vertical and horizontal components respectively of the ground reaction force on rear foot, which will become swing foot at the end of the double support phase.

During double support phase, the ZMP is always inside the support polygon (between the contact points of feet) as long as the contact constraints on both feet are verified. Thus ZMP is not calculated separately.

In addition to these constraints, it is also needed to add a set of constraints on the behavior of the robot during swing phase. The extremities of the swing foot must not touch the ground during entire swing phase *i.e.* the distance between swing foot's heel and toe must be positive. This constraint can be written as:

$$\begin{cases} y_{2\ heel} > 0 \\ y_{2\ toe} > 0 \end{cases} \tag{4.20}$$

here y_{heel} and y_{toe} are the vertical distances heel and toe of the swing foot respectively during the swing phase.

Another important phase of the bipedal walking is the impulsive impact phase. It is important to verify that the solution of the impact model is compatible with walking gait trajectory. Moreover, a constraint on the impulsive reaction forces during impact must be added to ensure no-slipping and no-take-off of the stance foot (4.21) that is the foot coming in contact with ground must not slip or bounce back during impact.

$$\begin{cases} I_{2y} > 0 \\ \mu I_{2y} \geq |I_{2x}| \end{cases} \tag{4.21}$$

The ZMP of the biped during impact must also remain inside the support polygon similar to that explained in equation (4.18). The ZMP at the time of impact (flat foot impact for gait type 2 and toe impact for gait type 3) is given by:

$$ZMP_x = \frac{-h_p I_{2x}}{I_{2y}} \tag{4.22}$$

Where I_x and I_y are the impulsive reaction forces of the ground on the foot at the time of impact.

It is also important to verify velocity of the swing foot just after impact. It is to be ensured that the foot do not enter into the ground. Therefore, heel and toe velocities of the foot leaving the ground just after impact must be positive to ensure proper take-off in case of gait type 2. This constraint can be formulated as presented in equation (4.23).

$$\begin{cases} V_{2\ heel} \geq 0 \\ V_{2\ toe} \geq 0 \end{cases} \tag{4.23}$$

Where V_{heel} and V_{toe} are the linear velocities of heel and toe of the foot 1 just after impact. I_x and I_y are the horizontal and tangential components of impulsive impact force during impact.

In case of gait type 3, at the time of first impact (heel impact), heel of the rear foot (foot 2) is allowed to take-off while the toe must remain on the ground to ensure double support phase. The constraint can be formulated such that:

$$\begin{cases} V_{2\ heel} \geq 0 \\ V_{2\ toe} = 0 \end{cases} \tag{4.24}$$

At the moment of second impact, the toe of the rear foot may take off the ground and the velocity should not be negative as presented in

$$V_{2\ toe} \geq 0 \tag{4.25}$$

4.9.2 Technological Constraints

These constraints consist of physical limitations of the biped's actuators and articulations. These are necessary to ensure that the biped will be able to follow the optimized trajectory without crossing the joints limitations. Depending on the selected actuators, each actuator can produce a limited torque and velocity.

$$\begin{cases} |\Gamma_i| - \Gamma_{i,max} \leq 0 \\ |\dot{q}_i| - \dot{q}_{i,max} \leq 0 \end{cases} \tag{4.26}$$

Where $\Gamma_{i,max}$ and $\dot{q}_{i,max}$ represents the maximum value of torque and velocity respectively for each actuator.

The upper and lower joint configuration limits must also be satisfied. These constraints on joint limits ensure a valid joint trajectory and prevent the actuators from damage by touching the mechanical limits.

$$q_{i,min} \leq q_i \leq q_{i,max} \tag{4.27}$$

Where $q_{i,min}$ and $q_{i,max}$ are the minimum and maximum joint position limits respectively.

4.9.3 Optimization using *fmincon*

For single objective constrained nonlinear optimization of an objective function $f(x)$, Matlab provides the function *fmincon*. It attempts to find a constrained minimum of a scalar function of several variables starting at an initial estimate [91, 30]. This is generally referred to as constrained nonlinear optimization or nonlinear programming. The problem is formulated to minimize $f(x)$ such that:

$$\min f(x) = \begin{cases} c(x) \leq 0 \\ ceq(x) = 0 \\ A.x \leq b \\ Aeq.x \leq beq \\ lb \leq x \leq ub \end{cases} \tag{4.28}$$

Here, x is the vector of optimization parameters, $ceq(x)$, and $c(x)$ describes the nonlinear equalities and inequalities receptively among parameters. A and b represents the linear inequalities and Aeq and beq describes the linear equalities among parameters. The syntax of the function in Matlab programing is presented in equation (4.29).

$$[x \quad fval] = fmincon(fun, x_0, A, b, Aeq, beq, lb, ub, nonlcon, options) \tag{4.29}$$

Where x is the set of estimated parameters on minimum value found by the optimization, $fval$ is value of objective function at minimum point, fun is the function to minimize. fun is a function that accepts a vector x and returns a scalar f, x_0 is the initial guess of the parameters, lb and ub are the lower and upper boundaries of the parameters and $options$ provides different options to the solver. *nonlcon* is the function that computes the nonlinear inequality constraints $c(x) \leq 0$ and the nonlinear equality constraints $ceq(x) = 0$.

4.9.4 Optimization using *fgoalattain*

As evident from the name, *fgoalattain* solves the goal attainment problem [46], which is one formulation for minimizing a multi-objective optimization problem. It attempts to find a constrained minimum of a vector function $F(x)$ of several variables starting at an initial estimate x. *fgoalattain* can also be used for single objective optimization. The problem is formulated to minimize γ such that:

$$\min\gamma = \begin{cases} F(x) - weight.\gamma \leq goal \\ c(x) \leq 0 \\ ceq(x) = 0 \\ A.x \leq b \\ Aeq.x \leq beq \\ lb \leq x \leq ub \end{cases} \tag{4.30}$$

The Matlab command line syntax of *fgoalattain* is presented in equation(4.31).

$$[x \quad fval] = fmincon(fun, x_0, goal, weight, A, b, Aeq, beq, lb, ub, nonlcon, options) \tag{4.31}$$

Where fun is the function to be minimized. It is a function that accepts a vector x and returns a vector F, the objective functions evaluated at x. *goal* is the vector of values that the objectives attempt to attain. The vector is the same length as the number of objectives F returned by fun. *weight* represents the weighting vector to control the relative under-attainment or over-attainment of the objectives.

It is a multi-objective optimization tool, which minimizes a set of objectives simultaneously. In the implementation of this function, the slack variable γ is used as a dummy argument to minimize the vector of objectives $F(x)$ simultaneously; goal is a set of values that the objectives attain. Generally, prior to the optimization, it is unknown whether the objectives will reach the goals (under attainment) or be minimized less than the goals (over attainment). A weighting vector, *weight*, controls the relative under-attainment or over-attainment of the objectives [46, 56].

4.9.5 Comparison of *fmincon* and *fgoalattain*

In this section, the simulation results for both optimization functions discussed above will be presented. To compare effectiveness of these algorithms, five sets of initial parameters were generated for different walking speeds with two different number of parameters. Each optimization function is then initialized with these data sets to observe the convergence toward global solution, time to converge and number of iterations. These simulation tests are done for gait type 1.

Following are the specifications of the system on which the optimization is done.

System Specifications:

- — Processor: Intel core i7 Q820 (Quad core 1.73GHz)
- — Operating System: Windows 8 Professional
- — System RAM: 4.0 Gb
- — Matlab version: 2012b

Figure 4.1 shows the value of objective function found by both functions at different walking speeds. The optimization algorithm is initialized at the same initial set of parameters. In Figure 4.1(a), criterion comparison for 16 parameters is presented. Results show that in 3 of 5 cases, *fgoalattain* finds the better solution. Although all the minima found are not the same as the global minimum, but still it gives solutions close to it. Comparison of criterion for 12 parameters is shown in Figure 4.1(b), which shows that both functions are able to find the same minimum when initialized at same initial conditions. Therefor, based on the criterion, *fgoalattain* is recommended for 16 parameters while both function can equally be used for optimization problem with 12 parameters.

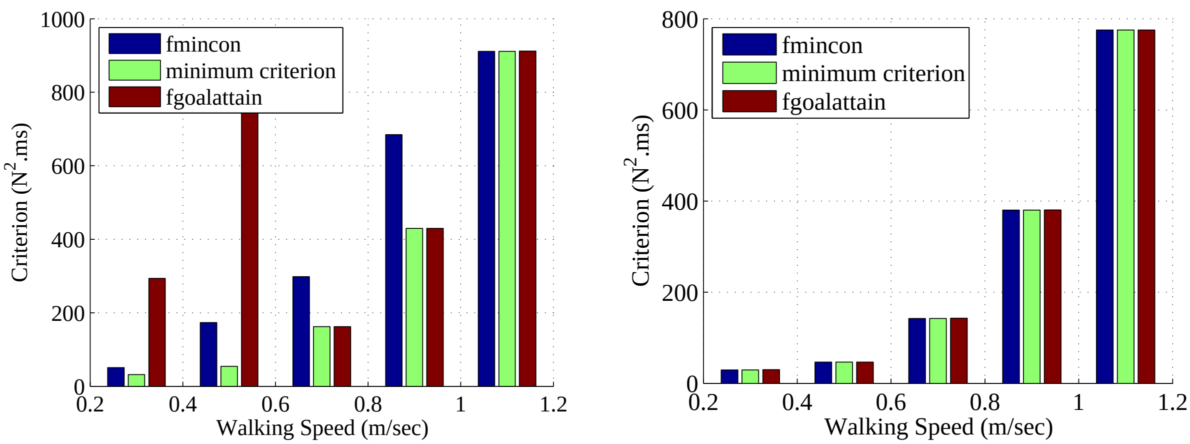

(a) 16 parameters (b) 12 parameters

Figure 4.1 – Comparison of criterion for *fmincon* and *fgoalattain*

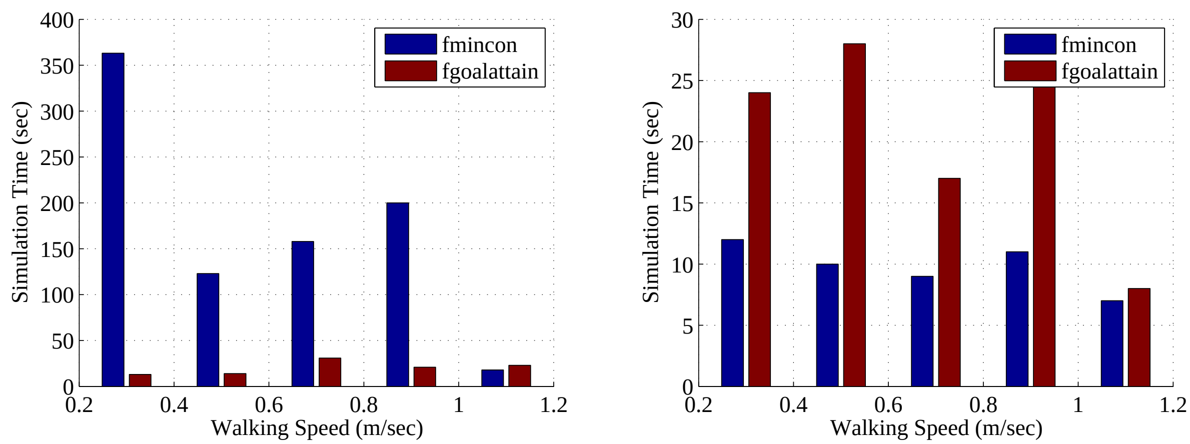

(a) 16 parameters (b) 12 parameters

Figure 4.2 – Comparison of simulation time for *fmincon* and *fgoalattain*

Figure 4.2 shows the comparison of time taken by optimization to converge towards feasible solution at different walking speeds. It is clear from figure 4.2(a) that *fgoalattain* converges much faster as compared to *fmincon* for 16 parameters. On the other hand, for 12 optimization parameters, *fmincon* proves its efficiency see figure 4.2(b). Based on time of simulation, it can be said that *fgoalattain* is better choice for large number of parameters and for small number of parameters, *fmincon* is recommended.

Figure 4.3 presents the comparison of number of iterations for both functions at different walking speeds. It is noted that *fgoalattain* do less iterations for 16 parameters and more iterations for 12 parameters compared to *fmincon*. Therefore, it can be concluded on the basis of number of iterations that fmincon is suitable for less parameters while *fgoalattain* is better option for optimization with large number of parameters.

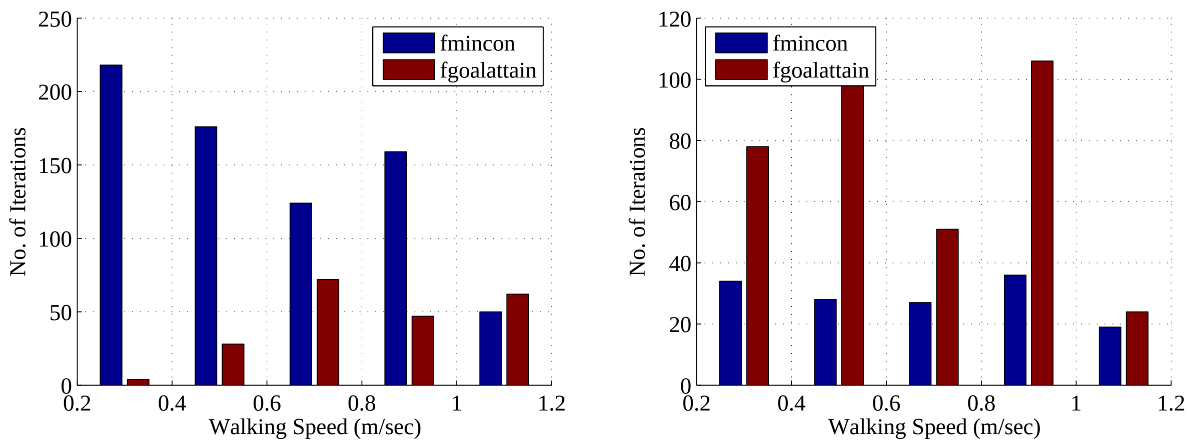

(a) 16 parameters (b) 12 parameters

Figure 4.3 – Comparison of number of iterations for *fmincon* and *fgoalattain*

Simulation results for 12 parameters are presented in Figures 4.1(b), 4.2(b), and 4.3(b), which show that in all tests, *fmincon* is able to find the minimum much faster than *fgoalattain*. Moreover, the solution found by *fmincon* corresponds to the minimum found after multiple optimizations, which is possibly the global minimum. This minimum will be called as *"global minimum"*.

From all the three evaluation criteria selected for comparison of Matlab optimization functions, it is observed that *fmincon* provides faster and better results for 12 parameters. It tends to converge quickly towards possible global minimum while for 16 parameters, the second optimization function *fgoalattain* has the tendency to converge faster towards a minimum point nearest to the global minimum. Hence it is concluded that *fmincon* is a better choice for 12 parameters while *fgoalattain* is a good options for 16 parameters. In the present study, both functions will be used to find an optimal walking gait trajectory by initializing the algorithms using several initial parameters for the same walking speed.

4.10 Conclusion

In this chapter, reference trajectory generation was explained, and different functions to generate joints reference trajectories as a function of time were presented. Trajectory generation procedure for three types of walking gaits was explained. A set of optimization parameters required to generate optimal gait trajectories for each gait was presented for knee locked case and without knee locked cases. The process of parametric trajectory optimization was discussed and different criteria for bipedal walking gait optimization were presented. The constraints required for successful stable walking were also presented. The first criteria presented is based on actuators torque and will be used in chapter 5 to optimize gait trajectories of a biped with electric actuators. The second is based on actuators energy and will be used in chapter 7 to optimize gait trajectories of studied biped with hydraulic actuator.

Finally, two different non-linear constrained optimization tools of Matlab were briefly explained and then the simulation results were compared. It was concluded from simulation results, that *fmincon* is the better solution for 12 optimization parameters while *fgoalattain* provides better results for 16 parameters. In practice, in the following chapters, to avoid local minima, several initializations will be used and both algorithms will be used to calculate the cost of walking of an optimal gait trajectory.

5

Comparison and Synthesis of 2D Bipedal Walking Gaits

Contents

5.1 Introduction

In this chapter, simulation results of different types of walking gait trajectories described in previous chapter will be presented. A number of strategies will be presented to reduce the energetic cost of walking of a biped. The objective of this study is to compare the performance of these strategies on different walking gaits. For this purpose, three types of walking gaits were defined along with dynamic and impact modeling in chapter 3. The procedure to generate optimal walking gait trajectories for each gait and optimization variables required were explained in chapter 4.

The simulation results presented in this chapter are for a biped having electric actuators. The criterion used is based on actuators torques, which is a quantity proportional to the losses by Joule effects of the electric motors. This criterion is given in (4.14). Simulation results obtained for each type of gait will be presented for different walking speeds. Initially, cost of walking will be calculated for a basic biped (biped without any modifications i.e. knee locking or spring addition). To improve the energetic efficiency of the biped during walking, two different strategies will be used. First, torsional springs will be added in parallel to the existing actuators. Secondly, knee joint of the stance leg will be mechanically locked. The torque required at knee joint is provided by the locking system and not by the actuator.

The simulation results are based on the definition of cyclic reference trajectory i.e. it is assumed that the step will repeat for infinite number of time without any change in characteristics. Therefore, only one cyclic step will be optimized and its energetic cost will be studied. The gait trajectory is re-optimized after adding springs or locking the knee joint to take maximum advantage of the springs or locking. Finally, the criterion obtained after adding springs or knee locking will be compared with that of basic robot and percentage energy savings will be presented in each case. The effects of walking speed on step length and time will also be discussed.

5.2 Studies Carried out

Following different types of studies are carried out on the biped:

case A. Gait trajectories are optimized and energetic cost of walking is calculated without adding springs or locking the knee.

case B. Springs are added to the hip, knee or ankle joints of the biped.

- **case B1.** Spring is added only to the support leg joints one at a time *i.e.* support ankle, knee or hip.
- **case B2.** Identical springs are added to a pair of ankle joints, knee joints, or hip joints.

In all cases where a spring is added to any of the joint, the spring constant K is optimized along with the gait and the spring offset or bias angle is zero.

case C. Support knee is mechanically locked at transition between single support phases without adding springs at any of the joint. The knee remains locked during the entire single support phase.

- **case C1.** Knee locking angle (β) is an optimization parameter for trajectory optimization.
- **case C2.** Based on the numerical values obtained in case **C1**, a constant value of β is selected and then gait is optimized.

case D. Support knee is mechanically locked and identical springs are added to both hip joints. The knee locking angle β and spring stiffness constant K are optimized along with gait trajectory.

5.3 Simulation Results of Walking Gait without Impact

In this section, simulation results for an impactless walking gait (type 1) presented in section 3.3.1 will be presented. This is the simplest walking gait studied. A number of walking gait trajectories at different walking speeds were generated and optimized using reference trajectory generation and optimization techniques presented earlier. Simulation results for walking speed of $0.5m/s$ will be presented, and then the effects of different studies (see section 5.2) on selected criterion will be compared. Moreover, effects of these techniques on other parameters like ZMP, CoG, and ground reactions etc will also be discussed.

Adding springs only to the support leg is possible by having a variable spring stiffness mechanism [128] capable of producing spring stiffness from zero to the required value. In [64] a light weight actuator AwAS (A new Actuator with Adjustable Stiffness) whose stiffness can be tuned from zero to rigid is proposed. In simulation tests, this mechanism is assumed to be mass-less and the energy consumed by the mechanism is supposed to be negligible, which is not the case in the real world. To avoid the variable stiffness mechanism, a simple option of adding identical torsional springs to both legs is preferred, and then the effects on energy consumption are also studied.

5.3.1 Results with Springs

Figure 5.1 shows a step of walking gait type 1 for different cases with identical springs installed at both ankles, knees, and hips joints of the biped at walking speed of 0.5 m/sec. It is observed that the step length when springs were added to both knees is significantly larger compared to that of other three cases. The step length of other cases (see figures 5.1(a), 5.1(b) and 5.1(d)) is almost the same, but the postures and joint trajectories are different in all cases.

Figure 5.2 presents the value of the selected criterion as a function of walking speed for a biped in cases where springs were added to different joints in parallel to the existing actuator. It is clear from Figure 5.2(a) that the effects of addition of springs can only be seen at very slow walking speeds in case **B1** where spring was introduced to the ankle of the support leg. When torsional springs were added to both ankle joints, the energetic effects during walking almost disappeared.

The optimization criterion was significantly reduced when spring was added only to the support knee joint (see Figure 5.2(b)). Hight reduction in energy consumption during walking was noted from low to medium and high walking speeds. Similar effects were observed in case **B2** where identical springs were added to both knee joints.

Figure 5.2(c) shows simulation results for hip joints in case **B1** where spring was added only to the support hip joint and in case **B2** where identical springs were added to both hip joints. The results show that addition of spring only at support hip is effective at slow as well as fast walking speeds while the addition of springs at both hips is effective at walking speeds above 0.6 m/sec (around 2 km/h).

Simulation results after adding springs to both ankle, knee or hip joints are presented in Figure 5.2(d), which shows that ankle springs are not at all effective for walking gait type 1. It also indicates that adding identical springs to knee joints are effective at slow walking speeds while hip springs can be used at high walking speeds (above 0.7 m/sec) to reduce walking cost.

Figure 5.3 gives the percentage energy savings as a function of walking speed for ankle, knee and hip joints in case **B2**. It confirms the observation in Figure 5.2(d) that knee springs are effective at

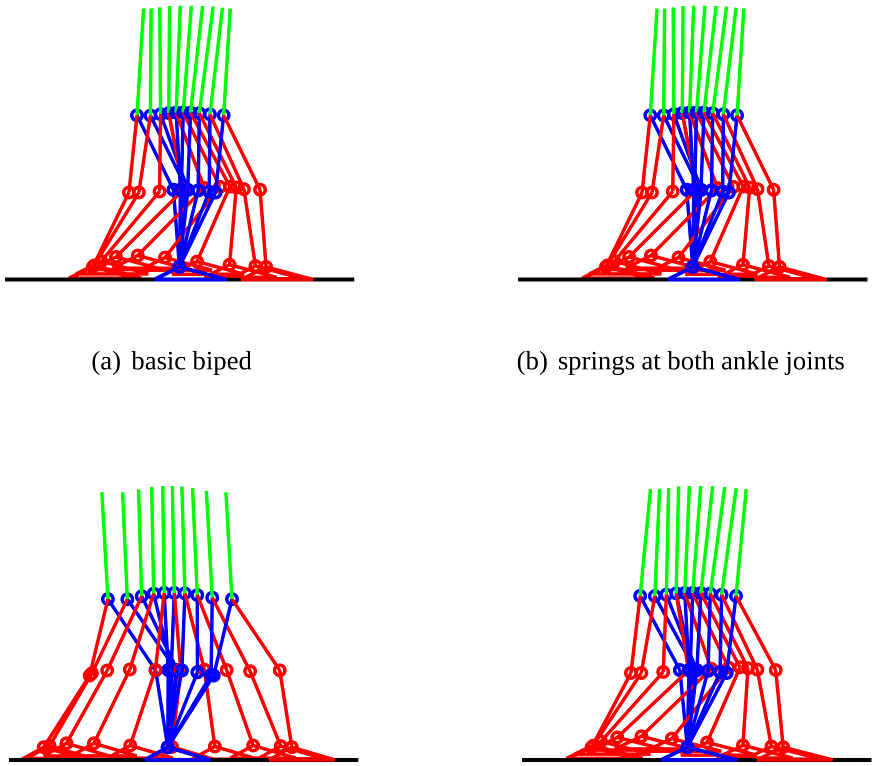

(a) basic biped

(b) springs at both ankle joints

(c) springs at both knee joints

(d) springs at both hip joints

Figure 5.1 – Walking gait of type 1 with springs at walking speed of 0.5 m/sec

slow while hip springs are effective at high walking speeds. Both curves intersect at walking speed of 0.7 m/sec. It means that if the application area of the biped is below this point then springs at knee joints are recommended otherwise springs at hip joints are to be used. Results show that up-to 65% of walking cost can be reduced by adding hip springs and up to 38% energy can be saved by adding identical springs at knee joints.

It was however observed, that adding springs to both ankle joints were not effective for the walking gait trajectories of type 1 of the studied biped. This is contrary to the work of T. Schauss [99] and M. Wisse [124], where they found ankle springs useful for stability as well as energetic efficiency. The negligible effects of ankle springs in the present study can be explained by the consideration of the flat foot contact on the ground and impactless walking gait. In addition, there is no rotation of the support foot during the entire swing phase.

Figure 5.4 presents the value of spring stiffness K at different walking speeds for case B2 where identical springs were added to similar joints of the feet, and for case D where knee was locked and identical springs were added to hip joints. It shows that it is possible to fix a constant spring stiffness at almost all walking speeds for knee joints. However, for hip joints, the variation of value of K is high, therefore, a constant value can not be fixed. In case of ankle joints, K is approximately zero at slower speeds and varies at high walking speeds. Identical springs are added to both joints because it is easy to implement a system, which can be tuned off-line for a

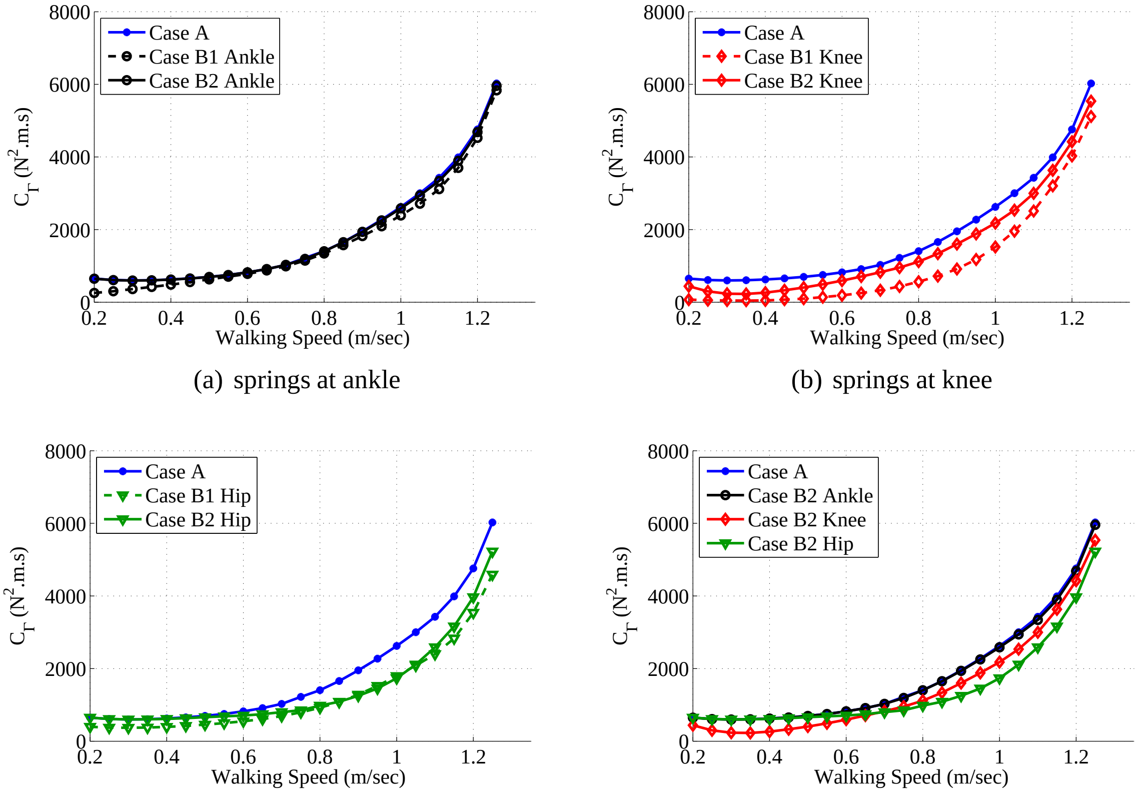

(a) springs at ankle

(b) springs at knee

(c) springs at hip

(d) springs at both ankles, knees, and hips

Figure 5.2 – Value of criterion ($C_\Gamma = \frac{1}{d}\int_0^T \mathbf{\Gamma}^t\mathbf{\Gamma}dt$) as a function of walking speed for gait type 1 (solid lines for springs at both legs and dashed lines for springs at support leg only)

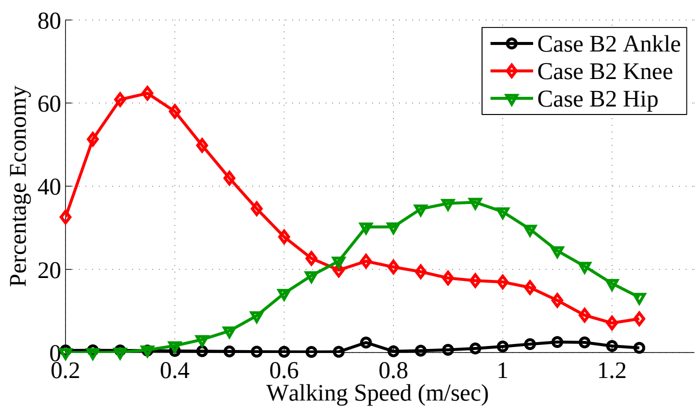

Figure 5.3 – Percentage energy savings as a function of walking speed for gait type 1 with springs

specific walking speed. On the other hand, to add springs with different stiffness at stance and swing joint, a active system capable of changing stiffness at each step is required.

Figure 5.5 gives the evolution of joint torques of gait type 1 with springs at walking speed of 0.5 m/sec for studies of basic biped, and biped with torsional springs at both ankles, knees and hips. It is to be noted that all joint torques during the step are far below the maximum allowable limits described by the constraint equation (4.26). Technological constraints for the bipedal robot

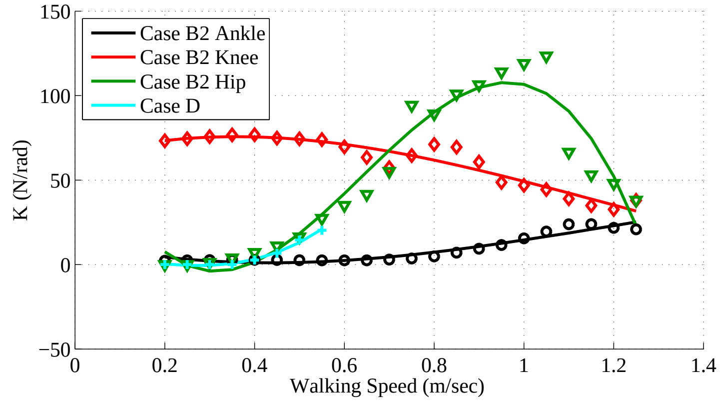

Figure 5.4 – Value of spring stiffness (K) as a functions of walking speed for gait type 1

HYDROïD are given in table 3.2. It shows that the swing foot torques ($\Gamma_4, \Gamma_5, \Gamma_6$) in all cases are less important than that of support foot torques. Joint torques are significantly reduced when springs are added to both knee joints in parallel with the existing actuator (see Figure 5.5(c)).

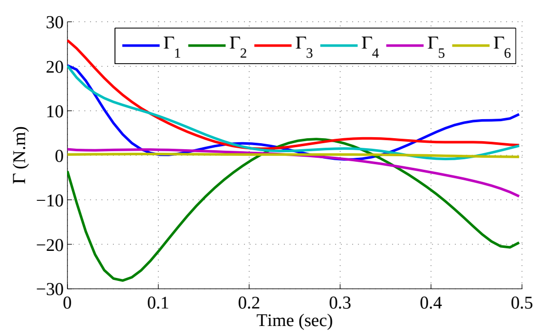

(a) basic biped

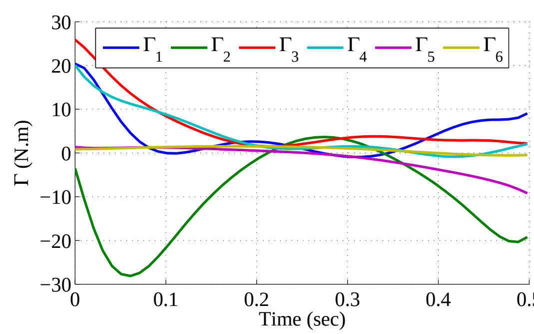

(b) springs at both ankles

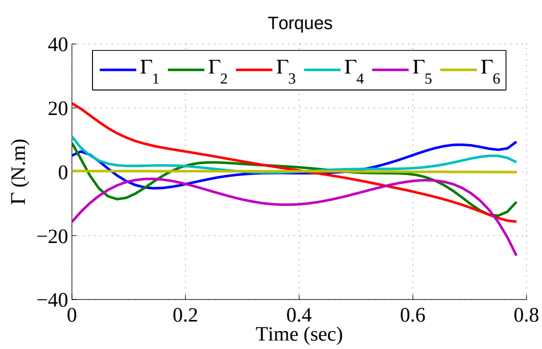

(c) springs at both knees

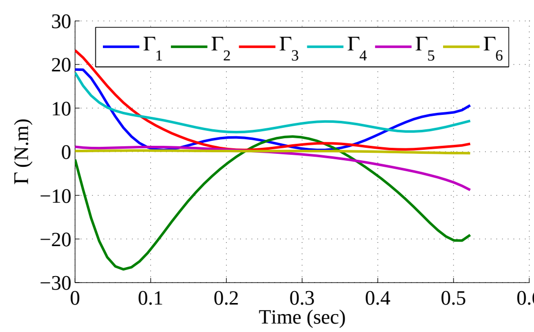

(d) springs at both hips

Figure 5.5 – Evolution of joint torques of gait type 1 with springs at walking speed of 0.5 m/sec. $\Gamma_1, \Gamma_2, \Gamma_3$ are the support ankle, knee and hip torques, and $\Gamma_4, \Gamma_5, \Gamma_6$ are the swing hip, knee, and ankle torques

The evolution of relative joint positions of gait type 1 for walking speed of 0.5 m/sec is presented in Figure 5.6. These results are for a cyclic step of a bipedal robot with identical springs at different joints. A significant reduction in swing knee angle (θ_5) can be seen when springs are added to both knee joints of the biped. The biped configuration in Figure 5.6(c) with knee springs is significantly different from other three figures, which can also be observed in Figure 5.1(c) of walking step. Addition of springs to hip joints does not significantly modify the trajectory but help to reduced the overall cost of walking.

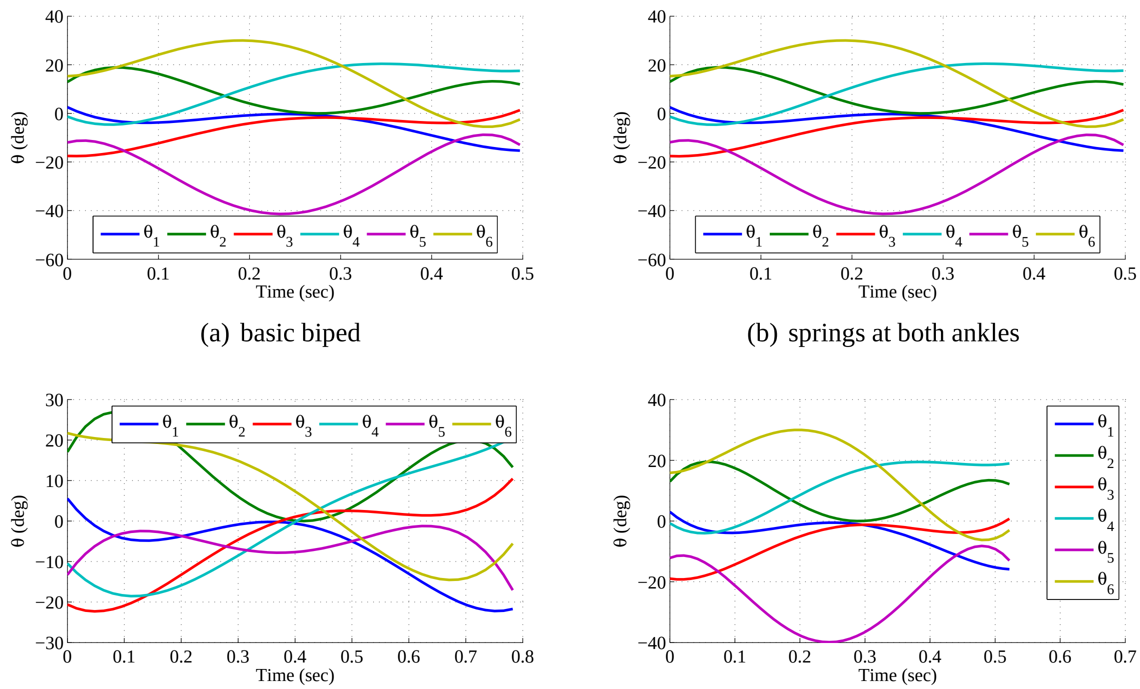

(a) basic biped

(b) springs at both ankles

(c) springs at both knees

(d) springs at both hips

Figure 5.6 – Evolution of joint positions of gait type 1 with springs at walking speed of 0.5 m/sec. $\theta_1, \theta_2, \theta_3$ are the support ankle, knee and hip angles, and $\theta_4, \theta_5, \theta_6$ are the swing hip, knee, and ankle angles

Figure 5.7 gives the evolution of joint angular velocities of optimal gait trajectory of type 1 with springs at walking speed of 0.5 m/sec. Like joint angles and torques, the joint velocities are also within the maximum allowable limits. It can be observed in all cases, that joint velocities start with relatively high values, decrease towards the middle of the step and then increase again at the end of the step. This evolution reflects the effect of the impact avoidance on the joint evolution.

5.3.2 Results with Knee Locked

Walking gait for different studies with knee locked (see case C1 and case D) is presented in Figure 5.8 at walking speed of 0.5 m/sec. It shows that the step length is reduced when springs were added to the knee locked case. Thus after optimizing the gait with springs, a new trajectory is found, which is more adapted to benefits from springs and reduces cost of walking. Although, the support knee was locked in this study, but the gait trajectory of knee locked case (Figure 5.8(a)) resembles that of knee springs in Figure 5.1(c) and Figure 5.8(b) also looks like Figure 5.1(a).

For all cases where support knee was locked, the optimization algorithm was unable to find a walking gait trajectory satisfying all the constraints at walking speeds above 0.55 m/sec. The phases of acceleration and deceleration at the beginning and end of the step limits the maximum attainable speed. Simulation results show that the most effective way to reduce energy consumption during walking for an impactless walking gait, is to add springs to the support joints only, and the most economical is the support knee joint (see fig. 5.3).

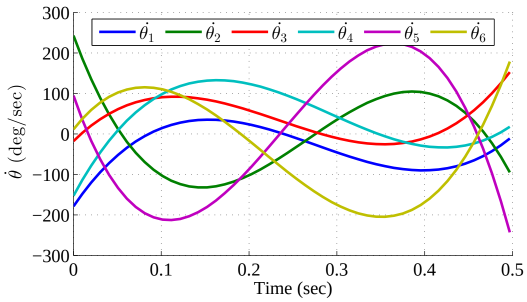

(a) basic biped

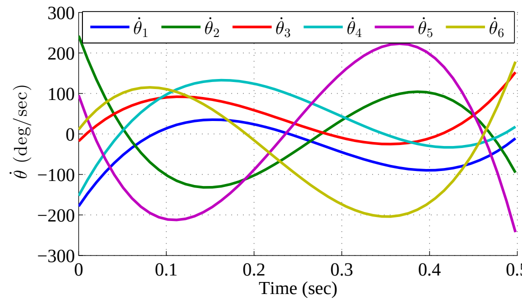

(b) both ankle springs

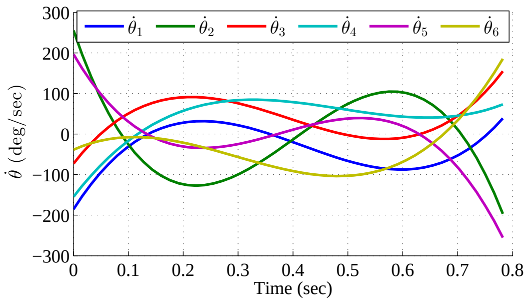

(c) both knee springs

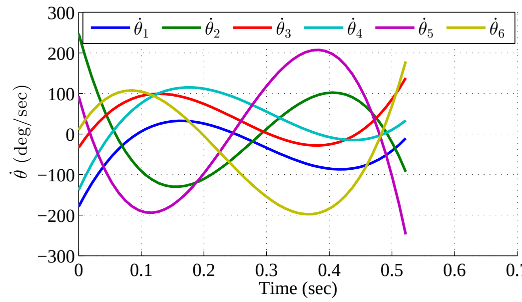

(d) both hip springs

Figure 5.7 – Evolution of joint angular velocity of gait type 1 with springs at walking speed of 0.5 m/sec. The subscript 1,2,3 represents stance ankle, knee, hip while 4,5,6 represents swing hip, knee, and ankle

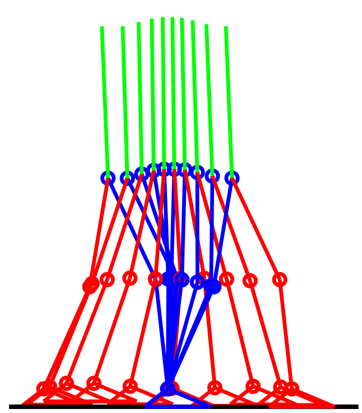
(a) knee locked

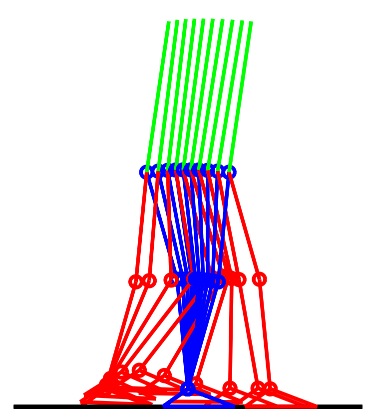
(b) knee locked and springs at both hips

Figure 5.8 – Walking gait of type 1 with knee locked at walking speed of 0.5 m/sec

Figure 5.9(a) gives the comparison of criteria curves as a function of walking speed in case **A**, case **C1** where knee locking angle β was optimized, case **C2** with constant value of β. An average value of 8.3 degree of knee locking angle β was calculated from optimization results in case **C1**. It also presents simulation results for a biped in case **D** with identical springs on both hips and support knee locked. Since it is not possible to study spring effects on the knee joint while the joint is locked, therefore, identical springs are added to both hip joints to study the combined effects of knee locking and spring addition.

Simulation results show that knee locking for an impactless bipedal walking gait is economical at slow walking speeds, and not possible at high walking speeds. Both curves in case **C1** and **C2** are superposed, which clearly indicate that the knee can be locked at a constant angle for all possible walking speeds. It is also evident from figure 5.9(a) that addition of springs at hip joints while support knee is locked has negligible effects on energy saving compared to knee locked only. Therefore, it is recommended to lock support knee for slow and add hip springs for high walking speeds without knee locking.

Figure 5.9(b) presents the percentage energy savings as a function of walking speed. It shows that the energetic efficiency in case **D** is almost the same as that of in case **C2**. It means that addition of springs has no effect on energetic efficiency when knee is locked. It is clear from simulation results that knee locking is effective at slow walking speeds (up to 0.55 m/sec), and for speeds above 0.55 m/sec, the only choice is the hip springs. Comparing Figures 5.3 and 5.9(b), it was observed that knee locking is more effective at slow walking speeds compared to the addition of springs at both knees.

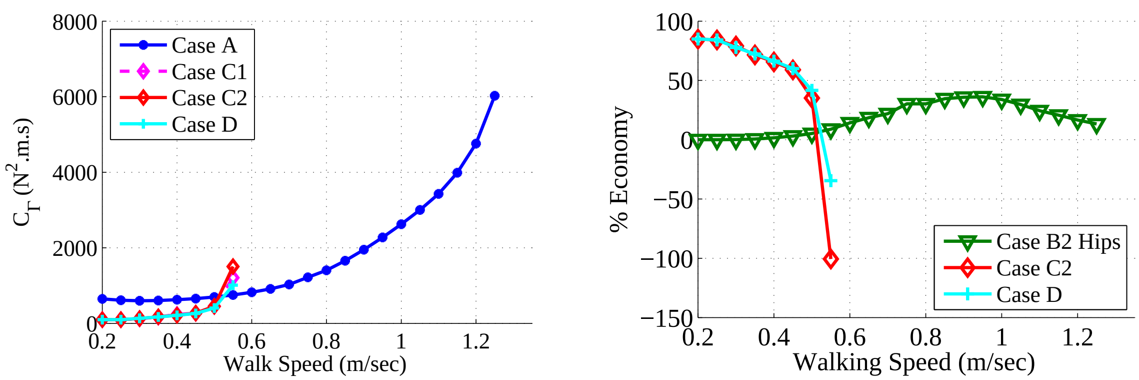

(a) criterion

(b) % ecocomy

Figure 5.9 – Value of criterion and percentage energy savings as a function of walking speed for gait type 1 with knee locked

Figure 5.10 presents the impulsive impact forces on foot 2 (the foot just came in contact with the ground) of the biped at different walking speeds. These results are for the cases where knee was locked. It is to be noted that gait type 1 is an impactless walking gait, and there are no impulsive forces when the knee is not locked. This is why impulsive reactions for studies without knee locking are not presented. The tangential and normal component of the impulsive reaction represented by I_{2t} and I_{2N} are presented in Figures 5.10(a) and 5.10(b) respectively. It shows that these forces are unidirectional and directly proportional to walking speed.

The value of knee locking angle β is presented in Figure 5.11(a) for different walking speeds of gait type 1. It shows that the angle varies between 8.2 and 8.6 degrees, which means that the knee joint is slightly bent. Since variation of β is not very high at complete range of walking speeds, it is possible to select a constant value of knee locking angle. This will reduce the number of optimization parameters by one, which is the case C2 in present studies. The average value of $\beta = 8.3^o$ was calculated from results obtained in the case C1 and then fixed in the optimization

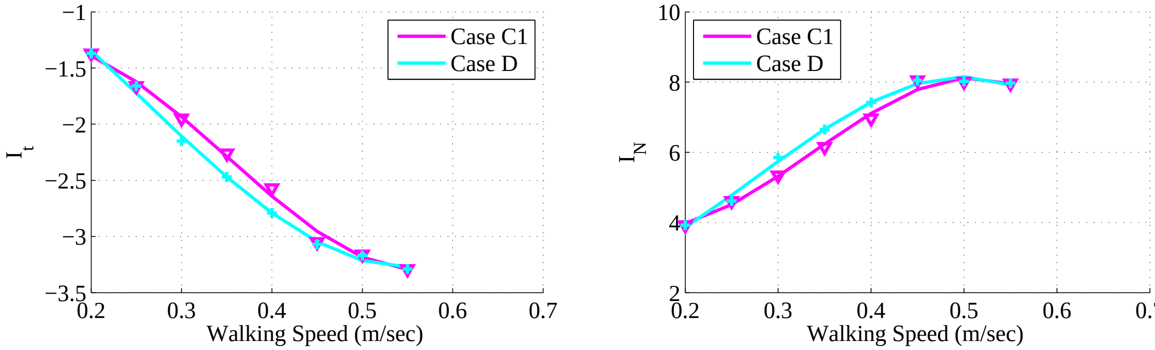

(a) tangential component (b) normal component

Figure 5.10 – Value of foot impulsive reaction (I_2) as a functions of walking speed for gait type 1

process. Figure 5.11(b) gives the value of impulsive reaction on the knee joint at different walking speeds for gait type 1. It is noted that the impulsive reaction on knee is unilateral and is almost directly proportional to walking speed.

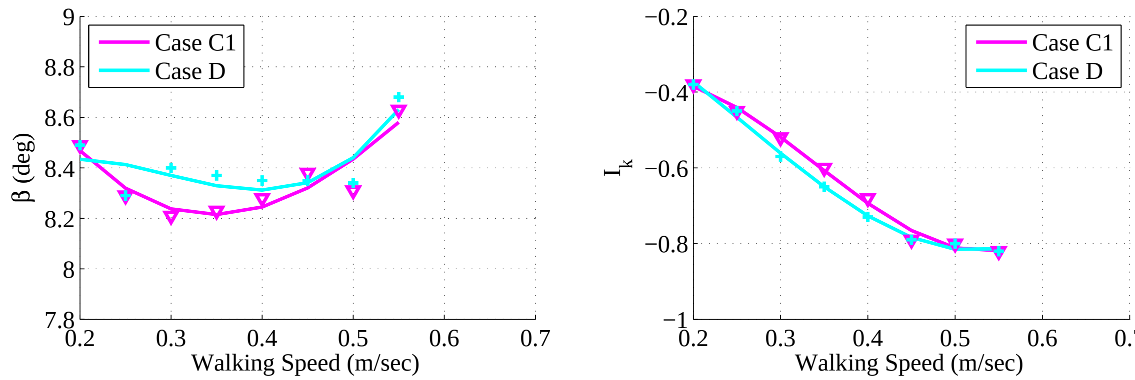

(a) knee locking angle (b) knee impulse

Figure 5.11 – Knee locking angle (β) and knee impact (I_k) as a functions of walking speed for gait type 1

Evolution of joint torques for knee locked and knee locked with hip springs is presented in Figure 5.12 for a walking speed of 0.5 m/sec. Here, the knee torque shown in figures is provided by the locking mechanism and the actuator's torque for the support knee joint is zero during the entire swing phase. It shows that the effects of adding springs when knee was locked are negligible.

Figure 5.13 gives evolution of joint positions of gait type 1 with knee locked at walking speed of 0.5 m/sec. It is clear from results that joint angle $\theta_2 = \beta$ of the support knee is constant throughout the walking step. It can also be observed that the locking angle β is about 8.4^o for case C1 (knee locked only) and about 9.0^o for case D (knee locked and springs at both hips).

Evolution of joint angular velocities of gait type 1 with knee locked at walking speed of 0.5 m/sec is given in Figure 5.14. Figure 5.14(a) shows that when knee is locked, the velocities of all the joints of the support leg are significantly reduced compared to basic biped (see figure 5.7(a)). There is very less variation in joint velocities during the entire step. It is also clear that the support knee angular velocity $\dot{\theta}_2$ is zero during the entire single support phase. Similar results can be seen

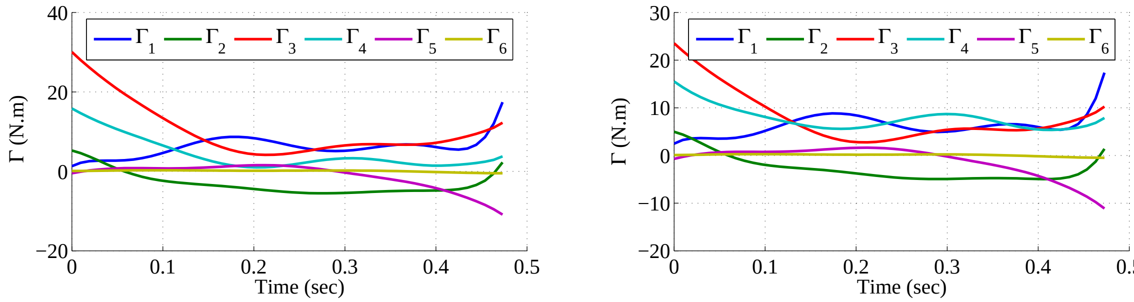

(a) support knee locked (b) knee locked and springs at both hips

Figure 5.12 – Evolution of joint's torque of gait type 1 with knee locked at walking speed of 0.5 m/sec. $\Gamma_1, \Gamma_2, \Gamma_3$ are the support ankle, knee and hip torques, and $\Gamma_4, \Gamma_5, \Gamma_6$ are the swing hip, knee, and ankle torques

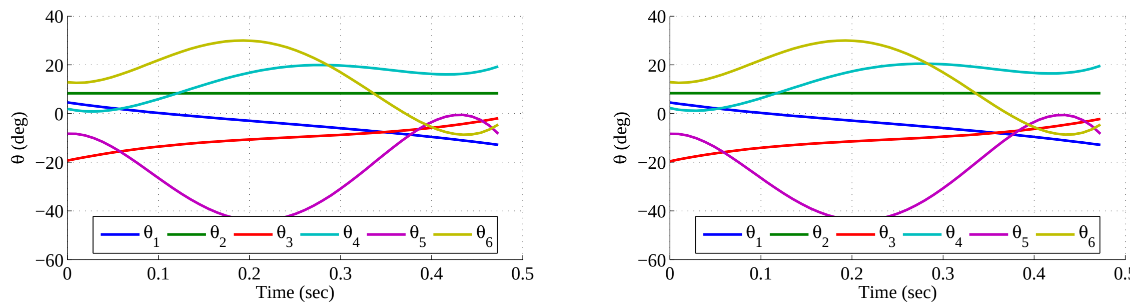

(a) support knee locked (b) knee locked and springs at both hips

Figure 5.13 – Evolution of joint positions of gait type 1 with knee locked at walking speed of 0.5 m/sec. $\theta_1, \theta_2, \theta_3$ are the support ankle, knee and hip angles, and $\theta_4, \theta_5, \theta_6$ are the swing hip, knee, and ankle angles

in Figure 5.14(b) where springs were added to both hips of the biped, and support knee was also locked.

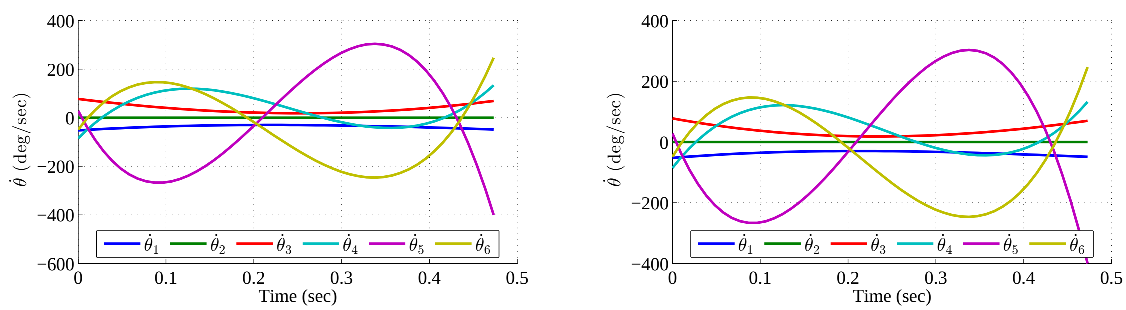

(a) knee locked (b) knee locked and hip springs

Figure 5.14 – Evolution of joint angular velocity of gait type 1 with knee locked at walking speed of 0.5 m/sec. The subscript 1,2,3 represents stance ankle, knee, hip while 4,5,6 represents swing hip, knee, and ankle

5.3.3 Combined Results with Springs and Knee Locked

Figure 5.15(a) shows the duration of step as a function of walking speed for gait type 1 for all studied cases, while Figure 5.15(b) presents the length of step for the same. It is clear from simulation results presented in Figure 5.15 that the duration of step decreases and the step length increases as walking speed increases. Therefore, it is deduced that duration of step is inversely proportional to walking speed while step length is directly proportional to it. These results (Figure 5.15) also confirm our observation made for Figure 5.1, that step length is significantly increased for almost all walking speeds when springs are added to both knees. This difference in duration of step and length is clearly visible in Figure 5.15.

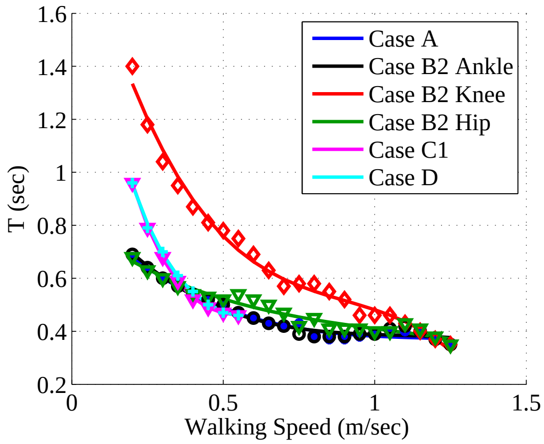

(a) duration of step

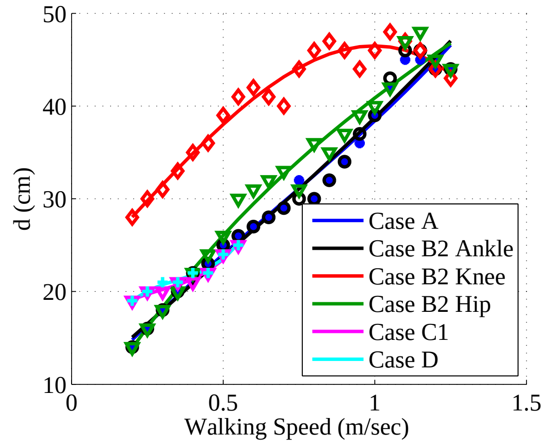

(b) step length

Figure 5.15 – Evolution of duration of step (T) and step length (d) as a functions of walking speed for gait type 1

Evolution of the normal component of ground reaction force and no-slipping constraint on stance foot are presented in Figure 5.16 at different walking speeds for all studied cases. Figure 5.16(a) gives the vertical reaction force at walking speed of 0.5 m/sec which shows that the shape of the curves resembles letter "M". This shape of vertical ground reaction forces during walking has been observed in several bio-mechanical studies on human walking [127, 22, 95]. Although, there is no impacts and double support phases in walking gait type 1, but still our results conform to bio-mechanical studies. It was also observed that neither the shape nor the amplitude is significantly modified when torsional springs were added to the biped joints in parallel to the existing actuators. Significant reduction in amplitude of the ground reaction force was observed when the support knee was locked. However, the shape of the curve remained unchanged.

During walking step, the biped must not slip and satisfy the constraint of no-slipping. The evolution of no-slipping constraint of gait type 1 is presented in Figure 5.16(b) at walking speeds of 0.5 m/sec for different studies carried out on the biped. This constraint is given by equation (4.17) and the value of this constraint should always be below the maximum allowable limit. Simulation results show that the ratio of tangential force versus normal force is far below the maximum limit. Therefore, the biped will not slip during walking even if the friction between floor and the feet is less than that of selected value. The value of friction coefficient μ between the ground and sole of foot of the bipedal robot was supposed to be 0.9. Results show that a coefficient of friction of 0.3 will be sufficient to generate feasible gait trajectory.

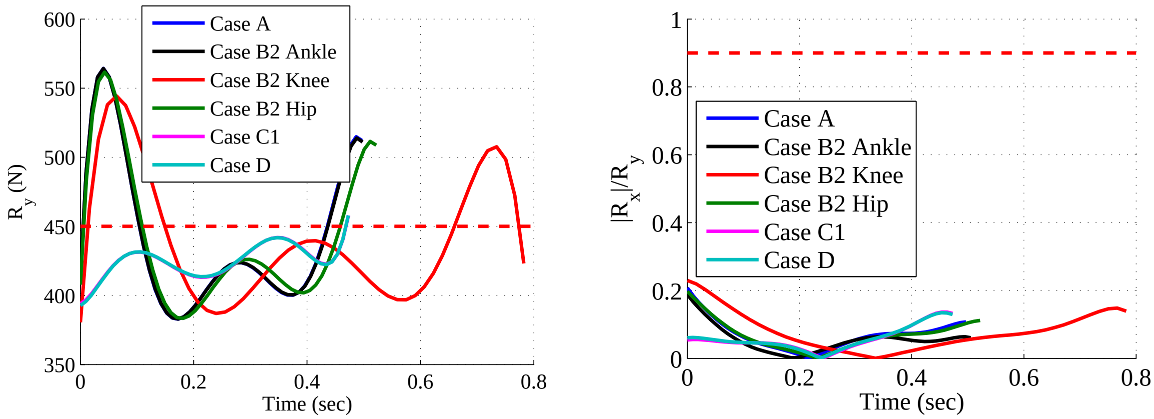

(a) vertical reaction (b) no slipping constraint

Figure 5.16 – Evolution of vertical reaction and no-slipping constraint on stance foot of gait type 1 at 0.5 m/sec. The horizontal red dotted line represents the weight of the biped in (a) and value of co-efficient of friction μ in (b)

Figure 5.17 shows the ZMP and CoG of the biped for gait type 1 at walking speed of 0.5 m/sec. Zero Moment Point (ZMP) is one of the important criterion which must be satisfied in bipedal gait trajectory generation. This constraint is presented in Figure 5.17(a), which shows that for all studies, ZMP remains inside the support polygon. The red dotted lines show the upper and lower limits of the support polygon. It also shows that it has low amplitude and is nearly below the ankle of the foot during the entire walking step.

Evolution of CoG of the biped during a walking step is presented in Figure 5.17(b) at 0.5 m/sec. It shows that there is very less variation in the vertical position of the CoG, and that the variations are significantly reduced when the knee is locked. This reduction in variation of CoG resulted in reduced variation of potential energy, which is directly proportional to CoG of the biped. The reduction in total criterion during walking is the result of less variations of the CoG and the locking of the support knee or springs.

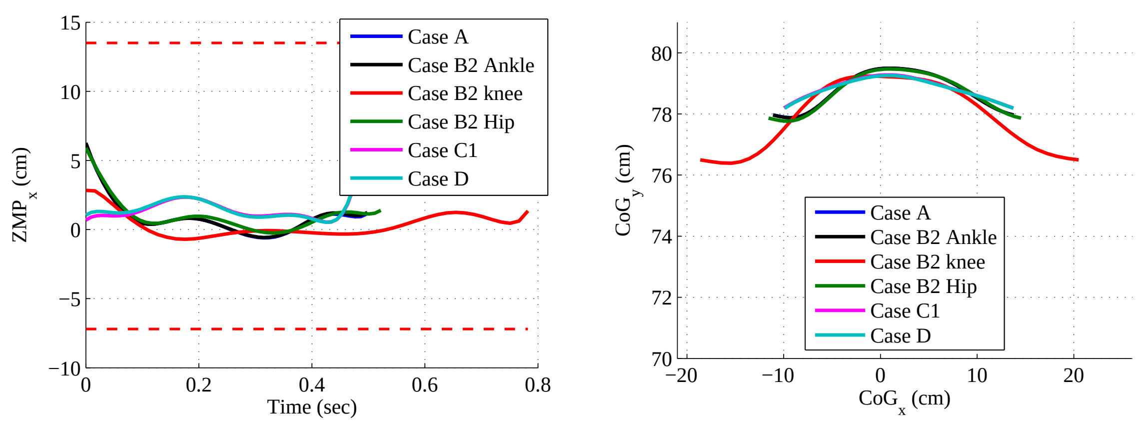

(a) ZMP (b) CoG

Figure 5.17 – Evolution ZMP and CoG of gait type 1 at walking speed of 0.5 m/sec

5.3.4 Summary of Walking Gait without Impact

In this section, impactless walking gait trajectories for a seven-link bipedal robot were presented with three different strategies, one by adding torsional springs to different joints, second by mechanically locking the knee and third by combining the two strategies *i.e.* locking the support knee and adding identical springs to hip joints. The key focus of the study was the energy consumption during walking.

It is concluded from this study that the energy consumption of a biped is significantly reduced by adding identical torsional springs at the hip joint and mechanically locking the knee. However, the maximum attainable walking speed was reduced to half. The energetic efficiency of blocking the knee alone at low speeds and adding springs only to the knee or hip joints is also noticeable. Practical implementation of this strategy will significantly improve the energetic efficiency as well as the autonomy of a biped. In the next section, walking gait trajectories of type 2 will be generated and optimized, and the effects of springs and knee locking on energy consumption during walking will also be explored.

5.4 Simulation Results of Walking Gait with Impact

In this section, simulation results for walking gait trajectories of gait type 2 will be presented for all cases discussed in Section 5.2. The optimization criteria will then be compared with that of the basic biped in case **A** for all studied cases. The percentage energy saved by using the above techniques will also be presented and explained. A number of walking gait trajectories at different walking speeds will be generated and optimized using cubic spline function presented earlier. Finally, simulation results for walking speeds of $0.5m/s$ will be presented, and the effects on energy consumption during walking of different studies will be compared. Energy consumption during walking and other parameters like step length, hip height, ZMP, CoG, impulsive forces and ground reactions etc will also be discussed.

5.4.1 Results with Springs

Figure 5.18 shows a step of walking gait type 2 for different cases with springs at walking speed of 0.5 m/sec. It can be observed that when springs are added to both knees, the step length is slightly larger than that of other three cases. The step length of other cases (see figures 5.18(a), 5.18(b) and 5.18(d)) is almost the same, but the postures are different like for gait type 1.

Figure 5.19 presents the evolution of criterion for the biped in case **A**, case **B1** where spring were introduced to the joints of the support leg, and case **B2** where identical springs were added to respective joints of both legs. Figure 5.19 shows that the optimization criterion is significantly reduced after introducing identical springs to both hip joints in parallel with the existing actuator. It was however observed, that adding springs to both knees or ankles were not effective in our case. It also shows that criterion is significantly reduced when identical springs with constant stiffness are added to both hip joints (see figures 5.19(d) and 5.19(c)). Therefore, it is possible to add passive torsional springs of constant stiffness at both hips, which are effective for almost all walking speeds. However, at very slow walking speeds, the energy consumption is high compared to that of basic biped. For gait type 2 an average value of $K = 40N/rad$ is selected based on results presented in Figure 5.21.

Figure 5.20 gives the evolution of percentage economy as a function of walking speed

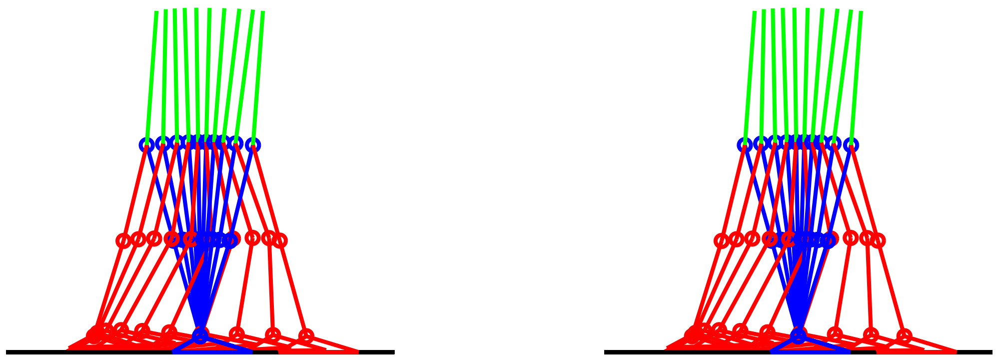

(a) basic biped (b) spring at support ankle joint

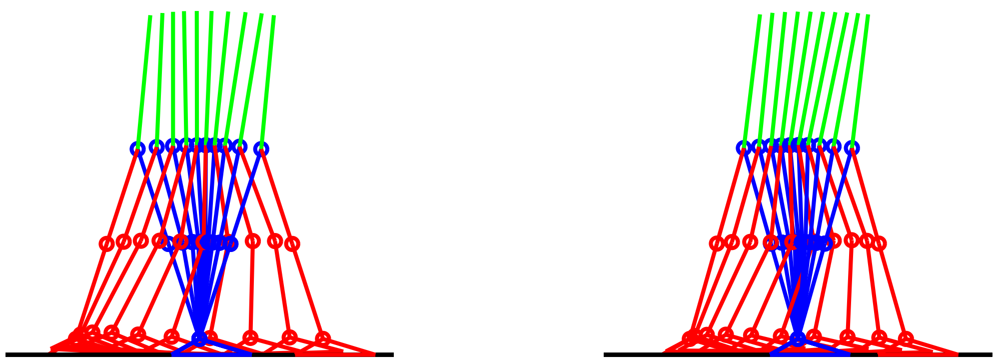

(c) spring at support knee joint (d) spring at support hip joint

Figure 5.18 – Walking gait of type 2 with springs at walking speed of 0.5 m/sec

corresponding to Figure 5.19 of gait type 2. It shows that the criterion is reduced to 50% by adding identical springs to both hip joints and maximum energetic efficiency is obtained at walking speeds from 0.7 m/sec to 1.0 m/sec.

Simulation results show that the most effective way to reduce energy consumption during walking is to add springs only to the support joints, and the most economical is the hip joint (see fig. 5.19(c)). Addition of springs to hip joints economizes up to 85% of energy at 0.85 m/sec as presented in figure 5.20. Figures 5.19(a) and 5.19(b) show that adding springs only to the support ankle or knee joint or to both joints are effective for gait type 2 while only knee springs were beneficial for gait type 1.

Figure 5.21 presents the value of spring stiffness K at different walking speeds for case B1 where springs were added to the joints of the support leg, case B2 with identical springs at both hips, and for case D where knee was locked and identical springs were added to hip joints. It shows that it is possible to fix a constant spring stiffness at slow walking speeds for support hip joint, and for fast walking speeds K can not be fixed. Similarly, for ankle joints K is zero for the entire range of

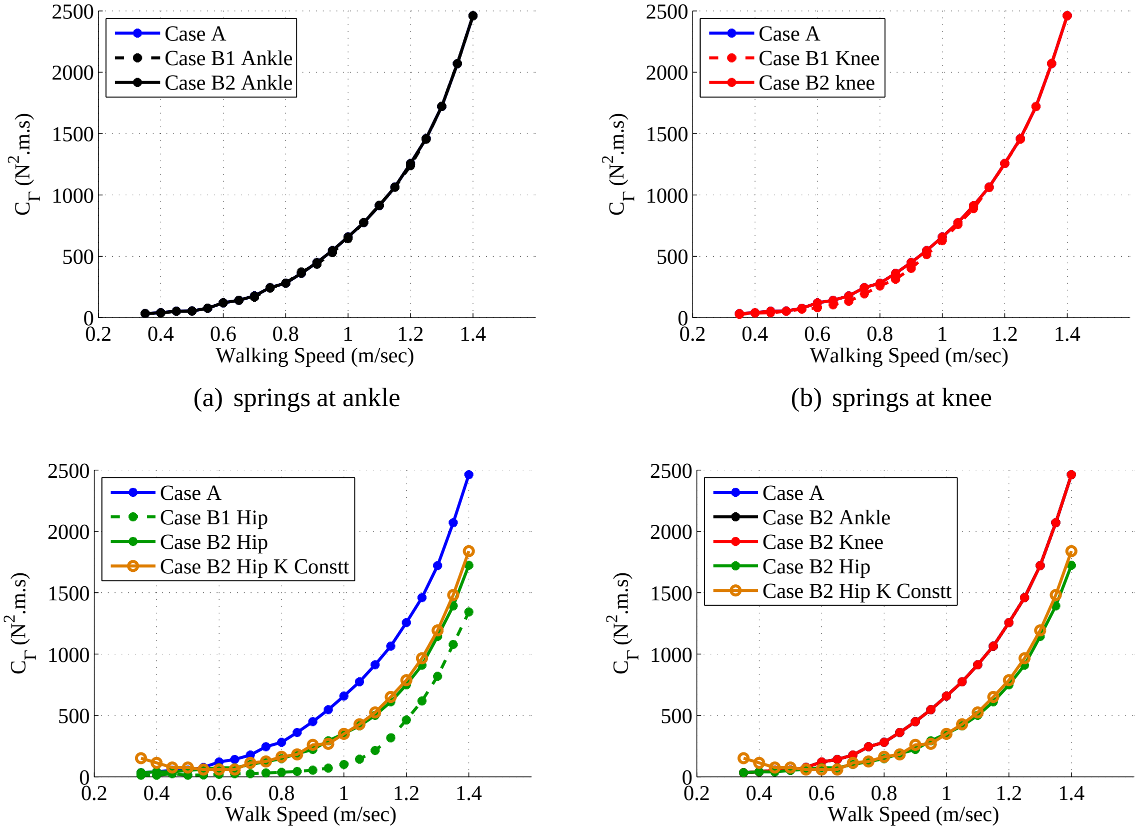

(a) springs at ankle

(b) springs at knee

(c) springs at hip

(d) springs at both ankle, knee and hip

Figure 5.19 – Value of criterion as a function of walking speed for gait type 2 (solid lines for springs at both legs and dashed lines for springs at support leg only)

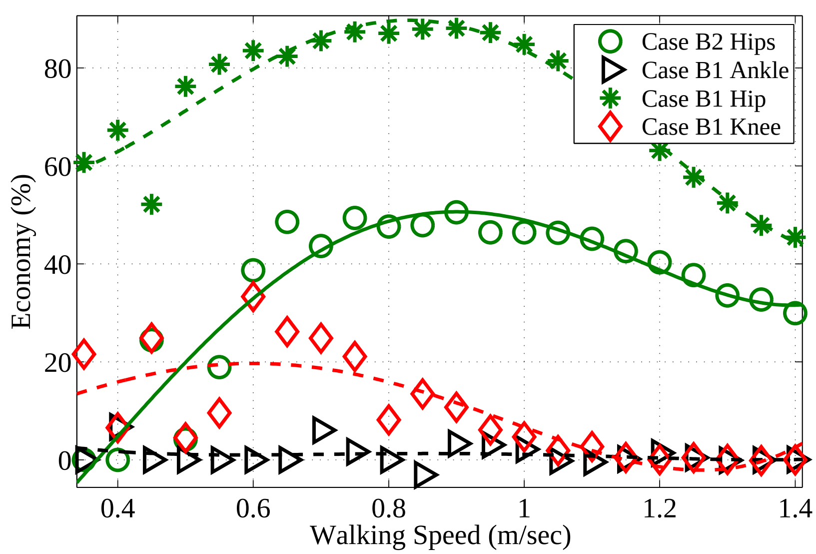

Figure 5.20 – Percentage energy saving as a function of walking speed for gait type 2 (solid lines for springs at both legs and dashed lines for springs at support leg only)

walking speed. In case of both hips joints, it seems that it is not possible to fix a constant value of K. However, by fixing $K = 40N/rad$ and optimizing the gait, optimal gait trajectories minimizing significant amount of energy consumption were found (see figure 5.19(d)). At slow walking speeds, the walking cost is increased with a constant value of spring stiffness..

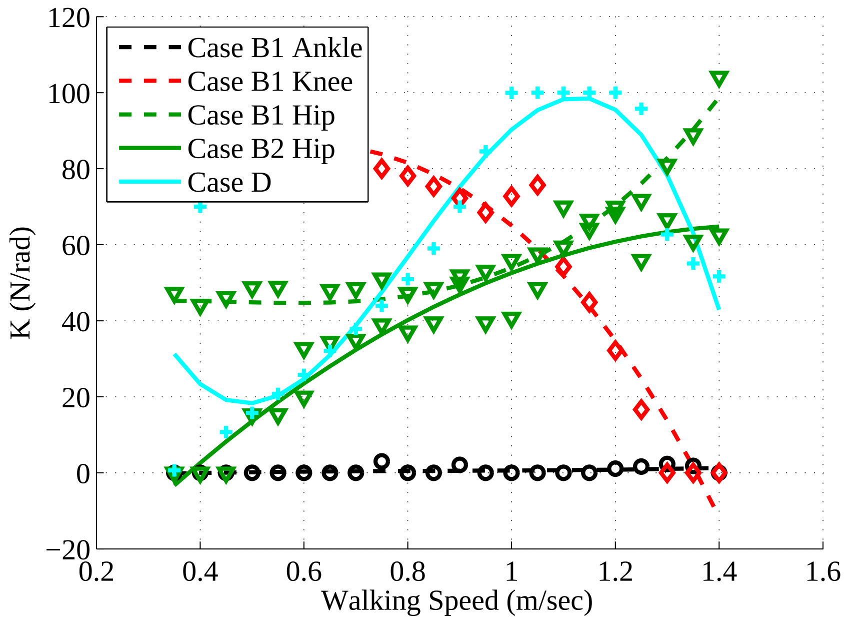

Figure 5.21 – Value of spring stiffness (K) as a functions of walking speed for gait type 2

Figure 5.22 presents the evolution of joint torques of gait type 2 with springs at walking speed of 0.5 m/sec for studies of basic biped, and biped with torsional springs at both hips. Since, ankle and knee springs were not effective, only results for both hip springs will be presented. It is to be noted that all the joint torques during the step are far below the maximum allowable limits described by the constraint equation (4.26). Technological constraints for the bipedal robot HYDROïD are given in table 3.2. Swing foot torques ($\Gamma_4, \Gamma_5, \Gamma_6$) in all cases are less important compared to that of the support foot. Joint torques are reduced when springs are added to joints of the biped in parallel with the existing actuator.

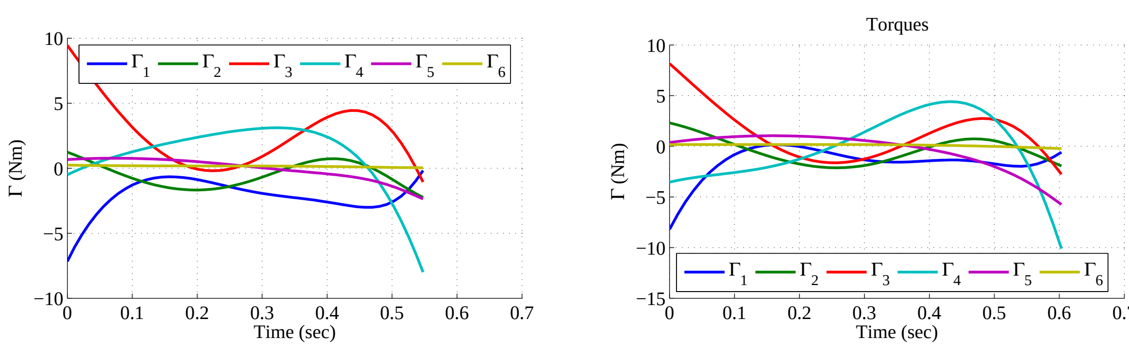

(a) basic biped (b) both hip springs

Figure 5.22 – Evolution of joint torques of gait type 2 with springs at walking speed of 0.5 m/sec. $\Gamma_1, \Gamma_2, \Gamma_3$ are the support ankle, knee and hip torques, and $\Gamma_4, \Gamma_5, \Gamma_6$ are the swing hip, knee, and ankle torques

Evolution of relative joint positions of gait type 2 for walking speed of 0.5 m/sec is presented in Figure 5.23. These results are for a cyclic walking step of a biped with identical springs at both hip joints. Results show that gait trajectory is slightly modified to improve the effectiveness of springs. A slight change in evolution of θ_5 and θ_6 is observed. It is also found that addition of springs improved the optimization criterion by providing additional toque to the actuator while keeping the trajectory almost unchanged. It also shows that the variation in magnitude of the knee angle θ_2 of stance leg is negligible during the entire walking step, which means that the joint can be locked to reduce walking cost without significantly modifying the gait trajectory.

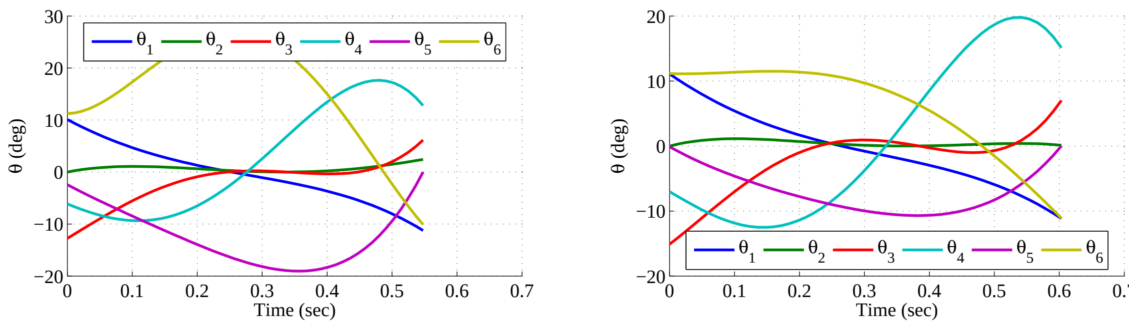

(a) basic biped (b) both hip springs

Figure 5.23 – Evolution of joint positions of gait type 2 with springs at walking speed of 0.5 m/sec. $\theta_1, \theta_2, \theta_3$ are the support ankle, knee and hip angles, and $\theta_4, \theta_5, \theta_6$ are the swing hip, knee, and ankle angles

Figure 5.24 gives the evolution of joint angular velocities of optimal gait trajectory of type 2 with springs at walking speed of 0.5 m/sec. Like joint angles, the joint velocities are also within the maximum allowable limits. It is clear that in all cases, joint velocities start with relatively low values and ends with high magnitudes at the end of the step.

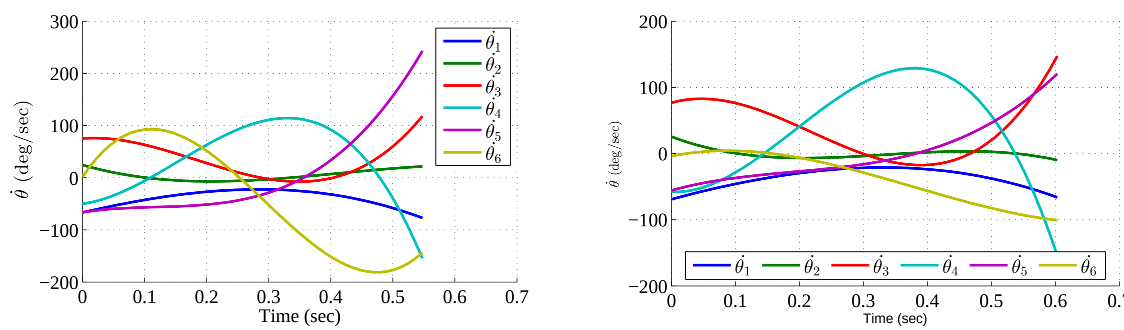

(a) basic biped (b) both hip springs

Figure 5.24 – Evolution of joint angular velocity of gait type 2 with springs at walking speed of 0.5 m/sec. The subscript 1,2,3 represents stance ankle, knee, hip while 4,5,6 represents swing hip, knee, and ankle

5.4.2 Results with Knee Locked

Walking gait trajectory for different studies with knee locked (see case C1 and case D) is presented in Figure 5.25 for walking speed of 0.5 m/sec. It shows that the step length and the joint configuration in all cases during walking step is almost the same. Although, the support knee was

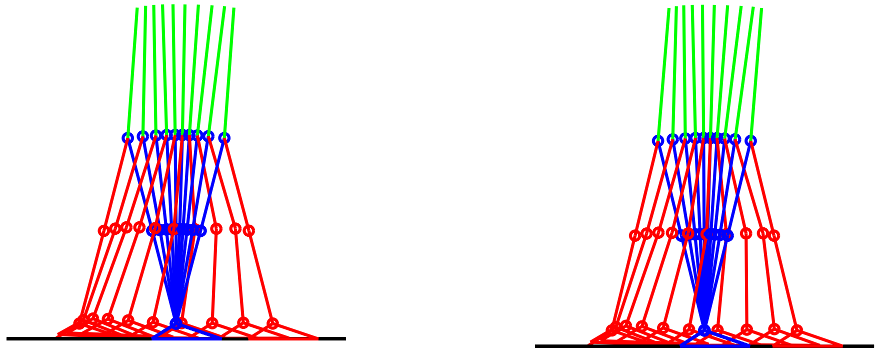

(a) knee locked

(b) knee locked and springs at both hip joints

Figure 5.25 – Walking gait of type 1 with knee locked at walking speed of 0.5 m/sec

locked in this study, the gait trajectory visually resembles that in figures 5.18(b) and 5.18(d). The average value of knee locking angle β is found to be 1.0^o, which was 8.3^o for impactless walking.

Figure 5.26(a) gives the evolutions of selected criteria as a function of walking speed for the biped in case **A**, case **B2** where identical springs were added to both hip joints, case **C2** where knee locking angle β of 1 degree was obtained from case **C1**, and for a biped in case **D** with identical springs on both hips with support knee locked. The energy consumption for a biped with support knee locked and springs on both hips (case **D**) is always less than that of a biped with only knee locked or hip springs. There is no limitation of the walking speed in case of support knee locked as was observed in gait type 1. Moreover, significantly high walking speeds can be achieved in all studied cases compared to gait type 1. Thus, the presence of impulsive impact increased the range of walking speeds in all cases.

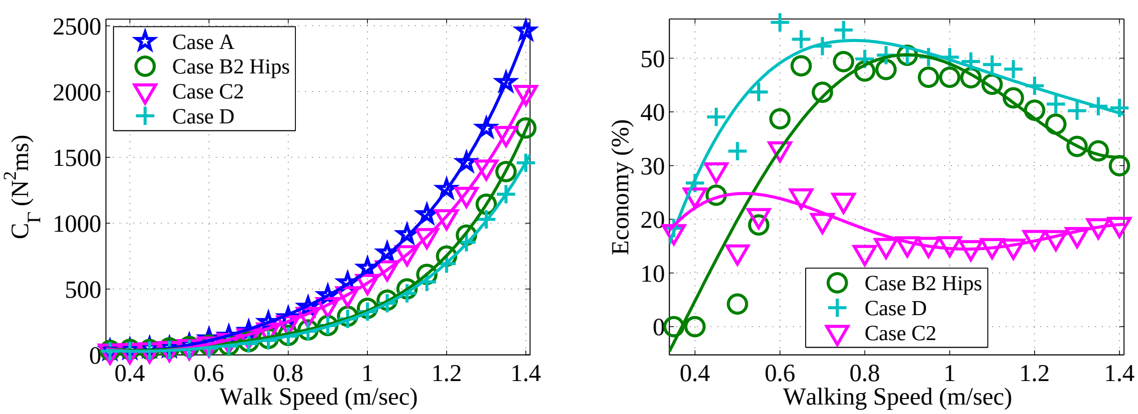

(a) criterion

(b) % economy

Figure 5.26 – Value of criterion and % economy as a function of walking speed for gait type 2 with knee locked

Evolution of percentage energy savings is presented in figure 5.26(b), which shows that the combined energetic efficiency of locking the support knee and adding identical torsional springs to both hip joints is always greater than the individual effect of locking the knee or adding springs to both hips. Previously for gait type 1, it was noted that springs addition had no effects when knee was locked. In the case of walking gait type 2, addition of springs has significantly improved the energetic efficiency of the biped during walking. Addition of springs to both hip joints with support knee locked is efficient for the complete range of possible walking speeds.

The value of knee locking angle β is presented in Figure 5.27(a) for different walking speeds. It can be seen that the β varies from zero to 2 degrees, therefore, it is possible to select a constant value of β for knee locking. This will reduce the number of optimization parameters by one, which is the case C2 in our studies. The average value of $\beta = 1^o$ was calculated from results obtained in case C1, and then fixed in optimization process. Figure 5.27(b) gives the value of impulsive impact on knee at different walking speeds and different cases with knee locked for gait type 2. It is to be noted that the impulsive reaction on knee is unilateral and is proportional to walking speed in both cases.

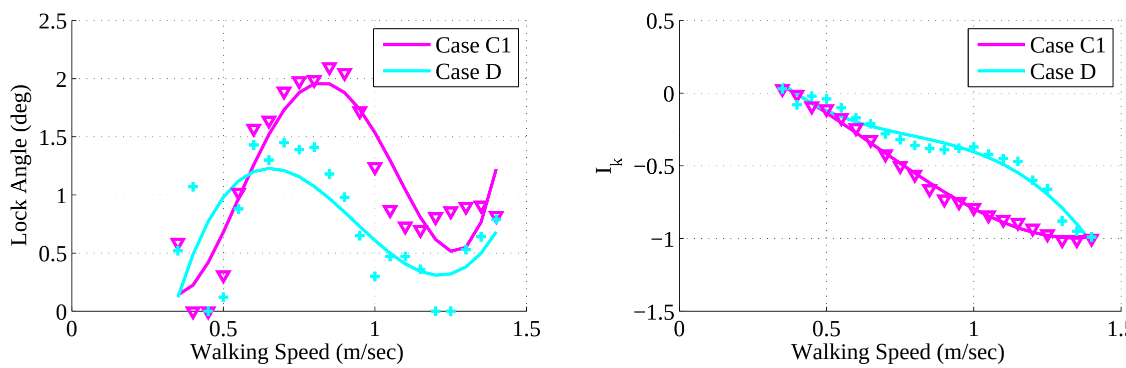

(a) knee locking angle (b) knee impulse

Figure 5.27 – Value of knee locking angle (β) and knee impulsive reaction (I_k) as a functions of walking speed for gait type 2

Evolution of joint torques for knee locked and knee locked with hip springs is presented in Figure 5.28 for a walking speed of 0.5 m/sec. It is to be noted that the knee torque shown in figures is provided by the locking mechanism, and the actuator's torque of the support knee is zero during the entire swing phase. Figure 5.28(b) shows that both hip torques are slightly reduced after adding springs. It is to be noted that the knee locking mechanism is assumed to be bilateral capable of providing torque in both directions.

Figure 5.29 gives the evolution of joint positions of gait type 2 with knee locked at walking speed of 0.5 m/sec. It can be observed that the joint angle $\theta_2 = \beta$ of support knee is constant throughout the walking step. It can also be observed that the locking angle β is about 1^o for case C1 (knee locked only) and case D (knee locked and springs at both hips). The joint configuration during walking step remains unchanged after adding springs to both hip joints.

Evolution of joint angular velocities of gait type 2 with knee locked at walking speed of 0.5 m/sec is given in Figure 5.30. It is clear from results that the support knee angular velocity $\dot{\theta}_2$ is zero during the entire single support phase, which confirms that the knee was locked during the entire

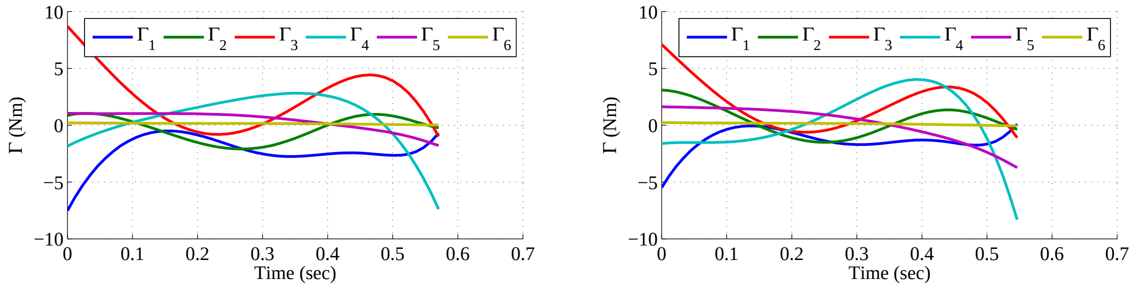

(a) knee locked (b) knee locked and hip springs

Figure 5.28 – Evolution of joint's torque of gait type 2 with knee locked at walking speed of 0.5 m/sec. $\Gamma_1, \Gamma_2, \Gamma_3$ are the support ankle, knee and hip torques, and $\Gamma_4, \Gamma_5, \Gamma_6$ are the swing hip, knee, and ankle torques

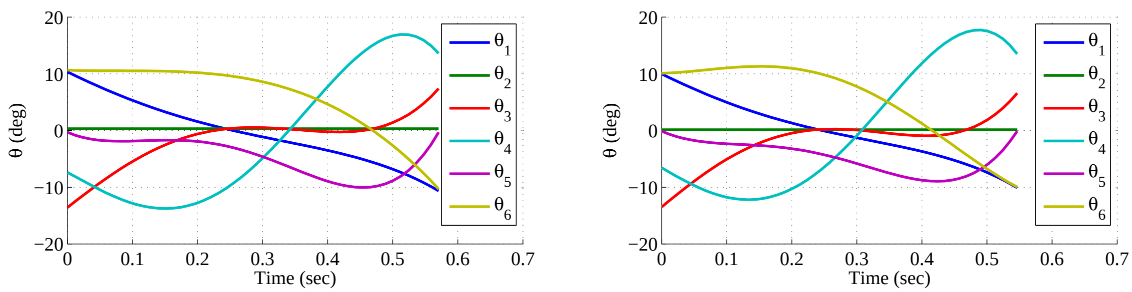

(a) knee locked (b) knee locked and hip springs

Figure 5.29 – Evolution of joint positions of gait type 2 with knee locked at walking speed of 0.5 m/sec. $\theta_1, \theta_2, \theta_3$ are the support ankle, knee and hip angles, and $\theta_4, \theta_5, \theta_6$ are the swing hip, knee, and ankle angles

walking step. Similar results can be seen in Figure 5.30(b) where springs are added to both hips of the biped, and support knee is also locked.

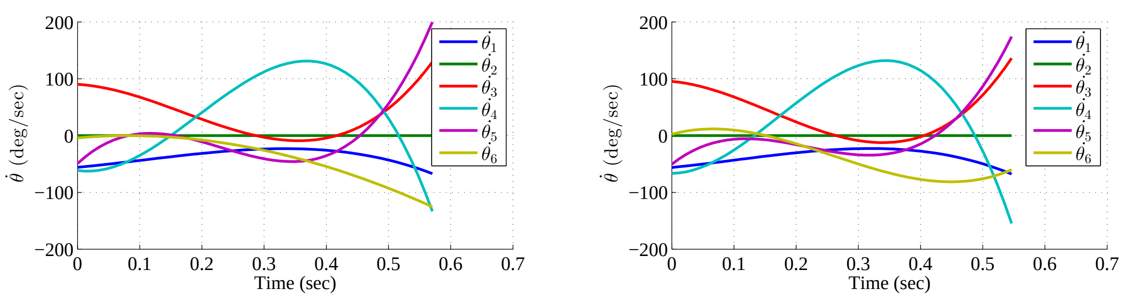

(a) knee locked (b) knee locked and hip springs

Figure 5.30 – Evolution of joint angular velocity of gait type 2 with knee locked at walking speed of 0.5 m/sec. The subscript 1,2,3 represents stance ankle, knee, hip while 4,5,6 represents swing hip, knee, and ankle

5.4.3 Combined Results with Springs and Knee Locked

Figure 5.31(a) shows the duration of step as a function of walking speed for all studied cases of gait type 2 while Figure 5.31(b) presents the length of step for the same. It is clear from results that the duration of step decreases and the step length increases as walking speed increases. Therefore, it is deduced that duration of step is inversely while step length is directly proportional to walking speed.

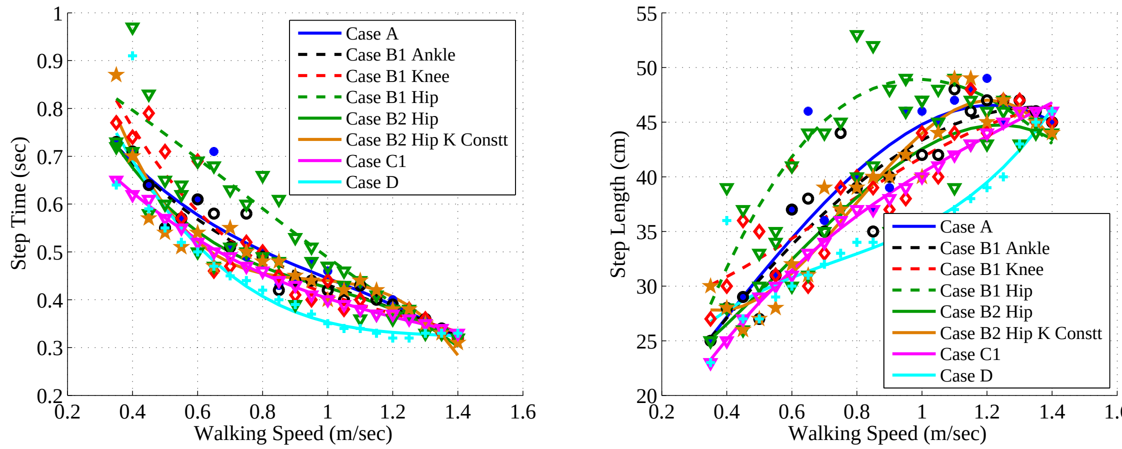

(a) duration of step (b) step length

Figure 5.31 – Evolution of duration of step (T) and step length (d) as a functions of walking speed for gait type 2

Figure 5.32 presents the impulsive impact forces on foot 2 at different walking speeds for all cases with springs and knee locked. It shows that the tangential and normal component of the impulsive reaction represented by I_t and I_N respectively are unidirectional and are directly proportional to walking speed.

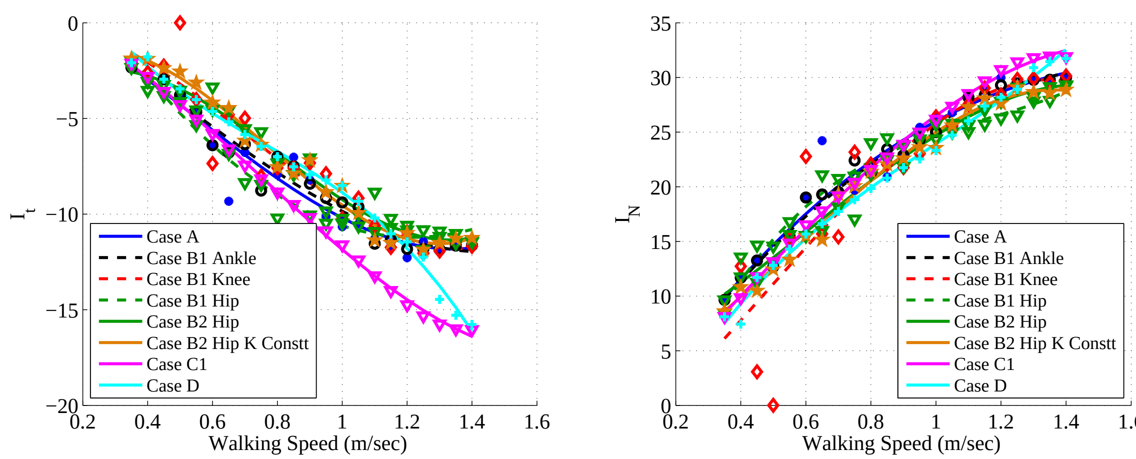

(a) tangential component (b) normal component

Figure 5.32 – Value of knee foot impulsive reaction (I_2) as a functions of walking speed for gait type 2

Evolution of normal component of the ground reaction force and no-slipping constraint on foot 1 at different walking speeds is presented in Figure 5.33 for all studied cases at walking speed of 0.5m/sec. Figure 5.33(a) gives the vertical reaction force, which shows that it is always positive for all cases. It also shows that the constraint of no-take-off is well satisfied. It was also observed that neither the shape nor the amplitude is significantly modified when torsional springs are added to the biped joints in parallel with the existing actuators or support knee is locked. However, it is observed that the vertical reaction forces is always less than the weight of the biped (average value of acceleration of CoG of the biped during singles support phase is not zero). By analyzing the impulsive reaction at impact (see figure 5.32(b)), it is found that the impulsive reaction is always positive, consequently vertical velocity after impact is greater than that before impact, which compensates for the non null average value of vertical acceleration, and the net average value for a complete cycle is null.

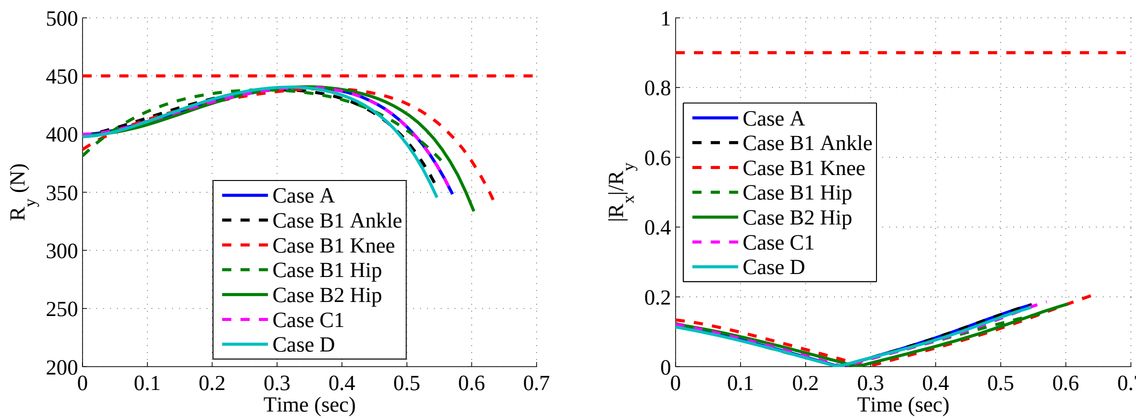

(a) vertical reaction (b) no slipping constraint

Figure 5.33 – Evolution of vertical reaction and no-slipping constraint on stance foot of gait type 2 at 0.5 m/sec. The horizontal red dotted line represents the weight of the biped in (a) and value of co-efficient of friction μ in (b)

Evolution of the calculated value of ration of tangential versus normal force during a walking step of gait type 2 is presented in Figure 5.33(b) at walking speeds of 0.5 m/sec. During walking step, the biped must not slip and satisfy the constraint of no-slipping i.e. the calculated value of μ should always be less than the maximum allowable limit. Simulation results show that the constraint of no-slipping is well satisfied and the calculated value of μ is significantly lower then the limit during the complete walking step for both walking speeds. The value of friction coefficient μ was supposed to be 0.9 between ground and sole of feet of the biped and is represented by the horizontal dotted line in Figure 5.33(b).

Figure 5.34(a) shows the position of ZMP for walking gait type 2 at walking speed of 0.5m/sec. It shows that the ZMP is always inside the support polygon. It has low amplitude and is just below the ankle axis of the foot during the entire walking step. During the walking step, it has very less variations compared to gait type 1. The upper and lower dotted lines represent the extremity of the toe and heel respectively.

Figure 5.34(b) gives the evolution of CoG of the biped during a walking step. It shows that there is very less variation in the vertical position of CoG of the biped at 0.5 m/sec in all studied cases, and the curves are almost superposed. It is observed that addition of springs or knee locking have

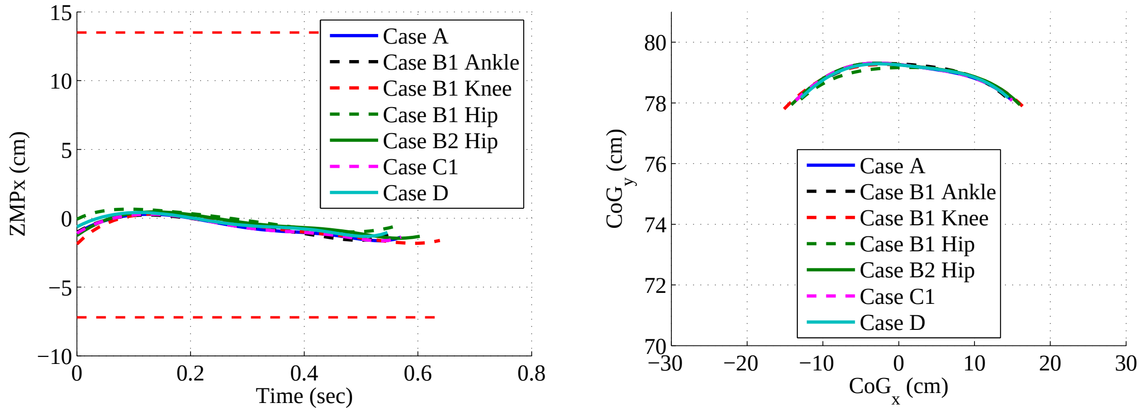

(a) ZMP (b) CoG

Figure 5.34 – Evolution ZMP and CoG of gait type 2 at walking speed of 0.5 m/sec

no significant effects on the position of CoG of the biped. Therefore, the reduction in consumption of total energy during walking is the result of effects of springs and or knee locking. Gait type 2 has less variation of CoG compared to gait type 1. This is due to the fact that there is no need to decelerate the foot before having impact contrary to gait type 1, which have phases of acceleration and deceleration at the start and end of the step respectively.

5.4.4 Summary of Walking Gait with Impact

In this section, walking gait trajectories of gait type 2 for planar biped were studied using three different strategies, first by adding torsional springs to different joints, second by mechanically locking the knee and third by combining the two strategies *i.e.* locking the support knee and adding identical springs to hip joints. It was concluded that the energy consumption of a biped during walking is significantly reduced by adding identical torsional springs at the hip joints and mechanically locking the knee. The energetic efficiency of locking the knee alone or adding springs only to the hip joints is also noticeable. This strategy will significantly improve the energetic efficiency as well as the autonomy of a bipedal robot.

In previous results for gait type 1, it was observed that walking speed is reduced when knee is locked, which is not the case for gait type 2. Results were presented showing that ankle and knee springs are not effective to reduce the cost of walking. In perspective of this study, the next step will be to explore the effects of springs and knee locking on gait type 3, which is composed of single and double support phases.

5.5 Studies Carried out on Walking Gait with Double Support

For the two previous gaits, we have analyzed the effects of springs in two cases, when identical springs are added during all phases of walking, and when the springs are added only during the support phase, cases denoted by B1 and B2. In the case of this gait that includes single support and double support phases, the case of spring used during all the phases can obviously be done. But if we accept to use the spring only during a part of the walking, during which phase(s) the spring must be used is not so obvious and depends on the joint where the spring is placed. Thus to study the effects of addition of springs on energetic efficiency of a biped robot during walking, and to take maximum advantage of the springs, a number of different combinations of spring addition is tested and the best option is selected for further analysis. First of all, optimal motions are defined for this gait using the model without spring at different walking velocities. In a preliminary study, the cost of walking is calculated as a function of spring stiffness by taking the optimal gait trajectory of basic robot (without addition of springs). It is to be noted that the trajectory is not re-optimized, only added spring stiffness K is varied to calculated criterion. Following are the different modes of addition of springs to different joints of the biped.

mode 1. Identical springs are added to both joints of a pair (ankles, knees, or hips). The springs are active all the time during single as well as double support phase.

mode 2. Spring is added only to the stance leg joints and is active only during single support phase.

mode 3. Spring is added only to the stance leg joints and is active during entire single support phase and double support phase on front foot.

mode 4. Springs are added to both legs and are active for both legs during double support phase and for stance leg during single support phase.

mode 5. Spring is active for stance leg during single support phase and during double support phase for rear foot.

mode 6. Spring is added to rear leg only during double support phase.

5.5.1 Springs at Ankle Joints

Results of tests carried out on addition of springs at ankle joints are presented in figure 5.35. Tests are carried out for three different walking speeds to get an overview of effectiveness of different modes at various walking speeds. It shows that the most effective mode to add springs to ankle joint is to activate the spring only during double support phase on rear foot (mode 6). The stiffness should change from zero to required value at the start of activation phase. The energy consumed by variables stiffness mechanism is assumed to be zero in present tests. Figure 5.35(d) presents the comparison of mode 1 and 6 with reference value of criterion. It is found that addition of identical springs to both joints, which are active all the time during single as well as double support phase minimize very less amount of energy (around 2%). Therefore, for ankle springs mode 6 will be selected and the trajectory will be optimized along with spring stiffness to take maximum advantage of the springs.

In mode 6, the role of the spring is to push the rear foot, this interest of the spring is coherent with the study done by T. Schauss [99] and M. Wisse [124], where they found ankle springs useful for stability as well as energetic efficiency. Figure 5.36(a) shows percentage economy for mode 1 and 6. It shows that mode 6 economizes about 12% at low walking speeds and the economy decreases as the walking speed increases. Figure 5.36(b) presents the value of K at different walking speeds. It shows that for mode 1, the optimal value of stiffness increases with walking speed while for mode 6 it is always at maximum allowable limit ($K = 50N/rad$). Therefore, it is possible to obtain high reduction in cost of walking by installing springs with hight stiffness.

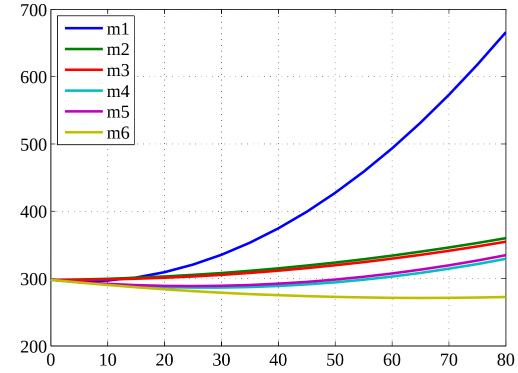

(a) 0.6 m/sec

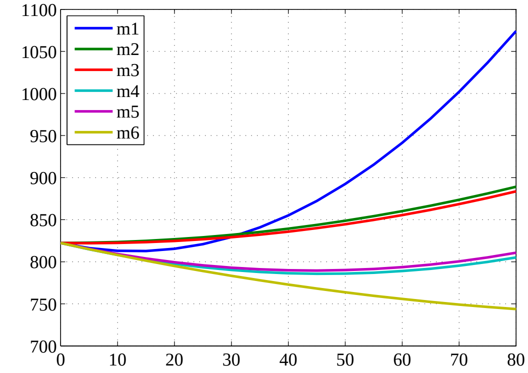

(b) 1.2 m/sec

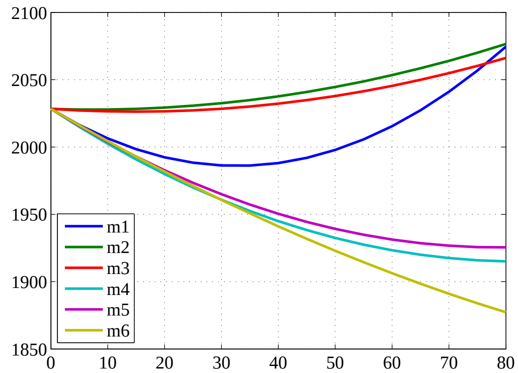

(c) 1.7 m/sec

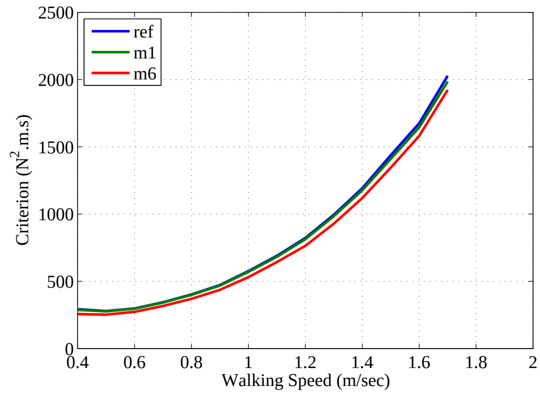

(d) comparison of reference with m1 and m6

Figure 5.35 – Evolution of criterion as a function of spring stiffness K for ankle joints

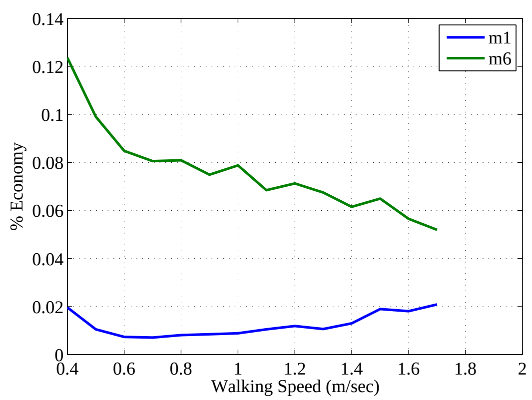

(a) % economy

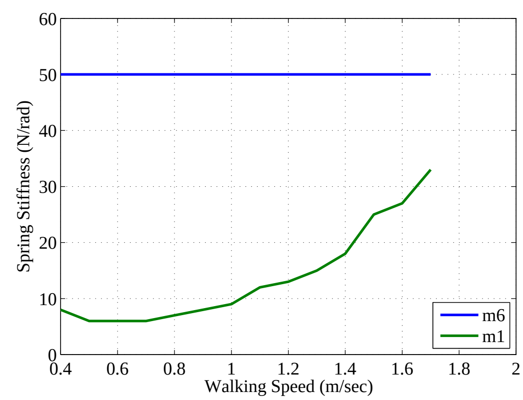

(b) Spring Stiffness

Figure 5.36 – Value of percentage economy and spring stiffness as a function of walking speed for ankle springs

5.5.2 Springs at Knee Joints

Similar to ankle springs, a number of test are carried out on knee joint to select the best available option of spring addition at knee joint. Results are produced for all studied modes presented in

5.5. Figures 5.37(a), 5.37(b), and 5.37(c) show that the best option to save energy during walking is to add springs to the stance knee joint during entire single support phase and to the the front leg during double support phase, which is mode 3 of the studies test modes.

Figure 5.37(d) compares the results of mode 1 and 3 with reference criterion. It shows that energy savings by applying mode 1 is negligible at low velocity and increase to 4% at hight velocity while mode 3 is a little more economical. The energetic efficiency of mode 3 can be further improved by allowing high spring stiffness and optimizing the gait along with stiffness.

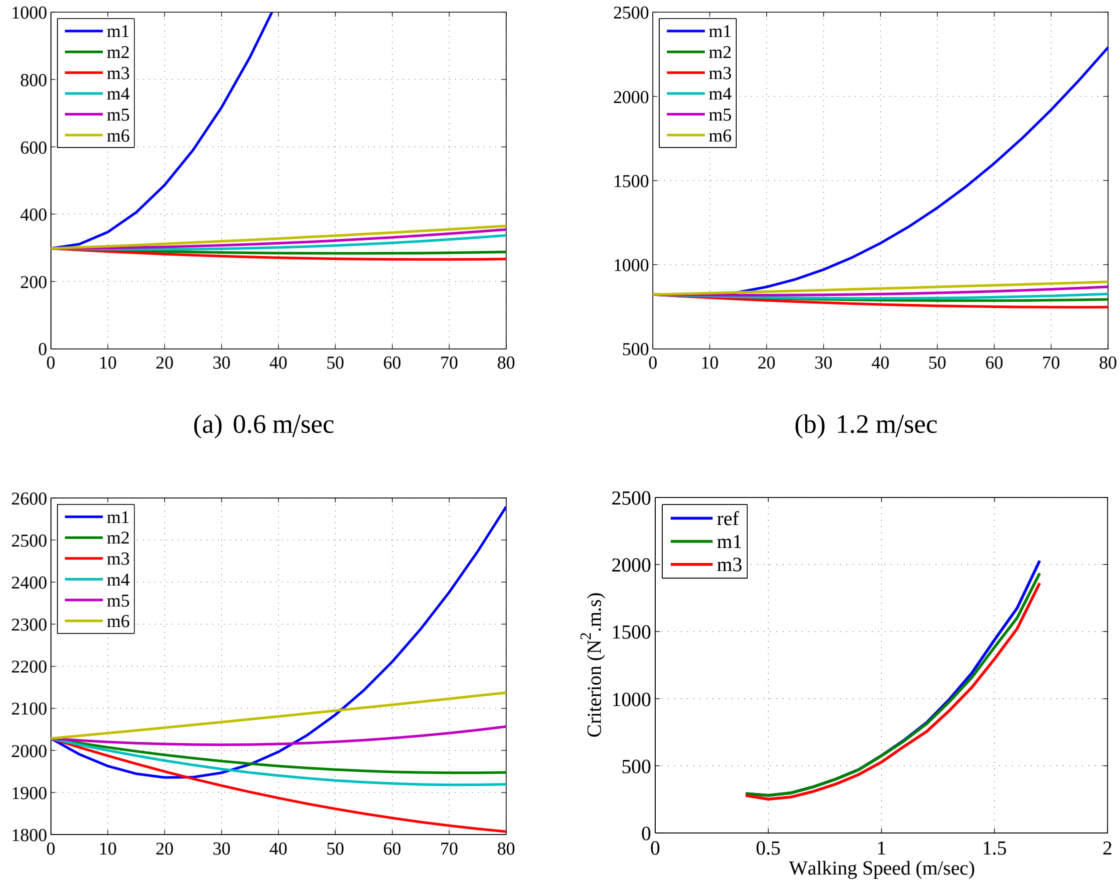

(a) 0.6 m/sec

(b) 1.2 m/sec

(c) 1.7 m/sec

(d) comparison refrence with m1 and m6

Figure 5.37 – Evolution of criterion as a function of spring stiffness K for knee joints

Figure 5.38(a) shows that percentage economy by adding springs at knee joint to the stance leg during single support phase and front leg during double support phase. It shows that mode 3 economizes around 10% of energy during walking for all walking speeds. Figure 5.38(b) gives the optimal value of spring stiffness as a function of walking speed. It shows that energetic efficiency of mode 3 can be improved by allowing hight stiffness springs.

5.5.3 Springs at Hip Joints

Figures 5.39(a), 5.39(b), and 5.39(c) present evolution of criterion as a function of spring stiffness at hip joints for all studied modes. It shows that modes 2 and 5 are superposed and have less effects on energetic efficiency during walking. It also shows that modes 3 and 4 are almost

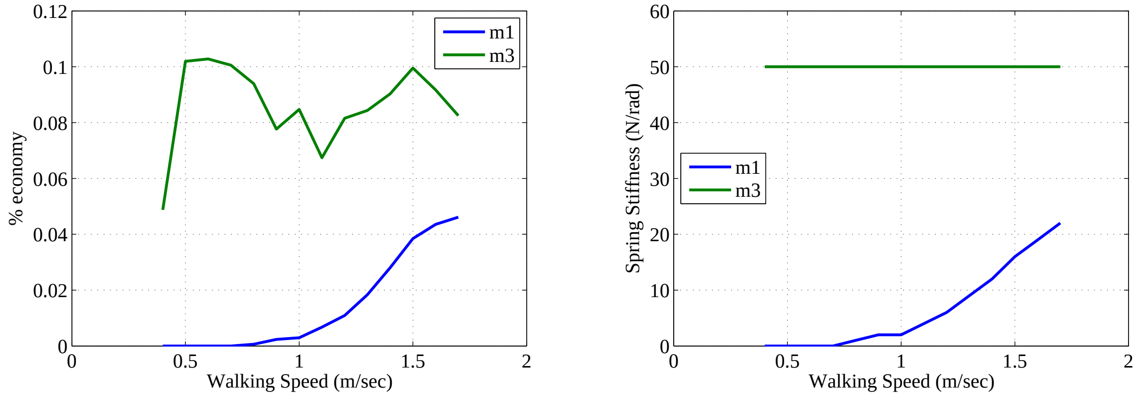

(a) % economy (b) Spring Stiffness

Figure 5.38 – Value of percentage economy and spring stiffness as a function of walking speed for knee springs

superposed and have significant effects on energetic efficiency. Contrary to results of spring addition at ankle joints, spring only at rear hip during double support phase is not as effective as it was for ankle joint. The best solution is to activate the spring at the beginning of double support until the end of the following double support phase (mode 4).

Figure 5.39(d) gives the comparison of criterion as a function of walking speed for modes 1 and 4 with reference values. It shows that spring addition at stance hip joint during single support phase and at both hips during double support economizes a significant amount of energy during walking at all walking speeds.

Figure 5.40(a) shows the percentage savings in modes 1 and 4. It is clear that the energetic efficiency of the biped is significantly improved in mode 4. The percentage savings decreases as walking speed increases starting at about 35% and ending at about 15% economy. Figure 5.40(b) gives the corresponding optimal values of spring stiffness for Figure 5.40(a). It shows that optimal value of spring stiffness for mode 4 varies between 40-50 N/rad and is below 10 N/rad for mode 1.

5.5.4 Summary of Simulation Tests with Springs

From simulation results done by adding springs to different joints and applying different modes of activation, we can conclude:

1. The energetic effects of adding identical springs to a pair of joint (ankle, knee, hip) are negligible.
2. Mode of activating a spring depends on the location where the spring is installed (ankle, knee, hip).
3. The most effective mode for ankle is to activate spring only on rear leg during double support phase (mode 6). It helps the ankle in propulsion phase.
4. The best option for the knee is to use mode 3: The spring is active at the beginning of double support until the end of next single support.
5. Addition of springs at hip joints is effective in mode 3 and 4. In present study only mode 4 will be studied for further analysis.

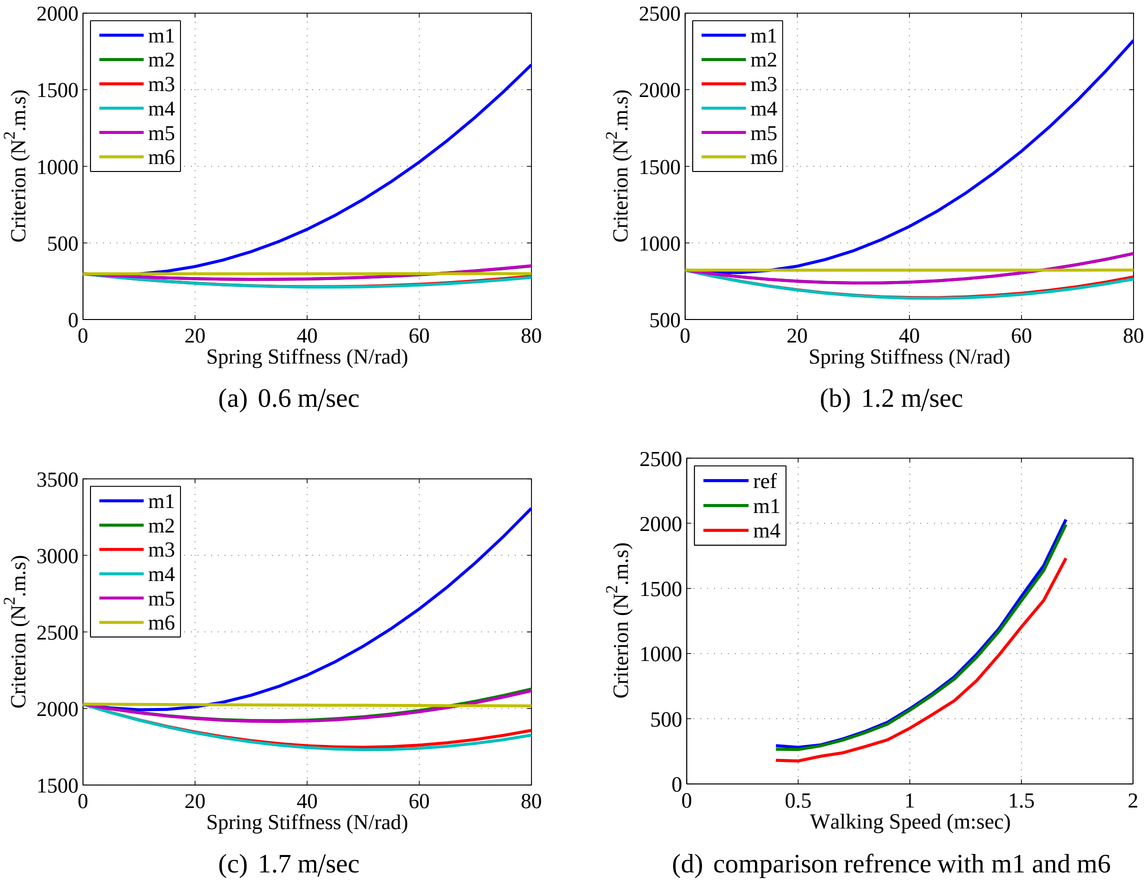

(a) 0.6 m/sec
(b) 1.2 m/sec
(c) 1.7 m/sec
(d) comparison refrence with m1 and m6

Figure 5.39 – Evolution of criterion as a function of spring stiffness K for hip joints

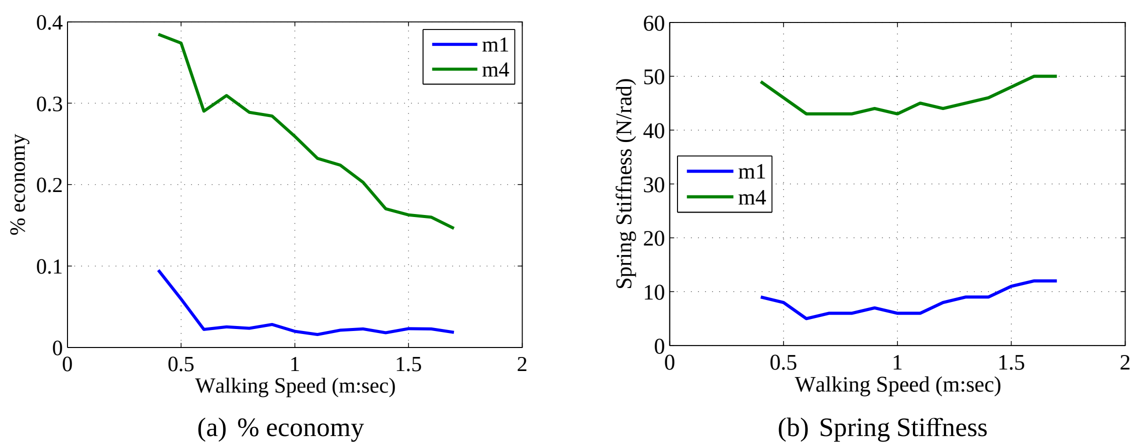

(a) % economy
(b) Spring Stiffness

Figure 5.40 – Value of percentage economy and spring stiffness as a function of walking speed for hip springs

As a result of above analysis, following different types of studies are carried out on the biped robot to further improve the energetic efficiency during walking.

case A. The biped trajectories are optimized and energetic cost of walk is calculated without adding springs or locking the support knee joint (reference criterion).

case B. Torsional springs are added to different joint of the biped in parallel to the existing actuators depending on the most effective mode obtained previously. The gait trajectory is optimized along with the spring stiffness. This study has the following sub cases:

- **case B1.** Mode 6 is applied to ankle joints: Spring is active only at rear leg during double support phase.
- **case B2.** Mode 3 is applied to knee joints: Spring is active during entire single support phase at stance leg and double support phase at front leg.
- **case B3.** Mode 4 is applied to hip joints: Springs are added to both legs and are active for both legs during double support phase and for stance leg during single support phase.

In all the cases where a spring is added to any of the joint, the spring constant K is optimized along with the gait and the spring offset or bias angle θ_0 is kept zero.

5.6 Simulation Results of Walking Gait with Double Support

A number of optimal walking gait trajectories of type 3 were generated at different walking speeds to study the effects of springs on selected performance criterion during walking. Moreover, effects of springs on other parameters like ZMP, CoG, ground reaction forces are also studies and the results are presented in this section. Since this gait is more realistic and human like, the range of simulation results is extended to walking speed of 1.7m/sec. Simulation results at walking speed of 1.2m/sec, which is close to normal human walking velocity will be presented.

Figure 5.41 shows the stick diagram of a walking step for the biped at walking speed of 1.2 m/sec for all studied cases. It is visually observed that gait trajectories of all cases with springs are slightly different from that of basic robot. It means that by optimizing the trajectory after adding springs, it is slightly modified to benefit from the torques provided by the torsional springs addition parallel to the existing actuators. During double support phase, rotation of front foot on its heel and rear foot on its toe can be clearly observed in the figure.

It was previously observed, that for gait type 2 in section 5.4, the amplitude of height of swing foot was very low during entire swing phase. In contrast to the results of gait type 2, the amplitude of height of swing foot during entire swing phase is increased. It means that by introducing finite double support phase, walking step is improved and the gait is close to human walking. Similar improvements in walking gait trajectory are also observed for a biped with hydraulic actuators (see 7.4.1).

Figure 5.42(a) presents the comparison of criteria curves as a function of walking speed for basic robot as well as all studied cases with springs according to the selected mode of activation. It shows that the optimization criterion is significantly reduced when torsional springs are added to ankle joints in mode 6, knee joint in mode 3, and hip joints in mode 4. It also shows that criteria curves in case B1 and case B2 are almost superposed. The most effective method to reduce the consumption of energy during walking is to add torsional springs to both hips during double support phase and only to stance hip during single support phase (mode 4). Simulation results of gait types 1 and 2 also showed the effectiveness of hip springs while ankle springs were not effective in case of gait types 1 and 2. In contrast to previous results presented in this study, and in line with recent research on bipedal walking, ankle springs showed their effectiveness only when added at rear leg during double support phase (propulsion phase) at all walking speeds.

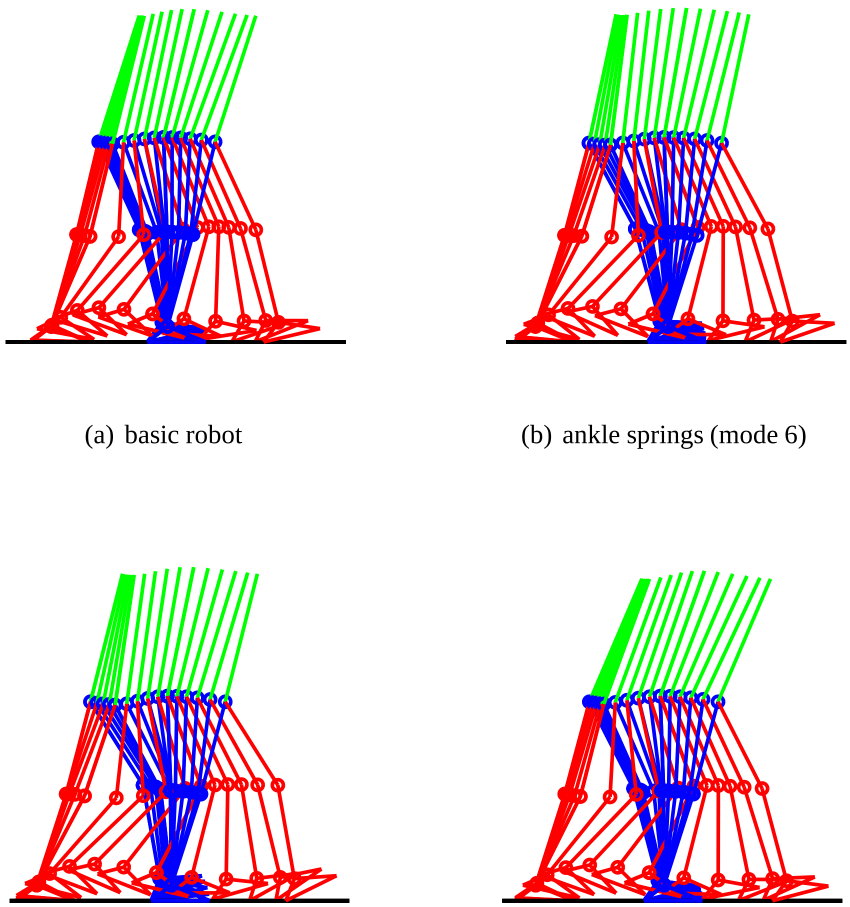

(a) basic robot (b) ankle springs (mode 6)

(c) knee springs (mode 3) (d) hip springs (mode 4)

Figure 5.41 – Walking step of the biped for all studies cases at 1.2 m/sec for gait type 3

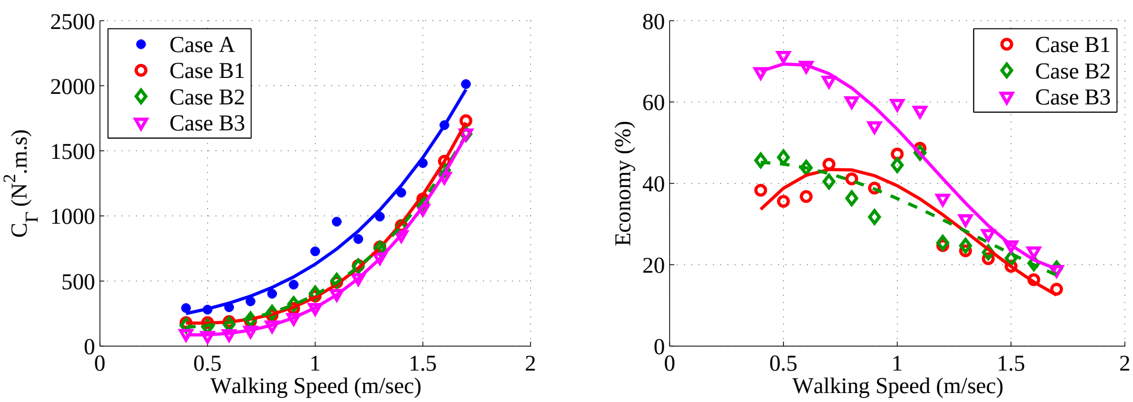

(a) criterion (b) % economy

Figure 5.42 – Value of criterion and percentage savings as a function of walking speed for gait type 3

Figure 5.42(b) gives the evolution of percentage savings of selected criterion as a function of walking speed for all studied cases. It shows that percentage economy decreases with increase in walking speed but even at high speeds, the percentage reduction is significant for all studied cases. The percentage saving of energy consumption varies between 18 to 40% in cases **B1** and **B2**. Percentage economy of case **B3** is very high at slow walking speeds, however it decreases and converges towards the other cases. It is observed that energetic efficiency is significantly improved in all case when trajectory is optimized alongside the spring stiffness compared to that obtained where only spring stiffness was optimized. It is therefore concluded from simulation results, that the best option to reduce bipedal walking cost is to us torsional springs at hip joints in mode 4. The spring is active from the beginning of double support phase until the end of following double support phase.

Evolution of spring stiffness (K) as a function of walking speed is presented in Figure 5.43. It shows that for sprigs at hip joints in mode 4 (case B3), the value of K is almost constant and significantly lower than that of other two cases. The springs keeps the torso in a slightly forward leaned position and works against the gravity. As a result the actuators work is reduced and consequently the cost of walking. For case B2, the spring constant increases with increase in walking speed. Since the maximum limit of K is 100 N/rad, it is constant at this value at speeds above 0.6m/sec. For ankle joint, the limit for springs stiffness is 150 N/rad. It is clear from results that the value of K is constant at maximum for all studied walking speeds. The spring is use only at rear ankle during double support phase. It helps to prepare for next single support phase and provides a push to move forward, thus require a high stiffness. It is concluded from results that a constant value of spring stiffness can be used for all joint using respective modes of activation, and the cost of walking can be significantly reduced.

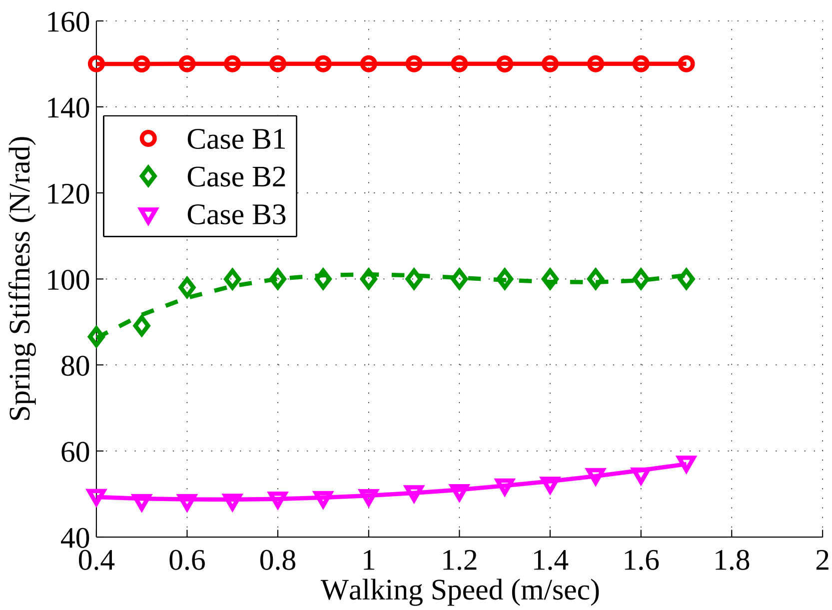

Figure 5.43 – Evolution of spring stiffness for gait type 3 in different cases

Figure 5.44 shows the duration of step and the length of step as a function of walking speed for gait type 3 for all studied cases. It is clear from results that the duration of step decreases and the step length increases as walking speed increases. Therefore, it is deduced that duration of step is inversely proportional to walking speed while step length is directly proportional to it. It is therefore, concluded that addition of identical springs to different joints of the biped have small effects on step length and duration. However, effects on energy consumption during walking are significant for springs at ankles in mode 6, at knees in mode 3, and hips in mode 4 (see Figure 5.42(a)). Similar correlation of duration of step and step length with walking speed was also observed in gait type 1 and gait type 2.

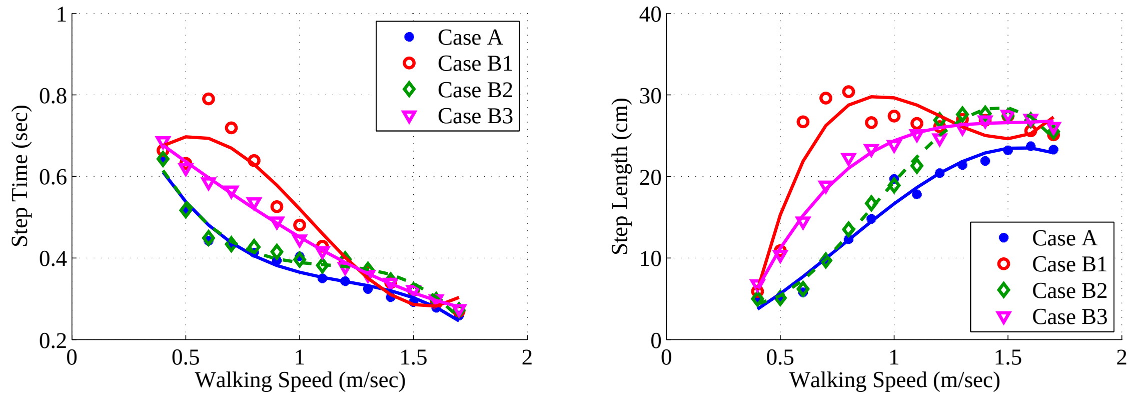

(a) duration of step (b) step length

Figure 5.44 – Evolution of duration of step (T) and step length (d) as a functions of walking speed for gait type 3

As previously discussed, that the optimal trajectory for walking gait type 3 is the trajectory without first impact. Therefore, there is no impulsive reactions when the heel of the front foot touches the ground. The second impact (toe impact see Figure 3.7) occurs when the front foot comes in flat contact on the ground. Figure 5.45 presents the impulsive impact force I_{r1ss} on the front foot of the biped at different walking speeds. It is the impulsive force on front foot at the end of double and the start of single support phase. The tangential and normal component of the impulsive reaction represented by I_{r1ss_x} and I_{r1ss_y} are presented in Figures 5.45(a) and 5.45(b) respectively. It shows that for all studied cases, these forces are unidirectional. The magnitude of tangential component increases towards medium walking speeds and then decreases again at high walking speeds for all cases. Similarly, the magnitude of normal components decreases towards medium speeds and then increases again at high walking speeds.

Figure 5.46 presents the evolution of joint torques of gait type 3 at walking speed of 1.2 m/sec for studies of basic robot, and all cases with torsional springs at respective joints according to selected activation modes. Discontinuities in joint torques at toe impact (second impact) are clearly visible in the figure. It shows that all joint torques during the entire step are far below the maximum allowable limits described by the constraint equation (4.26). It is observed that the joint torques in all studied cases during single support phase are less important than that of during double support phase particularly the swing ankle torque during single support phase is negligible. Figure 5.46(b) shows that joint torques of hip Γ_3 and ankle of rear foot Γ_6 during double support phase are significantly reduced by adding spring at the ankle of rear foot.

Evolution of relative joint positions as a function of time of gait type 3 at walking speed of 1.2 m/sec is presented in Figure 5.47. In all cases, the joint angles have small variations during double support phase compared to that during single support phase. After analyzing the results it

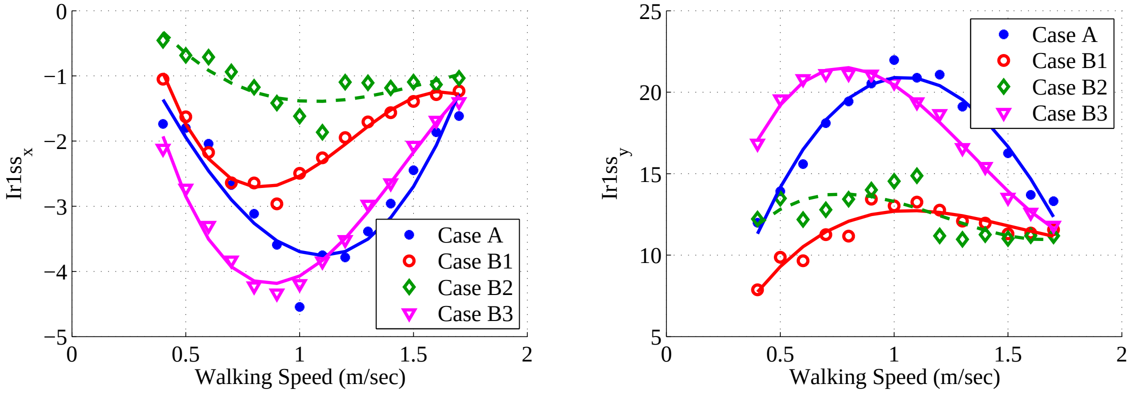

(a) tangential component (b) normal component

Figure 5.45 – Foot impulsive reaction (I_{r1ss}) on front foot at toe impact as a functions of walking speed for gait type 3

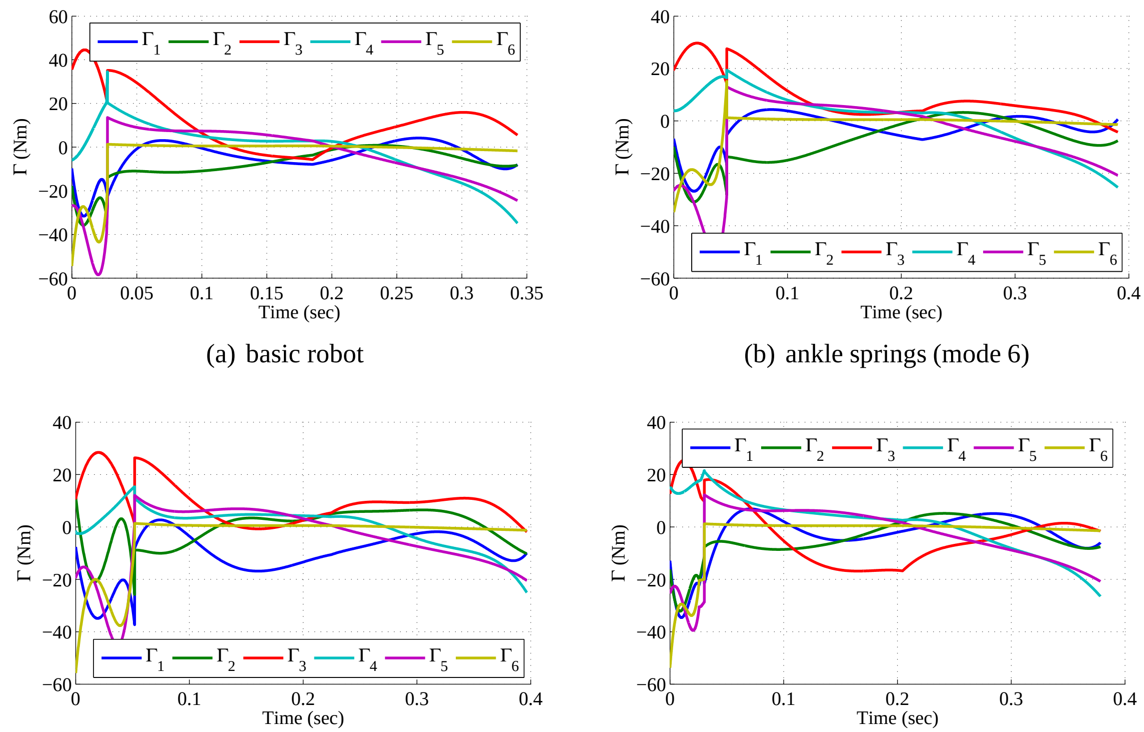

(a) basic robot (b) ankle springs (mode 6)

(c) knee springs (mode 3) (d) hip springs (mode 4)

Figure 5.46 – Evolution of joint torques of gait type 3 at walking speed of 1.2 m/sec. $\Gamma_1, \Gamma_2, \Gamma_3$ are the support ankle, knee and hip torques, and $\Gamma_4, \Gamma_5, \Gamma_6$ are the swing hip, knee, and ankle torques

is noted that joint trajectories in all cases are almost similar except the case **B3** (see figure 5.47(d)) where the support hip joint movement is relatively high. Figure 5.47 shows that in cases where springs are effective, the gait trajectory is slightly modified to get maximum advantage of the spring torque available to the actuators during different phases. Thus, the optimization algorithm found an optimal walking gait trajectory, which maximizes the effects of torsional springs added at a specific joint.

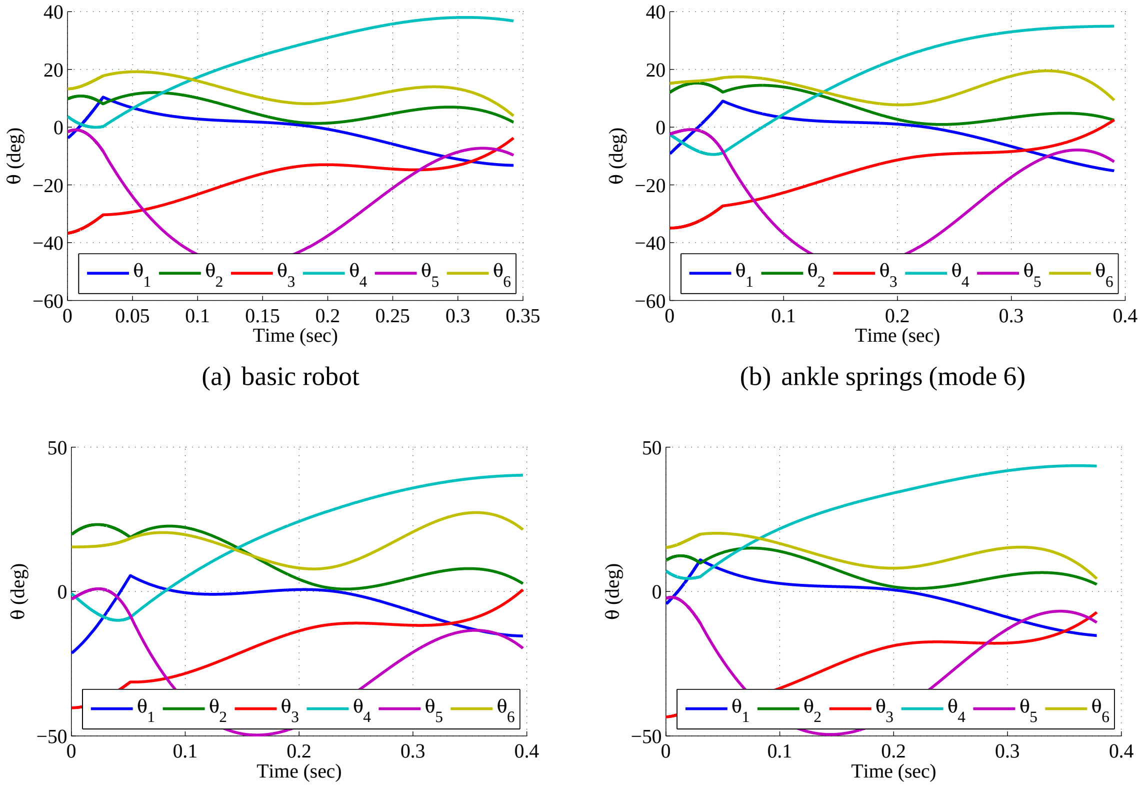

(a) basic robot (b) ankle springs (mode 6)

(c) knee springs (mode 3) (d) hip springs (mode 4)

Figure 5.47 – Evolution of joint positions of gait type 3 at walking speed of 1.2 m/sec. $\theta_1, \theta_2, \theta_3$ are the support ankle, knee and hip angles, and $\theta_4, \theta_5, \theta_6$ are the swing hip, knee, and ankle angles

Evolution of joint angular velocities of gait type 3 at walking speed of 1.2 m/sec is given in Figure 5.48. Similar observations made for joint positions can be made for joint angular velocities as well. Furthermore, it also shows that amplitude of joint velocities is high during double support phase compared to that during single support phase. Since there is no significant difference in joint velocities in all cases, therefore, the reduction in optimization criterion is due to the addition of torsional springs at different joints.

Evolution of normal component of the ground reaction force on both feet of the biped at walking speed of 1.2 m/sec is presented in Figure 5.49 for all studied cases. Figure 5.49(a) shows that the vertical component of the ground reaction force is always positive for all cases. It also shows that the constraint of no-take-off is well satisfied. It was also observed that neither the shape nor the amplitude is significantly modified when springs were added to different joints of the biped. In accordance with the ongoing research in bio-mechanics, the shape of ground reaction force on stance foot during single support phase resembles the letter "M". Similar "M" shaped curves for ground reaction force were also found in results of gait type 1.

Evolution of normal component of the ground reaction force on rear foot is presented in Figure 5.49(b) at 1.2 m/sec for all studied cases. It shows that the vertical component of the ground reaction force is always positive for all cases. It also shows that the constraint of no-take-off on rear foot is well satisfied during double support phase. The rear foot (foot 2) is in contact on the ground on its toe only during double support phase, and takes off the ground when second impact

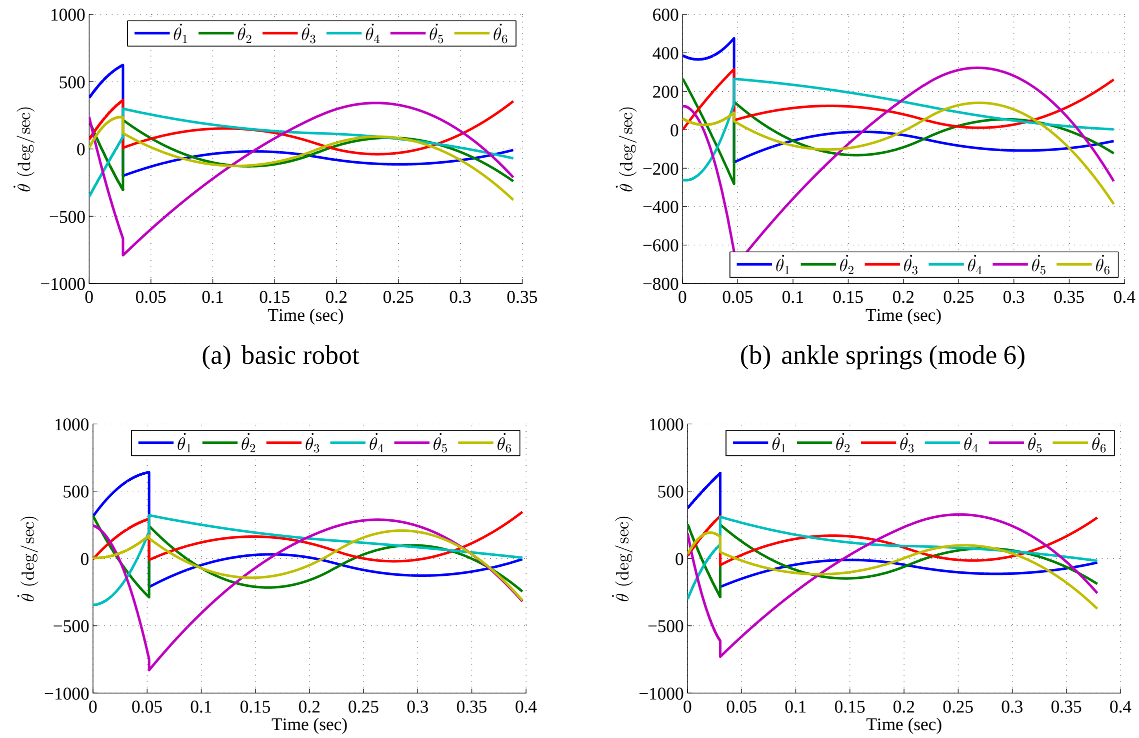

(a) basic robot (b) ankle springs (mode 6)

(c) knee springs (mode 3) (d) hip springs (mode 4)

Figure 5.48 – Evolution of joint velocities of gait type 3 at walking speed of 1.2 m/sec. The subscript 1,2,3 represents stance ankle, knee, hip while 4,5,6 represents swing hip, knee, and ankle

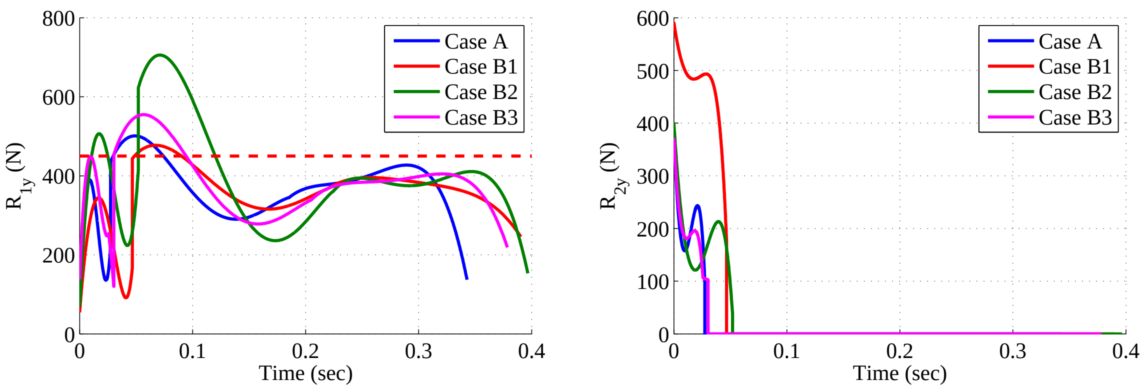

(a) stance foot (b) swing foot

Figure 5.49 – Evolution of vertical reaction force on feet of gait type 3 at 1.2 m/sec. The horizontal red dotted line represents the weight of the biped

occurs on toe of the front foot. Therefore, there is no reaction on the foot during single support phase.

The position of ZMP and no slipping constraint of the biped is presented in Figure 5.50. The Zero Moment Point (ZMP) of the biped must remain inside the support polygon during walking. This constraint is ensured in the optimization algorithm using the constraint equation (4.18), and can be calculated using (3.14) during the single support phase uniquely. The simulation results for

ZMP constraint are presented in Figure 5.50(a) for walking gait type 3 at walking speeds of 1.2 m/sec. Simulation results show that for all studies, ZMP is always inside the support polygon and is just below ankle axis.

The no-slipping constraint must be ensured during walking. The evolution of ratio of tangential force to normal force during a walking step of gait type 3 is presented in Figure 5.50(b) at walking speeds of 1.2 m/sec. The value of it should always be less than that of maximum allowable limit $\mu = 0.9$, which is the case in simulation results presented.

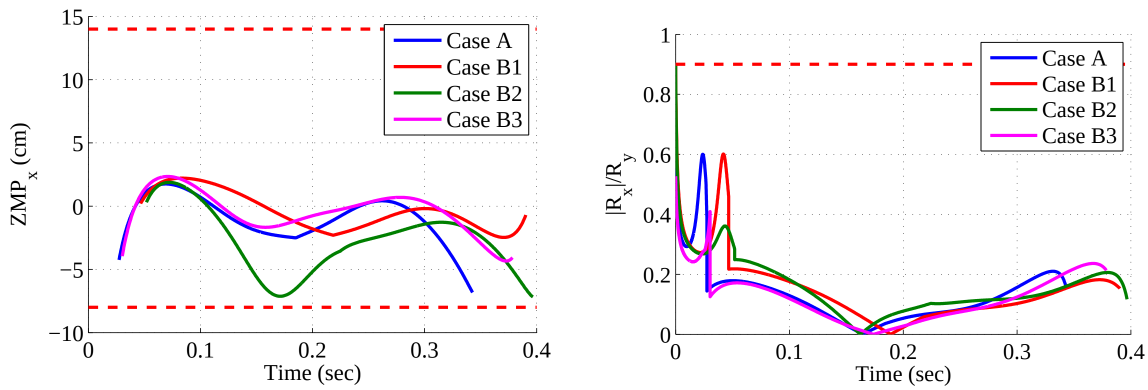

(a) ZMP (b) no slipping

Figure 5.50 – Evolution of ZMP and no-slipping constraint of gait type 3 at 1.2 m/sec

Evolution of CoG of the biped during a walking step is presented in Figure 5.51. It is observed that variations in amplitude of CoG are very small and that spring addition has no significant effects on the position of CoG of the biped in all cases.

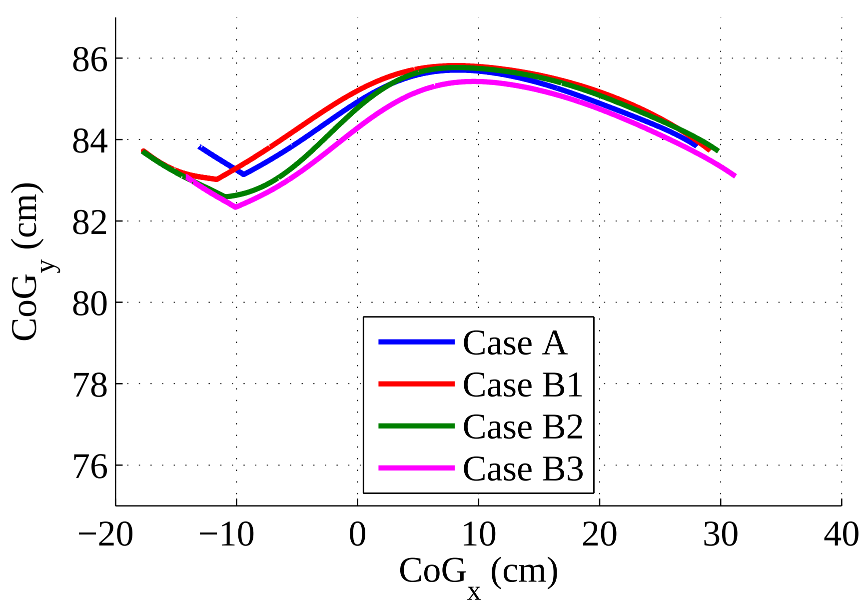

Figure 5.51 – Evolution of CoG of gait type 3 at walking speed of 1.2 m/sec

Duration of double support phase Tds_p in percentage of total time of a step is given in figure 5.52

as a function of walking speed for all studied cases. The duration of double support phase is an optimization parameter, and walking speed is a predefined value. Figure 5.52 shows that Tds_p is almost constant at slow walking speeds in cases 5.41(a) and 5.41(d) and it increases at high walking speeds. It can also be observed that Tds_p varies between 8% and 11% for these two cases. In case 5.41(b), duration of double support phase varies around 12%. Studies in bio-mechanics show that duration of double support phase is around 20% in human walking [116, 65, 121].

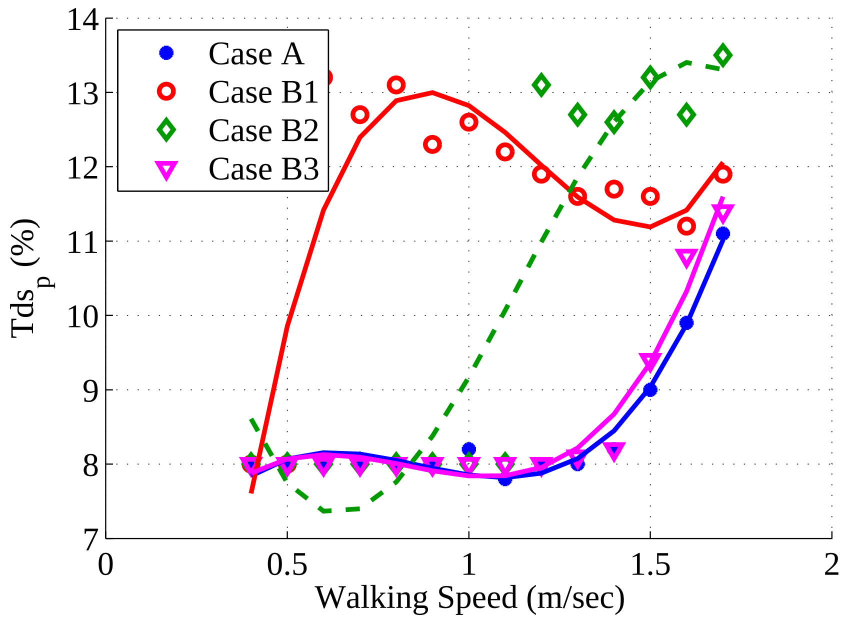

Figure 5.52 – Duration of double support phase in percentage of total time of step as a functions of walking speed for gait type 3

5.7 Simulation Results with Knee Locked

To study the effects of knee locking on walking gait type 3, the stance knee joint is locked during entire single support phase and then the gait trajectory is optimized. The locking mechanism is assumed to be massless and bidirectional. During locked mode, the joint torque is provided by the locking mechanism hence the torque of actuator is zero. Figure 5.53 presents the comparison of reference criterion for basic robot with that of knee locked. It is observed that at slow walking speeds the two curves are almost superposed while at high walking speeds knee locking is more costly. In contrast to previous results found in case of gait types 1 and 2, knee locking is not effective for gait type 3. Thus, it is concluded that gait type 3 does not support knee locking particularly at high walking speeds. Therefore, there is no need to lock knee joint for this gait.

5.8 Comparison of Studied Walking Gaits

Simulation results of three types of walking gaits were presented in this chapter. Figure 5.54 presents the comparison of selected criterion as a function of walking speed for basic biped for all studied walking gaits. It shows that cost of walking of the impactless gait with only single support phases is very high compared to other two gaits. However, the advantage of this gait is that is has

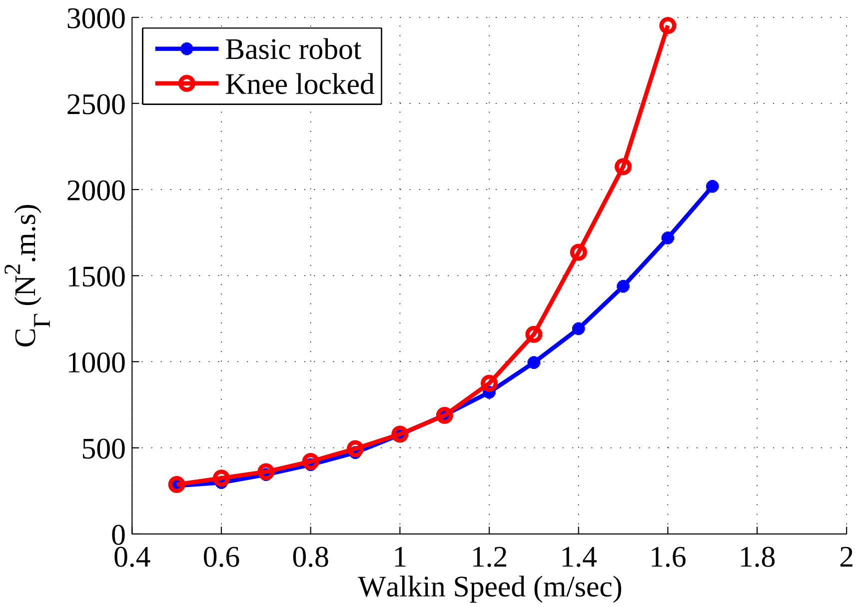

Figure 5.53 – Comparison of criteria of basic robot with knee locked for gait type 3

no impacts, which reduces the damages of the structure of the biped. It is also observed that energy consumed during a walking step for gait type 3 is significantly less than that of gait type 2 at high walking speeds. However, energy consumption of gait type 3 is slightly hight compared to gait type 2 at slow walking speeds. The criteria curves of both walking gaits intersects at around 0.9 m/sec. The low energy consumption of gait type 3 is due to the introduction of double support phase, which favors high walking speeds. Although it has slightly high consumption at slow walking speeds, but the gait is more anthropomorphic. It is also observed that impulsive impacts are significantly reduced compared to gait type 2 particularly at high walking speeds, thus having the advantages of impactless walking. Therefore, among the three studied gaits, the gait with finite double support (type 3) is the most realistic and human like.

5.9 Conclusion and Perspectives

In this chapter, three different types of walking gaits were studied and simulation results of each gait were presented. Three different studies on a seven-link bipedal robot were carried out for each gait type. First by adding torsional springs to different joints, second by mechanically locking the knee, and third by combining the two strategies *i.e.* locking the support knee and adding identical springs to different joints of the biped. The main focus of the study was to improve the energetic efficiency during walking of a bipedal robot.

Simulation results for walking gait with single support phases without impacts (type 1) show that the energy consumption of a biped during walking was significantly reduced by adding identical torsional springs at the hip joints and mechanically locking the knee. However, the maximum attainable walking speed was reduced to half in case where support knee joint was locked. In line with the previous research, this study reinforces the idea of using passive joint stiffness to improve energetic efficiency of the biped especially on the hip joints in our case. However, in contrast with previous work, ankle springs were not effective in for walking gait trajectories of type 1.

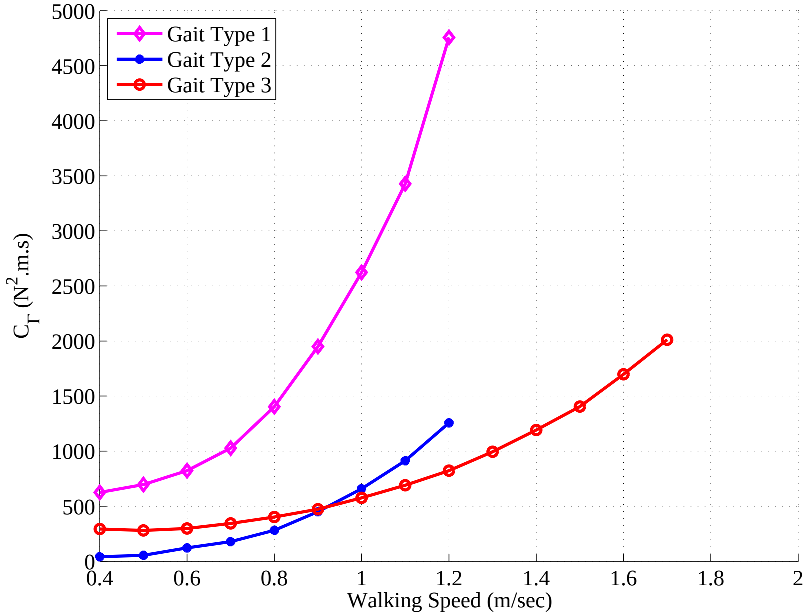

Figure 5.54 – Comparison of energy consumption of studied waling gaits at different walking speeds

In second part of this chapter, studies carried out on walking gait with single support phases and impulsive impacts (type 2) were described and then simulation results obtained using optimization algorithm were presented. Similar to gait type 1, it was concluded that the energy consumption of a biped during walking is significantly reduced by adding identical torsional springs at the hip joints and mechanically locking the support knee joint during the entire single support phase. In contrast to gait type 1, the maximum attainable walking speed was not reduced for cases with support knee locked. The presence of impulsive impacts at the end of each step allowed the biped to attain high walking speeds even if the support knee joint was locked.

A third type of walking gait, which is more complex and close to human walking was presented in the last part of this chapter. A number of tests were carried out to select the best possible mode of activation of springs to take maximum advantage of springs addition. Different studies with torsional springs in parallel to existing actuators at different joints of the biped were carried out and the results were presented. It was found that addition of springs at ankle, knee, or hip joints significantly reduce the energy consumption during walking when activated according to the selected mode. However, identical springs at a pair of joints when activated all the time during single and double support phases (mode 1) were not effective. In accordance with recent research [124, 99], ankle springs showed their effectiveness for gait type 3. It is also concluded that energetic efficiency is significantly increase when the trajectory is optimized alongside the spring stiffness compared to optimizing the spring stiffness alone. However, for this gait, the knee locking does not allow to improve the energetic efficiency during walking.

Finally, the selected criterion of the three studied gaits was compared. It was found that the impactless gait is the most energetically costly followed by gait type 2 at high walking speeds. The energetic cost of walking of gait type 3 is greater at slow walking speeds while less at high walking speeds than that of gait type 2. It was concluded that compared to other two gaits, gait type 3 is more realistic and human like.

In perspective of this study, the next step will be to explore the effects of springs and knee locking on more complex and human like walking gaits with foot rotation during single support phase on the energetic efficiency of bipedal robots. The effects of ankle springs and spring offset angle can also be studied for complex walking gaits. This study can also be extended to study the effects of proposed strategies on 3D bipeds.

6

Hydraulic Actuators

Contents

6.1 Introduction

One of the important and challenging issue in the field of robotics especially in humanoid robots is the design and selection of its actuating system. High performances in actuation are required to enhance energetic efficiency and stability of these systems. One of the possible and interesting aim of humanoid research was to build better orthosis and prosthesis for human beings. A few examples are: powered leg prosthesis for gait rehabilitation [35], ankle-foot orthosis [19, 50], dynamic knee-ankle-foot orthosis [63, 33], and forearm prosthesis. In the future, humanoid robots are expected to be integrated in human environment to perform human tasks like personal assistance, where they should be able to assist the sick and elderly people, and do dangerous jobs that can not be done by humans or too risky for them. To integrate robots into human environment, they should be safe and human friendly. For instance, in the field of humanoid robotics, essential and desirable properties for actuators are: (1) high power to mass ratio; (2)

ability to produce high torque at low speed; (3) highly integratable (reduction of occupied volume); (4) able to generate smooth joint motions resulting in human-like walking movements.

Generally, two main types of actuation Electric and Hydraulic are used to actuate robotics systems such as humanoid robots. The advantages of electric actuators overs its counter parts is that they have reduced cost and maintenance, and are easy to use and control. However, a number of disadvantages appear when electric motors are used with mechanical reduction gear box. First of all, due to the quasi-rigid connection between the motor and its payload, it is difficult to produce compliance in the joint required for safety. To introduce compliance in the joints, Hogan et al. developed an impedance control method to ensure compliant interaction with the environment [59]. On the other side, series elastic actuators are added to enable joint compliance [103, 92, 93].

Addition of mechanical components (passive or active) to achieve compliance in joints, leads to a substantial increase in size and complexity of the mechanical system. Although, a high gear box reduction ratio has to be chosen to have high joint torques, it is always limited and cannot be increased indefinitely, which is clearly a limitation of electric actuators [6]. Finally, electric actuators have to be sized for the worst case scenario, defined by satisfying the instantaneous highest torque required. This leads to a non-optimal over-sized electric actuator, which will not be used all the time at its full capacity.

Hydraulic and pneumatic actuators have been used for decades in the industry for heavy loads. Their applications include, but not limited to, lifting cranes, excavators, hydraulic presses, and braking systems etc. Recently, the use of these actuators significantly increased in field of robotics particularly humanoid robotic systems due to their exceptional performances and high power to weight ratio. A central pumping or pressure unit called "central hydraulic block" is used to provide required pressure to each actuator to produce desired motion. One huge motor-pump is usually used to produce the pressure and the flow necessary to actuate several joints. One of the drawbacks of central hydraulic block is the whole system dimensioning, which leads to the necessity of satisfying the worst case requirements in terms of flow and pressure needed by all joints of the robot. Another disadvantage is the increased size and weight of the system, due to the need of including a servo-valve for each hydraulic actuator. Therefore, central hydraulic blocks have limited mobility, which drastically limits their use in autonomous robotic systems. Other drawbacks include routing of the hydraulic tubes passing through the joints required to connect the actuator to the central block, which increases the chance of potential leakage and consequent pressure drops.

To overcome the above mentioned problems, and fulfill the requirements of bipedal robots, a high performance Integrated Electro-Hydraulic Actuator (IEHA) has been developed by S. Alfayad et al. [6, 7], which uses displacement of a micro valve to control hydraulic motor. The newly developed hydraulic actuator is a light weight solution satisfying all the performances needed for actuating a humanoid robot [3]. Advantages of IEHA include, but are not limited to, 1) Light weight, 2) complete actuator including micro hydraulic pump, 3) energy storage function, and 4) no central pumping system required.

The new Integrated Electro-Hydraulic Actuator (IEHA) has an integrated reservoir in which energy can be stored in the form of hydraulic pressure in order to optimize the power consumption of the joint. It is based on the use of the duty cycle phenomenon to store energy whenever no motion is needed on the joint [6, 7]. This energy will be used when it is needed resulting in a smaller actuating system. Hence, the energy consumption can be reduced during walking or performing manipulating tasks.

In this chapter, hydraulic actuators will be introduced and its different parts will be explained. Working principle of a classic hydraulic actuator will be presented with mathematical expressions. A newly designed high performance integrated electro-hydraulic actuator will be presented and its advantages over its counterparts will be enlisted. The simplified model of the actuator will be presented and its different parts will be explained in detail. The exploded CAD schematic of the actuator will also be presented to have an overview of different parts of the actuator.

The working principle of the IEHA will be explained with the help of its hydraulic schematic diagram. Its different working modes will be elaborated. The energy storage function, which is one of the main advantage of this actuator will be presented. Mathematical expressions for energy balance in hydraulic actuators will be developed, and the stored energy and energy available to the during different working stages will be calculated. Finally, different cases of power consumption of an actuator during its working cycle will be explained and generalized storage function will be developed, and the chapter will then be concluded.

6.2 Hydraulic Actuators

Hydraulic actuators are normally used when a large amount of force is required to operate a link. Hydraulic power is used in these actuators and then converted in mechanical power to carry out some work. Pneumatic actuators belong to the same family, which uses compressible fluid such as air for their operation instead of incompressible fluid such as oil used in hydraulic actuators [49].

A typical piston-type actuator is shown in the Figure 6.1. It consists of a cylinder, piston, supply and return lines, and direction and pressure regulating valve. The difference between the pressures P in two different chambers results in a relative pressure, which produces a force F in a given surface S, which yields $F = PS$. The pressure is the input quantity, performing the same function as the current in electro-mechanical actuators. For complete modeling and details please refer to [49].

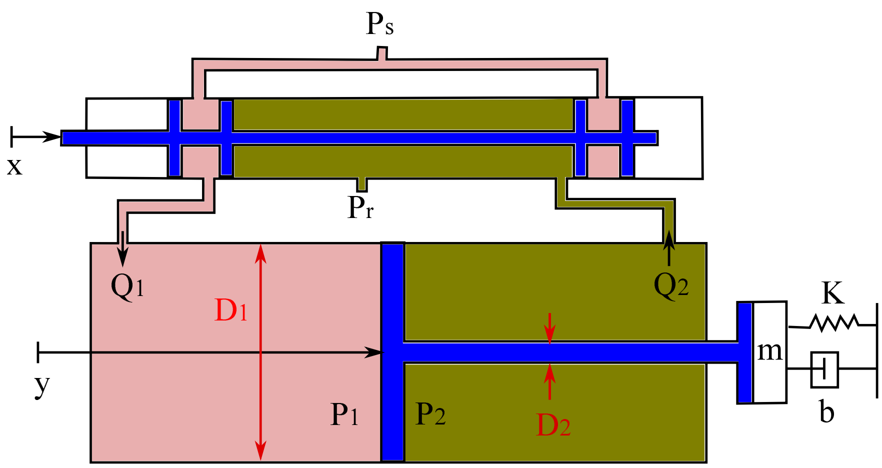

Figure 6.1 – Schematic diagram of a hydraulic actuator [49]

6.2.1 Working Principle

The piston or plunger of a hydraulic actuator operates in a cylindrical housing by the action of liquid under pressure. In a piston cylinder, a piston rod is connected to a piston to actuate a load (link in case of robotics). The amazing amount of force a cylinder exerts is due to the simple mechanical principle of pressure exerted on the surface area of the piston. The larger the diameter of the cylinder, the greater the capability of force it can apply. The hydraulic supply (Q_1) and return (Q_2) line is connected to the lower chamber and allows hydraulic fluid to flow to and from the lower chamber of the actuator.

The cylinder force can be expressed as $F = P_1A_1 - P_2A_2$ where P_i is the pressure in the chamber i and A_i is the effective section of the piston. It can be expressed as:

$$F = P_1\frac{\pi}{4}D_1^2 - P_2\frac{\pi}{4}(D_1^2 - D_2^2) \tag{6.1}$$

Since the section is different, therefore the force performed by the cylinder in steady-state conditions depends on whether the movement is done forward or backward. Assuming $P_2 = P_r = 0$ and $P_1 = P_s$, the forward force can be expressed as:

$$F_f = P_s\frac{\pi}{4}D_1^2 \tag{6.2}$$

Assuming that $P_2 = P_s$ and $P_1 = P_r = 0$, the backward force can be calculated as:

$$F_b = P_s\frac{\pi}{4}(D_1^2 - D_2^2) \tag{6.3}$$

The HYDROiD robot [5] is equipped with Integrated Electro-Hydraulic Actuator (IEHA). This new family of actuation is designated by integrated hydraulic actuation. The idea for this type of actuation is based on the capacity to produce hydraulic pressure for each liaison using an electric motor, independently of the others. An electric motor drives a micro-hydraulic pump of variable volumetric flow rate and is controlled electrically [6, 7]. Thus the central system to produce required pressure is completely integrated into the two elements, which form the link. The difference between IEHA hydraulic actuation system and the currently used systems is that it is a complete pressure producing unit installed on each joint, and is independent of the other joints. Generally, most of the present robots having hydraulic actuation are equipped with a central hydraulic system, and all the articulations depend on that unit.

Thanks to the high power density of hydraulics, actuator can easily produce the necessary torque for each link. The hydraulic modules installed on the HYDROiD robot allow to store and release energy during the gait cycle. This energy storage capacity of the system is exploited to obtain walking movements with a reduced energy consumption. The results described in this section focus on modeling, simulation and design function of storage of energy in the actuator and its use in the performance of cyclic walking of the HYDROiD.

6.3 Integrated Electro-Hydraulic Actuator (IEHA)

As discussed above, the Integrated Electro-Hydraulic Actuator (IEHA) is a new type high performance hydraulic actuator developed by S. Alfayad et al. [6, 7] intended to be used in robotics applications. According to the designers and developers of this actuator, their aim is to take advantage of the high power to mass ratio present by hydrostatic transmission systems. The basic idea and novel challenges in developing IEHA, concerns the integration of all required components in the smallest space possible while simplifying the control of the actuator. The proposed solution fulfills all these requirements using an unidirectional integrated micro-pump driven by an electric motor, which rotates at a constant speed. The micro-pump is connected through built-in reservoirs to a standard linear (non-symmetric) or rotary actuator. The design specific actuator and use of sophisticated control strategies are not required for the use of IEHA, which leads to reduction of its total cost, and hence making it attractive for robotic applications. Some of the main advantages of IEHA over its counterparts include:

- Light weight and highly integratable
- Central hydraulic system is not required
- Less hydraulic tubing
- No dead zone
- Simple control

6.3.1 IEHA Simplified Model

The simplified model of IEHA is shown in Figure 6.2. It is worth mentioning here that the diagrams and description presented in this section is taken from the original work published in [3, 5, 6, 7]. The shaft C_1 is connected to electric motor, which rotates at high angular velocity Ω. The pistons C_2 rotate with the shaft and slide on an inner roller bearing part, which is itself inserted in a carriage C_3. The distance E between the bearing and the shaft centers, called eccentricity, produces radial movement of the pistons C_2. This allows the pistons to aspirate liquid when moving away from the center and send it out when moving toward the axis of the shaft.

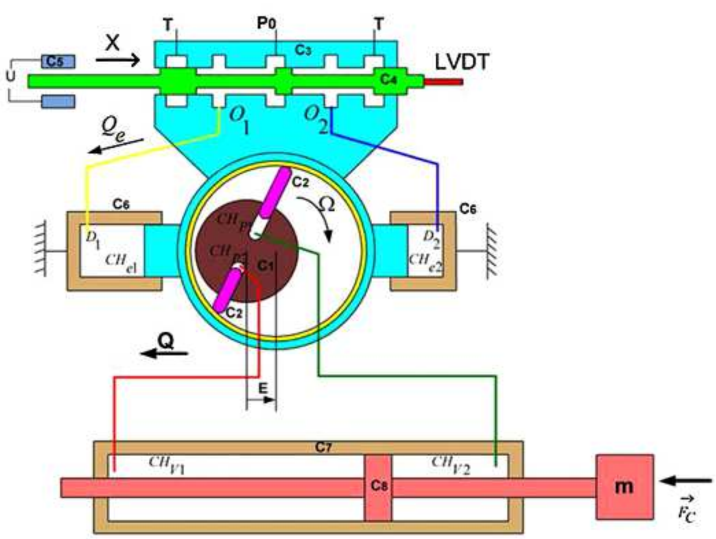

Figure 6.2 – IEHA simplified model [7]

The pressure and discharge produced by this phenomenon depend on eccentricity E. Increasing E will increase the flow and hence the hydraulic power produced by the pump. A constant value of E will maintain the flow constant and will increase the pressure. Changing the direction of the link motion can be obtained by using negative values of E while keeping the same direction of rotation of the electric motor. Hence, this will simplify the control of electric motor, as one of advantages of the IEHA. It is obvious that changing E will allows one to carry out both isometric and isotonic modes as described in section 6.3.3.

In the Integrated Electro-Hydraulic Actuator (IEHA), the eccentricity E is hydraulically controlled with the help of a micro-valve C_4 built inside the carriage C_3. This micro-valve C_4 is electrically actuated by an integrated induction coil C_5, which decides the position of micro-value to regulated hydraulic flow for the adjustment of eccentricity. Activating the coil will move the micro valve to the right permitting the high pressure P_0 to be connected to the left side of the carriage C_3. The low pressure T will be connected to the right side of the carriage C_3. Consequently, the carriage C_3 will move to the right, which will change the value of E. Therefore, this integrated actuator can be considered as a continuous transmission ratio varying system allowing to adjust the amount of power when needed. Figure 6.3 presents the CAD schematic diagram of the proposed IEHA.

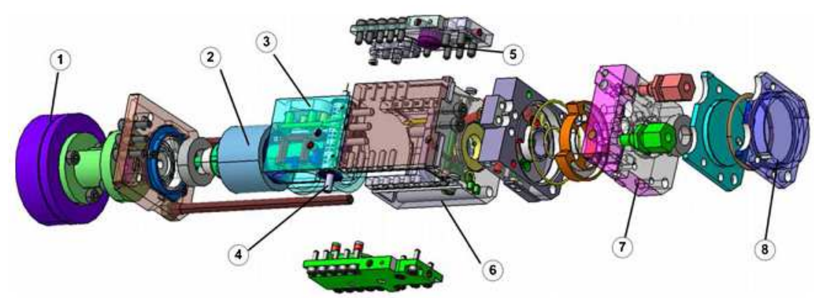

Figure 6.3 – IEHA CAD schematic diagram [6]

The integration of the micro-valve C_4 on the carriage C_3 gives a mechanical feedback. To illustrate this feedback, if at instant t_0, the micro valve moves to position X, then the distance between the carriage and the micro-valve will be $(X - E_0)$ (where E_0 is the eccentricity at t_0). This distance will permit connecting pressures P and T to the carriage making it to follow the micro-valve. Consequently, the distance between the micro-valve and the carriage $(X - E(t))$ will decrease until reaching zero. At this instance, the two lines T and P are completely disconnected from the two sides of the carriage. Hence, the carriage will be locked at a desired eccentricity E from the shaft center.

6.3.2 IEHA Working Principle

To explain the working of IEHA, its hydraulic scheme is detailed in Figure 6.4. Depending upon the pressure difference between line A and B, the passive distributor S takes one of three positions called, S_1, S_2 and S_3. If the pressure, in the line A, noted by P_A, is smaller than that in the line B, named P_B, the distributor takes the position S_1. In this position, the right chamber of the actuator linked to the segment of the robot, is connected to the atmospheric reservoir R. Line A is connected to a reservoir R while line B is connected to the left chamber of the actuator through line P. This activates the piston of the actuator to move to the right.

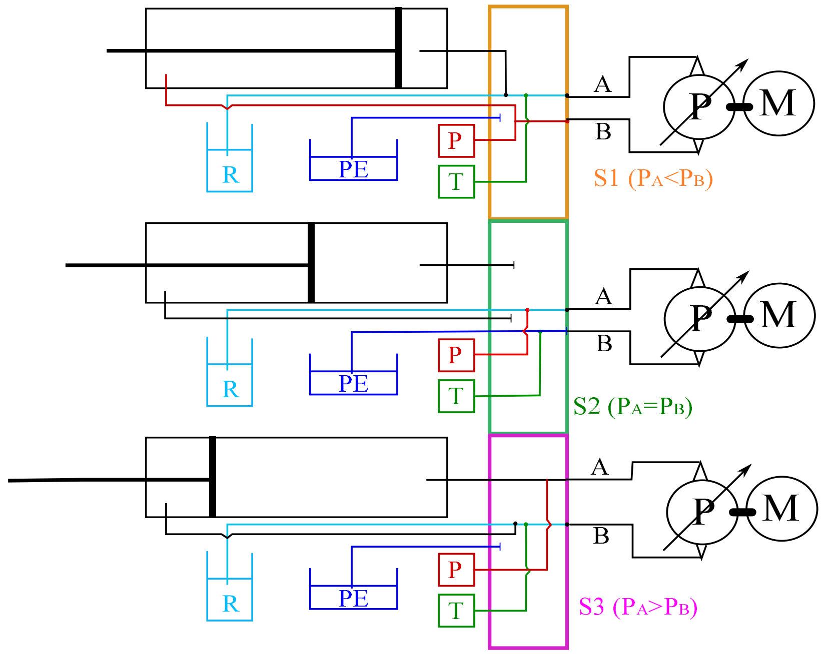

Figure 6.4 – IEHA hydraulic schematic diagram [6]

In position S_3, the role of lines A and B is reversed leading to motion generation of the actuator to the left. In the position S_2, both pressures P_A and P_B are equal and the payload represented by the actuator is completely disconnected from the micro-pump stage. Hence, the actuator keeps the same position without theoretically consuming any energy. In fact, it will only be necessary to compensate for the possible leaks, which would exist between both chambers of the actuator.

The passive distributor is non-symmetric rotary, thus allowing to have different durations whenever switching from position S_1 to S_3, and vice versa. Switching from S_1 to S_3 is designed such that it will take slightly more time than from S_3 to S_1, allowing to draw out the internal leakages present in the internal space where a pressure P_E occurs and to bring them to the reservoir R. On the other hand, as the passive distributor changes its position according to the difference between the pressures P_A and P_B, two lines, P and T can be added to the distributor outputs such that the line P is always connected to the high pressure while line T is linked to the reservoir R. Both lines P and T will be used to feed the micro-valve, making the IEHA completely autonomous, and enhance its high level of integration.

The position S_2 is an instantaneous one in which P_A and P_B are almost equivalent. In this position, the hydraulic actuator does not move (isometric mode), and its connections are almost locked. In this case, the lines A and B are connected to R and the P_E reservoirs respectively. Some offset is set in one direction allowing the distributor S to switch from S_1 to S_3 by passing through S_2 position. In this case, the pump will aspirate the leakage from reservoir P_E, and will deliver it to reservoir R. This phenomenon takes very short time and permits the system to reinsert all the liquid produced by the leakage in the hydraulic circuit.

6.3.3 Energy Storage in IEHA

Energy can be stored in hydraulic actuators during two types of link operation, first one is the *isometric* position when the link configuration is fixed ($\dot{q} = 0$), and the second one is the *isotonic* operation when the force applied is constant. In this study, isometric operation of the support knee joint will be used by locking the knee joint. Energy will be stored during the lock configuration and then re-utilized when needed during swing phase.

6.3.3.1 Normal Mode

The mode of energy storage is activated using a two-position distributor D. The first position corresponds to normal operation for which the pressure sent to the hydraulic actuator is instantaneously produced by micro-hydraulic pump. In normal functioning mode, the distributor S is either in position S_1 or S_3. Both positions of the distributor are previously explained in section 6.3.2. Further details of normal functioning mode can be found in [3].

6.3.3.2 Storage Mode

The second position of the distributor D is utilized when the link does not need to be moved (e.g. isometric mode). In this position, energy is stored in an integrated hydraulic reservoir of the IEHA whose connections are blocked. This position corresponds to S_2 as discussed in 6.3.2. Thus, the pump serves to increase the pressure in a reservoir to be used later during swing phase. This feature allows one to choose a smaller electric motor for the micro-hydraulic pump, thereby reducing the total weight of the system and increasing its autonomy. The storage mode can be activated during support phase for example for knee joint, which can be locked easily. The stored energy can be used for the same joint during swing phase by switching back to normal mode. Thus the energy available to the actuator will be the sum of stored energy during locked mode and energy produced by the micro-hydraulic pump during normal mode.

6.3.4 Energy Balance in Hydraulic Actuator

The energy required at each link will be represented by E_l and can be calculated for a cycle time of T such that:

$$E_l = \int_0^T |\Gamma(t)\dot{\theta}(t)|\mathrm{d}t \tag{6.4}$$

It is to be noted that energy must be provided in both phases of acceleration and braking that can not be recovered, which justifies the presence of the absolute values.

During isometric phases ($\dot{\theta} = 0$) of the links, the hydraulic actuators make it possible to lock the links resulting in no consumption of energy during lock phase. By introducing the number of useful phases ($\dot{q} \neq 0$) N_u, the required energy during a cycle can be written as:

$$E_l^u = \sum_{i=1}^{N_u} \left(\int_{t_i^s}^{t_i^f} |\Gamma(t)\dot{\theta}(t)|\mathrm{d}t \right) \tag{6.5}$$

where t_i^s is the start and t_i^f is the end of an useful phase i and $\dot{q} \neq 0$.

In the simplified case, when a joint is locked during the entire swing or support phase (half cycle), energy required is given by:

$$E_l = \int_0^{T/2} |\Gamma(t)\dot{\theta}(t)| \mathrm{d}t \tag{6.6}$$

This energy must be produced by the hydraulic actuator that has an electric motor, which rotates at a speed of $\Omega(t)$ and produces a motor torque $\Gamma_m(t)$. The energy input to the system is then defined by E_e whose expression is:

$$E_e = \int_0^{T} \Gamma_m(t)\Omega(t) \mathrm{d}t \tag{6.7}$$

Now, let ρ be the global efficiency of the actuation mechanism, and let suppose that there is no energy loss, then the energy balance can be written as:

$$E_e = \frac{1}{\rho} E_l^u \tag{6.8}$$

6.3.5 Stored and Available Energy

The ability of the hydraulic actuator to store energy in a reservoir will allow it to provide required energy that can not be provided by the actuator alone. Let T_s be the storage time during which the hydraulic actuator stores energy to be used during useful phases. The expression for T_s can be written in the form:

$$T_s = T - \sum_{i=1}^{N_u} \left(t_i^f - t_i^s \right) \tag{6.9}$$

The constant angular velocity Ω of the motor will ensure constant power at the input of the actuator. Consequently, motor torque Γ_m will also be constant. Therefore, the energy stored by hydraulic actuator can be expressed as:

$$E_s = \Gamma_m \omega T_s \tag{6.10}$$

To optimize the system operation and get closer to the goal of constant and minimum power supplied by the electric actuator located at the input of the hydraulic converter, the extra energy needed should be provided locally by this stored energy. One part of the required energy is being produced directly by the hydraulic actuator.

6.4 Modeling of Energy Storage Function in IEHA

6.4.1 Storage Function of Hydraulic Actuators

As the newly developed hydraulic actuator has an integrated reservoir to store energy, therefore the objective of the study is to define the actuator with a minimum capacity to produce desired torque by exploiting the energy storage capabilities of the actuator. As the motor driving hydraulic actuator rotates at constant speed, its optimal use corresponds to a constant power requirement. To evaluate the power required, the power supplied by the actuator is traced at every instance of time $|\Gamma(t)\dot{\theta}(t)|/\rho$. Figure 6.5 shows a working cycle of a joint having constant power requirements during the entire cycle. In humanoid robots, this case be found very rarely.

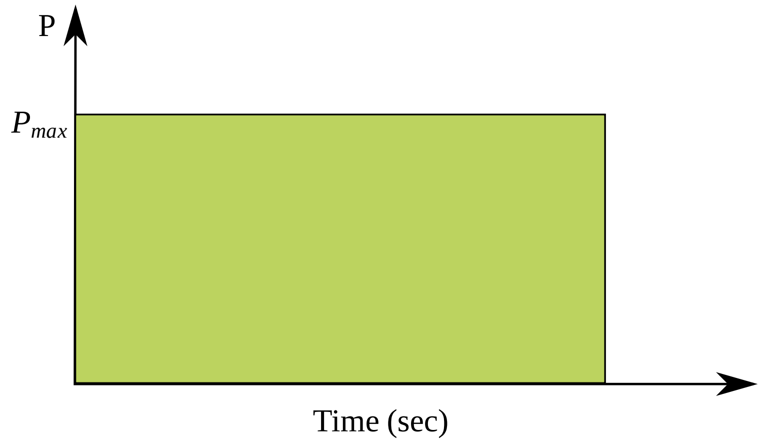

Figure 6.5 – Schematic diagram of constant power consumption

Two extreme cases can be distinguished during a complete working cycle of a joint. First, if there is no isometric phase, then it is not possible to store energy. In this case, if power consumption is not constant, the actuator must be dimensioned for maximum power requirements. During all stages where the maximum power is not used, the difference between the maximum power and power consumption is lost. Figure 6.6 represents the first case where power requirements varies during the working cycle and there is no isometric phase. In this case, the actuator is designed for the worse case to be able to provide maximum power (P_{max}) at any instant of time. This is the case in most of the robotic system, which uses electric motors for actuation.

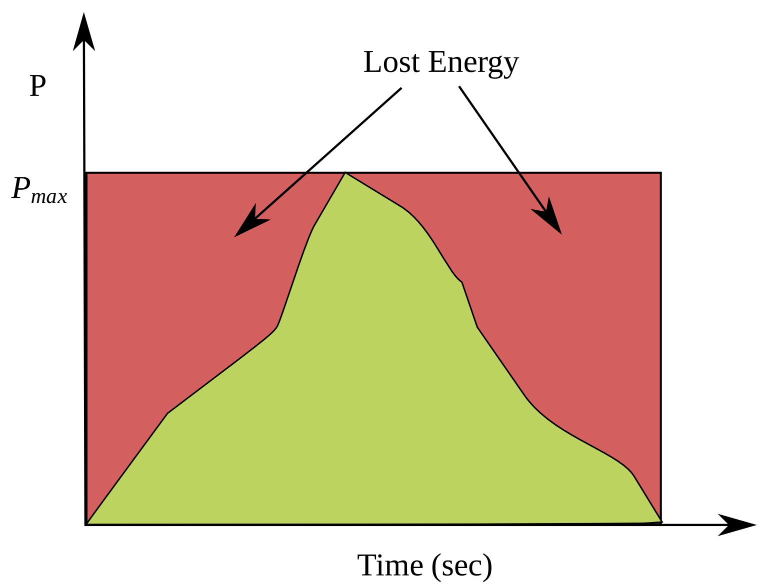

Figure 6.6 – Schematic diagram of variable power consumption

The opposite case is that during most of the cycle time T_s, the link is in an isometric configuration ($\dot{\theta} = 0$) with a short duration at the end where high power is required and consumed. In the isometric phase, the energy defined by equation (6.10) will be stored as represented in green in

Figure 6.7. This stored energy E_s will be returned to the system when needed. At the end of the period, between time $T - T_s$ and T, the energy available is that produced by the actuator, which is $\Gamma_m \omega (T - T_s)$ (android green) plus the stored energy E_s (green) (see Figure 6.7). It is to be noted that during a complete cycle, the stored and re-used energy must be equal to minimize lost energy.

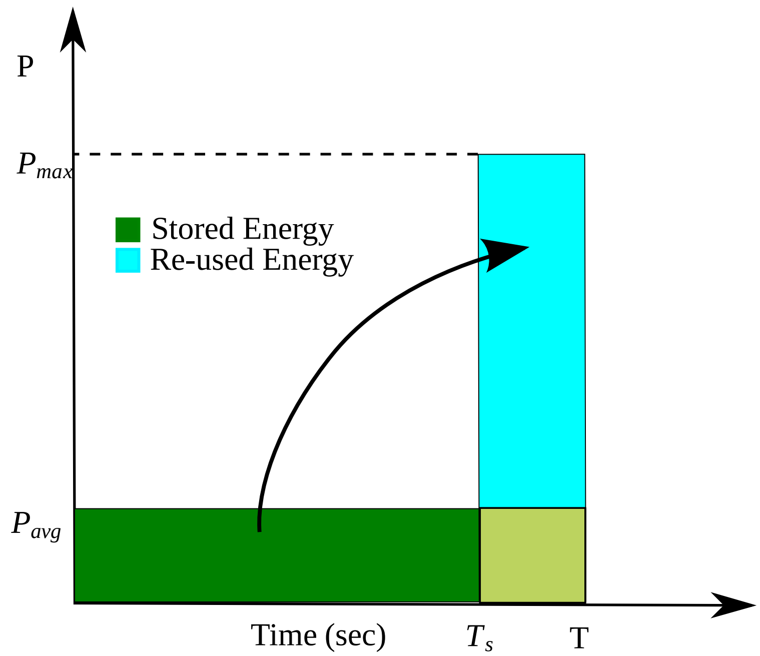

Figure 6.7 – Schematic diagram of power consumption with storage during major part of the time and then released during a short phase with high power demands

In Figure 6.7, the instantaneous available power provided by the actuator $P = \Gamma_m \omega$ is assumed to be constant during normal working mode, and available at any time. This can be determined based on the energy balance equation (6.8) such that:

$$|\Gamma(t)\dot{\theta}(t)| = \frac{\Gamma_m \omega T \rho}{(T - T_s)} \tag{6.11}$$

Now, for a known energetic consumption of $|\Gamma(t)\dot{\theta}(t)|$ corresponding to Figure 6.7, the required actuator torque can be calculated as:

$$\Gamma_m = \frac{|\Gamma(t)\dot{\theta}(t)|(T - T_s)}{\omega T \rho} \tag{6.12}$$

It may be noted that the design of the actuator is done on the basis of average power (P_{avg}) required and not on maximum power (P_{max}) required. In this case, the difference in actuator size is significant compared to that if it was designed for maximum power.

6.4.2 Generalization of Storage Function

During bipedal walking, the required joint torque is normally not constant and varies between minimum and maximum values. The power requirements of a joint in most common case is shown in Figure 6.8. It is based on the hypothesis of cyclic motion and the energy storage phase is assumed to be at the end of the step. Generally, during a complete cycle, the maximum power is required for a short period of time. It is important to note that the presence of energy storage phase $(T - T_s)$ reduces the maximum power that the actuator must produce. The output power P_m for the design of actuators is less than P_{max}, but the energy lost (brown area) is not zero. Motor design is done in such a way to ensure that the stored energy (green area) is used when the energy can not be made available directly by the hydraulic actuator. In stages of high demand, a part of energy is supplied directly by the actuator (android green area) and the rest of the energy is recovered from the stored energy (aqua blue area). The surface of the aqua blue area (re-used energy) is equal to the surface of the green zone (stored energy).

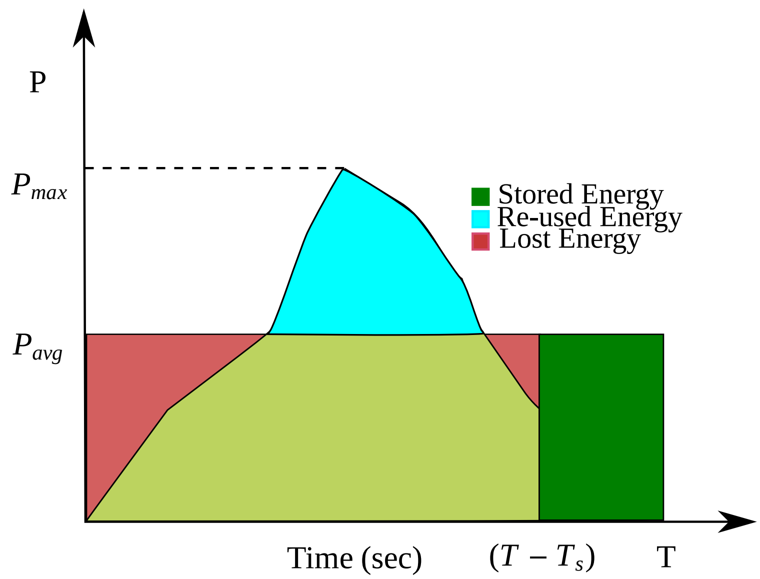

Figure 6.8 – Schematic diagram of power consumption with storage at the end of the cycle

For a given trajectory of the actuated joints, which may contain isometric phases ($\dot{\theta} = 0$), the minimum power of the actuator $P = \Gamma_m \omega$ should satisfy:

$$PT_s = \int_0^T max(0, |\Gamma(t)\dot{\theta}(t)|/\rho - P)\mathrm{d}t \tag{6.13}$$

Equation (6.13) gives equality between stored (green area) and re-used (aqua blue area) energy presented in Figure 6.8. One can easily verify that this general formulation describes well the two special cases initially described. In case where there is no storage of energy then $T_s = 0$ and the equation (6.13) can be written as:

$$P = max(|\Gamma(t)\dot{\theta}(t)|/\rho) \tag{6.14}$$

For a very special case in Figure 6.7, where energy storage is active from $t = 0$ to $t = T_s$, and $|\Gamma(t)\dot{\theta}(t)|$ is constant during the time $t = T - T_s$, the integral becomes:

$$\int_0^T max(0, |\Gamma(t)\dot{\theta}(t)|/\rho - P)\mathrm{d}t = \int_{T_s}^T max(0, |\Gamma(t)\dot{\theta}(t)|/\rho - P)\mathrm{d}t = (T - T_s)|\Gamma(t)\dot{\theta}(t)|/\rho - (T - T_s)P \tag{6.15}$$

The above equation can be solved for P such that:

$$P = \frac{(T - T_s)}{T}|\Gamma(t)\dot{q}(t)|/\rho \tag{6.16}$$

6.4.3 Optimization Criterion of Hydraulic Actuators with Energy Storage

The criterion used in the optimization algorithm is based on the actuators energy. It is used to optimize the trajectory, which minimizes the actuators effort to take one step *i.e.* cover a distance d for a motion on a half cycle of duration T. Equation (6.17) shows energy optimization criterion for a biped with electric actuators. Its calculation is based on the definition of cyclic gait trajectory, which is repeated every walking step. Therefore, only one cyclic step will be optimized and its energetic cost will be calculated.

$$C_E = \frac{1}{d}\int_0^T |\mathbf{\Gamma}(t)|^{\mathrm{t}}|\dot{\boldsymbol{\theta}}(t)|\mathrm{d}t \tag{6.17}$$

Where C_E is the objective function to minimize, $\mathbf{\Gamma}$ is the vector of joint torques, and $\dot{\boldsymbol{\theta}}$ represents the joints velocity vector.

The biped HYDROiD studied in this chapter is equipped with IEHA. The electric motor of the hydraulic actuator driving the micro hydraulic pump runs at a constant angular velocity to provide required power at a link. It should provide all the time the maximum instantaneous power required by the link. When the required power is less than maximum, the rest of the energy is lost. The motor consumption in this case is based on the maximum instantaneous power required. Therefore, the optimization criterion for the studied biped without energy storage can be expressed as:

$$C_{max} = \frac{1}{d}\sum_{i=1}^{n}(max(|\Gamma_i(t)\dot{\theta}_i(t)|)T) \tag{6.18}$$

Where Γ_i is the joint torque, $\dot{\theta}_i$ is the angular joint velocity of link i, d is the distance traveled in one step, T is the duration of the step, and n is the number of joints of the biped. The above criterion is valid for any biped equipped with classical hydraulic actuators driven by electric motors running at constant angular velocity.

In case of energy storage, it can be shown that the energy used by the electric motor driving the micro pump is given by the following criterion:

$$C_S = min(\frac{1}{d}\mathbf{P}\ T) \tag{6.19}$$

under the following constraint

$$P_i T_{is} = \int_0^T max(0, |\Gamma_i(t)\dot{\theta}_i(t)| - P_i)\mathrm{d}t \tag{6.20}$$

Where P_i is the motor power of joint i, $\mathbf{P} = [P_1, ..., P_n]$, T is step time and T_{is} is the time for which the articulation i was locked and energy was stored.

The objective is to minimize the optimization criterion C_S by finding the optimal values of optimization parameters X_0 under non-linear constraints, and polynomial function of degree four as basis of motion. The optimization problem is formulated as follows

$$\begin{cases} \text{Minimize} & C_S(X_0) \\ \text{Subject to} & g_j(X_0) \leq 0,\ j = 1, 2, ..., l \end{cases} \tag{6.21}$$

Where $C_E(X_0)$ is the objective function to minimize with l constraints $g_j(X_0) \leq 0$ to satisfy.

6.5 Conclusion

In this chapter, a classical piston-cylinder type hydraulic actuator was presented and its working principle was explained. Then a more complex newly designed integrated electro-hydraulic actuator was introduced and its advantages over its counterparts were enlisted. Different parts of the IEHA were detailed with the help of schematic and CAD diagrams and their working was explained. The energy storage capabilities of IEHA were explored and its different working modes (normal mode and energy storage mode) were discussed. Finally, mathematical expressions for energy balance in hydraulic actuators were developed, and a generalized expression of the power produced by the actuator by using the energy storage function during working cycle was proposed. Furthermore, optimization criterion for hydraulic actuators with storage function was presented.

7

Effects of Hydraulic Actuators on 2D Bipedal Walking

Contents

7.1 Introduction

In previous chapter, hydraulic actuators were presented and a special type of Integrated Electro-Hydraulic Actuator (IEHA) was introduced. Energy storage in IEHA and different working modes were also explained. In this chapter, energetic effects of hydraulic actuators and energy storage will be studied on different walking gaits of a bipedal robot. The goal is to develop a number of methodologies for this specific actuator that will improve the energetic efficiency of the studied biped during walking. This chapter is dedicated to IEHA, therefore, effects of springs on bipedal walking will not be covered.

The objective of the study is to compare the performance of knee locking and energy storage on different walking gaits. The performance criterion used in this chapter to compare different gaits is based on actuators energy and is different from that used in chapter 5. To compare performance of the gaits, optimal walking gait trajectories will be generated for gait types 2 and 3. Gait type 1 will not be studied in this chapter due to its high walking cost and resemblance with gait type 2.

Simulation results obtained from optimization algorithm for each type of gait will be presented at different walking speeds. Effects of knee locking and energy storage on consumption of energy during walking of different cyclic walking gaits will then be compared. Similarly, effects of walking speed on step length, time, CoG, ground reaction forces and other parameters will also be discussed.

7.2 Studies Carried out

Different types of studies will be carried out on both walking gaits studied in this chapter to analyze the energetic performance of the biped. A number of different methodologies used to improve energetic performance during walking are:

case A. The robot trajectories are optimized and energetic cost of walking is calculated without knee locking.

case B. Support knee is locked at impact and remains locked during the entire single support phase.

- **case B1.** Stance knee is locked without possibility of energy storage and locking angle (β) is optimized along with trajectory optimization.
- **case B2.** Stance knee is locked with possibility to store energy which can be used during swing phase and (β) is optimized along with trajectory optimization.
- **case B3.** Based on the numerical values obtained in case **B2**, a constant value of β is selected and then the gait is optimized.

7.3 Optimization of Walking Gait with Impact

The walking gait with impulsive impacts is the gait type 2 presented in section 3.3.2. A cubic spline function with one intermediate passage point is used to generate walking gait trajectories. All the optimization constraints and optimization variables presented earlier for gait type 2 apply to this gait as well. The only change is the optimization criterion which is calculated considering hydraulic actuators.

7.3.1 Simulation Results

In this section, simulation results for walking gait type 2 (see section 3.3.2) with hydraulic actuators will be presented. A number of walking gait trajectories at different walking speeds will be generated and optimized using reference trajectory generation and optimization techniques presented earlier. Simulation results for walking speeds of $0.5m/s$ will be presented and then the effects of different studies (see section 7.2) will be compared. Energy consumption during walking, and other parameters like gait trajectory, ZMP, CoG and ground reaction forces etc will also be discussed and compared.

Figure 7.1 shows a walking step stick diagram of the biped under study at walking speed of 0.5 m/sec for all studied cases. It can be observed that the step length is approximately the same in all four cases. The posture and joint trajectory of basic robot (see Figure 7.1(a)) is largely different than that of other three cases with support knee locked. A clear difference in the height of foot 2 during swing phase can be observed.

Figure 7.2(a) presents the comparison of criteria curves as a function of walking speed for all studied cases. Simulation results show that the most effective method to reduce energy

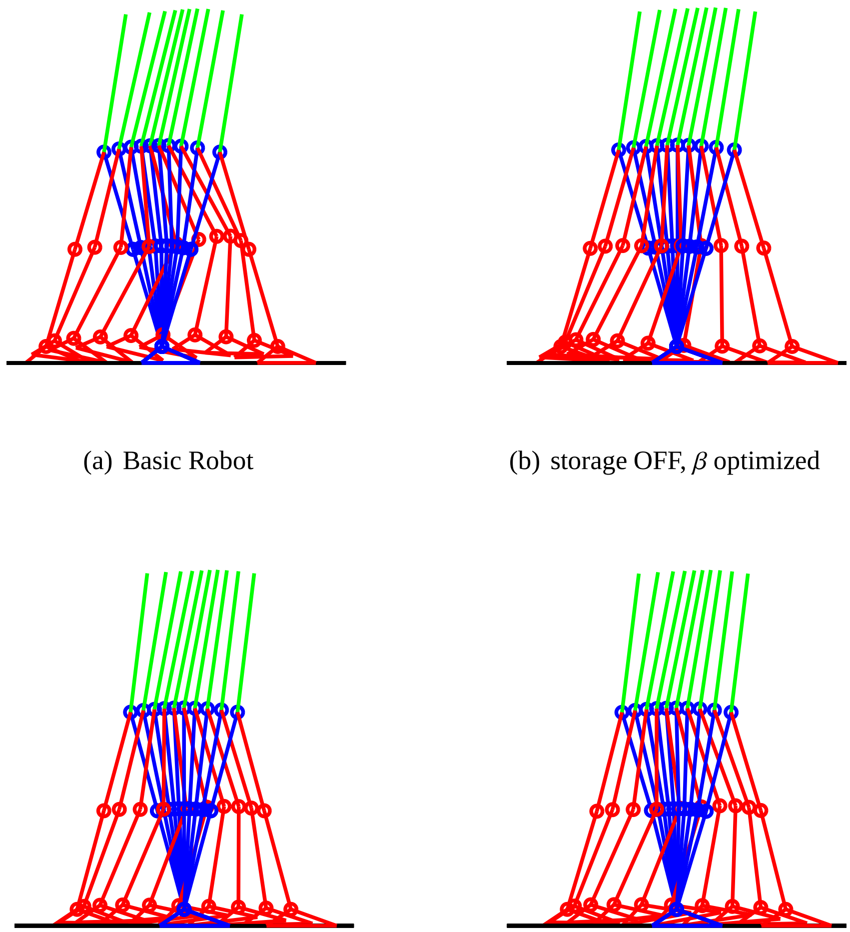

(a) Basic Robot

(b) storage OFF, β optimized

(c) storage ON, β optimized

(d) storage ON, β constant

Figure 7.1 – Walking step of the biped for all cases at 0.5 m/sec

consumption during walking is to lock the support knee joint, store energy during lock phase and re-utilize the stored energy when needed. It shows that the optimization criterion is significantly reduced after storing energy during the knee locking and then reusing during the swing phase. Energy is also reduced when the support knee is locked without energy storing mechanism. Since, energy consumption of knee joint is zero while in isometric position, and the hydraulic actuator consume no energy while locked, therefore, net consumption during walking is reduced. In the case where knee is locked without storing energy, the power requirements are calculated based on the swing knee, which consumes less power compared to support knee. In case **B2** where storage is ON and knee locking angle β is optimized, and case **B3** with storage ON and β constant, the criteria curves have almost same values for all walking speeds. Therefore it is possible to lock support knee at a constant value for all valid walking gait trajectories.

Percentage savings of selected criterion is given in Figure 7.2(b). It shows that only knee locking is the least effective method to save energy during bipedal walking. The percentage saving in case **B1** is directly proportional to walking speed. In other two cases **B2** and **B3** with storage ON, percentage economy decreases at the start, increases in the middle range of walking speeds and then decreases again at high walking speeds. Maximum energy saving of about 60 % can be achieved at high walking speeds between 1.0 to 1.1 m/sec.

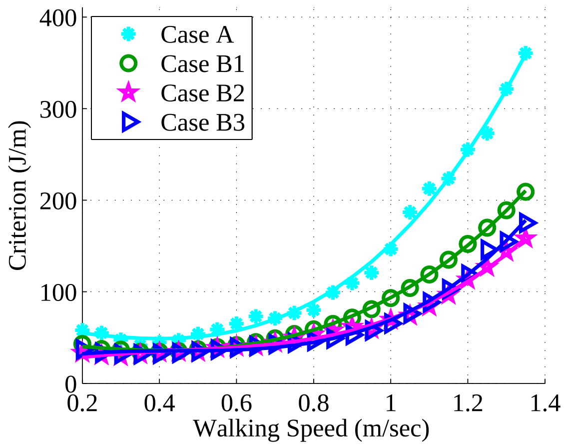

(a) criterion

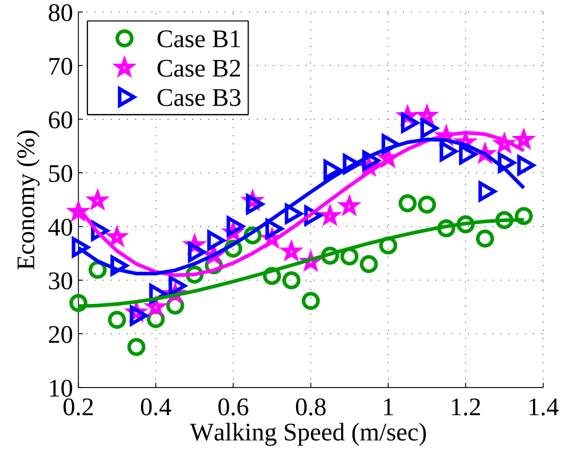

(b) % economy

Figure 7.2 – Value of criterion and percentage savings as a function of walking speed for gait type 2

Figure 7.3 gives the evolutions of maximum power required at knee joint of the robot as a function of walking speed. These are the values of motor power required to generate maximum joint torque required to follow reference trajectory of one cyclic step. It is observed that the magnitude of maximum motor power in cases **B2** and **B3** is drastically reduced. Consequently, energy consumed by the biped during walking is also significantly reduced, which is clear from criteria curves in Figure 7.2(a). Both curves are almost identical, which means that a constant value of knee locking angle β exists for complete range of walking speeds. However, the effects of knee locking without taking into consideration the energy storage, are less significant compared to those of knee locking with energy storage.

Figure 7.4(a) shows the step duration as a function of walking speed for gait type 2 for all studied cases, while Figure 7.4(b) presents the length of step for all studied cases as a function of walking speed. It is deduced that step duration is inversely proportional to walking speed while step length is directly proportional to it. Similar types of curves were also found in chapter 5 for all three studies walking gaits.

In all cases where the support knee is locked (cases **B1** , **B2**, and **B3**) just before impact, an impulsive reaction appears on the support knee joint. Figure 7.5 gives the value of this impulsive reaction on the knee joint at different walking speeds for gait type 2. It is noted that the impulsive reaction on knee is unilateral and is directly proportional to walking speed.

Figure 7.6 presents the impulsive impact forces on foot 2 (the foot touching the ground) of the studied biped at different walking speeds. The tangential and normal components of the impulsive reaction represented by I_{2t} and I_{2N} are presented in Figures 7.6(a) and 7.6(b) respectively. It shows that these forces are unidirectional and directly proportional to walking speed.

Figure 7.7 gives the evolution of joint's torque of gait type 2 at walking speed of 0.5 m/sec for studies of basic robot, and all cases with knee locked and storage OFF and ON. It shows that

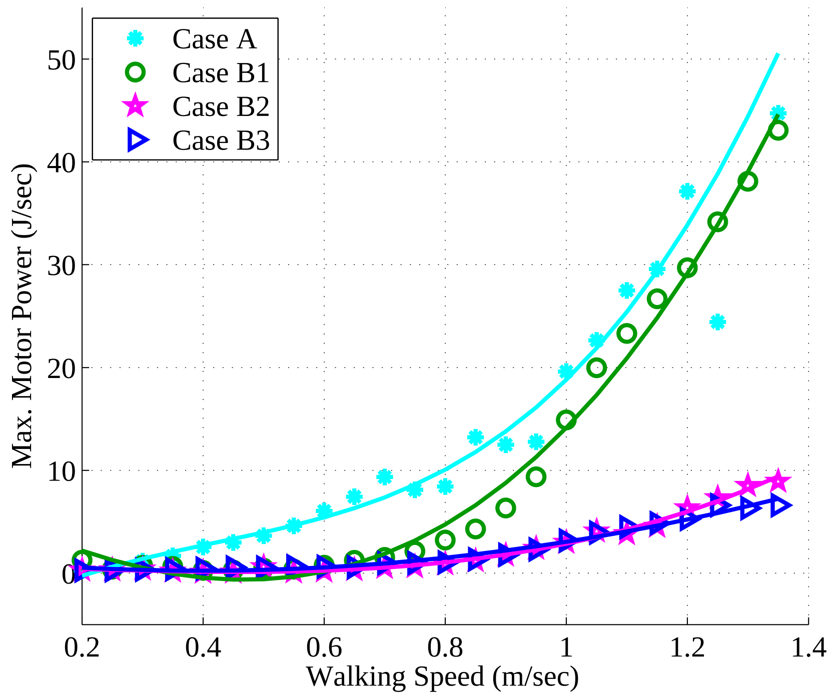

Figure 7.3 – Knee power as a function of walk speed for gait type 2

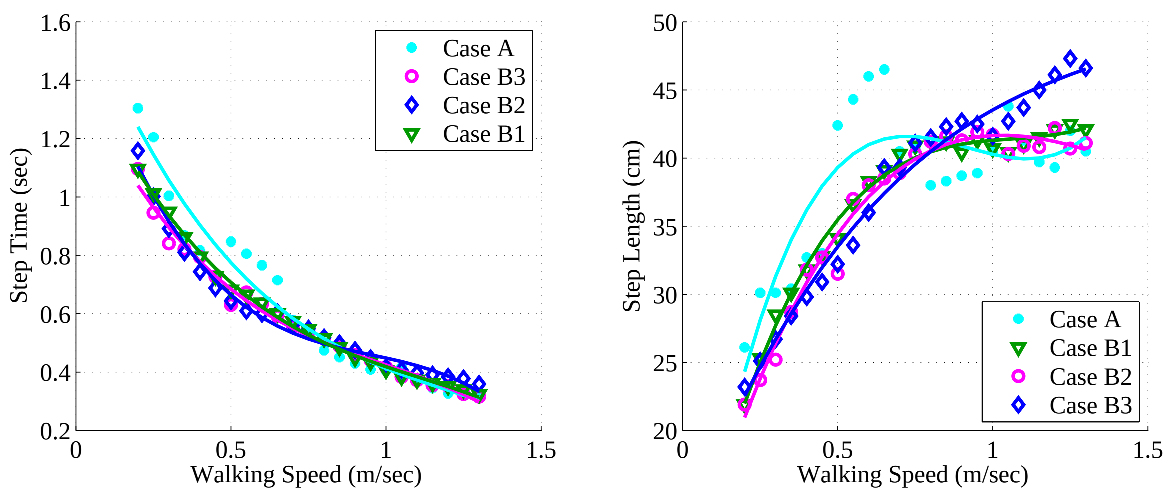

(a) step duration

(b) step length

Figure 7.4 – Evolution of step duration (T) and step length (d) as a functions of walking speed for gait type 2

support hip torque (Γ_3) is significantly reduced in all cases with knee locked. Torques of all other joints are also considerabblay reduced. It is to be noted that all joint torques during the step are below the maximum allowable limits. Results show that the swing foot torques ($\Gamma_4, \Gamma_5, \Gamma_6$) in all studied cases are less important than that of support foot. Joint torques are significantly reduced when the support knee is locked with or without storing energy (see Figures 7.7(b), 7.7(c), and

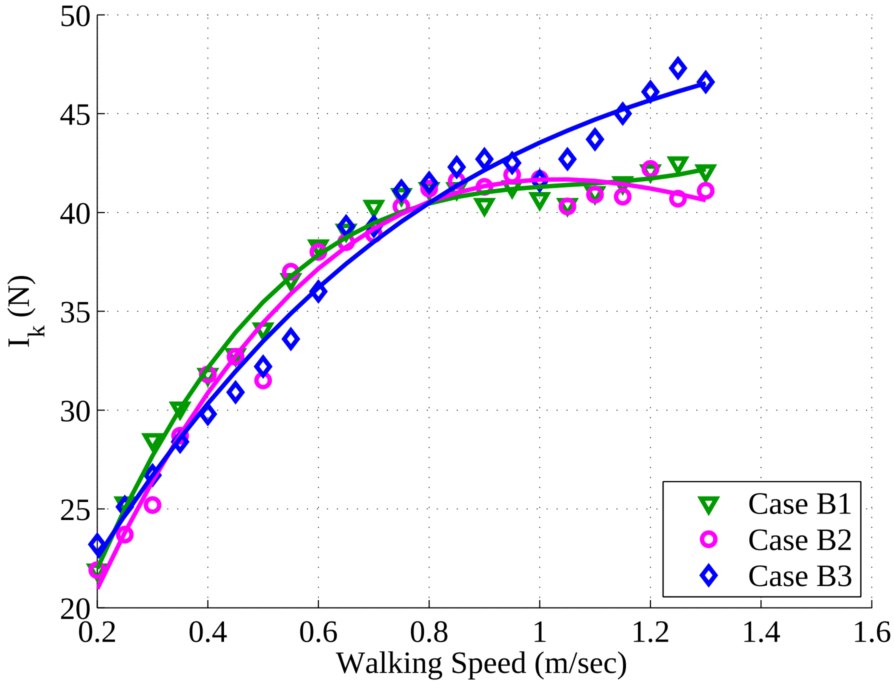

Figure 7.5 – Knee impact (I_k) as a functions of walking speed for gait type 2

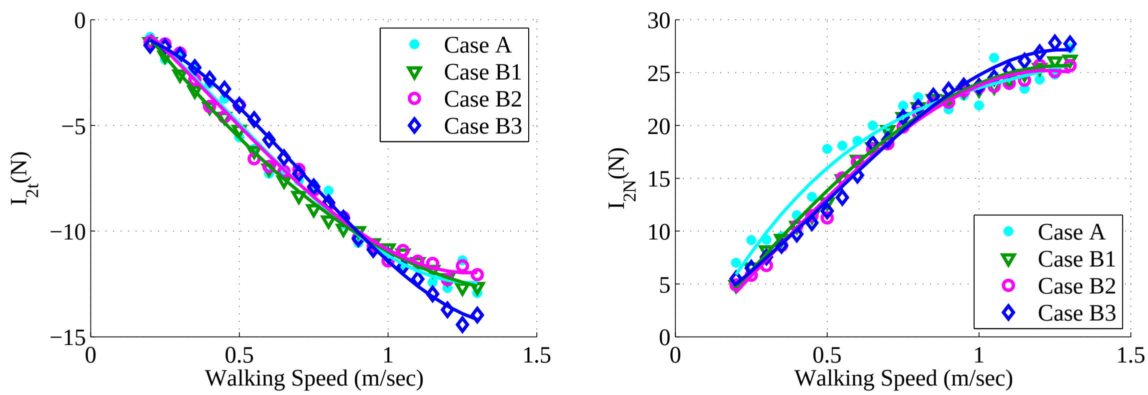

(a) tangential component (b) normal component

Figure 7.6 – Foot impulsive reaction (I_2) as a functions of walking speed for gait type 2

7.7(d)).

Figure 7.8 presents the amplitude of knee locking angle β as a function of walking speed for gait type 2. It shows that β is zero at slow walking speeds for both cases, and varies between zero and 3 degrees for case **B1**, and between zero and 1.5 degrees for case **B2** for walking speeds above 0.45 m/sec. Based on these results, an average value of $\beta = 1^o$ is selected to reduce the optimization parameters in case **B3**.

Figure 7.9 shows the evolution of relative joint positions as a function of time of gait type 2 at walking speed of 0.5 m/sec. These results are for a cyclic step of a bipedal robot with support knee locked and the possibility to activate or deactivate the energy storage function. In all cases

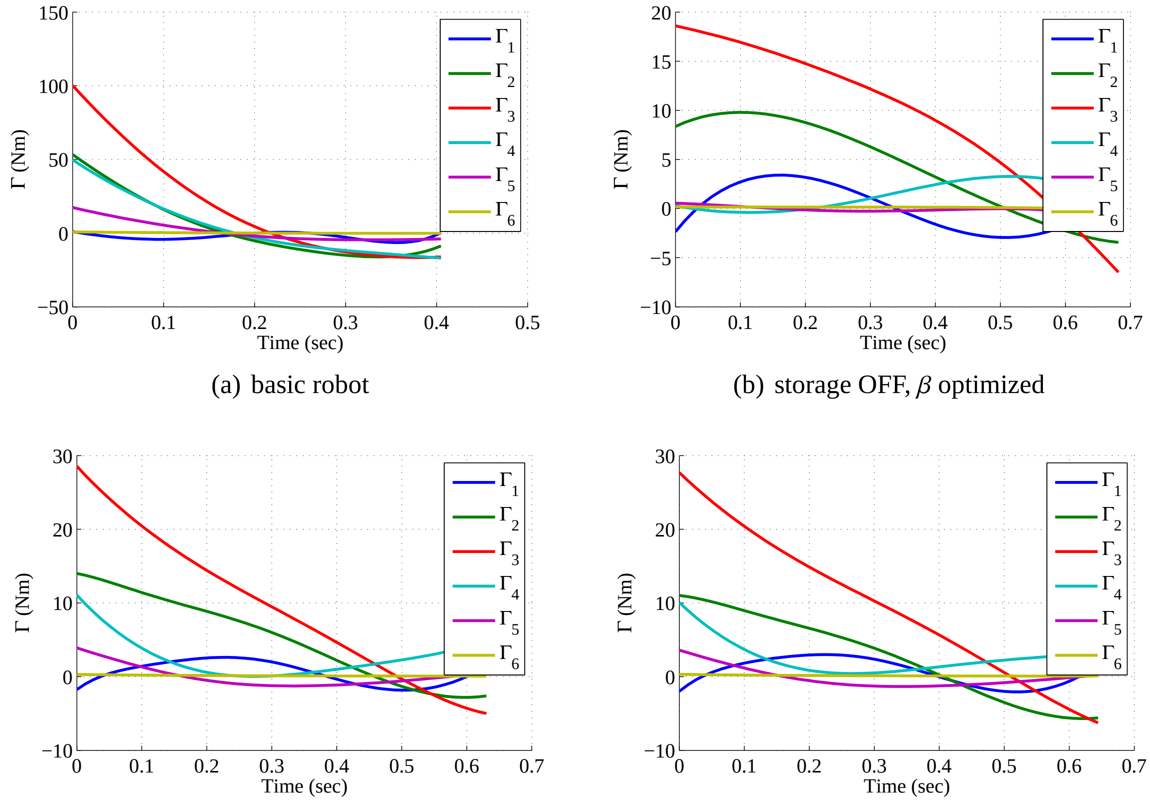

(a) basic robot

(b) storage OFF, β optimized

(c) storage ON, β optimized

(d) storage ON, β constant

Figure 7.7 – Joint torques of gait type 2 for different studied cases at walking speed of 0.5 m/sec

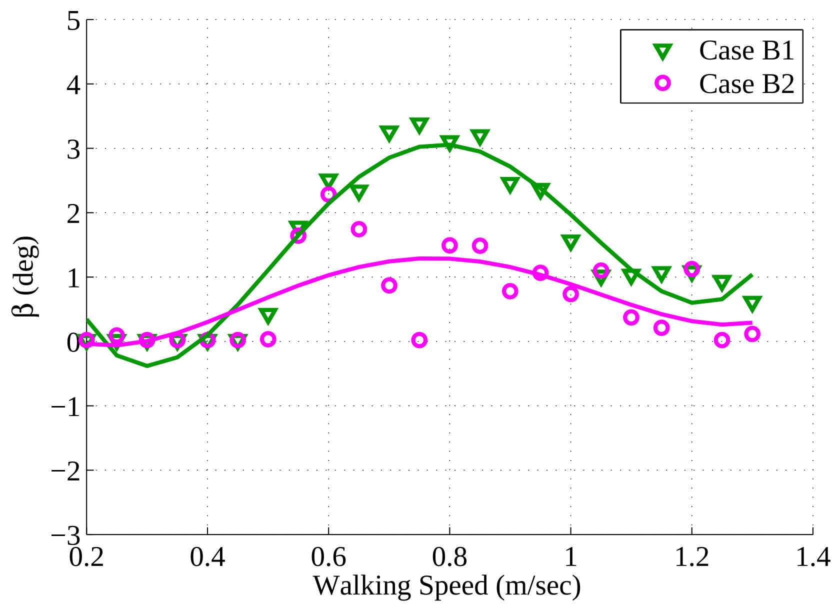

Figure 7.8 – Knee locking angle (β) as a functions of walking speed for gait type 2

with knee locked, a significant reduction in both hips angles (θ_3 and θ_4) can be observed in Figures 7.9(b), 7.9(c), and 7.9(d). It also shows that support knee angle is constant during the entire walking step.

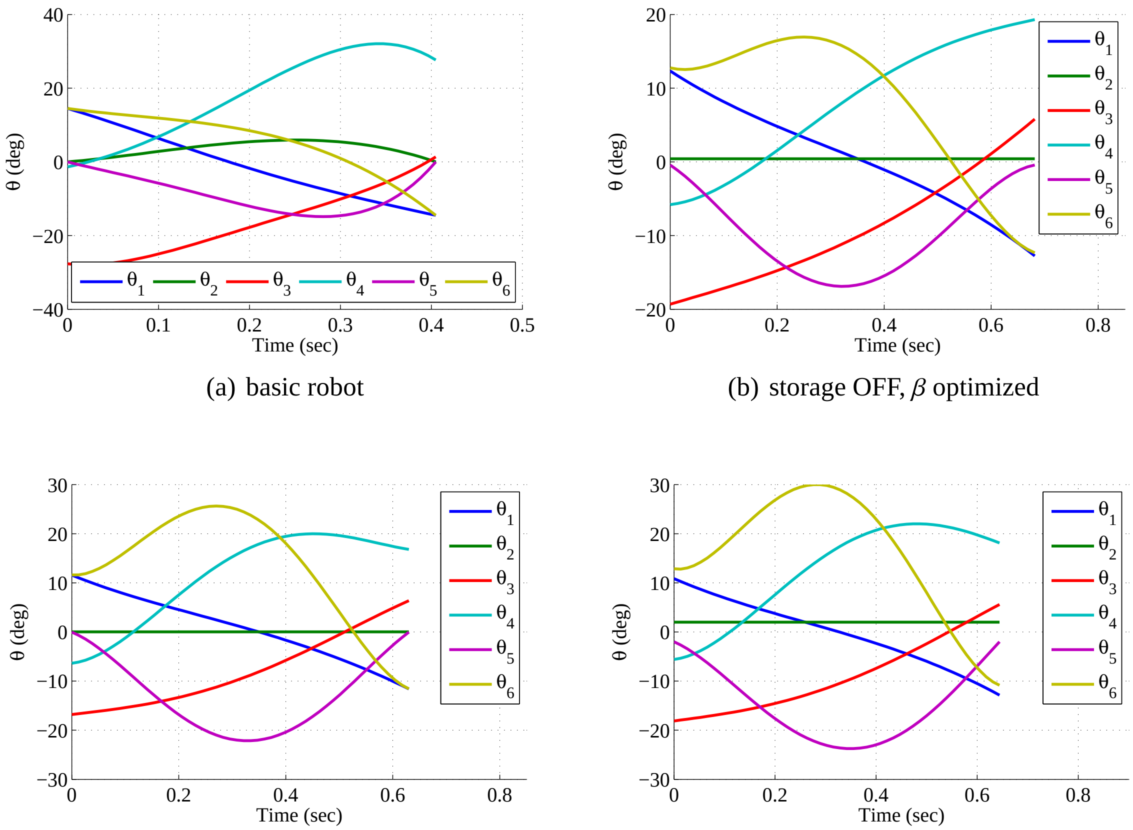

(a) basic robot

(b) storage OFF, β optimized

(c) storage ON, β optimized

(d) storage ON, β constant

Figure 7.9 – Evolution of joint positions of gait type 2 at walking speed of 0.5 m/sec

Evolution of joint angular velocities of gait type 2 with knee locked at walking speed of 0.5 m/sec is given in Figure 7.10. It is clear from results that the support knee angular velocity $\dot{\theta}_2$ is zero during the entire single support phase, which confirms that the knee is locked during the entire walking step. It also shows that amplitude of joint velocities is significantly reduced by locking the support knee. Since the optimization criterion is based on the product of joints torque and velocity, therefore, reduction in magnitudes of joint velocities resulted in reduced net criterion during walking.

Evolution of normal component of the ground reaction force on stance foot at 0.5 m/sec is presented in Figure 7.11(a) for all studied cases. It shows that the vertical component of the ground reaction force is always positive for all cases. It also shows that the constraint of no-take-off is well satisfied. It was also observed that neither the shape nor the amplitude is significantly modified when the support knee joint is locked. Normal ground reaction for cases **B2** and **B3** have identical curves, which represents that fixing β has no effect on it.

Evolution of no-slipping constraint as a function of step duration of gait type 2 is presented in Figure 7.11(b) at walking speeds of 0.5 m/sec. The calculated value of ratio of tangential force versus normal force should always be less than the maximum allowable limit. In present results, this value is significantly lower than limit, which was fixed at 0.9. It can be said that a value of $\mu = 0.3$ would be sufficient for the biped to follow the optimized trajectory. In other words, the

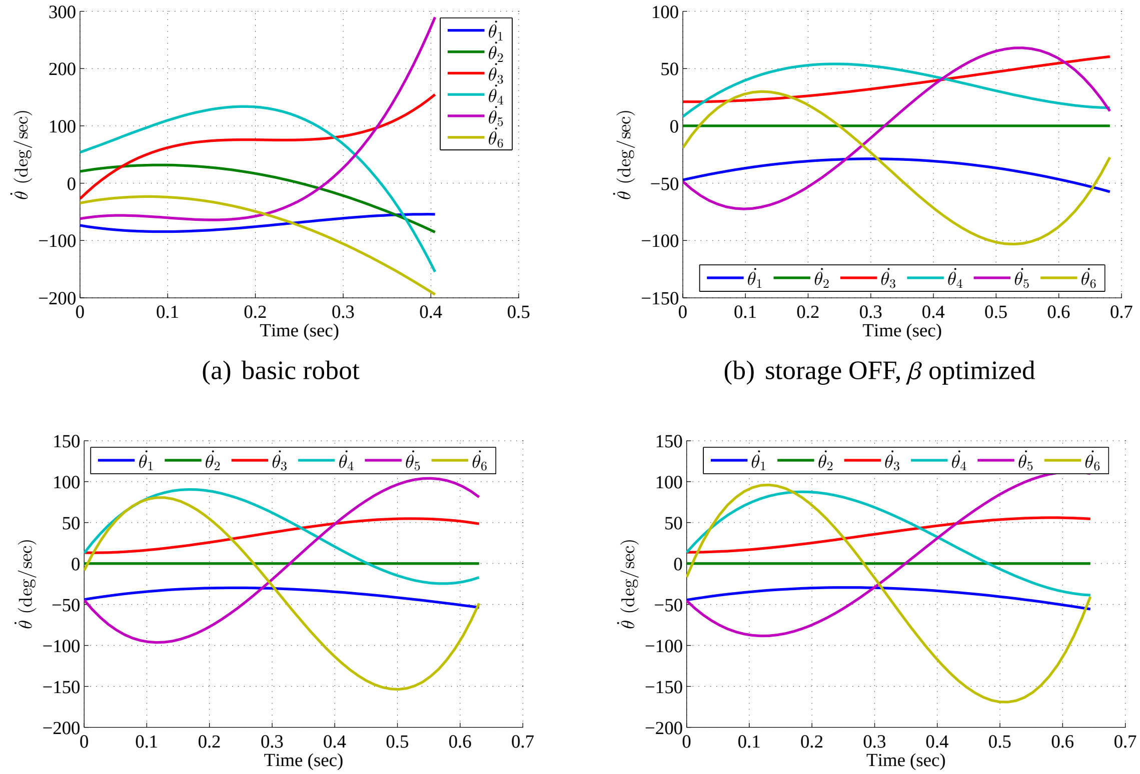

(a) basic robot
(b) storage OFF, β optimized
(c) storage ON, β optimized
(d) storage ON, β constant

Figure 7.10 – Evolution of joint velocities of gait type 2 at walking speed of 0.5 m/sec

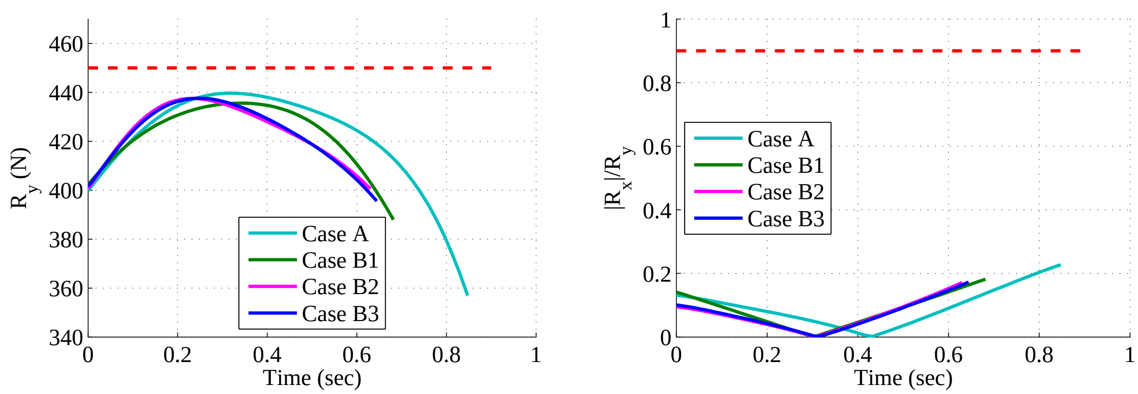

(a) vertical reaction on stance foot
(b) no slipping constraint

Figure 7.11 – Evolution of vertical reaction and no slipping of gait type 2 at 0.5 m/sec. The horizontal red dotted line represents the weight of the biped in (a) and shows the limit of coefficient of friction μ in (b)

biped will not slip and walk successfully even if the friction between feet and the ground is less than the designed value. Results also show that selecting a constant value of β has negligible effects on the constraint.

Figure 7.12 presents the evolution of ZMP and the vertical position of CoG as a function of its horizontal position for walking gait type 2 at 0.5m/sec. Simulation results show in Figure 7.12(a) show that for all studies, ZMP is always inside the support polygon. It also shows that ZMP has low amplitudes and is just below the ankle axis of the foot during the entire walking step. It is also observed that all the cases with knee locked have low variation of ZMP during a step compared to basic robot. Compared to results in chapter 5 (see figure 5.33(a)), the ZMP has very less variation and is shifted towards the center of the foot.

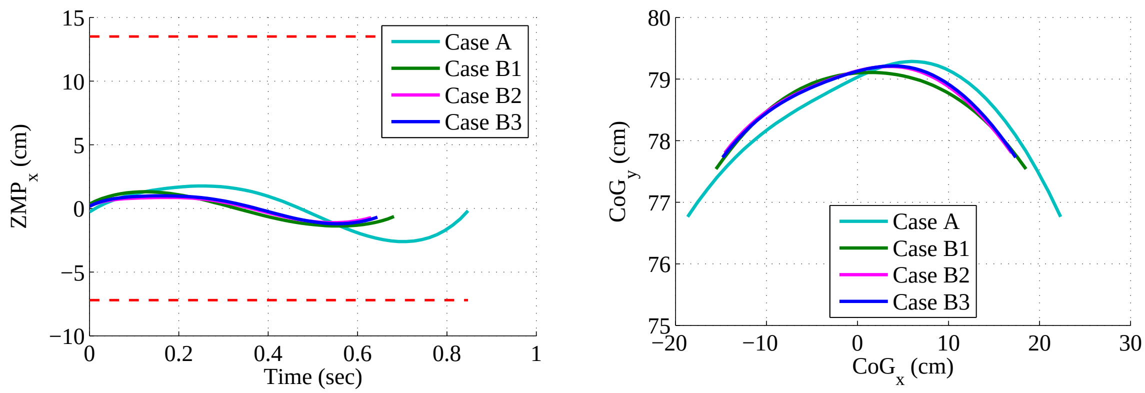

(a) ZMP (b) CoG

Figure 7.12 – Evolution of ZMP and CoG of gait type 2 at 0.5 m/sec

Evolution of CoG of the studied biped during a walking step is presented in Figure 7.12(b). It is observed that activation of storage function or knee locking have no significant effects on the position of CoG of the robot. Therefore, reduction in consumption of total energy during walking is the result of effects of knee locking and energy storage.

7.3.2 Summary of Gait Type 2

In this section, walking gait trajectories of a seven-link planar biped equipped with integrated electro-hydraulic actuators were studied under two different methodologies, first by locking the support knee without possibility of storing energy, second by locking the knee with possibility to store energy. It was concluded that the energy consumption of a biped during walking is significantly reduced by locking the support knee during the entire single support phase. It was also observed that additional energy can be saved by adding the possibility to store energy while knee joint is locked.

It was concluded that it is possible to lock support knee at a constant locking angle (β) for all possible walking gait trajectories without significantly effecting the energetic efficiency of the biped. The duration of step is inversely proportional to walking speed, and step length, impulsive reaction force of the ground on the foot, and impulsive reaction of knee joint are directly proportional to it.

Although optimization criterion in chapter 5 is different than that used in this chapter, a number of parameters can still be compared to highlight the effects of different criteria on bipedal waking gait type 2. It is observed that joint torques are significantly increased with respect to that found in chapter 5 for the same type of gait at the same walking speed. This is because the criterion in chapter 5 minimizes the square of joint torques while that in this chapter minimizes the actuators energy (product of joint's torque and angular velocity). Another significant difference is that the impulsive reaction on support knee joint is largely increased for the second criterion used in this chapter. Finally, the shape of curves of vertical reaction forces is largely different in all cases than that of the same gait in chapter 5 optimized using criterion based on joint torques.

It is deduced from simulation results of gait type 2 that applying these strategies will significantly improve the energetic efficiency as well as autonomy of the studied biped. In perspective of this study, the next step is to explore the effects these strategies on gait type 3, which is more complex and composed of single and double support phases with rotation of feet during double support phase.

7.4 Optimization of Walking Gait with Double Support

The walking gait with impulsive impacts and double support phases is the gait type 3 presented in section 3.3.3. The studies carried out on this gait are listed in section 7.2 except the case B3.

Walking gait trajectory for gait type 3 is generated and optimized in two parts. In first part, reference joint trajectory during double support phase is generated by a cubic spline having two nodes. In second part, joint trajectory during single support phase is generated using cubic spline function with on intermediate point. All constraints and optimization parameters enlisted before for gait type 3 apply to this gait as well. The only difference is the optimization criterion used.

7.4.1 Simulation Results

A number of gait trajectories at different walking speeds were generated and optimized using reference trajectory generation and optimization techniques presented earlier. In this section, simulation results for walking gait type 3 with hydraulic actuators will be presented at walking speeds of $1.2 m/s$. The effects of knee locking and energy storage function on energetic consumption of a biped during walking will be compared. Energetic efficiency during walking and other parameters like gait trajectory, ZMP, CoG, and ground reaction forces etc will also be discussed and compared at different walking speeds.

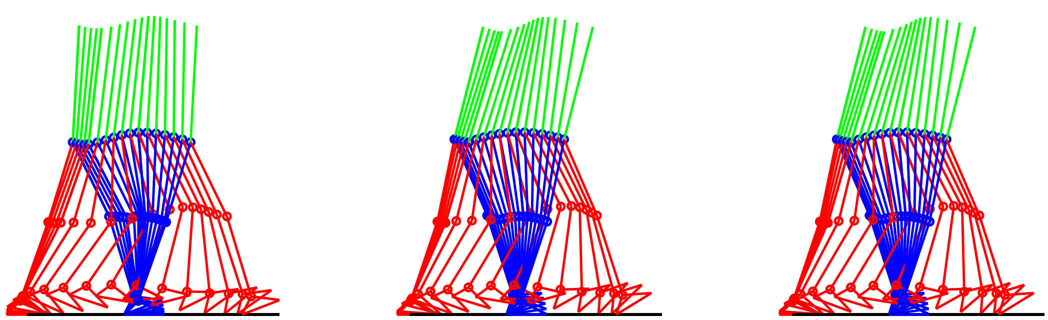

(a) basic robot (b) storage OFF (c) storage ON

Figure 7.13 – Walking step of the biped for all studies cases at 1.2 m/sec for gait type 3

Figure 7.13 shows the stick diagram of a walking step for the biped at walking speed of 1.2 m/sec (4.3 Km/h) in all studied cases. It is observed that gait trajectories of cases with knee locked are slightly different from that of basic case particularly the torso is slightly leaned forward. Previously, for gait type 2 in section 7.3.1, the visual impression of the gait was that the amplitude of height of swing foot is very low during entire swing phase. Contrary to results of gait type 2, the amplitude of height of swing foot during entire swing phase is increased during a walking step for gait type 3. It means that by introducing finite double support phase, walking step is improved and the gait more is anthropomorphic and close to human walking.

Figure 7.14(a) presents the comparison of criteria curves as a function of walking speed for all studied cases. Simulation results for gait type 3 show that similar to gait type 3 in chapter 5, knee locking is not effective and energetic efficiency during walking is decreased compared to that of basic robot. In chapter 5, the over-consumption in case of knee locking was increasing with increase of walking speed while in this chapter, the over-consumption is almost constant at about 15% for all walking speeds. The consumption of energy of walking is reduced by activating the energy storage function on the support knee while it is locked during the entire single support phase. The stored energy is re-used when needed particularly during swing phase. Energetic efficiency of the biped is slightly improved only at high walking speeds (above 1.0 m/sec) where about 10% of walking cost can be saved. It is to be noted that comfortable walking speed (speed at which energy consumption is minimum) for human walking is around 1.4 m/sec.

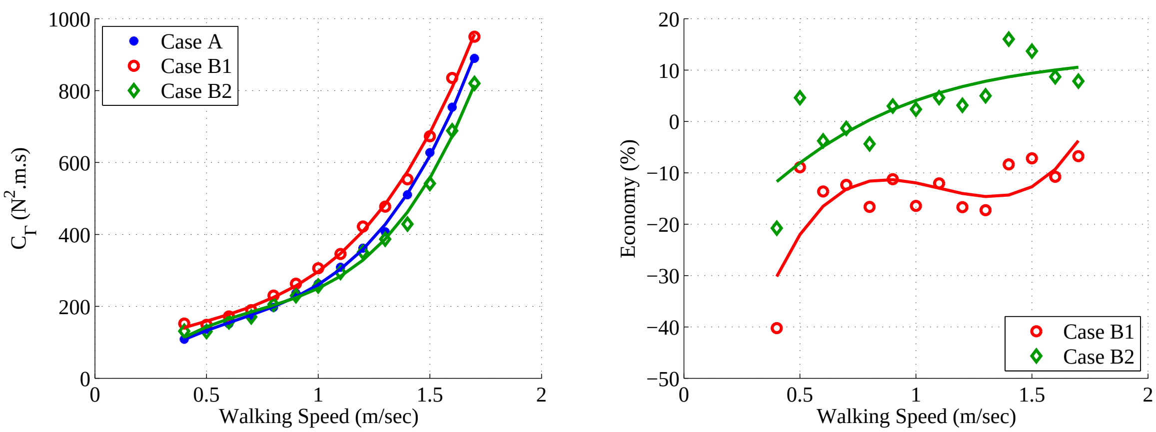

(a) criterion (b) % economy

Figure 7.14 – Value of criterion and percentage savings as a function of walking speed for gait type 3

Figure 7.14(b) gives the evolution of percentage economy as a function of walking speed for case **B1** where support knee was locked without storing energy and case **B2** where knee was locked with storage function ON and locking angle β was optimized. It shows that consumption of energy during walking is slightly reduced by locking the support knee and storing the energy during the entire single support phase. Up to 10% reduction in walking cost is observed at high walking speeds. However, the optimized criterion of knee locking without storing energy is always higher than that of basic robot. The percentage reduction is less important than that obtained for gait type 2. It is therefore concluded from simulation results, that the best option to reduce bipedal walking cost is to lock the support knee at high walking speeds and store energy for later use.

Figure 7.15 shows the duration and length of step as a function of walking speed for gait type 3 for all studied cases. It shows that the duration of step decreases and the step length increases as walking speed increases. It is concluded that knee locking and activating or deactivating storage function have negligible effects on step length and time. The curves in cases B1 and B2 are superposed, gait trajectories are identical except at 1.7 m/sec and the criterion in case B2 is lower than that of B1 due to the storage of energy.

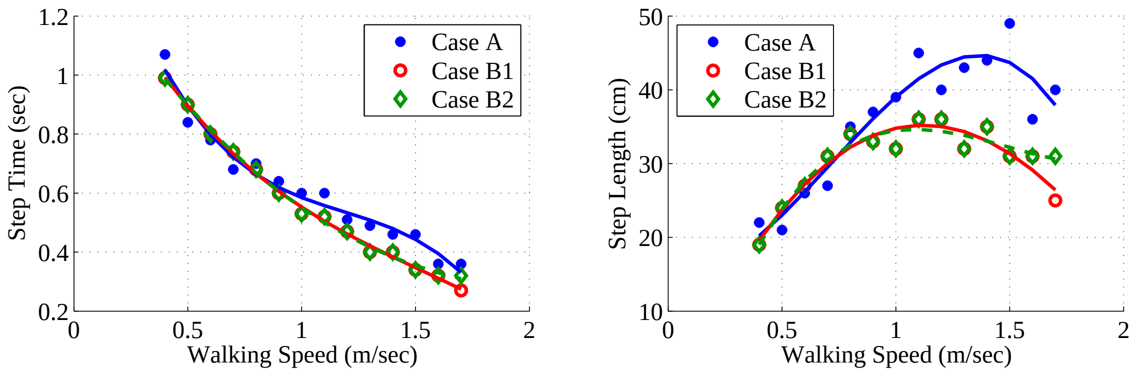

(a) duration of step (b) step length

Figure 7.15 – Evolution of duration of step (T) and step length (d) as a functions of walking speed for gait type 3

Figure 7.16 gives the value of impulsive reaction on the knee joint at different walking speeds for gait type 3. It is noted that impulsive reaction on support knee joint is unilateral, and is directly proportional to walking speed. Similar results were obtained for gait type 2 with significantly high amplitudes of impulsive reaction forces. Both curves are almost superposed.

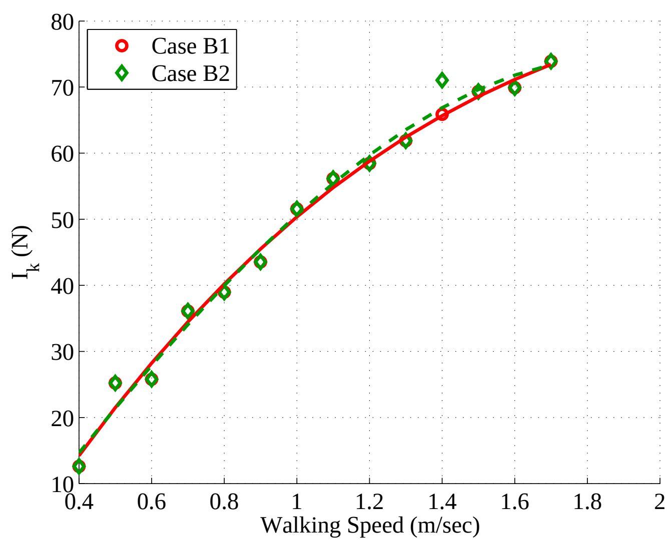

Figure 7.16 – Knee impact (I_k) as a functions of walking speed for gait type 3

As there is no impact on the heel of the front foot, there are no impulsive reaction forces neither on heel of front foot nor on toe of rear foot. An impulsive impact (toe impact see Figure 3.7) occurs when the front foot touches the ground with flat contact. Figure 7.17 presents the impulsive impact force I_{r1ss} on the front foot of the biped at different walking speeds. It is the impulsive force on front foot at the end of double and start of single support phase. The tangential and normal component of the impulsive reaction represented by I_{r1ss_x} and I_{r1ss_y} are presented in Figures 7.17(a) and 7.17(b) respectively. It shows that for all studied cases, the tangential and normal components of the impulsive reaction are unidirectional. In case of basic robot (case A), the impulsive reaction force has very low magnitudes and is almost constant on complete range of walking speeds. In cases where stance knee is locked during entire single support phase, impulsive reactions increase with increase in walking speed. These forces are significantly high at high walking speeds, which is the cause of high magnitudes of the selected criterion in all cases with knee locked.

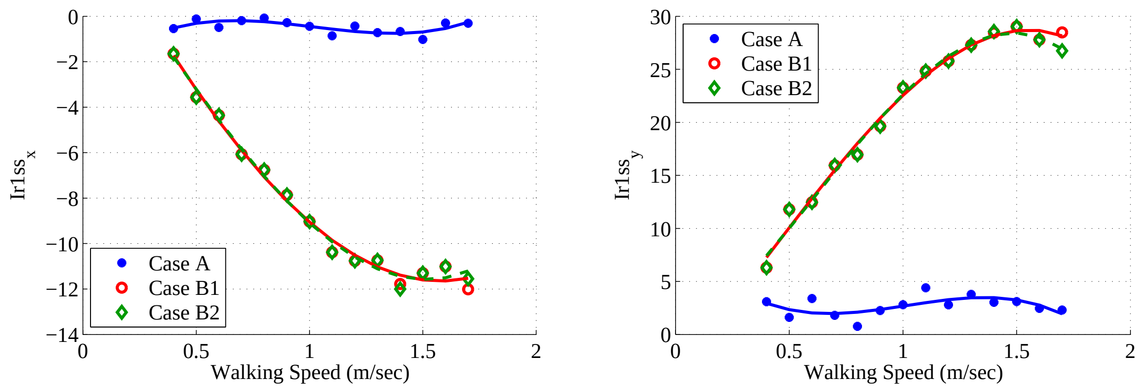

(a) tangential component

(b) normal component

Figure 7.17 – Foot impulsive reaction (I_{r1ss}) on front foot at toe impact as a functions of walking speed for gait type 3

Figure 7.18 presents the amplitude of knee locking angle β as a function of walking speed for gait type 3. It shows that β varies between 7.5 and 8.5 degrees, and for most of the walking speeds it is around 8.0 degree for all studied cases. Thus, based on these results, an average value of β can be selected for knee locking to reduce optimization parameters in case.

Figure 7.19 presents the evolution of joint torques of gait type 3 at walking speed of 1.2 m/sec for studies of basic robot, and all cases with knee locked and storage OFF or ON. Discontinuities in joint torques at toe impact are clearly visible in the figure. The results show that all joint torques during the entire step are far below the maximum allowable limits described by the constraint equation (4.26). Results show that joint torques during double support phase and at at the beginning of the single support phase are relatively high compared to that during rest of the the single support phase. It is also observed that the swing foot torques $(\Gamma_4, \Gamma_5, \Gamma_6)$ in all studied cases are less important than that of support foot. Since the gait trajectories with storage OFF and ON are same, only storage ON results are presented for simplicity. In case with support knee locked (see Figures 7.19(b)), stance knee torque Γ_2 and stance ankle torque Γ_1 during double support phase are significantly reduced.

Evolution of relative joint positions as a function of time for gait type 3 at walking speed of 1.2 m/sec is presented in Figure 7.20. These results are for a cyclic step of a bipedal robot with support knee locked during entire single support phase and the possibility to store energy. In case of basic robot, the knee joint angle has high variations, which resulted in high values of optimization criterion when it was locked.

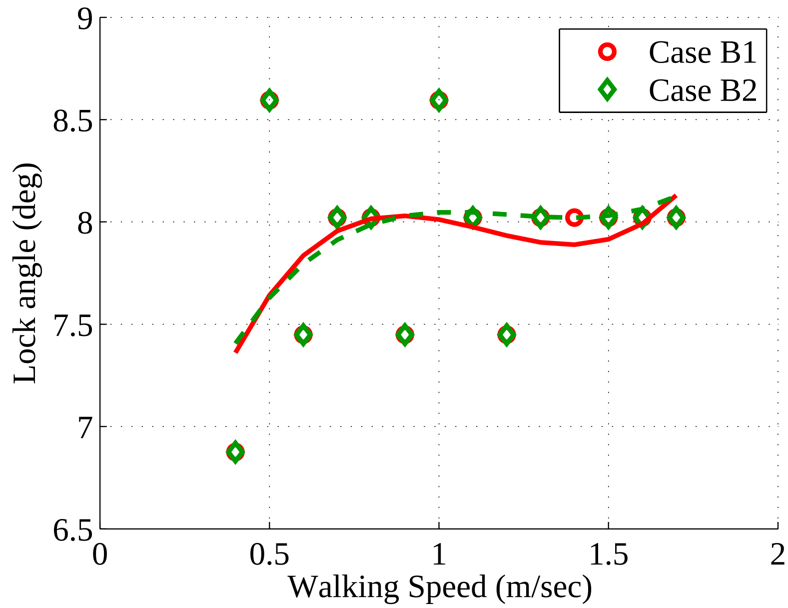

Figure 7.18 – Knee locking angle β in case **B2** as a functions of walking speed for gait type 3

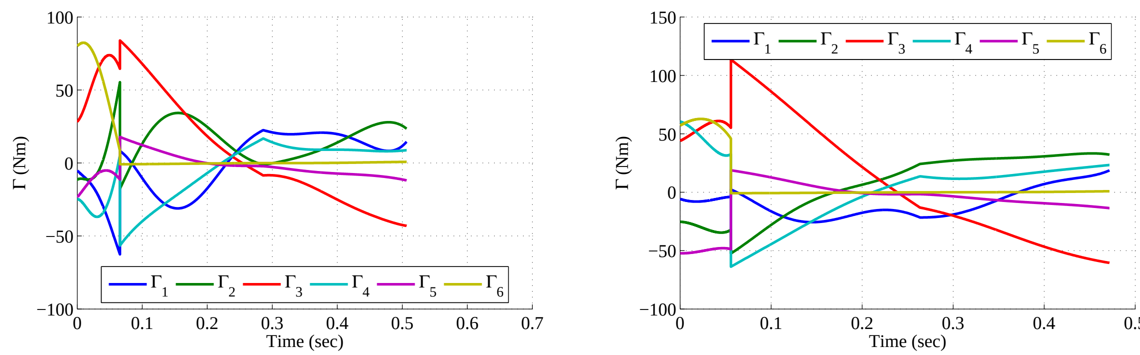

(a) basic robot

(b) storage ON, β optimized

Figure 7.19 – Evolution of joint torques of gait type 3 at walking speed of 1.2 m/sec. $\Gamma_1, \Gamma_2, \Gamma_3$ are the support ankle, knee and hip torques, and $\Gamma_4, \Gamma_5, \Gamma_6$ are the swing hip, knee, and ankle torques

Evolution of joint angular velocities of gait type 3 at walking speed of 1.2 m/sec is given in Figure 7.21. It is clear from results that the support knee angular velocity $\dot{\theta}_2$ is zero during the entire single support phase, which confirms that the knee is locked during the entire single support phase. It also shows that amplitude of swing hip velocities is significantly high compared to other joints. This is because that the swing leg has to move from rear to forward position.

Evolution of normal component of the ground reaction force on both feet of the biped at 1.2 m/sec during a walking step is presented in Figure 7.22 for all studied cases. Figure 7.22(a) shows that the vertical component of the ground reaction force on stance foot is always positive for all cases. It also shows that the constraint of no-take-off is well satisfied. It is observed that the shape and magnitude of ground reaction on front foot during double support phase is significantly modified after locking the knee. However, the amplitude during single support phase is slightly modified. It is observed that shape of curves of reaction force resembles the letter "M" during single support

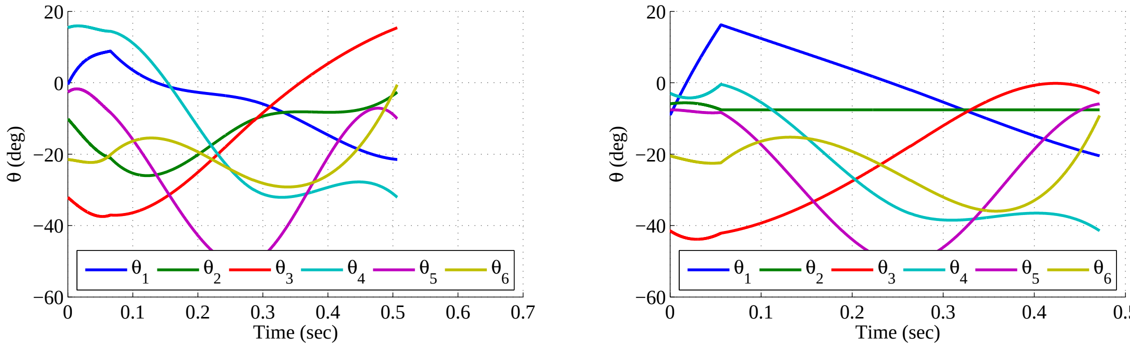

(a) basic robot (b) storage ON, β optimized

Figure 7.20 – Evolution of joint positions of gait type 3 at walking speed of 1.2 m/sec. $\theta_1, \theta_2, \theta_3$ are the support ankle, knee and hip angles, and $\theta_4, \theta_5, \theta_6$ are the swing hip, knee, and ankle angles

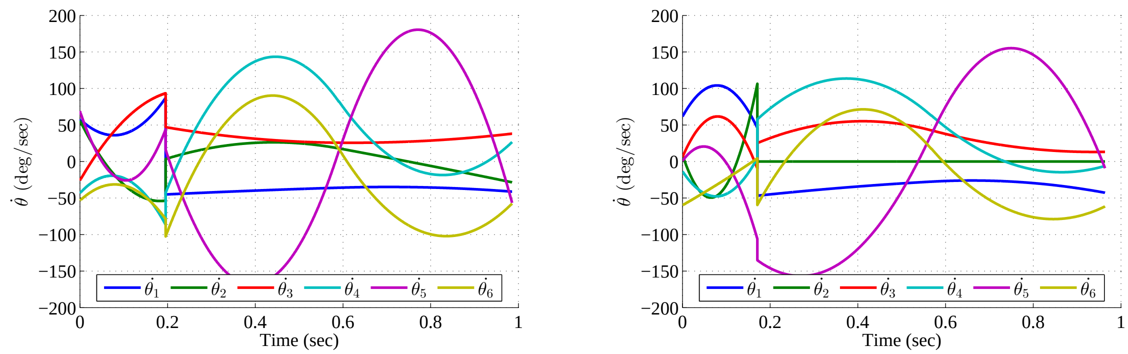

(a) basic robot (b) storage ON, β optimized

Figure 7.21 – Evolution of joint velocities of gait type 3 at walking speed of 1.2 m/sec. The subscript 1,2,3 represents stance ankle, knee, hip while 4,5,6 represents swing hip, knee, and ankle

phase. The "M" shaped curve of vertical component of ground reaction forces during walking has been found in a number of bio-mechanical studies on human walking [127, 22, 95].

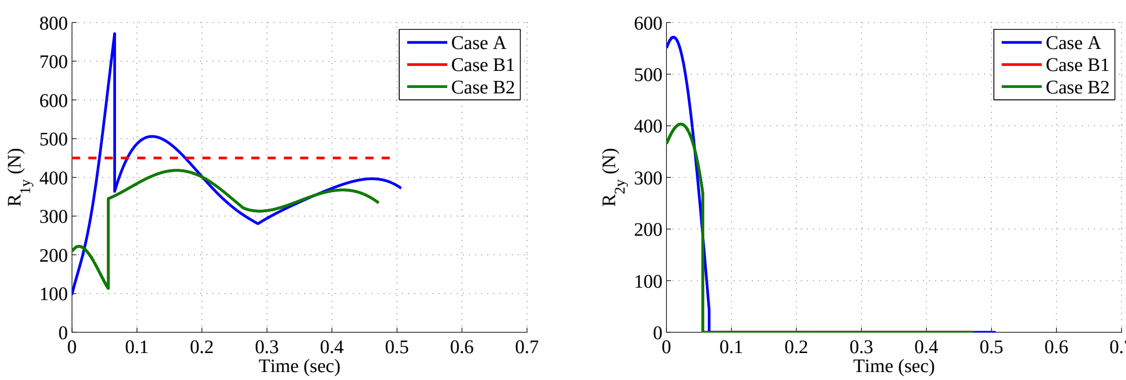

(a) front foot (b) rear foot

Figure 7.22 – Evolution of vertical reaction force on feet for gait type 3 at 1.2 m/sec. The horizontal red dotted line represents the weight of the biped

Evolution of normal component of the ground reaction force on rear foot (foot 2) at 1.2 m/sec is presented in Figure 7.22(b) for all studied cases. It shows that the vertical component of the ground reaction force is always positive and the constraint of no-take-off is well satisfied during double support phase for all cases. For both feet, reaction force curves in cases B1 and B2 are superposed.

The evolution of ratio of tangential reaction force to normal force (no-slipping constraint) during a walking step of gait type 3 is presented in Figure 7.23(a) at walking speeds of 1.2 m/sec. This constraint is given by equation (4.17). The value of μ should always be less than the maximum allowable limit represented by the red dotted line, which is the case in simulation results presented in Figure 7.23(a). It shows that the ratio between tangential and normal force is significantly less than the maximum limit, which means that the biped will not slip even if there are small variations in the friction between floor and foot of the biped. This ratio is higher particularly during double support phase when the knee is locked than for the basic gait.

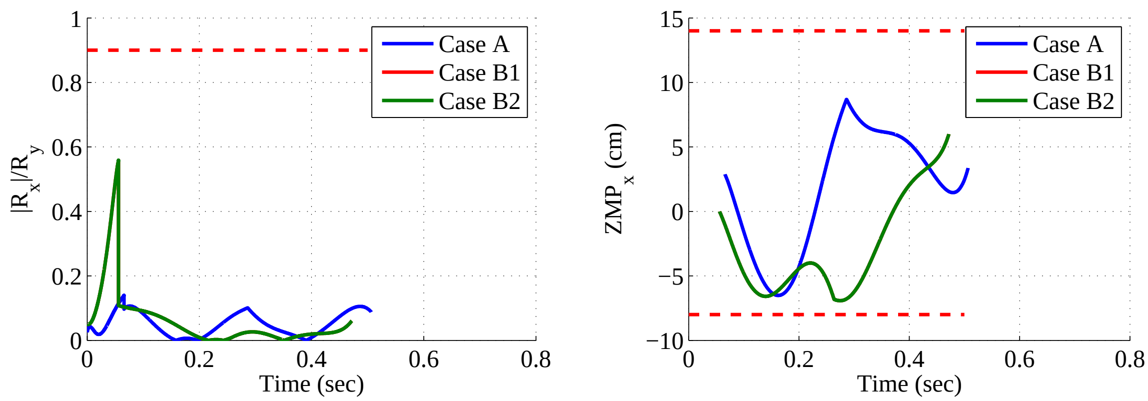

Figure 7.23 – Evolution of no-slipping and ZMP constraint of gait type 3 at 1.2 m/sec. The horizontal red dotted line shows the limit of coefficient of friction μ in (a)

An important criterion which must be satisfied in bipedal walking is the position of Zero Moment Point (ZMP), which should remain in the support polygon during walking. This constraint is presented in Figure 7.23(b) for walking gait type 3 at walking speeds of 1.2 m/sec. Simulation results show that for all studied cases, ZMP is always inside the support polygon. It also shows that ZMP moves towards heel of the foot till mid-swing and then moves back towards toe as the biped advances forward and the weigh of the biped is shifted forward. Here, negative and positive sign represents the position of ZMP towards the heel and toe of the foot respectively.

Figure 7.24 presents the evolution of vertical position of CoG as a function of its horizontal position at walking speed of 1.2 m/sec. It is observed that knee locking and storage function have no significant effects on the position of CoG of the robot. The CoG of cases B1 and B2 are superposed.

Duration of double support phase Tds_p in percentage of total time of a step is given in Figure 7.25 as a function of walking speed for all studied cases. It shows that Tds_p decreases with increase in walking speed, which allows the robot to have more time during single support phase to take longer step (see Figure 7.15). It can also be observed that Tds_p varies between 12% and 14% for

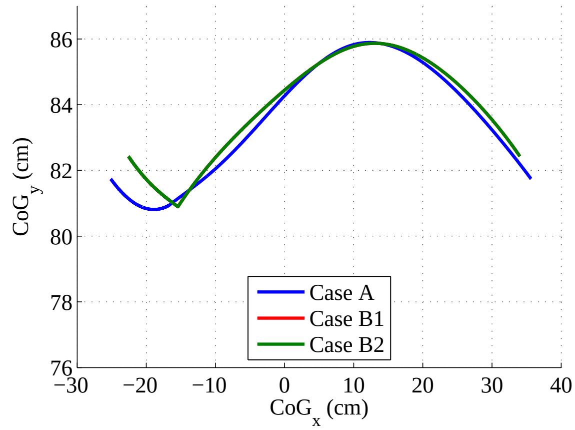

Figure 7.24 – Evolution of CoG of gait type 3 at 1.2 m/sec

basic robot in case **A**, and varies between 10% and 20% for all other cases with knee locked. Studies in bio-mechanics show that duration of double support phase is around 20% in human walking and decreases with increase in walking velocity until the double support phase disappears and the walking changes into running [116, 65, 121].

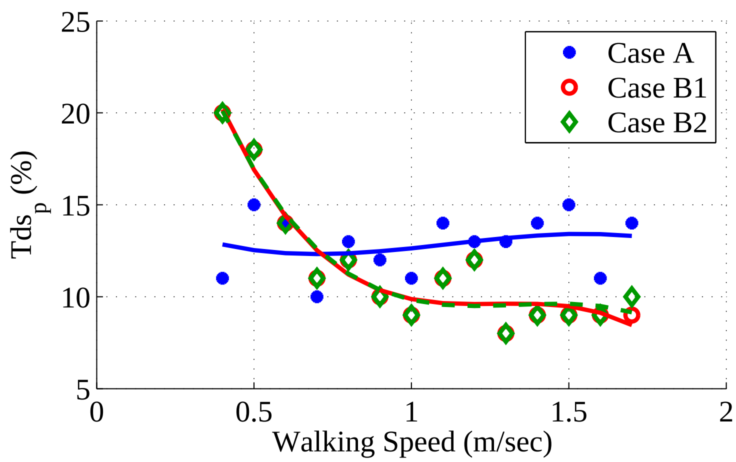

Figure 7.25 – Duration of double support phase in percentage of total time of step as a function of walking speed for gait type 3

7.4.2 Comparison of Gait Types 2 and 3

Two different types of walking gaits were presented in this chapter. The effects of knee locking and energy storage were also discussed on walking gait trajectories of these two bipedal walking gaits. Figure 7.26 presents the comparison of selected criterion as a function of walking speed for basic robot and knee locked with storage ON cases. It can be observed that in all cases the value of selected criterion during a walking step for gait type 3 is significantly higher than that of gait type 2 at all walking speeds. High magnitudes of selected criterion of gait type 3 is due to a number of differences like introduction of finite double support phase, impactless landing of the front foot at heel contact (beginning of the double support phase), and an impulsive impact on toe of the front foot at the end of the double support phase.

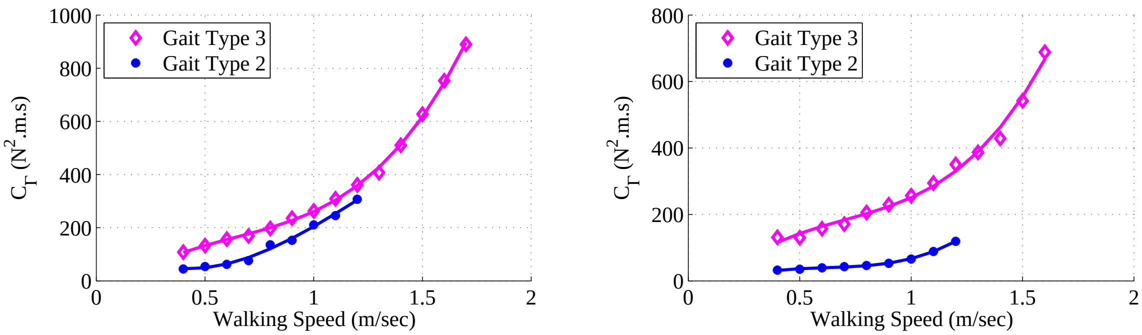

(a) basic robot (b) storage ON, β optimized

Figure 7.26 – Comparison of criteria of gait types 2 and 3 at different walking speeds

7.5 Conclusion

The work presented in this chapter is based on the use of hydraulic actuators, and the goal is to reduce the overall energy consumption of a humanoid robot during walking. A set of optimal walking gait trajectories were generated using parametric optimization algorithm for a biped equipped with hydraulic actuators. Two different types of walking gaits were studied, one with instantaneous double support and impulsive impact, and second with finite double support phase, impactless first contact of the swing foot on its heel, and an impulsive impact on its toe at the end of double support phase. Energetic effects of knee locking without possibility to store energy, storage function ON, and storage function OFF were explored. The simulation results were then compared with that of basic biped. The main focus of the study was to economize the energy consumption of a bipedal robot during walking by exploiting different characteristics of integrated elector-hydraulic actuators (IEHA).

It is concluded from the simulation results that energetic efficiency of the studied biped during walking is significantly improved by locking the support knee during the entire single support phase for gait type 2. Consumption of energy is further reduced by activating the energy storage function of the IEHA, and storing the energy in a reservoir in the form of hydraulic pressure. The stored energy is then re-used when needed particularly during swing phase. Moreover, the high power producing characteristics of hydraulic actuators allow to select a small electric motor that reduces the total mass of the biped and hence the energetic cost of walking. However, knee locking was not effective for gait type 3 and the energy consumption was increased after locking the knee. After activation the energy storage function for gait type 3, energetic efficiency was slightly improved at high walking speeds. It is therefore concluded that gait type 3 is not suitable for knee locking but it is more realistic and human like. Similar results of knee locking were also found in chapter 5 for gait type 3.

It is also observed that the support knee can be fixed at a constant value for all walking speeds without significantly affecting the energetic efficiency of the biped. This reduces the number of optimization parameters by one, and the algorithm converges relatively fast. Finally, optimization criteria of walking gait types 2 and 3 were compared. It was found that the selected criterion for gait type 3 is significantly higher than that of gait type 2 for all walking speeds. The increased cost of walking is because of the finite double support phase, the first impactless contact of heel of the front foot, and the presence of second impact on toe of the front foot at the end of the double support phase. In chapter 5, it was observed that energy consumption of impactless gait (type 1) is significantly high compared to other two gaits. Gait type 3 was less costly than gait type 2 at high walking speeds for criterion of chapter 5 and is more costly all the time for the criterion in this chapter. It is to be noted that criteria in chapter 5 and 7 are not the same and can not be compared with each other. Although walking gait type 3 is more costly, it is more realistic and closer to human walking.

8

Conclusion and Perspectives

8.1 Conclusion

This thesis addressed to some extent the problem of energy consumption of a planar biped during walking. A number of different strategies were proposed to minimize the selected criterion during a walking step. To apply these strategies and study their effects on walking gait, a seven link planar biped was presented with two different types of actuators. One with classical electric actuators and second with newly designed integrated hydro electrical actuators. In the first part of the study, effects of knee locking and torsional springs were studied on predefined performance criterion during walking of the biped with electric actuators. The same biped with hydraulic actuators was studied in the second part of the present work. The integrated electro-hydraulic actuator is capable of storing energy and lock the joint at any position by consuming no energy or negligible energy. Effects of knee locking and energy storage on the selected criterion were studied.

General introduction of the subject and organization of the thesis were presented in chapter 1. Human walking and its different statistics were presented in chapter 2. Furthermore, different phases and events occurring during a complete cycle of human walking gait were discussed and terminologies used to describe human gait were presented. The two major phases *stance phase* and *swing phase*, and their sub-phases were explained in detail. Moreover, robot locomotion was discussed, and then human walking was compared to bipedal walking. A relationship between these two was also established. Different characteristics of the biped required to be able to efficiently undergo a walking step were enlisted. Furthermore, a criterion to compare energetic performance of different machines was presented. A number of energy recovery approaches used to improve energetic efficiency of a biped during walking were also presented and discussed in detail. Effects of springs, knee locking, and knee joint design on energetic efficiency and stability of walking gait were discussed. Towards the end of chapter 2, different methods used in present study to improve energetic performance of bipedal walking were presented.

Chapter 3 was dedicated to presentation and modeling of the studied biped. The geometric and inertial parameters of the biped were presented and its dynamic model was formulated using the Lagrange method. The dynamic model in single support phase, double support phase, and in general case was developed depending on different phases of studied walking gaits. The impact model for a seven link bipedal robot was developed, and different possible solutions of foot contact with the ground just after impact were discussed. Moreover, the dynamic model was extended to incorporate the effects of adding springs in parallel with the existing actuators, and the locking of the knee joint. Furthermore, different walking gait types with or without impact, and with or without double support phase were defined.

To identify the advantages and energetic effects associated with the proposed strategies to improve the energetic efficiency of a biped, a parametric optimization method to generate walking gait trajectories for a planar biped was presented in Chapter 4. Different functions used to generate reference walking trajectories were introduced. Trajectory generation for all studied gaits was explained and optimization variables required to generate optimal gait trajectories for these gaits were enlisted. Optimization criterion based on joint's torque for electric actuators and based on joint's energy for hydraulic actuators was presented. To compare the performance of the biped at different walking speeds, optimal walking gait trajectories were generated for all walking gaits. A set of constraints required to generate an optimal gait trajectory was presented. Finally, different non-linear constrained optimization tools of MATLAB® were explained and simulation results for these optimization functions were compared.

Simulation results for the biped HYDROiD with electric actuators were presented in chapter 5. Optimal walking gait trajectories for each gait were generated as a function of time using cubic spline functions. The cost of walking was calculated for each gait type using different strategies proposed to improve energetic efficiency of the biped. For gait type 1, It was found that maximum energetic efficiency during walking can be achieved by adding identical torsional springs at the hip joint and mechanically locking the knee. However, the maximum attainable walking speed for gait type 1 only was reduced to half because the joint velocities were saturated. The energetic efficiency of locking the knee alone at low speeds and adding springs only to the knee or hip joints was also noticeable. Implementation of these energy saving techniques to physical biped will significantly improve the energetic efficiency as well as the autonomy. Furthermore, it was noted that the joint torques were lower in cases with springs at both hip joints and support knee joint locked. It is therefore possible to use a smaller gear box with lower gear reduction ratio to obtain high joint velocities while respecting the joint torques limits. The reduction in size of the gear box would consequently reduce the total mass of the biped and thus the energy consumption during walking.

Similarly, optimal walking gait trajectories were generated for gait type 2 for both solutions *i.e.*, adding torsional springs to different joints of the biped, and mechanically locking the support knee joint. Gait type 2 has only single support phases and impulsive impacts, there is no finite double support phase. Simulation results similar to that of gait type 1 were found in terms of criterion reduction and joint torques. Finally, it was observed that, in contrast to gait type 1, the biped's joint velocities were not saturated and it was able to attain the same maximum walking speed as were attained by a basic robot without springs and knee locking. The presence of impulsive impacts at the end of each step allowed the biped to attain high walking speeds even if the support knee joint was locked. Moreover, as for gait type 1, smaller motors and gear reduction box can be installed to perform walking. This will result in reduced overall mass of the biped and will therefore further reduce the consumption of energy during walking.

A third type of walking gait with single support phase, finite double support phase, and two impacts one at heel and second at toe of the front foot was also presented in chapter 5. Reference joint trajectory generation functions for both single and double support phase were presented.

Stick diagram of a walking step of gait type 3 showed that it is more close to human walking. Simulation results of the selected performance criterion showed that significant reduction in criterion can be achieved by adding springs to different joints of the biped depending on their mode of activation. However, identical springs on a pair of joint and active during the entire step (single and double support phases) were very less effective for all studied walking speeds. Moreover, it was observed that impulsive reactions on heel of the front foot at heel impact were almost zero, which were the result of zero landing velocity of the heel of front foot at impact. Therefore, it was concluded that the only optimal solution for gait type 3 is the trajectory without first impact. Consequently, the gait was modeled with zero velocity of the heel touching the ground to reduce the optimization parameter and improve convergence of the algorithm. Similarly, impulsive reactions on toe of rear foot at heel impact and toe of front foot at toe impact were significantly lower that those found for gait types 1 and 2. In accordance to previous research, ankle springs were only effective at rear leg during double support phase, which help to prepare for the next step and provide a thrust to move forward.

Finally, criterion for all three studied gaits was compared for basic biped, biped with identical torsional springs at both ankles joints, both knees joints, and both hips joints. It was observed that gait type 1 is the most energetically costly in all cases followed by gait type 2 at high walking speeds and gait type 3 at slow walking speeds. It was also found that gait type 3 is more costly at slow walking speeds and less costly at high walking speeds compared to gait type 2. The criteria curves for these two gaits intersects at about 0.9 m/sec. According to studies in bio-mechanics, the average human walking speed is about 1.4 m/sec. Hence, the studied biped has comfortable walking speed (less energy consuming), which is largely below than that of human.

The second part of the present work is based on the study of a bipedal robot with hydraulic actuators capable of storing energy while the joint is locked, and reuse the stored energy when needed. Hydraulic actuators were introduced in chapter 6 and working principal of a classical hydraulic actuator was presented. Furthermore, a newly designed high performance Integrated Electro-Hydraulic Actuator (IEHA) was presented and its advantages over its counterparts were enlisted. The simplified model of the actuator was presented and working of its different parts was explained in detail. Moreover, different working modes of IEHA were elaborated and its energy storage function, which is one of the main advantage of this actuator was presented. Mathematical expressions for energy balance in hydraulic actuators were developed, and the stored and available energy of a hydraulic actuator during different working stages was calculated. Finally, a number of cases of power consumption of an actuator during its working cycle were explained and calculation of the minimal power of the electric motor used in the hydraulic system is proposed in case of energy storage.

Finally, a comprehensive study of energetic effects of hydraulic actuators and energy storage was carried out in chapter 7 on different walking gaits of a bipedal robot. A number of methodologies were presented to improve the energetic efficiency of the studied biped during walking. A set of optimal walking gait trajectories were generated using parametric optimization algorithm on a robot equipped with hydraulic actuators. Two different types of walking gaits were studied. Energetic effects of knee locking without possibility to store energy, storage function ON, and storage function OFF were explored and the simulation results were then compared with that of basic robot. The main focus of the study was to economize the energy consumption of a bipedal robot during walking.

It was concluded from the simulation results that energetic efficiency of a bipedal robot during walking is significantly improved by locking the support knee during entire single support phase for gait types 2. Consumption of energy is further reduced by activating the energy storage function, and storing the energy in a hydraulic reservoir in the form of hydraulic pressure. The stored energy is then re-used when needed particularly during swing phase. It was also observed that the support knee can be fixed at a constant value for all walking speeds without significantly affecting the energetic efficiency of the biped. It was found that knee locking is not effective for gait type 3 and that storing energy is only effective at high walking speeds. Finally, optimization criteria of walking gait types 2 and 3 were compared, and it was found that gait type 3 is more energetically costly for the studied criterion than gait type 2 for all walking speeds. The increased cost of walking was because of the finite double support phase, zero landing velocity of the heel touching the ground, and the impulsive impact on toe of the biped.

The preset thesis presented different strategies, which can be used to improve the energetic efficiency of a bipedal robot during walking. These strategies include, 1) study of effects of torsional springs and support knee locking on the energy consumption during walking, 2) study of a new type of integrated electro-hydraulic actuator and the effects of energy storage of this type of actuator by locking the support knee joint, 3) study of three different types of walking gaits having impact and double support phase with heel take-off of the rear foot at heel impact of the front foot. Practical implementation of the proposed techniques will solve to some extent the issue of energy consumption of bipedal robots and hence improve their autonomy. The total mass of the biped will be reduced by selecting smaller gear box or motor as well as small batteries for equivalent autonomy. Consequently, the overall cost will also be reduced.

8.2 Perspectives

In line with previous research, this study reinforces the idea of using passive joint stiffness to improve energetic efficiency of a biped especially on the hip joints in our case. However, contrary to previous work, ankle springs were not effective in our study. Hydraulic actuators were also used to store energy and improve the performance of bipedal walking. In perspective of this study, a number of different studies can be done to explore the effects of springs, knee locking, and hydraulic actuators on bipedal walking.

The first step would be to generate walking trajectories for a planar biped as close as possible to human walking. This can be done by introducing rotation of toe of the rear foot during stance phase. In bipedal walking, this toe rotation will result in one degree of under-actuated system. It is therefore not possible to freely define the behavior of all the joints. The problem of under-actuation has been treated in a number of studies [38, 10]. The effects of knee locking and addition of torsional springs in parallel to the existing actuators can be studied on this type of walking gaits.

Secondly, the effects of spring offset or bias angle and the ankle springs with foot rotation during double support phase as well as during single support phase on the energetic efficiency of the biped needs to be studied. In case of hydraulic actuators, an algorithm can be developed to share the store energy between multiple actuators.

In present study, only identical springs were added to a pair of same joints (both ankles, both knees, both hips), the study can be extended to explore effects of different springs at different joints simultaneously, for example springs can be added to the pair of knee joints and hip joints.

Keeping in view the energetic effects of torsional springs in parallel to the existing actuators on a biped with electric actuators, it will be a good study to add springs to different joints of the biped with hydraulic actuators. Apart from torsional springs in parallel, series compression springs can be added to different links of the biped structure to explore their effects on energy consumption during walking.

In present study, only support knee joint was locked to study the effects on energy consumption during walking and store energy in case of hydraulic actuators. Similar to knee joint, locking of other joints particularly support hip joint can be studied. Furthermore, instead of locking the joint during the entire single support phase, it can be locked during a specific portion of the single support phase.

Finally, the study can be extended to generate walking gait trajectories for 3D bipedal robots and explore the effects of springs on different joints in different planes for example in frontal or traversal planes. Similarly, the idea of knee locking can also be extended to other joints like hip joint etc to minimize energy consumption. Moreover, effects of hydraulic actuators and energy storage function can also be explored on energetic efficiency of 3D bipedal walking.

A

Résumé Étendu en Français

A.1 Introduction générale

Actuellement, la recherche sur les robots bipèdes est l'un des sujet le plus passionnant et fascinant dans le domaine de la robotique. Le champ d'application est vaste, tant pour l'industrie ainsi que toute utilisation de la vie quotidienne, et beaucoup de problèmes scientifiques difficiles sont encore ouvertes. Un travail important a été fait pour générer des trajectoires de marche qui sont anthropomorphique et aussi proche que possible de la marche humaine tout en étant énergiquement efficace et dynamiquement stable [31, 88, 128]. Les chercheurs dans le domaine de la robotique humanoïde sont inspirés par la marche humaine et essaient de la reproduire pour les robots bipèdes. La recherche en biomécanique [65, 121, 2] montre que la marche humaine est un processus de locomotion dans lequel le tronc érigé est soutenu par une première jambe, puis l'autre. Lorsque le tronc mobile passe au-dessus de la jambe d'appui, l'autre jambe est transférée vers l'avant et se prépare pour sa prochaine phase d'appui. Un pied ou l'autre est toujours en contact sur le sol, et au cours de cette période, lorsque l'appui du corps est transféré de la jambe arrière à la jambe d'avant, il y a une brève période appelée «phase de double appui". Pendant la phase de double appui, les deux pieds sont en contact avec le sol [65]. Lorsque la vitesse de marche augmente, ces périodes de double appui deviennent plus brèves jusqu'à ce qu'elles disparaissent totalement et soient remplacés par de brèves périodes appelées "phase de vol" alors qu'aucun le pied ne soit au sol. A ce moment, la marche devient la course. Les alternances cycliques de la phase d'appui de chaque jambe et l'existence d'une phase de double appui lorsque les deux pieds sont au sol sont des éléments essentiels de la marche. Un pas cyclique de la marche humaine est composé de deux phases principales, *phase d'appui* et *phase de transfert*.

La notion de locomotion d'un robot englobe diverses méthodes qui permettent à des robots de se déplacer géographiquement d'un endroit à un autre. On peut distinguer deux catégories principales, la *locomotion à roues* et la *locomotion à pattes*. Les robots à roues sont couramment utilisés pour transporter des charges tels que PatrolBot [104] et PowerBot [83] et à des fins d'exploration des planètes comme Rover [70]. Actuellement, les robots à pattes sont généralement utilisés à des fins de recherche en laboratoire ou dans l'industrie du divertissement. Des exemples typiques de robots à pattes comprennent la série HRP [69, 68], ASIMO de Honda [97], NAO de Aldebran robotique [51], BidDog, RiSE et RHex de Boston Dynamics [15, 17, 16] etc.

En termes d'efficacité énergétique sur des surfaces planes, des robots à roues sont les plus efficaces. Cela est dû au fait que pour un roulement idéal non glissant, la roue ne perd pas d'énergie (en négligeant les pertes par frottement). Par contre les robots à pattes, perdent de l'énergie lors de l'impact du talon avec le sol. Bien que des robots à roues sont généralement très économes en terme de l'énergie et simple à contrôler, la locomotion à pattes peut être plus approprié pour traverser un sol irrégulier, se déplacer et interagir dans des environnements humains. En outre, l'étude de robots bipèdes peut avoir un impact bénéfique sur la biomécanique et l'amélioration de la conception et la performance des orthèses et prothèses. L'objectif de cette étude est de générer des allures de marche énergétiquement efficace pour un bipède. Le champ d'application de cette étude est limité aux bipèdes planaires, car le mouvement dans le plan sagittal a une contribution dominante vis à vis de la consommation énergétique durant la marche.

La recherche sur la marche bipède au cours des dernières décennies a permis d'obtenir des robots bipèdes avec une polyvalence impressionnante. Les bipèdes comme ASIMO [97] (Figure 2.9(a)) ou HRP-2 [68] (Figure 2.9(b)) peuvent marcher, monter les escaliers, et même courir. En plus de cette polyvalence, les propriétés souhaitables d'un robot humanoïde sont une faible consommation d'énergie et de mouvement de la marche proche de celui des humaines. En comparaison à la marche humaine, l'efficacité énergétique des robots bipèdes d'aujourd'hui est significativement inférieure. En outre, les allures de marche de la plupart des robots bipèdes ressemblent seulement vaguement à une marche humaine [99].

Au cours des deux dernières décennies, les études sur les robots passifs ont considérablement attiré l'attention des chercheurs par leur performance énergétique et par la proximité avec des allures humaines. Un robot est appelé passif lorsque aucune énergie externe (actionneur) est nécessaire pour la marche. En 1990 McGeer [80] a présenté son travail sur la marche dynamique passive et démontré qu'il est possible d'exploiter la distribution de masse du robot pour le faire marcher sur une pente faible sans actionnement [48].

S'inspirant du travail du McGeer sur les marcheurs passifs, la communauté des chercheurs du domaine de la robotique humanoïde a développé les robots bipèdes dynamiques semi-passifs à actionnement minimal pour leur permettre marcher sur des surfaces horizontales [31, 32]. Ces robots sont capables de marcher sur des surfaces horizontales avec un coût énergétique à peu près égal à celle de l'humain. Les trois robots marcheurs les plus célèbres capable de marcher sur les surfaces plats basés sur la conception de robot passif sont le bipède Cornell, le bipède Denise (Delft) [8, 124] et le bipède du MIT [32]. Ces bipèdes motorisés ont des mouvements proches de ceux de leurs homologues passifs [32]. Gini et all [48] ont étendu ces principes à des robots complètement actionnés et construit un robot avec des compliances articulaires et un genou de conception original afin d'améliorer l'efficacité de la marche.

Les robots humanoïdes sont les robots biologiquement inspirés. Ils ressemblent à un humain ayant deux jambes, un torse, et deux bras, bien que certains robots bipèdes puissent être limités à une partie seulement du corps. Par exemple, la plupart des bipèdes marchant dans les laboratoires de recherche ont seulement deux jambes et un torse [100, 107, 44]. Comme le robot bipède RABBIT [25] ils peuvent aussi ne pas avoir de pieds, c'est à dire avoir des pieds ponctuels. Cependant, le nombre de robots humanoïdes ayant des bras, la tête et les pieds sont en hausse. Les chercheurs s'intéressent aux effets énergétiques de la compliance sur les allures de marche en ajoutant des ressorts aux différentes articulations des bipèdes. La plupart des chercheurs, y compris [42, 99, 100, 86] sont motivés par l'hypothèse que les bipèdes avec des ressorts aux chevilles peuvent être en mesure de présenter des allures plus naturelles avec une meilleure efficacité énergétique et une plus grande stabilité de marche que les bipèdes sans ressorts aux articulations. Plusieurs chercheurs ont étudié la conception de l'articulation du genou pour aider à améliorer l'efficacité de marche [53, 79] et d'autres se sont concentrés sur l'ajout d'éléments élastiques passifs dans le genou et la hanche. La compliance de la jambe de transfert peut aussi réduire le coût énergétique en produisant des couples anti-gravité qui réduisent la quantité de travail de l'actionneur nécessaire pour avancer la jambe libre [81].

L'un des problèmes essentiels dans le domaine de la robotique en particulier dans la génération de trajectoires de marche de robot humanoïde est la consommation d'énergie lors de la marche. Des études montrent que les jambes des robots humanoïdes consomment plus d'énergie dans la phase d'appui que dans la phase de transfert [36]. Cette différence dans la consommation d'énergie est due à la demande des couples élevés pour appuyer le poids du robot sur le sol. Par conséquent, il y a place pour une amélioration significative en optimisant la consommation d'énergie de la jambe d'appui. Förg [36] a montré que le l'articulation la plus énergivore est l'articulation du genou d'appui.

Récemment, des éléments élastiques linéaires (ressorts) ont été utilisés afin de récupérer l'énergie perdue, diminuer la consommation d'énergie, et stabiliser l'allure de marche. Dans la plupart des cas, les ressorts sont ajoutés à la cheville du bipède pour stocker l'énergie et de l'utiliser en cas de besoin. Cette énergie stockée est principalement utilisé lors de la phase de propulsion de la cheville juste avant l'impact du talon de la jambe libre. Geyer et al. [47] ont introduit l'idée de jambes compliantes avec ressorts de compression pour marcher et courir. Ils ont montré que les jambes avec compliance sont essentielles pour expliquer la mécanique de la marche. Ils ont étudié un modèle masse-ressort du bipède, qui contient la phase de double appui comme une partie essentielle de mouvement et reproduit les caractéristiques dynamiques de la marche. Leur modèle combine la dynamique fondamentale de marche et de course dans un seul système mécanique. Dans une autre étude, un contrôleur avec compliance est utilisé pour régler la raideur de l'actionneur avec ressort adaptable et ainsi réduire la consommation d'énergie du bipède pendant la marche du robot Lucy [119]. Lucy est actionnée par des muscles artificiels pneumatiques et est capable de marcher à une vitesse de marche lente de 0,15 m/s.

Une autre méthode de réduction de la consommation d'énergie est de bloqué mécaniquement le genou d'appui à l'impact et de libérer l'articulation à la fin de la phase de double appui. Le blocage du genou avec mécanisme de déclenchement actif est jugée technologiquement simple et énergiquement efficace [114]. Toutefois, les effets combinés de blocage du genou et l'ajout de ressorts n'ont pas été explorées, les effets de la compliance sur la consommation d'énergie n'ont pas non plus été étudiés pour plusieurs vitesses de marche. Notre travail explorera donc ces deux domaines et présentera des résultats des simulations détaillées et la comparaison des différentes techniques pour améliorer l'efficacité de marche.

Afin d'avoir des allures de marche efficace, un travail significatif a été réalisé sur la récupération de l'énergie perdue au cours de chaque pas de marche [80, 73, 31, 76]. Cependant, les effets énergétiques de ressorts de torsion en parallèle à l'actionneur existant, n'ont pas été suffisamment explorés. La première partie de cette étude se concentre sur deux stratégies différentes pour améliorer l'efficacité énergétique d'un robot bipède planaire. Dans la première méthode, des ressorts de torsion seront ajoutés à différentes articulations du robot en parallèle aux actionneurs existants, et les effets énergétiques seront étudiés. Ensuite, le genou d'appui du bipède est bloqué mécaniquement pendant toute la phase de transfert afin de réduire la consommation d'énergie. Les deux techniques seront appliquées à différentes allures de marche du bipède planaire en commençant par l'allure le plus simple pour finir par une allure relativement complexe et plus naturelle incluant une phase de double appui fini.

Dans le domaine de la robotique humanoïde, un autre problème plus important et difficile est la conception et le choix du système d'actionnement. De hautes performances en actionnement sont nécessaires. Dans le futur, les robots humanoïdes vont être intégrés dans l'environnement humain pour effectuer des tâches telles que l'assistance personnelle, où ils aideront les personnes malades et les personnes âgées. Afin d'intégrer les robots dans l'environnement humain, ils doivent être sûrs pour les humains. Par exemple, dans le domaine de la robotique humanoïde, les propriétés essentielles et souhaitables pour les actionneurs sont: (1) grand rapport puissance masse, (2) capacité à produire un couple élevé à basse vitesse; (3) haute intégrabilité (réduction du volume occupé), (4) capacité de générer des mouvements articulaires lisses produisant de mouvements de marche proche les humains.

Les systèmes robotiques tels que des robots humanoïdes sont généralement actionnées par deux principaux types d'actionneurs, électrique et hydraulique (ou pneumatique). Les robots humanoïdes les plus connues utilisant des actionneurs électriques sont ASIMO de HONDA [58], WABIAN-2 [89], et HRP-2 [68] etc. et ceux utilisant l'actionnement hydraulique sont HYDROïD [3], et l'humanoïde UT-Theta 2 de l'Université de Tokyo [67]. Il est à noter que les actionneurs électriques ont l'avantage d'un coût réduit et sont faciles à programmer dans la loi de commande. Cependant, un certain nombre d'inconvénients apparaissent lorsque les moteurs électriques sont utilisés avec un réducteur à engrenages mécanique. Tout d'abord, en raison de la connexion quasi-rigide entre le moteur et sa charge, il est difficile de produire le compliance de l'articulation nécessaire à la sécurité. Deuxièmement, des actionneurs électriques doivent être dimensionnés pour le pire des cas, pour être capable de fournir le couple instantané le plus élevé nécessaire. Cela conduit à un actionneur électrique surdimensionné non-optimal, qui ne sera pas utilisé tout le temps à sa pleine capacité.

A partir de l'analyse des solutions existantes, et les exigences de robots bipèdes, un actionneur à haute performance électro-hydraulique intégré (IEHA) a été développé par S. Alfayad et al. [6, 7]. Il utilise le déplacement d'une micro valve afin de contrôler le moteur hydraulique. Cet actionneur hydraulique nouvellement développé a une faible masse et satisfait toutes les performances nécessaires pour actionner un robot humanoïde [3]. Les avantages de IEHA sont, 1) un poids léger, 2) actionneur complet incluant un micro pompe hydraulique, 3) fonction de stockage d'énergie, et 4) aucun système de pompage centrale requis. Cet actionneur est capable de stocker de l'énergie qui peut être utilisée en cas de besoin. Le bipède HYDROïD équipé de nouveaux actionneurs IEHA est développé dans le cadre du projet intitulé R2A2 soutenu par l'Agence Nationale de la Recherche (ANR). Dans ce travail nous examinerons les effets du stockage de l'énergie sur différentes allures de marche d'un robot bipède.

A.2 Organisation de la thèse

L'objectif de cette thèse est d'explorer différentes techniques pour améliorer la performance énergétique d'un robot bipède pendant la marche, et de proposer la meilleure option disponible selon le type d'allure du bipède. Les stratégies d'optimisation de l'énergie étudiées dans ce manuscrit comprennent, blocage mécanique du genou d'appui, l'ajout de ressorts à différents articulations du bipède, et l'intégration des actionneurs hydrauliques capables de stocker de l'énergie. Ces techniques sont appliquées à trois allures de marche d'un robot planaire de la plus simple à la plus complexe. Des algorithmes d'optimisation paramétriques [38] sont utilisés afin de générer des trajectoires de marche pour toutes ces allures. Le critère énergétique est calculé après l'application des techniques mentionnées ci-dessus, puis comparé à celui du robot de référence sans blocage du genou et sans ressort.

Ce manuscrit est composé de six chapitres principaux d'un chapitre d'introduction générale et d'un de conclusions. Dans le chapitre 2, la marche humaine est expliquée et différentes statistiques sur la marche humain sont présentées. Différentes phases et événements survenant au cours d'un cycle complet de la marche humain sont discutés et les termes utilisés pour décrire l'allure de marche humaine sont présentés. Les deux phases principales *phase d'appui* et *phase de double appui* et leurs sous-phases expliquées en détail. En outre, la locomotion des robots est discutée et en particulier la marche bipède. La marche humaine est comparée à la marche de robot bipède et la relation entre les deux est établie. Différentes caractéristiques nécessaire à un bipède pour avoir une marche efficace sont présentées. En outre, un critère pour comparer l'efficacité énergétique des différentes machines est présenté. Différentes approches de récupération d'énergie utilisées afin d'améliorer l'efficacité énergétique d'un bipède pendant la marche sont présentés et discutés en détail. L?effet des ressorts, du blocage du genou, et de la conception d'articulation du genou sur l'efficacité énergétique et la stabilité de l'allure de marche sont discutées. Enfin, différentes méthodes utilisées dans cette étude pour améliorer la performance énergétique de la marche bipède sont présentées ce qui conclut le chapitre.

Les paramètres géométriques et dynamiques du bipède étudié sont présentées dans le chapitre 3. Trois types d'allures de marche étudiés dans ce travail sont présentés et leurs différentes phases au cours d?un cycle de marche sont expliquées. Le modèle dynamique est ensuite formulé pour un robot bipède planaire en utilisant la formulation de Lagrange pour les trois allures de marche. Le modèle dynamique pendant simple appui et double appui est élaboré en fonction du type d'allure de marche. Le modèle d'impact pour un robot bipède est développé, et les différentes solutions possibles de contact du pied avec le sol juste après l'impact sont discutées. De plus, le modèle dynamique est étendu afin d'intégrer les effets de ressorts ajoutés en parallèle avec les actionneurs existants.

Dans le chapitre 4, la génération et l'optimisation de trajectoire de référence pour un robot bipède planaire est discutée. Par ailleurs, différentes fonctions pour générer les trajectoires de référence de marche d'un robot bipède sont présentées. L'optimisation de la trajectoire de chacun des trois types d'allures de marche présentés dans le chapitre précédent est expliquée et les paramètres d'optimisation requis pour chaque allure dans les différents cas sont présentés. Les contraintes d'optimisation sont introduites pour une allure de marche cyclique du robot bipède étudié. Deux critères d'optimisation différents, l'un pour les actionneurs électriques et l'autre pour les actionneurs hydrauliques sont présentés. Différents outils d'optimisation sous contrainte non-linéaires sont expliqués. Enfin, les résultats de simulation pour les fonctions d'optimisation *fmincon* et *fgoalattain* sont comparés.

Après avoir présenté le bipède, développé des modèles dynamique et d'impact, et avoir expliqué les différentes techniques de génération de trajectoire, les résultats de simulation des différents types d'allure de marche pour un robot bipède sont présentés dans le chapitre 5. Un certain nombre de stratégies seront présentées pour réduire le critère énergétique lors de la marche.

L'objectif de ce chapitre est de comparer les performances de ces techniques pour les différentes allures de marche. A cet effet, trois types d'allure de marches ont été définie dans le chapitre 3. Les trajectoires de marche optimales pour chaque allure sont générées et le coût de la marche est calculé dans le chapitre 5. Les résultats de simulation obtenus pour chaque type d'allure de marche sont présentés pour différentes vitesses de marche. L'effet de ressorts et blocage du genou sont ensuite comparés sur la base du critère énergétique pour les différentes allures de marche cycliques.

Le chapitre 6 de cette thèse est consacrée à l'introduction d'actionneurs hydrauliques. Dans ce chapitre, le principe de fonctionnement d'un actionneur hydraulique classique est présenté. Un Actionneur électro-hydraulique Intégré (IEHA) à haute performance nouvellement conçu[6, 7] est présenté et ses avantages par rapport à ses homologues sont détaillés. Le modèle simplifié de cet actionneur est présenté et le fonctionnement de ses différentes parties est expliqué en détail. Le schéma CAD éclaté de l'actionneur sera également présenté pour avoir un aperçu des différentes parties de l'actionneur. En outre, les différents modes de fonctionnement du IEHA sont donnés, et sa fonction de stockage d'énergie, qui est l'un des principaux avantages de cet actionneur sera présentée. Les expressions mathématiques traduisant les transferts d'énergie dans les actionneurs hydrauliques seront développées. L?énergie stockée et l'énergie disponible pour l'actionneur au cours des différentes phases de travail sont calculées. Enfin, différents cas de consommation d'énergie d'un actionneur au cours de son cycle de fonctionnement seront expliqués. La fonction de stockage généralisé sera développée et suivie par la conclusion de ce chapitre.

L'étude énergétique des actionneurs hydrauliques et du stockage d'énergie seront étudiées dans le chapitre 7 pour différentes allures de marche d'un robot bipède. Un certain nombre de méthodologies seront présentées pour améliorer l'efficacité énergétique d'un robot humanoïde pendant la marche. Les trajectoires de marche optimales seront générées pour deux types d'allures de marche et un critère fondé sur la consommation d'énergie du bipède sera défini afin de comparer les performances des différentes allures. Un algorithme d'optimisation sera développé, et les paramètres requis pour définir une trajectoire de marche de référence seront également présentés pour chaque allure de marche. Les résultats de simulation obtenus à partir de l'algorithme d'optimisation pour chaque type d'allure seront présentés aux différentes vitesses de marche. Les effets du blocage du genou et du stockage de l'énergie sur la consommation d'énergie lors de la marche de différentes allures de marche cyclique seront ensuite comparés. De même, les effets de la vitesse de marche sur la longueur du pas, la durée du pas, le centre de gravité (CG) du bipède, les forces de réaction du sol, et d'autres paramètres seront également abordés.

Enfin, le travail sera conclu dans le chapitre 8 qui présente un certain nombre de conclusions tirées de cet étude. Des recommandations pour les travaux futurs dans la continuité de ce travail seront également présentées.

A.3 Présentation et modélisation dynamique du bipède

A.3.1 Présentation du bipède

Le bipède planaire, présenté dans la figure 3.1, est composé de deux jambes identiques et un torse. Chaque jambe est composée d'une cuisse, un tibia et un pied rigide. Tous les articulations sont rotoïdes, sans friction et ne peuvent se déplacer que dans le plan sagittal. Le pied droit (pied 1) et le pied gauche (pied 2) sont respectivement le pied d'appui et le pied libre.

A.3.2 Paramètres géométriques du bipède

Les paramètres géométriques et dynamiques du bipède sont donnés dans le tableau 3.1. Ces paramètres sont définis pour le robot humanoïde "HYDROïD" [4] qui a des masses et des longueurs corporelles similaires à ceux d'un être humain, ces paramètres correspondent au modèle du corps humain géométrique conçu par Hanavan [57]. L'inertie du corps présenté est calculé par rapport au centre de masse du corps autour de l'axe z perpendiculaire au plan sagittal. Le robot HYDROïD a aussi des bras, mais dans cette étude, la masse des bras est fusionnée dans la masse du torse. Le centre de gravité et d'inertie du torse est recalculé en prenant compte les effets des bras et en considérant que les bras sont fixés en position étendu au long du torse. La géométrie du pied est présentée dans la figure 3.11 qui explique les différents termes utilisés dans le tableau 3.1.

A.4 Définition des allures de marche étudiées

Différents types d'allures de marche peuvent être considérés afin de tester la performance d'une allure de marche d'un robot bipède. Les trajectoires de marche optimales seront générées pour le robot bipède étudié en utilisant l'algorithme d'optimisation paramétrique présentée dans le chapitre 4. L'objectif est de générer des trajectoires d'allure de marche qui ressemblent étroitement à la marche humaine. En outre, toutes les trajectoires de marche sont supposées être cycliques.

A.4.1 Allure sans impact

Dans cette étude, l'allure le plus simple étudiée est l'allure sans impact. Elle est constituée uniquement de phases de simple appui séparées par des phases de transition instantanées sans impact. Cette allure sera appelée *allure de type 1* pour plus de simplicité. Dans une allure de type 1, la vitesse du pied libre au contact avec le sol est nulle. Le pied d'appui est le pied 1 et le pied de transfert est pied 2. Le pas de marche commence par une phase de simple appui et se termine avec un contact sans impact pied à plat sur le sol, où les pieds échangent leur rôle. Le pied d'appui devient pied de transfert et vice versa. Le pied d'appui reste en contact à plat sur le sol pendant toute la phase de simple appui. En phase de transition, les articulations sont renumérotées de telle sorte que le pied d'appui est toujours le pied 1. Cela nous permet d'utiliser les mêmes modèles pour le deuxième pas lorsque le pied de transfert devient le pied d'appui. Il n'y a pas de changement dans la configuration, la vitesse et l'accélération des articulations pendant la phase de transition, seulement un re-paramétrage est fait. La figure 3.2 présente l'allure de marche de type 1 pour un bipède. Cette allure a le nombre minimum de paramètres d'optimisation parmi toutes les autres allures de marche étudiés dans cette thèse. Un autre avantage de cette allure est qu'elle n'a pas d'impact et par conséquent, la structure mécanique et les articulations du bipède sont préservées.

A.4.2 Allure avec impact

La trajectoire de marche de cette allure n'est composée que de phases d'appui simple appui séparés par des impacts impulsionnels. Cette allure sera appelée *allure de type 2*. Le pas de marche de l'allure de type 2 commence par une phase de simple appui et se termine par un impact pied à plat avec le sol sur le pied libre. En effet, les pieds échangent leur rôle: le pied d'appui devient le pied de transfert et vice versa. Il n'y a pas de rotation sur le talon ou la pointe du pied d'appui pendant toute la phase de simple appui. Le pied d'appui est considéré comme le base du bipède. Cette allure est illustrée dans la figure 3.4. L'avantage de cette allure est qu'elle a un relativement faible nombre de paramètres à optimiser, ce qui se traduit par une convergence rapide et un coût de calcul limité. En outre, cette allure est énergiquement plus efficace que l'allure de type 1.

A.4.3 Allure avec une phase de double appui

Après l'impact, différents comportements sont possibles. Par exemple, le pied déjà en contact avec le sol peut décoller ou rester sur le sol. Dans le cadre de l'obtention d'un mouvement optimisé, certaines conditions sont imposées après l'impact et il est vérifié que les contraintes liées à ces conditions sont satisfaites. Des trajectoires de marche ayant une phase de double appui sans décollage du pied déjà en contact ont été étudiées par Hobon [79] sans succès. Cependant, il a été constaté qu'une allure de marche ayant une phase de double appui fini peut être réalisée en permettant un décollage partiel du talon et une rotation autour des orteils du pied arrière et du talon du pied avant. Dans cette étude, un décollage du talon du pied arrière à l'impact sur le talon du pied avant est autorisé à obtenir une trajectoire de marche proche de la marche humaine.

L'allure de marche avec phase de double appui appelée *allure de type 3* est la marche plus réaliste et proche de la marche humaine parmi toutes les allures étudiées. Elle est composée de phases de simple appui et de phases de double appui séparées par des impacts impulsionnels instantanées, comme montré sur la figure 3.6. Il y a deux impacts impulsionnels au cours de chaque pas de la marche, l'un au moment du contact du talon et le second lorsque l'orteil du pied avant touche le sol. Ces impacts seront appelés « l'impact du talon » et "l'impact d'orteil", respectivement. Le pas de marche commence avec le premier impact sur le talon du pied de transfert. A cet instant, les deux pieds doivent rester sur le sol pour avoir une phase de double appui. Le talon du pied avant et les orteils du pied arrière restent sur le sol tandis que le talon du pied arrière est autorisé à décoller. C'est le début de la phase de double appui et au cours de cette phase, le pied avant tourne autour de son talon tandis que le pied arrière tourne autour de son orteil.

La phase de double appui se termine lorsque le second impact se produit sur l'orteil du pied avant. C'est la fin de la phase de double appui et début de la phase de simple appui. A cet instant, l'orteil du pied arrière décolle du sol et le pied avant est à plat sur le sol. Le pied avant (pied d'appui) reste en contact plat avec le sol pendant toute la phase de simple appui. Pour des allures cycliques, ce processus est répété à chaque pas de marche. La figure 3.7 présente la position des pieds du bipède pendant les différente phases d'un cycle de marche.

A.5 Modèle dynamique du bipède

Le modèle dynamique est utilisé pour exprimer et modéliser le comportement du système en fonction du temps. Dans le cas d'un bipède, le modèle dynamique inverse fournit les couples et les forces de contact en fonction des positions, vitesses et accélérations articulaires [71].

Modèle dynamique en phase de double appui avec contact explicite :

Pour représenter un bipède planaire ayant 6 ddl, 9 paramètres sont nécessaires pour exprimer le mouvement articulaire et la position et l'orientation d'un corps dans un plan. Ainsi, le vecteur de coordonnées généralisées pour le bipède étudié est définit par $\mathbf{q} = [q_{P1}\ q_{p2}\ q_1\ q_2\ q_3\ q_4\ q_5\ x_h\ y_h]^t$.

Le bipède est représenté sur la figure 3.1. Le modèle dynamique peut être écrit comme:

$$\mathbf{A}(\mathbf{q})\ddot{\mathbf{q}} + \mathbf{C}(\mathbf{q}, \dot{\mathbf{q}})\dot{\mathbf{q}} + \mathbf{G}(\mathbf{q}) = \mathbf{B}\boldsymbol{\Gamma} + \mathbf{J}_1^t\mathbf{R}_1 + \mathbf{J}_2^t\mathbf{R}_2 \tag{A.1}$$

où $\mathbf{A}(\mathbf{q}) \in \mathbb{R}^{9\times9}$ est la matrice d'inertie définie positive, $\mathbf{C}(\mathbf{q}, \dot{\mathbf{q}}) \in \mathbb{R}^{9\times9}$ contient les forces de Coriolis et centrifuges, $\mathbf{G}(\mathbf{q}) \in \mathbb{R}^{9\times1}$ est le vecteur des forces de gravité, $\mathbf{B} \in \mathbb{R}^{9\times6}$ est la matrice d'actionnement qui contient des zéros et un, $\mathbf{J}_1^t$ et $\mathbf{J}_2^t$ sont les matrices Jacobiennes correspondant à l?application d?un torseur d?effort sur le pied 1 et 2 respectivement, et $\mathbf{R}_1$ et $\mathbf{R}_2$ sont les torseurs d'efforts du sol sur le pied 1 et 2 respectivement.

Pour assurer le contact des pieds sur le sol, les contraintes dynamiques de contact doivent être ajoutées. Les équations de contraintes peuvent être exprimées comme suit:

$$\mathbf{J}_1\ddot{\mathbf{q}} + \dot{\mathbf{J}}_1\dot{\mathbf{q}} = 0 \tag{A.2}$$

$$\mathbf{J}_2\ddot{\mathbf{q}} + \dot{\mathbf{J}}_2\dot{\mathbf{q}} = 0 \tag{A.3}$$

Les pieds du bipède peuvent avoir trois types de contacts sur le sol, 1) contact pied à plat, 2) contact au talon, et 3) contact à l'orteil ou pas de contact du tout. Les dimensions de la matrice jacobienne $\mathbf{J}_i$ et le torseur de réactions du sol $\mathbf{R}_i$ dépendent du type de contact du pied i sur le sol. Si le pied i est en contact à plat, alors $\mathbf{J}_i \in \mathbb{R}^{3\times9}$, $\mathbf{R}_i \in \mathbb{R}^{3\times1}$ avec $\mathbf{R}_i = [R_{ix}, R_{iy}, M_i]^t$, et l'équation de contact contient 3 contraintes pour le pied i. De même, si le pied i a un contact ponctuel à la cheville ou à l'orteil avec le sol, alors $\mathbf{J}_i \in \mathbb{R}^{2\times9}$, $\mathbf{R}_i \in \mathbb{R}^{2\times1}$ avec $\mathbf{R}_i = [R_{ix}, R_{iy}]^t$, et l'équation de contact contient 2 contraintes pour le pied i.

Modèle dynamique en phase de simple appui :

Lors de la phase de simple appui, toutes les allures de marche étudiées (type 1, 2, 3) ont un contact pied à plat sur le sol. En phase de simple appui, une liaison implicite du pied d'appui (pied 1) avec le sol est considéré (voir la figure 3.8). Le pied d'appui ne décolle pas et ne glisse pas pendant la phase de simple appui. La configuration du bipède peut alors être exprimée par un vecteur réduit de coordonnée généralisée $\mathbf{q}_{ss}$ tel que:

$$\mathbf{q}_{ss} = [q_{p2}\ q_1\ q_2\ q_3\ q_4\ q_5]^t$$

D'après formulation de Lagrange, le modèle dynamique peut être écrit comme :

$$\mathbf{A}_{ss}(\mathbf{q}_{ss})\ddot{\mathbf{q}}_{ss} + \mathbf{C}_{ss}(\mathbf{q}_{ss}, \dot{\mathbf{q}}_{ss})\dot{\mathbf{q}}_{ss} + \mathbf{G}_{ss}(\mathbf{q}_{ss}) = \mathbf{B}_{ss}\boldsymbol{\Gamma} \tag{A.4}$$

où $\mathbf{A}_{ss}(\mathbf{q}_{ss}) \in \mathbb{R}^{6\times6}$ est la matrice d'inertie définie positive, $\mathbf{C}_{ss}(\mathbf{q}_{ss}, \dot{\mathbf{q}}_{ss}) \in \mathbb{R}^{6\times6}$ contient les forces de Coriolis et centrifuges, $\mathbf{G}_{ss}(\mathbf{q}_{ss}) \in \mathbb{R}^{6\times1}$ est le vecteur des forces de gravité, $\mathbf{B}_{ss} \in \mathbb{R}^{6\times6}$ est la matrice d'actionnement qui contient des zéros et un mais qui diffère de la matrice identité parce que les variables articulaires sont exprimées par des angles absolus, $\boldsymbol{\Gamma} \in \mathbb{R}^{6\times1}$ est le vecteur de couple articulaire.

Modèle dynamique en phase de double appui :

L'allure de type 3 est composé de phases de simples appui et de double appui séparées par des impacts impulsionnels. Pendant la phase de double appui, le bipède est en contact avec le sol par le talon du pied avant et l'orteil du pied arrière comme le montre la figure 3.12. Ainsi, il est possible de modéliser le contact entre le talon du pied avant et le sol par un pivot parfait. Le vecteur de coordonnées généralisées réduite au cours de double appui est donnée par $\mathbf{q}_{ds} = [q_{p1}, q_{p2}, q_1, q_2, q_3, q_4, q_5]^t$. Par conséquent, le modèle dynamique en phase de double appui peut être écrit en prenant compte les forces de réaction du sol sur le pied arrière comme:

$$\mathbf{A}_{ds}(\mathbf{q}_{ds})\ddot{\mathbf{q}}_{ds} + \mathbf{C}_{ds}(\mathbf{q}_{ds}, \dot{\mathbf{q}}_{ds})\dot{\mathbf{q}}_{ds} + \mathbf{G}_{ds}(\mathbf{q}_{ds}) = \mathbf{B}_{ds}\mathbf{\Gamma} + \mathbf{J}^t_{2\,ds}\mathbf{R}_{2\,ds} \tag{A.5}$$

où $\mathbf{A}_{ds}(\mathbf{q}_{ds}) \in \mathbb{R}^{7\times7}$ est la matrice d'inertie définie positive, $\mathbf{C}_{ds}(\mathbf{q}_{ds}, \dot{\mathbf{q}}_{ds}) \in \mathbb{R}^{7\times7}$ contient les forces de Coriolis et centrifuges, $\mathbf{G}_{ds}(\mathbf{q}_{ds}) \in \mathbb{R}^{7\times1}$ est le vecteur des forces de gravité, $\mathbf{B}_{ds} \in \mathbb{R}^{7\times6}$ est la matrice d'actionnement qui contient des zéros et un, et $\mathbf{\Gamma} \in \mathbb{R}^{6\times1}$ est le vecteur de couple articulaire.

Les forces de réaction sur le pied arrière $\mathbf{R}_{2\,ds} \in \mathbb{R}^{2\times1}$ sont prises en compte par la matrice Jacobienne $\mathbf{J}_{2\,ds} \in \mathbb{R}^{2\times7}$. La matrice Jacobienne pour un contact sur l'orteil du pied 2 est donnée par (C.7) (voir Annex C). La force de réaction R_1 n'a aucun effet sur ce modèle dynamique car un contact implicite de type pivot est supposé au talon de la jambe 1, donc cette force de réaction n'a pas de travail virtuel.

Pour assurer un bon contact sur le sol, les équations de contraintes dynamiques doivent être ajoutées.

$$\mathbf{J}_{2\,ds}\ddot{\mathbf{q}}_{ds} + \dot{\mathbf{J}}_{2\,ds}\dot{\mathbf{q}}_{ds} = 0 \tag{A.6}$$

A.5.1 Modèle dynamique avec ressorts

Afin d'intégrer les effets des ressorts dans la dynamique du robot bipède, une modification du modèle dynamique du bipède est nécessaire. Le modèle dynamique inverse du robot bipède ayant un ressort de torsion en parallèle de l'actionneur existant peut être écrit [100] :

$$\mathbf{A}(\mathbf{q})\ddot{\mathbf{q}} + \mathbf{C}(\mathbf{q}, \dot{\mathbf{q}})\dot{\mathbf{q}} + \mathbf{G}(\mathbf{q}) + \mathbf{\Gamma}_s = \mathbf{B}\mathbf{\Gamma} + \mathbf{J}_1^t\mathbf{R}_1 + \mathbf{J}_2^t\mathbf{R}_2 \tag{A.7}$$

où $\mathbf{\Gamma}_s$ est le vecteur de couple fournit par des ressorts et est obtenu par :

$$\mathbf{\Gamma}_s = \sum_{j=1}^{m} \mathbf{\Gamma}_{sj} \tag{A.8}$$

où j est l'articulation sur lequel le ressort est installé, m est le nombre total d'articulations ayant un ressort en parallèle avec l'actionneur, et $\mathbf{\Gamma}_{sj}$ est le vecteur de couple fournit par le ressort de l'articulation j.

A.6 Modèle d'impact

Le sol et le pied du bipède sont supposé rigides, par conséquent, l'impact entre deux corps rigide peut produire des discontinuités sur les vitesses. Les discontinuités produites à la suite de l'impact impulsionnel pourrait être problématique, surtout dans le cas d'une allure de type 3 où les deux pieds sont supposé rester sur le sol après l'impact. L'impact est modélisé par des équations algébriques de l'impact passive [9]. Le mot "passive" signifie qu'aucun couple impulsionnel n?est appliqué lors de l'impact. Dans les sections suivantes, le modèle d'impact pour l'allure de types 2 et 3 sera développé.

Modèle d'impact : contact pied à plat

Le contact pied à plat se produit dans une allure de type 2 à la fin de la phase de simple appui. De même, dans l'allure de type 3, le pied avant est à plat à la fin de la phase de double appui. A l?impact, le pied 1 qui était en support quitte le sol dans les deux types d'allures de marche. Le modèle s'écrit :

$$\mathbf{A}(\mathbf{q}(T))(\dot{\mathbf{q}}^{+} - \dot{\mathbf{q}}^{-}) = \mathbf{J}_j^{\mathrm{t}} \mathbf{I}_j \tag{A.9}$$

où j représente le pied qui reste au sol après l'impact.

Pour assurer le contact du pied qui reste sur le sol, la contrainte ci-dessous doit être satisfaite.

$$\mathbf{J}_j \dot{\mathbf{q}}^{+} = 0 \tag{A.10}$$

Modèle d'impact : contact au talon

Dans le cas d'allure de type 3, l'impact du talon se produit lorsque le talon du pied en transfert touche le sol. Cet impact est suivi d'une phase de double appui où les deux pieds restent au sol. Le modèle d'impact s'écrit :

$$\mathbf{A}(\mathbf{q})(\dot{\mathbf{q}}^{+} - \dot{\mathbf{q}}^{-}) = \mathbf{J}_{2\,toe}^{\mathrm{t}} \mathbf{I}_{2\,toe} + \mathbf{J}_{1\,heel}^{\mathrm{t}} \mathbf{I}_{1\,heel} \tag{A.11}$$

Les contacts au talon du pied avant et à l'orteil du pied arrière sur le sol doivent être assurés en ajoutant des contraintes suivantes :

$$\mathbf{J}_{1heel} \dot{\mathbf{q}}^{+} = 0 \tag{A.12}$$

$$\mathbf{J}_{2\,toe} \dot{\mathbf{q}}^{+} = 0 \tag{A.13}$$

Modèle d'impact : genou bloqué

On suppose pour certaines allures que le genou se bloque lors de l?impact avec le sol. Le blocage est supposé possible mécaniquement à n'importe quelle position présélectionnée. Le blocage du genou modifie le modèle d'impact que l'on peut écrire comme :

$$\mathbf{A}(\mathbf{q}(T))(\dot{\mathbf{q}}^{+} - \dot{\mathbf{q}}^{-}) = \mathbf{J}_2^{\mathrm{t}} \mathbf{I}_2 + \mathbf{J}_k^{\mathrm{t}} \mathbf{I}_k \tag{A.14}$$

où $\mathbf{I}_k$ est la réaction impulsionelle au genou bloqué, et $\mathbf{J}_k \in \mathbb{R}^{1\times 9}$ représente le Jacobian du genou bloqué et contient des zéros et un un.

A.7 Simulation d'allure de marche d'un bipède équipé des actionneurs électriques

Les effets énergétiques de ressorts de torsion et de blocage du genou pendant la marche sont étudiés pour un bipède muni d'actionneurs électriques. Les trajectoires de marche de différent type d'allures sont optimisées en réduisant le critère suivant.

$$C_\Gamma = \frac{1}{d}\int_0^T \mathbf{\Gamma}^t \mathbf{\Gamma} \mathrm{d}t \tag{A.15}$$

où C_Γ est la fonction objectif à optimiser, d est le longueur du pas T représente la durée du pas et $\mathbf{\Gamma}$ est le vecteur des couples articulaires.

Différentes études menées sur le robot bipède sont présentées ci-dessous :

case A. Les trajectoires du robot sont optimisées et le coût énergétique de la marche est calculé sans ajouter des ressorts et sans bloquer le genou.

case B. Les ressorts sont ajoutés à la hanche, au genou ou à la cheville du bipède.

- **case B1.** Le ressort est ajouté uniquement sur les articulations de la jambe d'appui (cheville, genou ou hanche).
- **case B2.** Des ressorts identiques sont ajoutés à la fois sur les articulations des deux jambes (cheville, genou ou hanche).

Dans tous les cas où un ressort est ajouté à l'une des articulations, le coefficient de raideur du ressort K est optimisé avec la trajectoire. L'angle d?offset (ou l'angle de repos du ressort) de ressort q_{sj} est fixé à zéro pour permettre de garder le bipède en position verticale et réduire le couple de l'actionneur.

case C. Le genou d'appui est bloqué mécaniquement à l'impact et pendant toute la phase d?appui sans ajout de ressorts à aucune des articulations. Le genou reste bloqué pendant toute la phase de simple appui.

- **case C1.** L'angle de blocage du genou (β) et l'allure de marche sont optimisés.
- **case C2.** A partir sur les valeurs numériques obtenues dans le cas **C1**, une valeur constante de β est sélectionnée, puis la trajectoire de la marche est optimisée.

case D. Le genou d'appui est bloqué mécaniquement et des ressorts identiques sont ajoutés à la hanche. L'angle de blocage du genou β et la raideur du ressort K sont optimisés avec la trajectoire de marche.

A.7.1 Simulation de la marche de type 1

Résultats avec ressorts

Figure A.1 présente la valeur du critère choisi en fonction de la vitesse de marche d'un bipède dans les cas où les ressorts ont été ajoutés à différentes articulations du bipède en parallèle à l'actionneur existant. Il est clair à partir de la figure A.1(a) que l?effet de l'ajout de ressorts n?est sensible qu?à des vitesses de marche très lentes dans le cas **B1** où le ressort a été introduit sur la cheville de la jambe d'appui. Lorsque les ressorts de torsion ont été ajoutés aux deux articulations des chevilles, les effets énergétiques disparaissent presque.

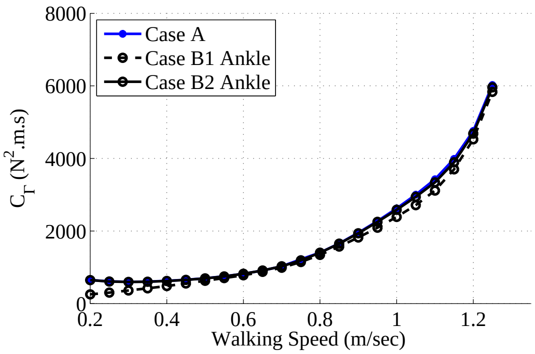

(a) ressorts au cheville

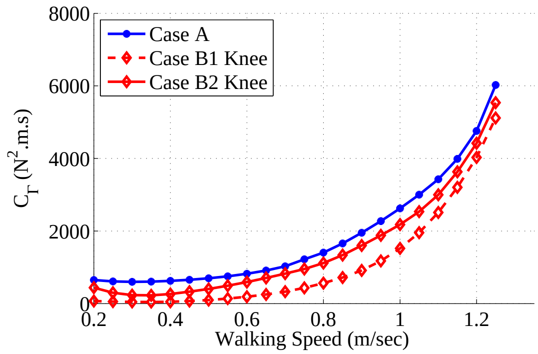

(b) ressorts au genou

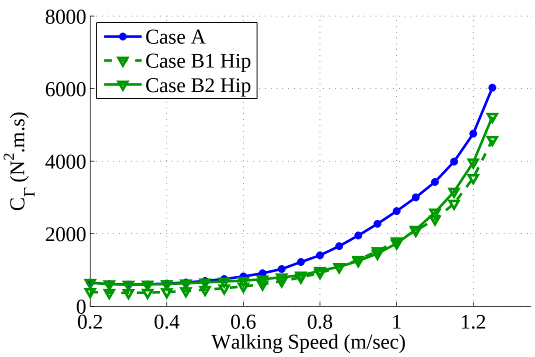

(c) ressorts à la hanche

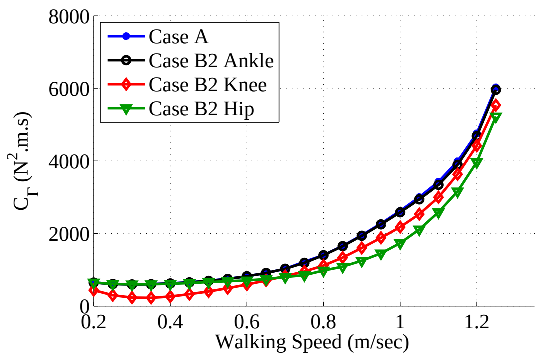

(d) ressorts aux chevilles, genoux, et hanches

Figure A.1 – valeur du critère ($C_\Gamma = \frac{1}{d}\int_0^T \mathbf{\Gamma}^t\mathbf{\Gamma}dt$) en fonction de la vitesse de marche pour allure de type 1 (lignes pleines : ressorts aux deux jambes et lignes pointillées : ressorts à la jambe d'appui)

Le critère d'optimisation a été significativement réduit quand le ressort a été ajouté uniquement à l'articulation du genou d'appui (voir figure A.1(b)). Une réduction significative de la consommation d'énergie pendant la marche a été notée pour une large gamme de vitesse de marche. Des effets similaires ont été observés dans le cas **B2** où des ressorts identiques ont été ajoutés aux deux articulations des genoux.

La figure A.1(c) montre les résultats de simulation pour les articulations de la hanche pour le cas **B1** où le ressort a été ajouté uniquement à la hanche d'appui et pour le cas **B2** où des ressorts identiques ont été ajoutés aux deux articulations des hanches. Les résultats montrent que l'ajout de ressort uniquement à la hanche d'appui est efficace à des vitesses de marche rapide aussi bien que lent. L'ajout de ressorts aux deux hanches est efficace à des vitesses de marche supérieure à 0,6 m/sec (autour de 2 km/h).

Les résultats de simulation en ajoutant des ressorts aux articulations des deux jambes sur les chevilles, les genoux ou les hanches sont présentés simultanément sur la figure A.1(d). Il montre que les ressorts de la cheville ne sont pas du tout efficace pour l'allure de type 1. Il indique également que l'ajout de ressorts identiques aux articulations du genou est efficace aux vitesses lentes de marche tandis que les ressorts aux hanches peuvent être utilisés à des vitesses de marche élevées (supérieures à 0,7 m/sec) pour réduire le coût de marche.

Résultats avec genou bloqué

La figure A.2 donne la comparaison des courbes de critères en fonction de la vitesse de marche dans le cas **A**, le cas **C1** où l'angle de blocage du genou β a été optimisé, et le cas **C2** avec une valeur constante de β. Une valeur moyenne de $8,3$ degré de l'angle blocage du genou β a été calculée à partir des résultats d'optimisation en cas **C1**. Il présente également les résultats de la simulation pour un bipède dans le cas **D** avec des ressorts identiques sur les deux hanches, et un blocage du genou d'appui. C?est le seul cas de combinaison de l?effet des ressorts et du blocage du genou qui est étudié car il n?est pas possible d'étudier simultanément un blocage du genou avec un ressort sur les genoux, et que les ressorts sur les chevilles ne sont pas efficaces.

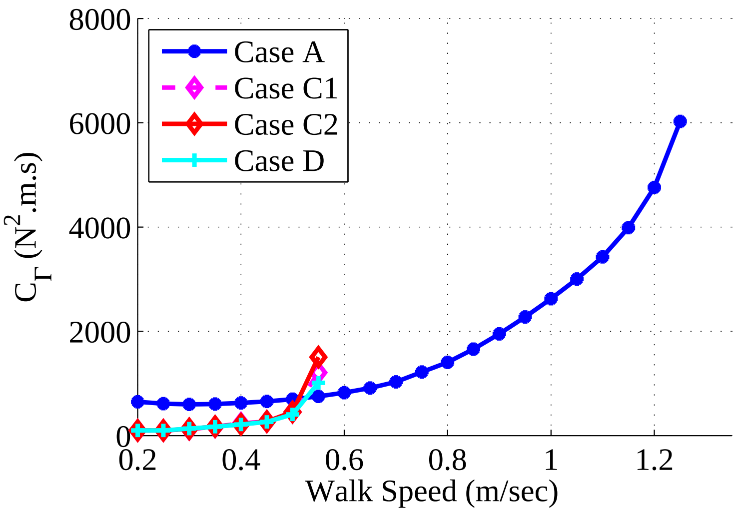

Figure A.2 – Valeur du critère en fonction de la vitesse de marche pour allure de type 1 avec genou bloqué

Les résultats des simulations montrent que le blocage du genou pour une allure de marche sans impact est économique pour des vitesses lentes de marche, mais rend impossible des marches à vitesse élevée. Les deux courbes pour les cas **C1** et **C2** sont superposées, ce qui indique clairement que le genou peut être bloqué à un angle constant pour toutes les vitesses de marche possibles. Il est également claire sur la figure A.2 que l'ajout de ressorts au niveau des articulations de la hanche tandis que le genou d'appui est bloqué a des effets négligeables sur l'économie d'énergie par rapport à genou bloqué uniquement. Par conséquent, il est recommandé d?ajouter des ressorts à l'articulation des genoux et de bloquer le genou d'appui à des vitesses lentes mais pas à des vitesses élevées.

A.7.2 Simulation de la marche de type 2

Résultats avec ressorts

La figure A.3 présente l'évolution du critère pour l'allure de type 2 pour les différents cas étudiés. La figure A.3 montre que le critère d'optimisation est considérablement réduit après l'introduction de ressorts identiques pour les deux articulations des hanches. Il est par contre observé que l'ajout de ressorts aux deux genoux ou aux deux chevilles n'est pas efficace. Cette figure montre également que le critère est considérablement réduit lorsque des ressorts identiques avec une raideur constante sont ajoutés aux deux articulations des hanches (voir les figures A.3(d) et A.3(c)). Par conséquent, il est possible d'ajouter des ressorts de torsion passifs de raideur constante aux hanches, cette démarche est efficace pour presque toutes les vitesses de marche. Cependant, à très lente vitesse de marche, la consommation d'énergie est plus élevé que celle de bipède de référence.

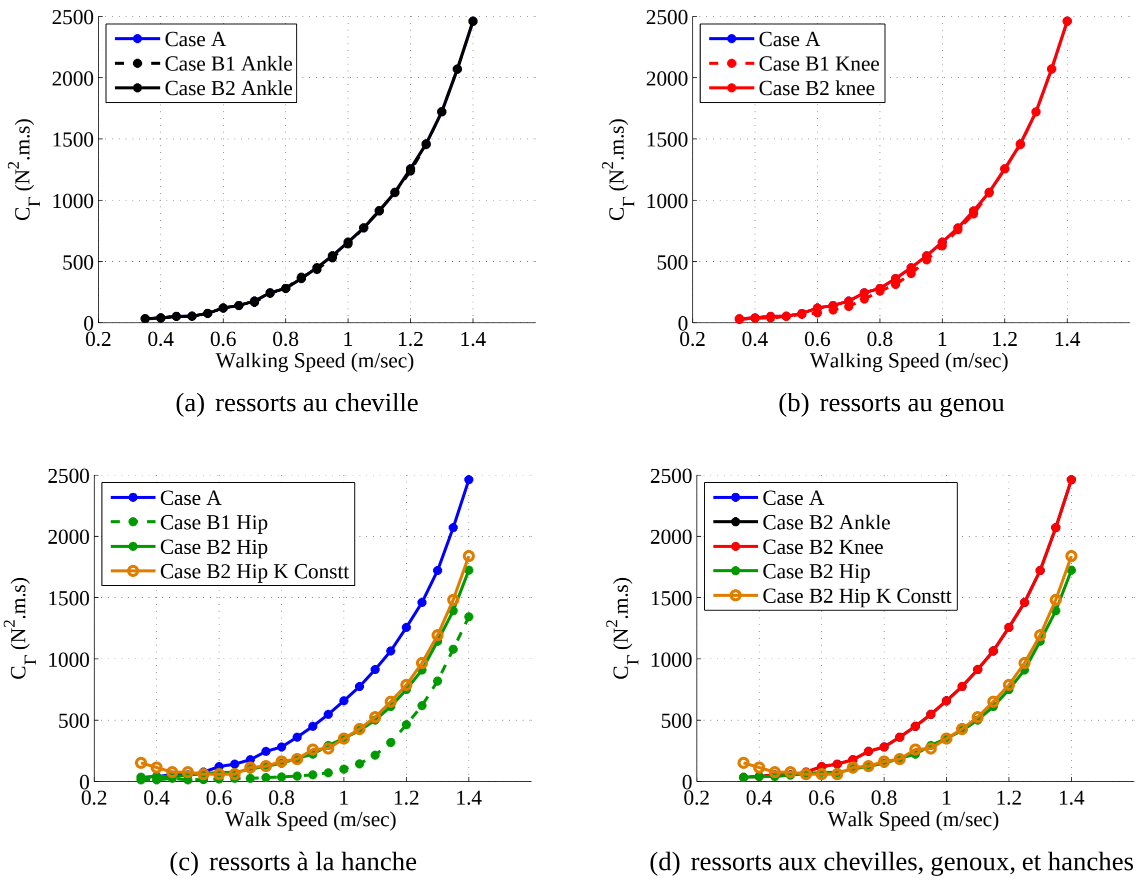

(a) ressorts au cheville

(b) ressorts au genou

(c) ressorts à la hanche

(d) ressorts aux chevilles, genoux, et hanches

Figure A.3 – Valeur du critère en fonction de la vitesse de marche pour l'allure de type 2 (traits pleins : pour les ressorts sur les deux jambes et traits pointillés pour les ressorts sur la jambe d'appui seulement)

Les résultats de simulation montrent que le moyen le plus efficace pour réduire la consommation d'énergie lors de la marche est d'ajouter des ressorts uniquement aux articulations de la jambe d'appui, et la plus efficace est l'articulation de la hanche (voire fig. A.3(c)). L?ajout de ressorts à l?articulation de la hanche économise jusqu'à 85 % de l'énergie à 0,85 m/sec. Les figures A.3(a) et A.3(b) montrent que l'ajout de ressorts uniquement à la cheville d'appui ou au genou ou des deux articulations ne sont pas efficaces pour l'allure de type 2, tandis que les ressorts au genou uniquement ont été bénéfiques pour l'allure de type 1.

Résultats avec genou bloqué

La figure A.4 donne l'évolution des critères sélectionnés en fonction de la vitesse de marche pour le bipède dans le cas **A**, le cas **B2** où des ressorts identiques ont été ajoutés aux deux articulations des hanches, le cas **C2** où l'angle de blocage du genou β de 1 a été défini à partir du cas **C1**, et pour le cas **D** où des ressorts identiques sont utilisés sur les deux hanches simultanément avec un genou d'appui bloqué. La consommation d'énergie dans le cas du blocage du genou et des ressorts sur les deux hanches (cas **D**) est toujours aux autres cas. Il n'y a pas de limitation de la vitesse de marche en cas de blocage du genou comme cela a été observé dans l'allure de type 1. En outre, les vitesses de marche significativement élevées peuvent être obtenues pour tous les cas étudiés par rapport à l'allure de type 1. Ainsi, la présence de l'impact impulsionnel augmente la plage de vitesses dans tous les cas étudiés.

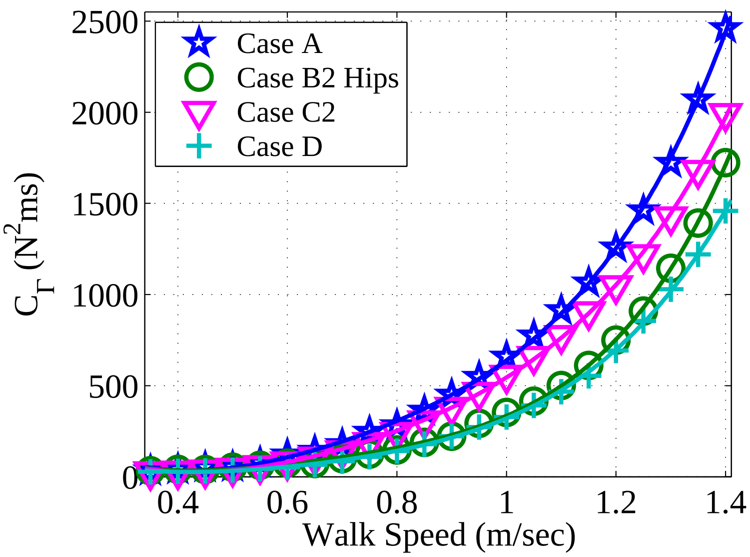

Figure A.4 – Valeur du critère en fonction de la vitesse de marche d'allure de type 2 avec genou bloqué

A.7.3 Simulation de la marche de type 3

Pour les deux allures précédentes, nous avons analysé les effets des ressorts dans les deux cas, lorsque des ressorts identiques sont ajoutés pendant toutes les phases de la marche, et lorsque des ressorts sont ajoutés uniquement pendant la phase d'appui. Dans le cas de cette allure qui inclut des phases de simple appui et des phases de double appui, le cas du ressort utilisé pendant toutes les phases peut évidemment être aussi traité. Mais si nous acceptons d'utiliser un ressort que pendant une partie de la marche, le choix de des phases pendant lesquelles le ressort doit être utilisé n'est pas trivial et dépend de l'articulation où le ressort est placé. Ainsi, afin d'étudier les effets de l'ajout de ressorts sur l'efficacité énergétique d'un robot bipède pendant la marche, et profiter au maximum des ressorts, un certain nombre de combinaisons différentes en ajoutant des ressorts ont été testées et ont permis de sélectionner la meilleure option pour les différents cas de positions des ressorts. Ces différents

Les différentes d'études suivantes sont réalisées sur le robot bipède pour améliorer encore l'efficacité énergétique lors de la marche.

case A. Les trajectoires du robot sont optimisées et le coût énergétique de la marche est calculé sans ajouter des ressorts et sans bloquer le genou.

case B. Des ressorts de torsion sont ajoutés aux différentes articulations du bipède en parallèle avec les actionneurs existants, seul le mode d?activation le plus efficace obtenu précédemment est retenu. L'allure est optimisée avec la raideur du ressort. Cette étude porte sur les sous cas suivants :

case B1. Ressort à l?articulation de la cheville : Le ressort est actif uniquement sur la jambe arrière pendant la phase de double appui.

case B2. Ressort à l?articulation du genou : Le ressort est actif pendant toute la phase de simple appui sur la jambe d'appui et pendant la phase de double appui sur la jambe avant.

case B3. Ressort à l?articulation de la hanche : Les ressorts sont ajoutés aux deux hanches et ils sont actifs pour les deux jambes lors de la phase de double appui et sur la jambe d'appui lors de la phase de simple appui.

Résultats avec ressorts

La figure A.5 présente la comparaison des courbes de critères en fonction de la vitesse de marche pour le robot de référence ainsi que pour tous les cas étudiés avec des ressorts décrit précédemment. Il montre que le critère d'optimisation est considérablement réduit en ajoutant des ressorts de torsion aux articulations de cheville, l'articulation du genou, et les articulations des hanches. Il montre également que les courbes des critères en cas B1 et cas B2 sont presque superposées. La méthode la plus efficace pour réduire la consommation d'énergie lors de la marche est d'ajouter des ressorts de torsion aux deux hanches pendant la phase de double appui, et à la hanche d'appui uniquement lors de la phase de simple appui. Les résultats de simulation des allures de types 1 et 2 ont également montré l'efficacité des ressorts de la hanche alors que les ressorts de la cheville ne sont pas efficaces pour les allures de types 1 et 2. Contrairement aux résultats précédents présentés dans cette étude, et en accord avec les recherches récentes sur la marche bipède, les ressorts de la cheville ont montré leur efficacité uniquement lorsqu'il est ajouté à la jambe arrière pendant la phase de double appui (phase de propulsion) à toutes les vitesses de marche.

Résultats avec genou bloqué

Pour étudier les effets de blocage du genou sur l'allure de type 3, l'articulation du genou d'appui est bloqué pendant toute la phase de simple appui, puis l'allure est optimisée. Le mécanisme de blocage est supposé sans masse et bidirectionnelle. Pendant le blocage, le couple articulaire est fourni par le mécanisme de blocage et le couple d'actionneur est nul. La figure A.6 présente la comparaison du critère de référence pour le robot de référence avec celle du genou bloqué. On observe qu?aux basse vitesses les deux courbes sont presque superposées tandis qu?aux vitesse plus élevées le blocage du genou est plus coûteux. Contrairement aux résultats précédents dans le cas de la marche types 1 et 2, le blocage du genou n'est pas efficace pour l'allure de type 3. Par conséquent, il n'est pas nécessaire de bloquer l'articulation du genou pour cette allure.

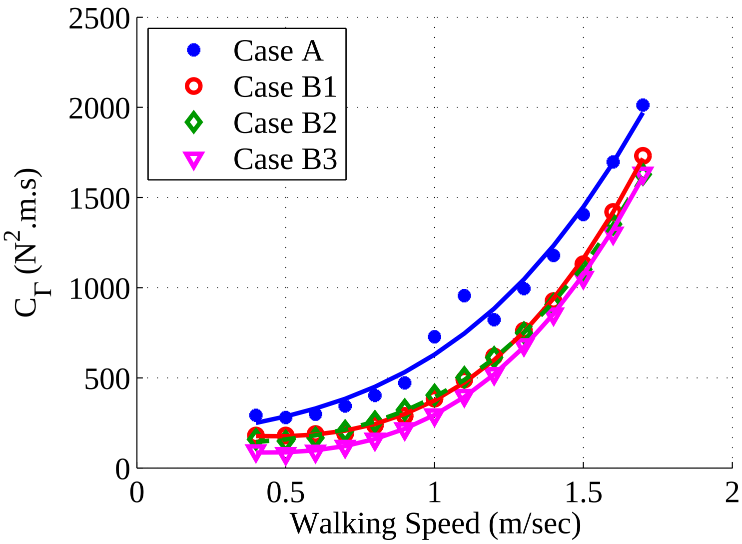

Figure A.5 – Valeur du critère en fonction de la vitesse de marche d'allure de type 3 avec ressorts

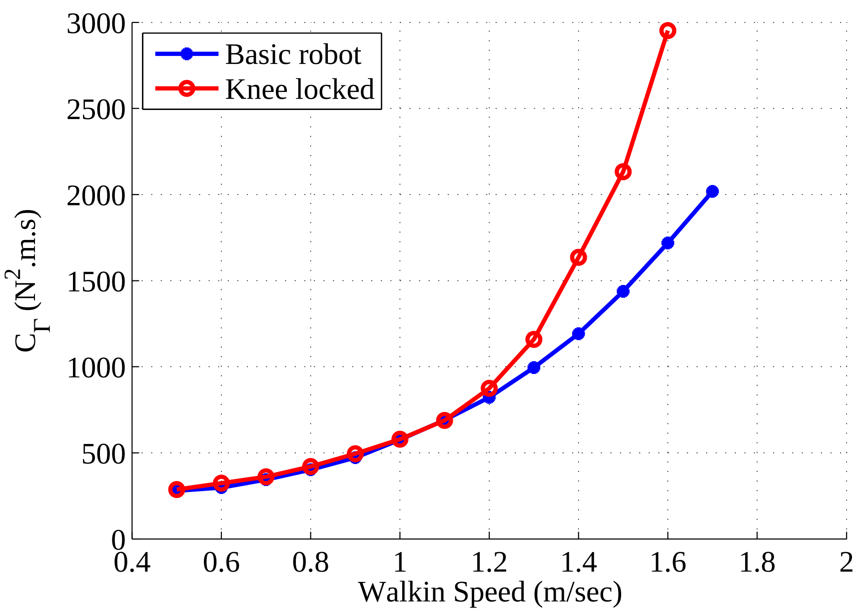

Figure A.6 – Comparaison des critères de référence avec genou d'appui bloqué pour l'allure de type 3

A.7.4 Comparaison des allures de marche étudiées

Les résultats de simulation de trois types d'allures de marche ont été présentés dans cette section. La figure A.7 présente la comparaison du critère choisi en fonction de la vitesse de marche de bipède de référence pour toutes les allures de marche étudiées. Le coût de l'allure sans impact avec des phases de simple appui uniquement est très élevé par rapport aux deux autres allures. Cependant, l'avantage de cette allure est qu'aucun impact n?a lieu, ce qui réduit les dommages de la structure du bipède. On observe également que l'énergie consommée lors d'un pas de marche pour l'allure de type 3 est nettement inférieure à celle d'allure de type 2 à une vitesse de marche élevé. Cependant, la consommation d'énergie de l?allure de type 3 est légèrement plus élevé que l'allure de type 2 à basse vitesse de marche. Les courbes critères des deux allures de marche se croisent à environ 0,9 m/sec. La faible consommation d'énergie de l'allure de type 3 est due à la présence d'une phase de double appui, ce qui favorise des vitesses de marche plus élevés. Même si elle a une plus forte consommation énergétique à basse vitesse, cette allure est plus anthropomorphique. On observe également que les forces impultioneles sont considérablement réduites par rapport l'allure de type 2 en particulier à des vitesses élevées, les risques d?endommagement de la structure mécanique sont ainsi réduits. Par conséquent, parmi les trois allures étudiés, l'allure avec double appui finie (type 3) est la plus réaliste et plus proche de la marche humaine.

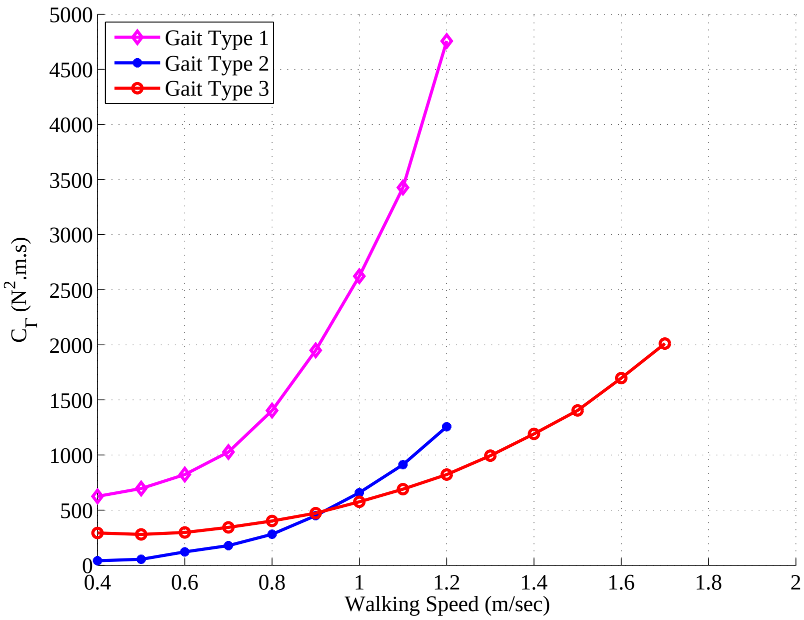

Figure A.7 – Comparaison de la consommation d'énergie des allures de marche étudiées à différentes vitesses de marche

A.8 Simulation d'allure de marche d'un bipède équipé des actionneurs hydrauliques

Dans cette section, le bipède doté d'un l'actionneur haute performance électro-hydraulique intégré (IEHA) développé par S. Alfayad et al. [6, 7] est étudié. L'objectif de l'étude est d'explorer les capacités de stockage d'énergie de l?IEHA et de comparer ses performances sur différentes allures de marche. Le critère de performance utilisé dans ce section afin de comparer différentes allures est basé sur l'énergie d'actionneur et est différente de celle utilisée dans la section A.7.

Le critère d'optimisation pour le bipède étudié sans stockage d'énergie peut être exprimé comme :

$$C_{max} = \frac{1}{d}\sum_{i=1}^{n}(max(|\Gamma_i(t)\dot{\theta}_i(t)|)T) \tag{A.16}$$

Où Γ_i est le couple articulaire, $\dot{\theta}_i$ est la vitesse articulaire i, d est la distance parcourue en un pas, T est la durée du pas, et n est le nombre d'articulations du bipède. Le critère ci-dessus est valable pour n'importe quel bipède équipé d'actionneurs hydrauliques classiques alimentés par des moteurs électriques fonctionnant à une vitesse angulaire constante.

En cas de stockage de l'énergie, il peut être démontré que l'énergie utilisée par le moteur électrique alimentant la micro pompe est donnée par le critère suivant :

$$C_S = min(\frac{1}{d}\mathbf{P}\ T) \tag{A.17}$$

sous la contrainte suivante

$$P_i T_{is} = \int_0^T max(0, |\Gamma_i(t)\dot{\theta}_i(t)| - P_i)\mathrm{d}t \tag{A.18}$$

Où P_i est la puissance de moteur de l?articulation i, $\mathbf{P} = [P_1, ..., P_n]$, T est la durée du pas et T_{is} et la durée pour laquelle l'articulation i est bloquée et l'énergie est stockée.

Les différentes méthodes utilisées dans cette étude pour améliorer la performance énergétique d'un robot bipède lors de la marche sont :

case A. Les trajectoires de marche sont optimisées et le coût énergétique de la marche est calculé sans ajouter de ressorts et sans bloquer le genou.

case B. Genou d'appui est bloqué à l'impact et reste bloqué pendant toute la phase de simple appui.

- **case B1.** Genou d'appui est bloqué sans possibilité de stockage de l'énergie. L'angle de blocage (β) est optimisé avec la trajectoire de marche.
- **case B2.** Genou d'appui est bloqué avec possibilité de stockage de l'énergie qui peut être utilisé pendant la phase de simple appui. L'angle de blocage (β) est optimisé avec la trajectoire de marche.
- **case B3.** A partir de valeur obtenu en cas **B2**, une valeur constante de β est sélectionnée et l'allure de marche est optimisé.

A.8.1 Simulation de la marche de type 2

La figure 7.2(a) présente la comparaison des courbes de critères en fonction de la vitesse de marche pour tous les cas étudiés. Les résultats de simulation montrent que la méthode la plus efficace pour réduire la consommation d'énergie lors de la marche est de bloquer l'articulation du genou d'appui, de stocker l'énergie pendant la phase de blocage et de réutiliser l'énergie stockée lorsque cela est nécessaire. Elle montre que le critère d'optimisation est considérablement réduit, après stockage de l'énergie lors du blocage du genou et la réutilisation pendant la phase de transfert. L'énergie est également réduite lorsque le genou d'appui est bloqué sans l'activation du stockage d'énergie. La consommation d'énergie de l'articulation du genou est nul dans la position isométrique, par conséquent, la consommation nette pendant la marche est réduite. Aucun dispositif supplémentaire de stockage d?énergie n?est nécessaire. Dans le cas où genou est bloqué sans stockage d'énergie, les besoins en énergie sont calculés sur la base du genou libre, qui consomme moins d'énergie par rapport au genou d'appui. En cas **??** où le stockage est activé et l'angle de blocage du genou β est optimisé, et le cas **??** avec stockage activé et β constant, les courbes de critères ont presque mêmes valeurs pour toutes les vitesses de marche. Par conséquent, il est possible de bloquer le genou d'appui à une valeur constante pour toutes les trajectoires valides d'allure de type 2.

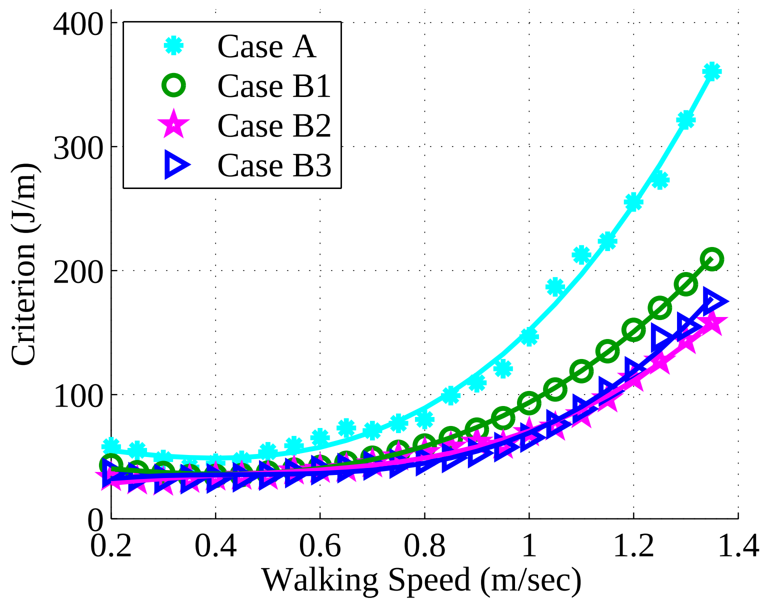

Figure A.8 – Valeur du critère en fonction de la vitesse de marche pour une allure de type 2

Il est conclu que la consommation d'énergie d'un bipède pendant la marche est considérablement réduite en bloquant le genou d'appui pendant toute la phase de simple appui. On observe également que l'énergie supplémentaire peut être économisée en ajoutant la possibilité de stocker de l'énergie tandis que l'articulation du genou est bloqué.

Les résultats de simulation d'allure de type 2 montrent que l'application de ces stratégies permettra d'améliorer considérablement l'efficacité énergétique ainsi que l'autonomie du bipède étudié. En perspective de cette étude, l'étape suivante consiste à étudier les effets de ces stratégies sur la allure de type 3, qui est la plus complexe et composée de phases de simple appui et double appui avec rotation de pieds pendant la phase de double appui.

A.8.2 Simulation de la marche de type 3

La figure A.9 présente la comparaison des courbes critères en fonction de la vitesse de marche pour tous les cas étudiés. Les résultats de simulation de l?allure de type 3 ressemblent aux résultats pour l'allure de type 3 avec des moteurs électriques même si le critère optimisé est différent. Les résultats montrent également que le blocage du genou n'est pas efficace et entraine même un surcoût par rapport aux marches sans blocage du genou. Dans le chapitre 5, la surconsommation en cas de blocage du genou a augmenté avec l'augmentation de la vitesse de marche tandis que dans ce chapitre, la surconsommation est presque constante à environ 15 % pour toutes les vitesses de marche. La consommation d'énergie de la marche est réduite par l'activation de la fonction de stockage de l'énergie sur le genou d?appui alors qu'il est bloqué pendant toute la phase de simple appui. L'énergie stockée est restituée en cas de besoin particulièrement pendant la phase transfert. L?efficacité énergétique du bipède est alors légèrement améliorée à haute vitesse de marche (plus de 1,0 m/sec), où environ 10 % du coût de marche peut être économisé. Il est à noter que la vitesse de marche confortable (vitesse à laquelle la consommation d'énergie est minimale) pour la marche humaine est d'environ 1,4 m/sec.

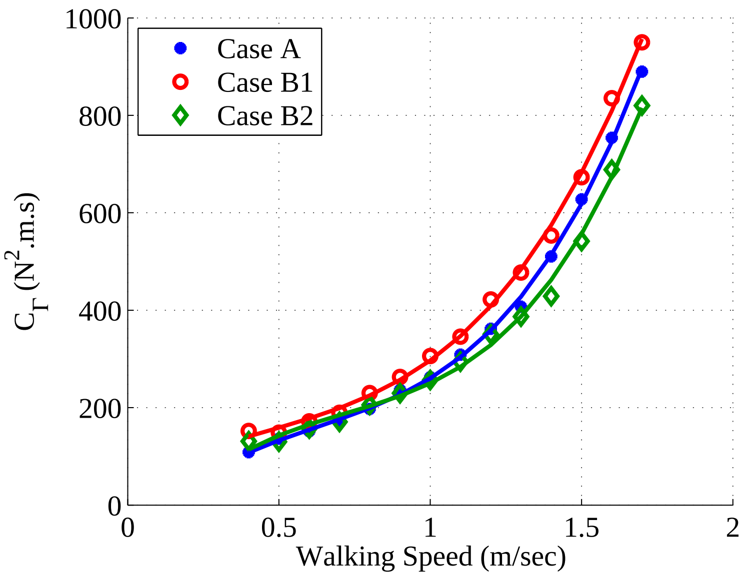

Figure A.9 – Valeur du critère en fonction de la vitesse de marche d'allure de type 3

A.8.3 Comparaison des allures de type 2 et 3

Dans cette partie de la thèse, deux types d'allures de marche ont été présentés. Les effets de blocage du genou et de stockage de l'énergie ont également été discutés sur les trajectoires de marche d'un robot bipède. La figure A.10 présente la comparaison du critère choisi en fonction de la vitesse de marche pour le robot de référence et avec le genou bloqué pour le cas avec le stockage de l'énergie activé. On peut observer que dans tous les cas, la valeur du critère sélectionnée lors de la marche pour l'allure de type 3 est nettement plus élevé que celui d'allure de type 2 à toutes les vitesses de marche. Les valeurs du critère plus élevés pour l'allure de type 3 est due à un certain nombre de différences, comme l'introduction de la phase de double appui fini, un contact sans impact du pied d'avant avec le sol au moment du contact du talon (début de la phase de double appui), et un impact impulsif sur l'orteil du pied avant à la fin de la phase de double appui.

A.9 Conclusion et Perspectives

A.9.1 Conclusion

Cette thèse aborde dans une certaine mesure le problème de la consommation d'énergie d'un bipède planaire pendant une allure de marche. Un certain nombre de stratégies ont été proposées afin de minimiser le critère choisi lors d'un pas de marche. Afin d'appliquer ces stratégies et d'étudier leurs effets sur la marche, un robot bipède planaire a été présenté avec deux types d'actionneurs. Dans le premier cas, des actionneurs électriques classiques sont utilisés et dans le second cas des actionneurs électro-hydraulique intégrés nouvellement conçus sont étudiés. Dans la première partie de l'étude, les effets de blocage du genou et de ressorts de torsion ont été

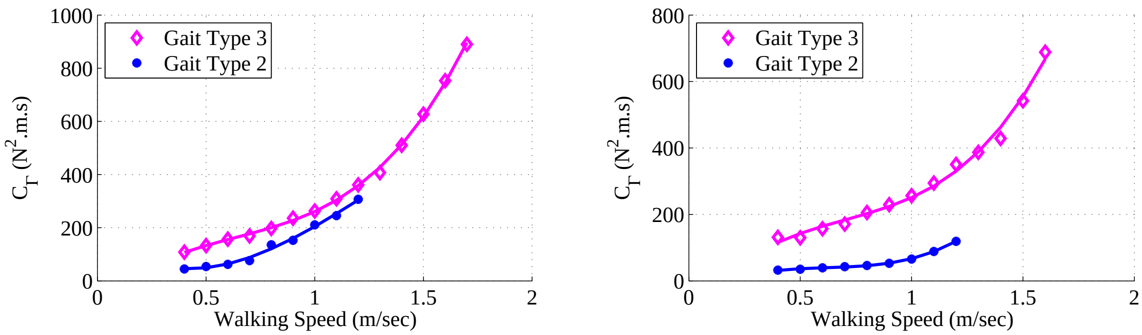

(a) robot de référence (b) stockage activé, β optimisée

Figure A.10 – Comparaison du critère pour l'allure de type 2 et 3 at à différentes vitesses de marche

étudiés sur le critère de performance prédéfini lors de la marche du bipède avec actionneurs électriques. La même bipède avec des actionneurs hydrauliques a été étudié dans la deuxième partie du manuscrit. L'actionneur électro-hydraulique intégré est capable de stocker de l'énergie et de bloquer une articulation à une position quelconque sans consommation énergétique (ou plus exactement avec une consommation d?énergie négligeable. Les effets du blocage du genou et du stockage de l'énergie sur le critère choisi ont été étudiés.

L?introduction générale du sujet et de l'organisation de la thèse ont été présentés dans le chapitre 1. La marche humaine et ses différentes statistiques ont été présentées dans le chapitre 2. En outre, les différentes phases et événements survenant au cours d'un cycle complet d'une allure de marche humaine ont été discutés et des terminologies utilisées pour décrire l'allure de marche humaine ont été présentés. Les deux phases principales *phase d'appui* et *phase d'oscillation*, et leurs sous-phases ont été expliquées en détail. En outre, la locomotion robotique a été discutée, puis la marche humaine a été comparée à celle du bipède. Une relation entre ces deux marches a également été établie. En outre, un critère pour comparer la performance énergétique des différentes machines a été présenté. Un certain nombre d'approches de récupération d'énergie utilisées pour améliorer l'efficacité énergétique d'un bipède pendant la marche ont également été présentées et discutées en détail. L?effet de ressorts, du blocage du genou et de la conception d'articulation du genou sur l'efficacité énergétique et la stabilité de la marche ont été discutés. A la fin du chapitre 2, les différentes méthodes utilisées dans la présente étude afin d'améliorer la performance énergétique de la marche bipède ont été présentées.

Le chapitre 3 a été consacré à la présentation et à la modélisation du bipède étudié. Les paramètres géométriques et inertiels du bipède ont été présentés et le modèle dynamique a été formulé en utilisant la méthode de Lagrange. Le modèle dynamique pendant la phase de simple appui, double appui, et dans le cas général est développé en fonction des différentes phases présentes dans des allures de marche étudiées. Le modèle d'impact pour un robot bipède planaire ayant sept corps a été développé. Les différentes solutions de contact du pied avec le sol juste après l'impact ont été discutées. En outre, le modèle dynamique a été étendu afin d'intégrer l?effet de l'ajout de ressorts en parallèle avec les actionneurs existants et le blocage de l'articulation du genou. En outre, différents types d'allure de marche avec ou sans impact, et avec ou sans phase de double appui ont été définis.

Afin d'identifier les avantages et les effets énergétiques associés aux stratégies proposées afin d’améliorer l’efficacité énergétique d’un bipède, une méthode d’optimisation paramétrique pour générer des trajectoires de marche pour un bipède planaire a été présentée dans le chapitre 4. Les différents outils utilisées afin de produire des trajectoires de marche de référence ont été introduites. La génération de trajectoire pour toutes les allures étudiées a été expliquée et les variables d’optimisation nécessaires pour générer des trajectoires de marche optimale pour ces allures ont été définies. Le critère d’optimisation basée sur le couple actionneur pour des actionneurs électriques et basé sur l’énergie consommée pour des actionneurs hydrauliques a été présenté. Afin de comparer les performances du bipède à différentes vitesses de marche, les trajectoires de marche optimales seront générées pour toutes les allures de marche étudiées. Un ensemble de contraintes nécessaires pour générer une trajectoire de marche optimale faisable a été présenté. Enfin, différents outils d’optimisation sous contrainte non-linéaires de MATLAB ® ont été expliquées et les résultats de simulation pour ces fonctions d’optimisation ont été comparées.

Les résultats de simulation pour le robot bipède HYDROïD avec des actionneurs électriques ont été présentés dans le chapitre 5. Les trajectoires de marche optimales pour chaque allure de marche ont été générées en utilisant des fonctions splines cubiques fonction du temps. Le coût de la marche a été calculé pour chaque type d’allure en utilisant différentes stratégies proposées afin d’améliorer l’efficacité énergétique du bipède. Pour l’allure de type 1, on a constaté que l’efficacité énergétique maximale peut être obtenue en ajoutant des ressorts de torsion aux articulations des hanches et un blocage mécanique du genou de support. Cependant, la vitesse de marche maximale atteignable pour une allure de type 1 uniquement a été réduite de moitié parce que les vitesses articulaires saturent. L’efficacité énergétique de blocage du genou seul à basse vitesse et en ajoutant des ressorts uniquement à l’articulation du genou ou à la hanche à haute vitesse est aussi uns stratégie intéressante. La mise en ouvre de ces techniques d’économie d’énergie permettra d’améliorer l’efficacité énergétique et ainsi l’autonomie des robots bipèdes. En outre, il a été noté que les couples articulaires étaient plus faibles dans le cas avec des ressorts aux hanches et un blocage du genou. Il est alors possible d’utiliser un réducteur avec un rapport de réduction plus petit afin d’obtenir des vitesses articulaires élevées tout en obtenant les couples désirées avec les mêmes moteurs. La réduction du rapport de réduction aurait aussi pour conséquence de réduire la masse du réducteur et donc la masse totale du bipède et donc la consommation d’énergie lors de la marche.

Des trajectoires optimales de marche ont aussi été générées pour l’allure de type 2 pour les deux solutions *i.e.* soit en ajoutant des ressorts de torsion à différentes articulations du bipède, soit en bloquant mécaniquement l’articulation du genou d?appui. L’allure de type 2 a des phases de simples appui et les impacts impulsionnels, il n’y a pas de phase de double appui fini. Des résultats de simulation similaire à ceux de l’allure de type 1 ont été trouvées en termes de réduction de critère basé sur les couples articulaires. Enfin, il a été observé que contrairement à l’allure de type 1, les vitesses articulaires du bipèdes ne sont pas saturés et que le robot était en mesure d’atteindre la même vitesse de marche maximale que celle atteinte par un robot de référence sans ressorts et sans blocage du genou. La présence d’impacts impulsionnels à la fin de chaque pas a permis au bipède d’atteindre des vitesses de marche plus élevées, même avec l’articulation du genou d’appui bloqué. Par ailleurs, comme pour l?allure de type 1, les approches proposées pour réduire la consommation d?énergie permettrait d?utiliser des moteurs de plus faibles puissances. Cela se traduira par une réduction de la masse totale du bipède et permettrait donc encore de réduire la consommation d’énergie lors de la marche.

Un troisième type d’allure de marche composée d’une phase de simple appui, une phase de double appui fini, et deux impacts au niveau du talon puis au niveau des orteils du pied avant a également été présenté dans le chapitre 5. Ce type d'allure de type 3 est plus proche de la marche humaine par rapport aux deux autres allures de marche. Il a été observé pour les trajectoires optimales que les réactions impulsives sur le talon du pied avant à l'impact du talon étaient quasiment zéro, ce qui correspond à une vitesse d'atterrissage du talon de pied avant à l'impact quasiment nulle. Par conséquent, il a été conclu que la solution optimale (pour nos critèes) pour une allure de type 3 est une trajectoire sans premier impact. En conséquence, l'allure a été modélisée pour satisfaire cette condition afin de réduire le nombre de paramètres d'optimisation et améliorer la convergence de l'algorithme d'optimisation. On peut noter que réactions impulsionnels sur l'orteil des pieds arrière et avant lors du second impact sont significativement plus faibles que ceux trouvés pour les allures de types 2. Les résultats de simulation du critère de performance choisi ont montré qu?une réduction significative du critère peut être obtenue en ajoutant des ressorts à différentes articulations du bipède en fonction de leur mode d'activation. Toutefois, les ressorts actifs pendant toutes les phases de la marche (phases de simple appui et doubles appui) étaient moins efficace pour toutes les vitesses de marche étudiées que pour les allures de type 1 et 2. Il est donc opportun, pour cette allure complexe, de n?activer les ressorts que pendant certaines phases de la marche. Conformément aux recherches antérieures, les ressorts sur la cheville ne sont utiles que sur la jambe arrière pendant la phase de double appui, pour aider le robot à se préparer à l'étape suivante et donner une poussée d'avancer vers l'avant.

Enfin, le critère a été comparé pour les trois allures étudiées pour le bipède de référence, le bipède avec ressorts de torsion identiques aux deux articulations de chevilles, les deux articulations de genoux joints, et les deux articulations de hanches. Il a été observé que l'allure de type 1 est le plus coûteuses en énergie parmi tous les cas. Il a également été constaté que l'allure de type 3 est plus coûteuse aux basses vitesses de marche et moins coûteuse aux vitesses de marche élevés par rapport à l'allure de type 2. Les courbes de critères de ces deux allures se croisent à environ 0,9 m/sec. Selon des études de bio-mécanique, la vitesse moyenne de marche humaine est d'environ 1,4 m/sec. La deuxième partie de ce travail a porté sur l'étude d'un robot bipède avec des actionneurs hydrauliques capables de stocker de l'énergie tandis que l'articulation est bloquée, et réutiliser l'énergie stockée lorsque cela est nécessaire. Les actionneurs hydrauliques ont été introduits dans le chapitre 6 et le mode de fonctionnement d'un actionneur hydraulique classique a été présenté. En outre, un actionneur à haute performance électro-hydraulique intégré (IEHA) a été présenté et ses avantages par rapport à ses homologues ont été détaillés. Le modèle simplifié de l'actionneur a été présenté et le fonctionnement de ses différentes parties a été expliqué en détail. En outre, les différents modes de fonctionnement du IEHA ont été élaborés et sa fonction de stockage d'énergie, qui est l'un des principaux avantages de cet actionneur a été présenté. Les expressions mathématiques pour l'équilibre de l'énergie dans les actionneurs hydrauliques ont été développés, et l'énergie stockée et disponible d'un actionneur hydraulique au cours des différentes étapes de travail a été calculé. Enfin, un certain nombre de cas de consommation d'énergie d'un actionneur au cours de son cycle de fonctionnement ont été expliqués et le calcul de la puissance minimale du moteur électrique utilisé dans le système hydraulique a été proposé en cas de stockage d'énergie. Enfin, une étude approfondie des effets énergétiques des actionneurs hydrauliques et de stockage de l'énergie a été réalisée dans le chapitre 7 sur différentes allures de marche d'un robot bipède planaire. Un certain nombre de méthodes ont été présentées pour améliorer l'efficacité énergétique du bipède étudié lors de la marche. Un ensemble de trajectoires optimales de marche ont été générés en utilisant l'algorithme d'optimisation paramétrique sur un robot équipé des actionneurs hydrauliques. Deux types d'allures de marche ont été étudiés : les allures 2 et 3. L?effet énergétique du blocage du genou sans possibilité de stocker de l'énergie, ou avec stockage de l?énergie ont été explorées et les résultats de simulations ont ensuite été comparées avec celle de robot de référence. L'objectif principal de l'étude était de réduire la consommation d'énergie d'un robot bipède pendant la marche.

Il a été conclu à partir des résultats de simulation que l'efficacité énergétique d'un robot bipède pendant la marche est significativement améliorée en bloquant le genou d'appui pendant toute la phase de simple appui pour l'allure de type 2. La consommation d'énergie est encore réduite en activant le mode de stockage de l'énergie dans un réservoir hydraulique sous la forme de pression hydraulique. L'énergie stockée est ensuite réutilisé en cas de besoin particulier pendant la phase de transfert. On a également observé que le genou d?appui peut être fixé à une valeur constante pour toutes les vitesses de marche sans affecter de manière significative l'efficacité énergétique du bipède. Il a été constaté que le blocage du genou n'est pas efficace pour une allure de type 3 et que le stockage d'énergie est uniquement efficace à des vitesses de marche élevés. Enfin, les critères d'optimisation de la marche d'allure de types 2 et 3 ont été comparés. Il a été constaté que l'allure de type 3 est plus coûteuse en énergie pour le critère étudié que l'allure de type 2 pour toutes les vitesses de marche. Ce manuscrit a présenté différentes stratégies, qui peuvent être utilisées afin d'améliorer l'efficacité énergétique d'un robot bipède pendant la marche. Ces stratégies comprennent, 1) l'étude des effets des ressorts de torsion et le blocage du genou d'appui sur la consommation d'énergie lors de la marche, 2) l'étude d'un nouveau type d'actionneur électro-hydraulique intégré et les effets du stockage de l'énergie de ce type d'actionneur en bloquant l'articulation du genou de la jambe d'appui, 3) une étude de trois types d'allures ayant un impact et une phase de double appui. La mise en ouvre de ces techniques proposées vont réduire la consommation énergétique des robot bipèdes et en conséquence l'autonomie de ces robots va être améliorée. La réduction de consommation énergétique peut aussi permettre de choisir des moteurs plus petits et ainsi de réduire la masse du robot et sa consommation énergétique ?

A.9.2 Perspectives

Conformément à des recherches antérieures, cette étude renforce l'idée d'utiliser des ressorts afin d'améliorer l'efficacité énergétique d'un bipède en particulier sur les articulations de la hanche dans notre cas. Cependant, contrairement aux travaux précédents, nous avons montré que l?efficacité des ressorts placés sur l?articulation des chevilles dépend du type d?allure étudié. Des actionneurs hydrauliques ont également été utilisés pour stocker de l'énergie et améliorer la performance de la marche bipède. En perspective de cette étude, un certain nombre d?études complémentaires peuvent être menées pour explorer les effets de ressorts, blocage du genou, et les actionneurs hydrauliques sur la marche bipède.

La première étape serait de générer des trajectoires de marche aussi proche que possible de la marche humaine pour un bipède planaire. Cela peut être fait par l'introduction de rotation des orteils du pied arrière au cours de la phase de simple appui. Dans la marche bipède, cette rotation des orteils se traduira par une rotation passive du robot autour de l?axe des orteils. Il n'est donc plus possible de définir arbitrairement le comportement de toutes les articulations. Le problème du sous-actionnement a été traité dans un certain nombre d'études [38, 10]. Les effets de blocage du genou et l'ajout de ressorts de torsion en parallèle aux actionneurs existants peuvent être étudiés sur ce type d'allures de marche qui sont en elle-même approprié pour permettre des marches rapides énergétiquement efficaces [38].

Deuxièmement, les effets de la position d'équilibre de ressort de la cheville avec la rotation du pied lors de la phase de double appui, ainsi que durant la phase de simple appui sur l'efficacité énergétique du bipède doit être étudiée. En cas des actionneurs hydrauliques, un algorithme peut être développé pour partager l'énergie stockée entre plusieurs actionneurs.

Dans cette étude, nous avons principalement étudié le cas d?un ressort constamment actif (soit identique pour la jambe d?appui et de transfert) pour les allures 1 et 2 et de ressort que l?on peut activer ou désactiver en fonction des phases pour l?allure 3. L'étude peut être étendue pour explorer les effets de ressorts à raideurs variables.

Les ressorts en parallèle avec les actionneurs électriques ayant montré leur efficacité, il serait pertinent de mener le même type d?étude avec des actionneurs hydrauliques. En dehors de ressorts de torsion en parallèle avec les moteurs, des ressorts de compression en série peuvent être ajoutés à différents corps de la structure du bipède pour explorer leurs effets sur la consommation énergétique lors de la marche.

Dans cette étude, l'articulation du genou d'appui uniquement a été bloquée afin d'étudier les effets sur la consommation d'énergie lors de la marche et de stocker l'énergie en cas des actionneurs hydrauliques. Comme l'articulation du genou, le blocage des autres articulations particulièrement l?articulation de la hanche d'appui peut être étudiée. En outre, au lieu de bloquer une articulation au cours de toute la phase de simple appui, l?articulation peut être bloquée pendant une partie seulement de la phase de simple appui.

Enfin, l'étude peut être étendue pour générer des trajectoires de marche des robots bipèdes en 3D et explorer les effets de ressorts sur les différentes articulations dans des plans différents, par exemple dans des plans frontaux ou traverse. De même, l'idée de blocage du genou peut également être étendue à d'autres articulations comme l'abduction de la hanche afin de minimiser la consommation d'énergie. En outre, les effets des actionneurs hydrauliques et de la fonction de stockage d'énergie peuvent aussi être explorés sur l'efficacité énergétique de la marche bipède en 3D.

B

Inverse Geometric Model of the Biped

B.1 Inverse Geometric Model for Gait Type 1 and 2

The joint configuration during double support phase can be calculated as a function of hip position (h_x, h_y) and step length d when the biped is in flat foot contact on the ground. The step length d is the distance between axis of ankles of the feet. The joint angles of both legs are calculated by solving the Inverse Geometric Model (IGM), which ensures flat foot contact on the ground during double support phase. This configuration represents joint angles at the end of the single support phase as well as at the start of the next single support phase. The studied biped with both feet on the ground is shown in the Figure B.1.

B.1.1 Calculations of joint angles of the stance foot

Joint angles of the stance leg can be found from the Cartesian coordinates of hip of the biped. Since the biped is in flat foot contact on the ground, therefore, the reference frame is fixed at the ankle axis of the front foot. The hip coordinates can be expressed as:

$$\begin{cases} h_x = -l_1 \sin(q_1) - l_2 \sin(q_2) \\ h_y = l_1 \cos(q_1) + l_2 \cos(q_2) \end{cases} \tag{B.1}$$

The solution of system of equation B.1 can be found by using the Paul's method. These equations form a system of type 7 such that:

$$\begin{cases} W \sin(q_1) = X \sin(q_2) + Z_2 \\ W \cos(q_1) = X \cos(q_2) + Z_1 \end{cases} \tag{B.2}$$

Where $W = l_1$, $X = -l_2$, $Z_2 = -h_x$, and $Z_1 = h_y$. The joint angle q_2 can be found such that:

$$q_2 = tan^{-1}\left(\frac{\sin(q_2)}{\cos(q_2)}\right) \tag{B.3}$$

where,

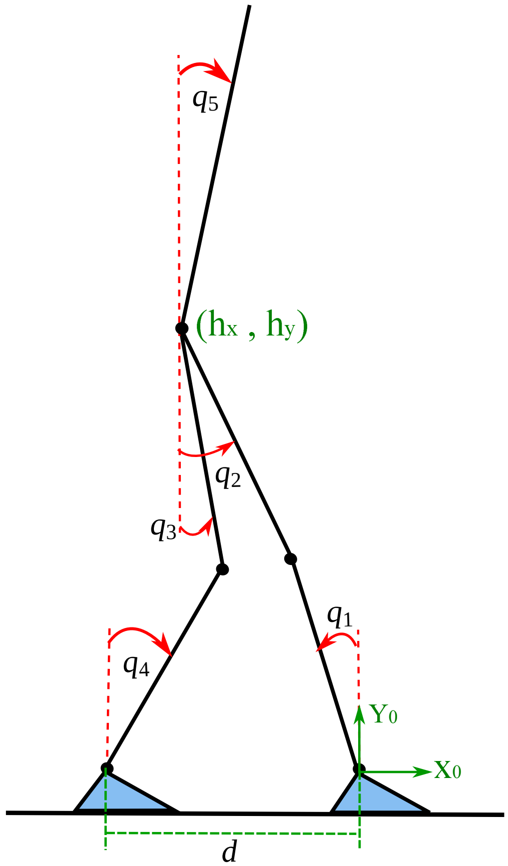

Figure B.1 – Position of biped's feet during instantaneous double support phase of gait type 1 and 2

$$\begin{cases} \sin(q_2) = \dfrac{B_1\,B_3 + e\,B_2\sqrt{B_1^2 + B_2^2 - B_3^2}}{B_1^2 + B_2^2} \\ \cos(q_2) = \dfrac{B_2\,B_3 - e\,B_1\sqrt{B_1^2 + B_2^2 - B_3^2}}{B_1^2 + B_2^2} \end{cases} \tag{B.4}$$

with

$$\begin{cases} B_1 = 2\,Z_2\,X \\ B_2 = 2\,Z_1\,X \\ B_3 = W^2 - X^2 - Z_1^2 - Z_2^2 \end{cases} \tag{B.5}$$

Where $e = +-1$ permits to select one of the two possible solutions of the inverse geometric model. Similarly, q_1 can be calculated by solving equation B.1 using system of equation of type 3 such that:

$$q_1 = tan^{-1}\left(\frac{\sin(q_1)}{\cos(q_1)}\right) \tag{B.6}$$

where,

$$\begin{cases} \sin(q_1) = \dfrac{W_1}{V_1} \\ \cos(q_1) = \dfrac{W_2}{V_2} \end{cases} \tag{B.7}$$

with,

$$\begin{cases} V_1 = l_1 \\ V_2 = l_1 \\ W_1 = -h_x - l_2 \sin(q_2) \\ W_2 = h_y - l_2 \cos(q_2) \end{cases} \tag{B.8}$$

B.1.2 Calculations of joint angles of the swing foot

Joint angles of the swing foot can be found as a function of hip position and step length such that:

$$\begin{cases} h_x + l_3 \sin(q_3) + l_4 \sin(q_4) = d \\ h_y - l_3 \cos(q_3) - l_4 \cos(q_4) = 0 \end{cases} \tag{B.9}$$

The equations B.9 also form a system of equations of type 7 such that:

$$\begin{cases} W \sin(q_3) = X \sin(q_4) + Z_2 \\ W \cos(q_3) = X \cos(q_4) + Z_1 \end{cases} \tag{B.10}$$

Where $W = l_3$, $X = -l_4$, $Z_2 = d - h_x$, and $Z_1 = h_y$. The joint angle q_4 can be found such that:

$$q_4 = tan^{-1}\left(\frac{\sin(q_4)}{\cos(q_4)}\right) \tag{B.11}$$

where,

$$\begin{cases} \sin(q_4) = \dfrac{B_1 B_3 + e B_2 \sqrt{B_1^2 + B_2^2 - B_3^2}}{B_1^2 + B_2^2} \\ \cos(q_4) = \dfrac{B_2 B_3 - e B_1 \sqrt{B_1^2 + B_2^2 - B_3^2}}{B_1^2 + B_2^2} \end{cases} \tag{B.12}$$

with

$$\begin{cases} B_1 = 2 Z_2 X \\ B_2 = 2 Z_1 X \\ B_3 = W^2 - X^2 - Z_1^2 - Z_2^2 \end{cases} \tag{B.13}$$

Similarly, q_3 can be calculated by solving equation B.9 using system of equation of type 3 such that:

$$q_3 = tan^{-1}\left(\frac{\sin(q_3)}{\cos(q_3)}\right) \tag{B.14}$$

where,

$$\begin{cases} \sin(q_3) = \dfrac{W_1}{V_1} \\ \cos(q_3) = \dfrac{W_2}{V_2} \end{cases} \tag{B.15}$$

with,

$$\begin{cases} V_1 = l_3 \\ V_2 = l_3 \\ W_1 = d - h_x - l_4\sin(q_4) \\ W_2 = h_y - l_4\cos(q_4) \end{cases} \tag{B.16}$$

B.2 Inverse Geometric Model for Gait Type 3

During double support phase of gait type 3, the biped is in contact on the ground with heel of the front foot and toe of the back foot with a distance d between the feet as shown in Figure B.2. In this configuration $\mathbf{q}_{ss}(0)$ (end of the single support phase just before heel impact), it is possible to calculate two joint angles as a function of the others by solving the IGM. Similarly, two angles of the joint configuration $\mathbf{q}_{ds}(T_{ds})$ at the end of double support phase can also be calculated from other joint angles. This is the joint configuration at the end of single support phase as well as at the start of double support phase after permutation. We chose to calculate the orientation of shin (q_3) and tight (q_4) of the swing foot as a function of other angles of the biped and step length.

From Figure B.2, **OC** can be written as:

$$\mathbf{OC} = \mathbf{OA} + \mathbf{AC} \tag{B.17}$$

$$\begin{bmatrix} d \\ 0 \end{bmatrix} = \begin{bmatrix} A_x + l_3\sin(q_3) + l_4\sin(q_4) + h_p\sin(q_{p2}) + (L_p - l_p)\cos(q_{p2}) \\ A_y - l_3\cos(q_3) - l_4\cos(q_4) - h_p\cos(q_{p2}) + (L_p - l_p)\sin(q_{p2}) \end{bmatrix} \tag{B.18}$$

Where d is the distance between heel of the front foot and toe of the rear foot during double support phase, and A_x and A_y are given by:

$$\begin{bmatrix} A_x \\ A_y \end{bmatrix} = \begin{bmatrix} l_p\cos(q_{p1}) - h_p\sin(q_{p1}) - l_1\sin(q_1) - l_2\sin(q_2) \\ l_p\sin(q_{p1}) + h_p\cos(q_{p1}) + l_1\cos(q_1) + l_2\cos(q_2) \end{bmatrix} \tag{B.19}$$

Let

$$\begin{bmatrix} C_x \\ C_y \end{bmatrix} = \begin{bmatrix} h_p\sin(q_{p2}) + (L_p - l_p)\cos(q_{p2}) \\ -h_p\cos(q_{p2}) + (L_p - l_p)\sin(q_{p2}) \end{bmatrix} \tag{B.20}$$

Now, by putting the values of C_x and C_y in equation B.18, we have:

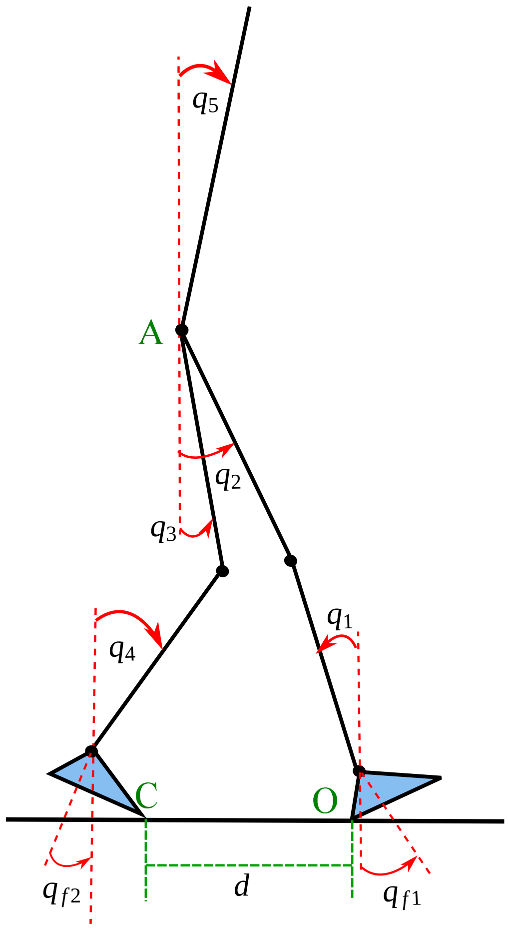

Figure B.2 – Position of biped's feet during double support phase of gait type 3

$$\begin{bmatrix} l_3\sin(q_3) \\ l_3\cos(q_3) \end{bmatrix} = \begin{bmatrix} -l_4\sin(q_4) - d - A_x - C_x \\ -l_4\cos(q_4) + A_y + C_y \end{bmatrix} \tag{B.21}$$

The solution of system of equation B.21 can be found by using the Paul's method. These equations form a system of type 7 such that:

$$\begin{cases} W\sin(q_3) = X\sin(q_4) + Z_2 \\ W\cos(q_3) = X\cos(q_4) + Z_1 \end{cases} \tag{B.22}$$

Where $W = l_3$, $X = -l_4$, $Z_2 = -d - A_x - C_x$, and $Z_1 = A_y + C_y$. The joint angle q_4 can be found such that:

$$q_4 = tan^{-1}\left(\frac{\sin(q_4)}{\cos(q_4)}\right) \tag{B.23}$$

where,

$$\begin{cases} \sin(q_4) = \dfrac{B_1\, B_3 + e\, B_2 \sqrt{B_1^2 + B_2^2 - B_3^2}}{B_1^2 + B_2^2} \\ \cos(q_4) = \dfrac{B_2\, B_3 - e\, B_1 \sqrt{B_1^2 + B_2^2 - B_3^2}}{B_1^2 + B_2^2} \end{cases} \tag{B.24}$$

with

$$\begin{cases} B_1 = 2\, Z_2\, X \\ B_2 = 2\, Z_1\, X \\ B_3 = W^2 - X^2 - Z_1^2 - Z_2^2 \end{cases} \tag{B.25}$$

Similarly, q_3 can be calculated by solving equation B.21 using system of equation of type 3 such that:

$$q_3 = tan^{-1}\left(\frac{\sin(q_3)}{\cos(q_3)}\right) \tag{B.26}$$

where,

$$\begin{cases} \sin(q_3) = \dfrac{W_1}{V_1} \\ \cos(q_3) = \dfrac{W_2}{V_2} \end{cases} \tag{B.27}$$

with,

$$\begin{cases} V_1 = l_3 \\ V_2 = l_3 \\ W_1 = -l_4 \sin(q_4) + d - A_x - C_x \\ W_2 = -l_4 \cos(q_4) + A_y + C_y \end{cases} \tag{B.28}$$

C

Calculation of Jacobian Matrices

C.1 General Expression

The Jacobian matrix is the matrix of all first-order partial derivatives of a vector or scalar-valued function with respect to another vector. Given a set of $\mathbf{F} = \mathbf{f}(\mathbf{x}) \in \mathbb{R}^m$ equations in $\mathbf{x} \in \mathbb{R}^n$ variables, the Jacobian matrix, sometimes simply called "the Jacobian" [108] is defined by:

$$\mathbf{J} = \begin{bmatrix} \dfrac{\partial F_1}{\partial x_1} & \cdots & \dfrac{\partial F_1}{\partial x_n} \\ \vdots & \ddots & \vdots \\ \dfrac{\partial F_m}{\partial x_1} & \cdots & \dfrac{\partial F_m}{\partial x_n} \end{bmatrix} \tag{C.1}$$

C.2 Jacobian Matrices for Walking Gait Type 1 and 2

The walking gait types 1 and 2 presented in present study are composed of only single support phases separated by tradition phases (gait type 1) or impulsive impacts (gait type 2). These walking gaits have flat foot contact on the ground at the time of impact as well as during the entire stance phase. Jacobian matrix of swing foot (foot coming in contact with the ground) is needed to solve the impact model. In our case, the Jacobian matrix $\mathbf{J}_2 \in \mathbb{R}^{3\times 9}$ is the first-order partial derivatives of the position vector of the swing foot with respect to generalized coordinate vector $\mathbf{q} = [q_{p1}\ q_{p2}\ q_1\ q_2\ q_3\ q_4\ q_5\ x_h\ y_h]^t$. Thus, the position and Jacobian of swing foot (foot 2) can be calculated such that:

$$\mathbf{P}_2 = \begin{bmatrix} x_h + L_3\sin(q_3) + L_4\sin(q_4) + h_p\sin(q_{p2}) \\ y_h - L_3\cos(q_3) - L_4\cos(q_4) - h_p\cos(q_{p2}) \end{bmatrix} \tag{C.2}$$

$$\mathbf{J_2} = \begin{bmatrix} 0 & h_p\cos(q_{p2}) & 0 & 0 & L_3\cos(q_3) & L_4\cos(q_4) & 0 & 1 & 0 \\ 0 & h_p\sin(q_{p2}) & 0 & 0 & L_3\sin(q_3) & L_4\sin(q_4) & 0 & 0 & 1 \\ 0 & 1 & 0 & 0 & 0 & 0 & 0 & 0 & 0 \end{bmatrix} \tag{C.3}$$

Here, a third row is added to the Jacobian of the feet to take into account the rotation of the foot.

In case where the knee joint is locked just before impact, the Jacobian of knee has to be added to the impact model. The Jacobian of the knee joint $\mathbf{J}_k \in \mathbb{R}^{1\times 9}$ of the swing leg can be calculated from derivative of the knee angle θ_5.

$$\theta_5 = q_3 - q_4 \tag{C.4}$$

$$\mathbf{J_k} = \begin{bmatrix} 0 & 0 & 0 & 0 & 1 & -1 & 0 & 0 & 0 \end{bmatrix} \tag{C.5}$$

C.3 Jacobian Matrices for Walking Gait Type 3

Walking gait type 3 consists of single and double support phases separated by impulsive impacts. During double support phase, the biped is in contact on the ground with heel of the front foot and toe of the back foot as shown in Figure 3.7. In this configuration, considering implicit liaison and perfect pivot contact on heel of stance foot, the generalized coordinate vector is expressed by $\mathbf{q}_{ds} = [q_{p1}\ q_{p2}\ q_1\ q_2\ q_3\ q_4\ q_5]^t$. The Jacobian matrix of toe of rear foot during double support phase is given by:

$$\mathbf{P}_{2\,ds} = \left[\begin{array}{c} l_p\cos(q_{p1}) - h_p\sin(q_{p1}) + (L_p - l_p)\cos(q_{p2}) + h_p\sin(q_{p2}) - L_1\sin(q_1) - L_2\sin(q_2) + L_3\sin(q_3) + L_4\sin(q_4) \\ -l_p\sin(q_{p1}) - h_p\cos(q_{p1}) - (L_p - l_p)\sin(q_{p2}) + h_p\cos(q_{p2}) - L_1\cos(q_1) - L_2\cos(q_2) + L_3\cos(q_3) + L_4\cos(q \end{array} \right. \tag{C.6}$$

$$\mathbf{J}_{2\,ds} = \left[\begin{array}{cccccc} -l_p\sin(q_{p1}) - h_p\cos(q_{p1}) & h_p\cos(q_{p2}) - (L_p - l_p)\sin(q_{p2}) & -L_1\cos(q_1) & -L_2\cos(q_2) & L_3\cos(q_3) & L_4\cos(q \\ l_p\cos(q_{p1}) - h_p\sin(q_{p1}) & h_p\sin(q_{p2}) + (L_p - l_p)\cos(q_{p2}) & -L_1\sin(q_1) & -L_2\sin(q_2) & L_3\sin(q_3) & L_4\sin(q \end{array} \right. \tag{C.7}$$

During a walking step of gait type 3, first impact occurs when the heel of the swing foot touches the ground. To have double support, the heel of foot 1 ($\mathbf{J}_{1\,heel} * \mathbf{q} = 0$) and the toe of foot 2 ($\mathbf{J}_{2\,toe}\mathbf{q} = 0$) must remain on ground. The generalized coordinate vector is expressed by $\mathbf{q} = [q_{p1}\ q_{p2}\ q_1\ q_2\ q_3\ q_4\ q_5\ x_h\ y_h]^t$. The position of heel of front foot and toe of rear foot during double support phase is given by:

$$\mathbf{P}_{1\,heel} = \begin{bmatrix} x_h + L_1\sin(q_1) + L_2\sin(q_2) - l_p\cos(q_{p1}) + h_p\sin(q_{p1}) \\ y_h - L_1\cos(q_1) - L_2\cos(q_2) - l_p\sin(q_{p1}) - h_p\cos(q_{p1}) \end{bmatrix} \tag{C.8}$$

$$\mathbf{P}_{2\,toe} = \begin{bmatrix} x_h + L_3\sin(q_3) + L_4\sin(q_4) + (L_p - l_p)\cos(q_{p2}) + h_p\sin(q_{p2}) \\ y_h - L_3\cos(q_3) - L_4\cos(q_4) + (L_p - l_p)\sin(q_{p2}) - h_p\cos(q_{p2}) \end{bmatrix} \tag{C.9}$$

At the instance of heel impact, the Jacobian $\mathbf{J}_{1\,heel} \in \mathbb{R}^{2\times 9}$ at heel of the front foot, and $\mathbf{J}_{2\,toe} \in \mathbb{R}^{2\times 9}$ at toe of the rear foot are given by:

$$\mathbf{J}_{1\,heel} = \begin{bmatrix} h_p\cos(q_{p1}) + l_p\sin(q_{p1}) & 0 & L_1\cos(q_1) & L_2\cos(q_2) & 0 & 0 & 0 & 1 & 0 \\ h_p\sin(q_{p1}) - l_p\cos(q_{p1}) & 0 & L_1\sin(q_1) & L_2\sin(q_2) & 0 & 0 & 0 & 0 & 1 \end{bmatrix} \tag{C.10}$$

$$\mathbf{J}_{2\,toe} = \begin{bmatrix} 0 & h_p\cos(q_{p2}) - (L_p - l_p)\sin(q_{p2}) & 0 & 0 & L_3\cos(q_3) & L_4\cos(q_4) & 0 & 1 & 0 \\ 0 & h_p\sin(q_{p2}) + (L_p - l_p)\cos(q_{p2}) & 0 & 0 & L_3\sin(q_3) & L_4\sin(q_4) & 0 & 0 & 1 \end{bmatrix} \tag{C.11}$$

The Jacobian matrices $\mathbf{J}_{1\,heel}$ and $\mathbf{J}_{2\,toe}$ have only two rows because at the instance of first impact, the front foot rotates on its heel while the rear foot rotates on its toe.

The second impact occurs when toe of the front foot comes in contact with the ground. At the moment of second impact, the foot is in flat contact on the ground. The position and Jacobian matrix is given by (C.12) and (C.13) respectively. It is to be noted that a third row is added to take into account the rotation on the foot.

$$\mathbf{P}_1 = \begin{bmatrix} x_h + L_1\sin(q_1) + L_2\sin(q_2) + h_p\sin(q_{p1}) \\ y_h - L_1\cos(q_1) - L_2\cos(q_2) - h_p\cos(q_{p1}) \end{bmatrix} \tag{C.12}$$

$$\mathbf{J_1} = \begin{bmatrix} h_p\cos(q_{p1}) & 0 & L_1\cos(q_1) & L_2\cos(q_2) & 0 & 0 & 0 & 1 & 0 \\ h_p\sin(q_{p1}) & 0 & L_1\sin(q_1) & L_2\sin(q_2) & 0 & 0 & 0 & 0 & 1 \\ 1 & 0 & 0 & 0 & 0 & 0 & 0 & 0 & 0 \end{bmatrix} \tag{C.13}$$

D

Calculation of R_{2x} by Minimizing the Criterion

D.1 Calculating R_{2x} by Minimizing the Criterion

The joint torques as well as vertical component of the ground reaction force on rear foot can be calculated as a function of R_{2x} by decomposing the equation of dynamic model in double support (3.15) such that:

$$\begin{bmatrix} \mathbf{\Gamma} \\ R_{2y} \end{bmatrix} = \begin{bmatrix} \mathbf{B} & \mathbf{J}^t_{2y} \end{bmatrix}^{-1} \begin{bmatrix} \mathbf{A}(\mathbf{q})\ddot{\mathbf{q}} + \mathbf{C}(\mathbf{q}, \dot{\mathbf{q}})\dot{\mathbf{q}} + \mathbf{G}(\mathbf{q}) - \mathbf{J}^t_{2x} R_{2x} \end{bmatrix} \tag{D.1}$$

where $\mathbf{A}(\mathbf{q}) \in \mathbb{R}^{7\times7}$ is the positive definitive inertia matrix, $\mathbf{C}(\mathbf{q}, \dot{\mathbf{q}}) \in \mathbb{R}^{7\times7}$ contains the Coriolis and centrifugal forces, $\mathbf{G}(\mathbf{q}) \in \mathbb{R}^{7\times1}$ is the vector of gravity forces, $\mathbf{B} \in \mathbb{R}^{7\times6}$ is the actuation matrix composed of 1 and 0, and $\mathbf{\Gamma} \in \mathbb{R}^{6\times1}$ is the joints torque vector. The ground reaction forces on rear foot $\mathbf{R}_2 \in \mathbb{R}^{2\times1}$ are taken into account through the Jacobian matrix $\mathbf{J}_2 \in \mathbb{R}^{2\times7}$.

The ground reaction force on front foot can be calculated by writing the force balance equations on center of mass of the biped. This can be written as:

$$\begin{cases} R_{1x} = m\ddot{x}_g - R_{2x} \\ R_{1y} = m\ddot{y}_g - R_{2y} + mg \end{cases} \tag{D.2}$$

From the second line of (D.1) and (D.2), for a given acceleration of the biped there is only one solution for R_{1y} and R_{2y}, independent of the torques. The torques only influence R_{1x} and R_{2x}. For this reason, a solution for the torques can be found as a function of R_{1x} or R_{2x} as parameter. Let us chooseR_{2x} and define the minimization problem with the associated constraint on component R_{2x}. To calculate R_{2x}, the dynamic equation will be solved in such a way that R_{2x} will minimize the optimization criterion based on joint torques.

$$\min_{R_{2x}} \mathbf{\Gamma}^t \mathbf{\Gamma} \tag{D.3}$$

with

$$\begin{cases} -\mu R_{1y} - R_{1x} \leq 0 \\ -\mu R_{1y} + R_{1x} \leq 0 \\ -\mu R_{2y} - R_{2x} \leq 0 \\ -\mu R_{2y} + R_{2x} \leq 0 \end{cases} \tag{D.4}$$

Let us suppose that left hand side of the dynamic equation (3.15) is constant (say ϕ), and rearranging the equation such that:

$$\phi = \mathbf{B}\boldsymbol{\Gamma} + \mathbf{J}^{t}_{2x} R_{2x} + \mathbf{J}^{t}_{2y} R_{2y} \tag{D.5}$$

$$\begin{bmatrix} \mathbf{B} & \mathbf{J}^{t}_{2y} \end{bmatrix} \begin{bmatrix} \boldsymbol{\Gamma} \\ R_{2y} \end{bmatrix} - \mathbf{J}^{t}_{2x} R_{2x} = \phi \tag{D.6}$$

$$\begin{bmatrix} \boldsymbol{\Gamma} \\ R_{2y} \end{bmatrix} = \begin{bmatrix} \mathbf{B} & \mathbf{J}^{t}_{2y} \end{bmatrix}^{-1} \phi + \begin{bmatrix} \mathbf{B} & \mathbf{J}^{t}_{2y} \end{bmatrix}^{-1} \mathbf{J}^{t}_{2x} R_{2x} \tag{D.7}$$

The first 6 lines of equation (D.7) can be written as:

$$\boldsymbol{\Gamma} = \left(\begin{bmatrix} \mathbf{B} & \mathbf{J}^{t}_{2y} \end{bmatrix}^{-1} \phi \right)_{(1:6)} + \left(\begin{bmatrix} \mathbf{B} & \mathbf{J}^{t}_{2y} \end{bmatrix}^{-1} \mathbf{J}^{t}_{2x} \right)_{(1:6)} R_{2x} \tag{D.8}$$

Let $\mathbf{E} = ([\mathbf{B} \quad \mathbf{J}^{t}_{2y}]^{-1}\phi)_{(1:6)}$ and $\mathbf{F} = ([\mathbf{B} \quad \mathbf{J}^{t}_{2y}]^{-1}\mathbf{J}^{t}_{2x})_{(1:6)}$ then we have:

$$\boldsymbol{\Gamma} = \mathbf{E} + \mathbf{F} R_{2x} \tag{D.9}$$

Now, the expression C^{*}_{Γ} as a function of joint torques which needs to be minimized can be written as:

$$C^{*}_{\Gamma} = \boldsymbol{\Gamma}^{t}\boldsymbol{\Gamma} = (\mathbf{E} + \mathbf{F} R_{2x})^{t}(\mathbf{E} + \mathbf{F} R_{2x})$$

$$C^{*}_{\Gamma} = \mathbf{E}^{t}\mathbf{E} + 2\mathbf{E}^{t}\mathbf{F} R_{2x} + R^{t}_{2x}\mathbf{F}^{t}\mathbf{F} R_{2x} \tag{D.10}$$

Finally, the value of R_{2x} which will minimize C^{*}_{Γ}, can be calculated by putting the derivative of C^{*}_{Γ} with respect to R_{2x} equal to zero.

$$\frac{\partial C^{*}_{\Gamma}}{\partial R_{2x}} = 0 \Rightarrow \quad 2\mathbf{F}^{t}\mathbf{E} + 2\mathbf{F}^{t}\mathbf{F} R_{2x} = 0$$

$$R_{2x\,opt\,\Gamma} = -\frac{\mathbf{F}^{t}\mathbf{E}}{\mathbf{F}^{t}\mathbf{F}} \tag{D.11}$$

This solution minimizes the optimization criterion C_{Γ} (4.14).

The solution of R_{2x} found in (D.11) minimizes the square of the torques without constraints. A constraint needs to be imposed on this solution to satisfy the maximum and minimum limits of R_{2x}. Let $R_{2x\,min}$ be the minimum and $R_{2x\,max}$ be the maximum value of R_{2x}, then the constraint on R_{2x} can be written as:

$$R_{2x\,min} \leq R_{2x} \leq R_{2x\,max} \tag{D.12}$$

Thus a solution of the minimization problem D.3 is given by following three cases:

$$\begin{cases} \text{If} \quad R_{2x\,min} \leq R_{2x\,opt\,\Gamma} \leq R_{2x\,max} \quad \text{then} \quad R_{2x} = R_{2x\,opt\,\Gamma} \\ \text{If} \quad R_{2x\,opt\,\Gamma} \leq R_{2x\,min} \quad \text{then} \quad R_{2x} = R_{2x\,min} \\ \text{If} \quad R_{2x\,opt\,\Gamma} \geq R_{2x\,max} \quad \text{then} \quad R_{2x} = R_{2x\,max} \end{cases} \tag{D.13}$$

In the case where there is no solution, *i.e* $R_{2x\,min} \geq R_{2x\,max}$, the value of R_{2x} is selected to minimize the violation of constraints such as:

$$R_{2x} = R_{2x\,opt\,\Gamma} \tag{D.14}$$

In this last situation, the constraints are not satisfied. However, the optimization algorithm will tend to satisfy the constraints of the motion, and the final solution will always satisfy $R_{2x\,min} \leq R_{2x\,max}$. This violation will only occur during the optimization process and will not appear in the final optimal walking gait trajectory.

D.1.1 Constraints of contact

The optimal walking gait trajectory should satisfy all the constraints presented in (D.4). Similar to equation (D.9), the reaction force can also be expressed as a function of R_{2x}. From the last row of (D.7), we have:

$$R_{2y} = \mathbf{M}_{2y} + \mathbf{N}_y R_{2x} \tag{D.15}$$

where $\mathbf{M}_{2y} = ([\mathbf{B} \quad \mathbf{J}^{t}_{(:,2)}]^{-1}\phi)_{(end)}$ and $\mathbf{N}_y = ([\mathbf{B} \quad \mathbf{J}^{t}_{(:,2)}]^{-1}\mathbf{J}^{t}_{(:,1)})_{(end)}$.

Similarly, from (D.2), reaction force on foot 1 can be expressed such that:

$$R_{1x} = \mathbf{M}_{1x} - R_{2x} \tag{D.16}$$

$$R_{1y} = \mathbf{M}_{1y} - \mathbf{N}_y R_{2x} \tag{D.17}$$

where $\mathbf{M}_{1x} = m\ddot{x}_g$ and $\mathbf{M}_{1y} = m\ddot{y}_g + mg - \mathbf{M}_{2y}$. It is to be noted that $\mathbf{N}_y$ is the same as in (D.15) but with negative sign.

For a given value of $(\mathbf{q}, \dot{\mathbf{q}}, \ddot{\mathbf{q}})$, the terms $\mathbf{M}_i$ and $\mathbf{N}_i$ are know, and the reaction forces are calculated with $R_{2x} = R_{2x\,opt\,\Gamma}$. If all the constraints given in (D.4) are satisfied, then this solution is used.

D.1.1.1 Constraint of no-take-off

In a case where all the constraints in (D.4) are not satisfied, the constraint of no-take-off needs to be verified first, because the constraint of no-slipping can be considered only if the foot stays on the ground.

If $\mathbf{N}_y \neq 0$, there exist some values of R_{2x} that can be used to satisfy the constraint of no-take-off ($R_{1y} > 0, R_{2y} > 0$) using (D.15) and (D.17). The maximum and minimum limits of R_{2x} can be calculated as:

$$R_{2x\,min} = \begin{cases} \dfrac{-\mathbf{M}_{2y}}{\mathbf{N}_y} & \text{if} \quad \mathbf{N}_y > 0 \\ \dfrac{\mathbf{M}_{1y}}{\mathbf{N}_y} & \text{if} \quad \mathbf{N}_y < 0 \end{cases} \tag{D.18}$$

$$R_{2x\,max} = \begin{cases} \dfrac{\mathbf{M}_{1y}}{\mathbf{N}_y} & \text{if} \quad \mathbf{N}_y > 0 \\ \dfrac{-\mathbf{M}_{2y}}{\mathbf{N}_y} & \text{if} \quad \mathbf{N}_y < 0 \end{cases} \tag{D.19}$$

If the constraint of no-take-off is not satisfied with the solution $R_{2x} = R_{2x\,opt\,\Gamma}$ and if there is no satisfactory solution ($R_{2x\,max} < R_{2x\,min}$), then (D.14) is used with limits calculated in (D.18) and (D.19).

The above limits of R_{2x} are calculated by ensuring positive normal reaction force on both feet ($R_{2y} > 0$ and $R_{1y} > 0$) during double support phase. Thus from (D.15) for $\mathbf{N}_y > 0$, we have:

$$\begin{cases} \mathbf{M}_{2y} + \mathbf{N}_y R_{2x} > 0 \\ \mathbf{N}_y R_{2x} > -\mathbf{M}_{2y} \\ R_{2x} > \dfrac{-\mathbf{M}_{2y}}{\mathbf{N}_y} \end{cases} \tag{D.20}$$

Similarly, from (D.17), we have:

$$\begin{cases} \mathbf{M}_{1y} - \mathbf{N}_y R_{2x} > 0 \\ -\mathbf{N}_y R_{2x} > -\mathbf{M}_{1y} \\ R_{2x} > \dfrac{\mathbf{M}_{1y}}{\mathbf{N}_y} \end{cases} \tag{D.21}$$

For $\mathbf{N}_y < 0$, the signs are inversed.

D.1.1.2 Constraint of no-slipping

If the constraint of no-take-off is satisfied, then the constraint of no-slipping needs to be verified and a solution which satisfies this constraint is to be found. The no-slipping constraint on foot 2 can be written as:

$$\begin{cases} -\mu R_{2y} - R_{2x} \leq 0 \\ -\mu R_{2y} + R_{2x} \leq 0 \end{cases} \tag{D.22}$$

Now, putting the value of R_{2y} from (D.15) we have:

$$\begin{cases} -\mu \mathbf{M}_{2y} - (\mu \mathbf{N}_y + 1) R_{2x} \leq 0 \\ -\mu \mathbf{M}_{2y} - (\mu \mathbf{N}_y - 1) R_{2x} \leq 0 \end{cases} \tag{D.23}$$

Similarly, the no-slipping constraint for foot 1 can be expressed as:

$$\begin{cases} -\mu R_{1y} - R_{1x} \leq 0 \\ -\mu R_{1y} + R_{1x} \leq 0 \end{cases} \tag{D.24}$$

Putting the values from (D.16) and (D.17), we have:

$$\begin{cases} -\mu \mathbf{M}_{1y} - \mathbf{M}_{1x} + (\mu \mathbf{N}_y + 1) R_{2x} \leq 0 \\ -\mu \mathbf{M}_{1y} + \mathbf{M}_{1x} + (\mu \mathbf{N}_y - 1) R_{2x} \leq 0 \end{cases} \tag{D.25}$$

Therefore, the minimum and maximum values of R_{2x} for no slipping constraint can be deduced from (D.23) and (D.25) such that:

$$R^{\mu}_{2x\,min} = \begin{cases} \dfrac{\min(-\mu \mathbf{M}_{2y}, \mu \mathbf{M}_{1y} + \mathbf{M}_{1x})}{(\mu \mathbf{N}_y + 1)} & \text{if} \quad (\mu \mathbf{N}_y + 1) > 0 \\ \dfrac{\min(-\mu \mathbf{M}_{2y}, \mu \mathbf{M}_{1y} - \mathbf{M}_{1x})}{(\mu \mathbf{N}_y - 1)} & \text{if} \quad (\mu \mathbf{N}_y - 1) > 0 \end{cases} \tag{D.26}$$

$$R^{\mu}_{2x\,max} = \begin{cases} \dfrac{\max(-\mu \mathbf{M}_{2y}, \mu \mathbf{M}_{1y} + \mathbf{M}_{1x})}{(\mu \mathbf{N}_y + 1)} & \text{if} \quad (\mu \mathbf{N}_y + 1) < 0 \\ \dfrac{\max(-\mu \mathbf{M}_{2y}, \mu \mathbf{M}_{1y} - \mathbf{M}_{1x})}{(\mu \mathbf{N}_y - 1)} & \text{if} \quad (\mu \mathbf{N}_y - 1) < 0 \end{cases} \tag{D.27}$$

Finally, to avoid take-off and slipping of the feet, the maximum and minimum of R_{2x} can be written as:

$$\begin{cases} R_{2x\,min} = \min(R^{\mu}_{2x\,min}, R_{2x\,min}) \\ R_{2x\,max} = \max(R^{\mu}_{2x\,max}, R_{2x\,max}) \end{cases} \tag{D.28}$$

E

Calculation of Centers of Mass of Links of the Biped

To calculate the dynamic model of the biped, it is necessary to determine the position of the centers of mass of each link.. In this part, the centers of mass of all the links of the studied biped will be calculated with respect to a reference frame $R_h(h_x, h_y)$ at the hip of the biped. The seven link planar biped is shown in Figure E.1(a), and its foot geometry is shown in Figure E.1(b). It is composed of two feet, two shin, two thigh, and a torso. All the joints are supposed to be perfect revolute joints.

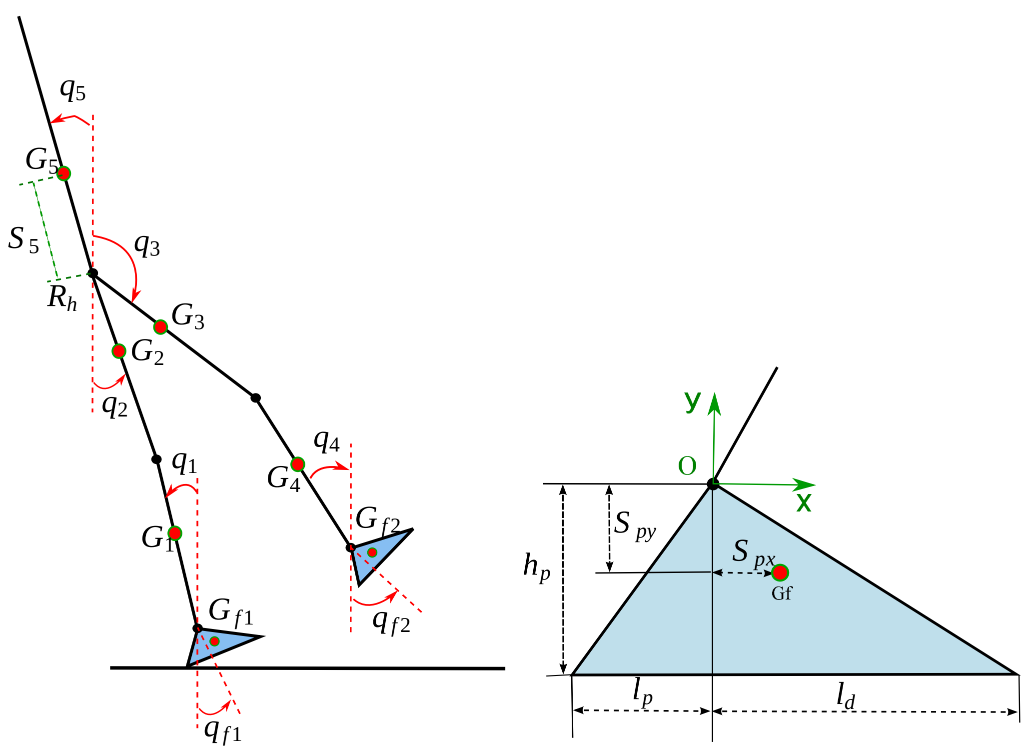

(a) biped's centers of mass (b) foot geometry

Figure E.1 – Position of centers of mass and foot geometry of the biped

The position of the centers of masses of the body is given by:

$$
\begin{aligned}
G_1 &= [h_x + l_2\sin(q_2) + s_1\sin(q_1);\, h_y - l_2\cos(q_2) - s_1\cos(q_1)] \\
G_2 &= [h_x + s_2\sin(q_2);\, h_y - s_2\cos(q_2)] \\
G_3 &= [h_x + s_3\sin(q_3);\, h_y - s_3\cos(q_3)] \\
G_4 &= [h_x + l_3\sin(q_3) + s_4\sin(q_4);\, h_y - l_3\cos(q_3) - s_4\cos(q_4)] \\
G_5 &= [h_x - s_5\sin(q_5);\, h_y + s_5\cos(q_5)] \\
G_{f1} &= [h_x + l_2\sin(q_2) + l_1\sin(q_1) + S_{p1x}\cos(q_{p1}) + S_{p1y}\sin(q_{p1}); \\
&\qquad h_y - l_2\cos(q_2) - l_1\cos(q_1) + S_{p1x}\sin(q_{p1}) - S_{p1y}\cos(q_{p1})] \\
G_{f2} &= [h_x + l_3\sin(q_3) + l_4\sin(q_4) + S_{p2x}\cos(q_{p2}) + S_{p2y}\sin(q_{p2}); \\
&\qquad h_y - l_3\cos(q_3) - l_4\cos(q_4) + S_{p2x}\sin(q_{p2}) - S_{p2y}\cos(q_{p2})]
\end{aligned}
\tag{E.1}
$$

Where (h_x, h_y) are the Cartesian coordinates of the hip of the biped, G_i is the position of center of mass of link i, and q_i is the absolute angle of link i with vertical axis.

The mass center of gravity (CoG) of the biped can be calculated from the individual centers of mass of all the links such that:

$$
CoG = (m_1G_1 + m_2G_2 + m_3G_3 + m_4G_4 + m_5G_5 + m_{f1}G_{f1} + m_{f2}G_{f2})/M \tag{E.2}
$$

Here, M is the total mass of the biped and m_i is the mass of link i.

Bibliography

[1] A. Agrawal and S.K. Agrawal. Effect of gravity balancing on biped stability. In *proceedings of the 2004 IEEE International Conference on Robotics and Automation (ICRA '04)*, volume 4, pages 4228–4233, 2004.

[2] R.M.N. Alexander. *Principles of animal locomotion*. Princeton University Press, 2002.

[3] S. Alfayad, F. B. Ouezdou, F. Namoun, and G. Cheng. Lightweight high performance integrated actuator for humanoid robotic applications: Modeling, design and realization. In *proceedings of the IEEE International Conference on Robotics and Automation (ICRA '09)*, pages 562–567, 2009.

[4] S. Alfayad, F.B. Ouezdou, and F. Namoun. New three dof ankle mechanism for humanoid robotic application: Modeling, design and realization. In *proceedings of the 2009 IEEE/RSJ International Conference on Intelligent Robots and Systems (IROS 2009)*, pages 4969–4976, 2009.

[5] Samer ALFAYAD. *Robot humanoïde HYDROïD : Actionnement, Structure Cinématique et Stratégie de contrôle*. PhD thesis, Institut Universitaire de Technologie de Velizy, 2009.

[6] Samer Alfayad, Fethi B. Ouezdou, Faycal Namoun, and Gordon Gheng. High performance integrated electro-hydraulic actuator for robotics part i: Principle, prototype design and first experiments. *Sensors and Actuators A: Physical*, 169(1):115–123, September 2011.

[7] Samer Alfayad, Fethi B. Ouezdou, Faycal Namoun, and Gordon Gheng. High performance integrated electro-hydraulic actuator for robotics. part ii: Theoretical modelling, simulation, control & amp; comparison with real measurements. *Sensors and Actuators A: Physical*, 169(1):124–132, September 2011.

[8] S.O. Anderson, M. Wisse, C.G. Atkeson, J.K. Hodgins, G.J. Zeglin, and B. Moyer. Powered bipeds based on passive dynamic principles. In *proceedings of the 2005 5^{th} IEEE-RAS International Conference on Humanoid Robots*, pages 110–116, 2005.

[9] Y. Aoustin and A.M. Formal'skii. On optimal swinging of the biped arms. In *Intelligent Robots and Systems, 2008. IROS 2008. IEEE/RSJ International Conference on*, pages 2922–2927, 2008.

[10] Hamon Arnaud. *Influence de la cinématique d'une articulation de genou polycentrique sur la marche d'un robot bipède*. PhD thesis, Université de Nantes, 2011.

[11] Richard Baker. Isb recommendation on definition of joint coordinate systems for the reporting of human joint motion part i: ankle, hip and spine. *Journal of Biomechanics*, 36(2):300–302, February 2003.

[12] F.P. Beer and E. R. Johnston. *Vector Mechanics for Engineers: Dynamics*. McGraw Hill, 9th edition, 2010.

[13] A.A. Biewener. *Animal locomotion*. Oxford University Press, USA, 2003.

[14] Carl de. Boor. *A Practical Guide to Splines*, volume 27. Springer, 2001.

[15] BostonDynamics. Boston dynamics bigdog. Online available: http://www.bostondynamics.com/robot_bigdog.html. Accessed: 23/01/2013.

[16] BostonDynamics. Boston dynamics rhex. Online available: http://www.bostondynamics.com/robot_rhex.html. Accessed: 23/01/2013.

[17] BostonDynamics. Boston dynamics rise. Online available: http://www.bostondynamics.com/robot_rise.html. Accessed: 23/01/2013.

[18] Ronan Boulic, NadiaMagnenat Thalmann, and Daniel Thalmann. A global human walking model with real-time kinematic personification. 6(6):344–358–, 1990.

[19] D.J.J. Bregman, M.M. van der Krogt, V. de Groot, J. Harlaar, M. Wisse, and S.H. Collins. The effect of ankle foot orthosis stiffness on the energy cost of walking: A simulation study. *Clinical Biomechanics*, (0):–.

[20] G. Cabodevila, N. Chaillet, and G. Abba. Energy-minimized gait for a biped robot. In *AMS*, pages 90–99, 1995.

[21] Selene L. Cardenas-Maciel, Oscar Castillo, and Luis T. Aguilar. Generation of walking periodic motions for a biped robot via genetic algorithms. *Applied Soft Computing*, 11(8):5306–5314, December 2011.

[22] Jean-Charles Ceccato, Mathieu de Séze, Christine Azevedo, and Jean-René Cazalets. Comparison of trunk activity during gait initiation and walking in humans. *PLoS ONE*, 4(12):e8193, December 2009.

[23] Hao Chen, Shuwen Pan, Rong Xiong, and Jun Wu. Optimal on-line walking pattern generation for biped robots. In *Networking and Distributed Computing (ICNDC), 2010 First International Conference on*, pages 331–335, 2010.

[24] Y. C. Chen. Solving robot trajectory planning plroblems with uniform cubic b-splines. *Optimal Control Applications and Methods*, 12(4):247–262, 1991.

[25] C. Chevallereau, G. Abba, Y. Aoustin, F. Plestan, E.R. Westervelt, C. Canudas-de Wit, and J.W. Grizzle. Rabbit: a testbed for advanced control theory. *Control Systems, IEEE*, 23(5):57–79, 2003.

[26] C. Chevallereau and Y. Aoustin. Optimal reference trajectories for walking and running of a biped. *Robotica*, 19(5):557–569, 2001.

[27] C. Chevallereau, D. Djoudi, and J.W. Grizzle. Stable bipedal walking with foot rotation through direct regulation of the zero moment point. *IEEE Transactions on Robotics*, 24(2):390–401, 2008.

[28] C. Chevallereau, J.W. Grizzle, and Ching-Long Shih. Asymptotically stable walking of a five-link underactuated 3-D bipedal robot. *IEEE Transactions on Robotics*, 25(1):37–50, 2009.

[29] Christine Chevallereau, Guy Bessonnet, Gabriel Abba, and Yannick Aoustin. *Bipedal Robots: Modeling, Design and Walking Synthesis*. John Wiley & Sons, Inc., 2007.

[30] T.F. Coleman and Y. Li. An interior, trust region approach for nonlinear minimization subject to bounds. *SIAM Journal on Optimization*, 6:418–445, 1996.

[31] S.H. Collins and A. Ruina. A bipedal walking robot with efficient and human-like gait. In *proceedings of the 2005 IEEE International Conference on Robotics and Automation (ICRA 2005)*, pages 1983–1988, 2005.

[32] Steve Collins, Andy Ruina, Russ Tedrake, and Martijn Wisse. Efficient bipedal robots based on passive-dynamic walkers. *Science*, 307(5712):1082–1085, 2005.

[33] A. Cullell, J.C. Moreno, E. Rocon, A. Forner-Cordero, and J.L. Pons. Biologically based design of an actuator system for a knee-ankle-foot orthosis. *Mechanism and Machine Theory*, 44(4):860–872, April 2009.

[34] Winnie Daamen and Serge Hoogendoorn. Experimental research of pedestrian walking behavior. *Transportation Research Record: Journal of the Transportation Research Board*, 1828(-1):20–30, January 2003.

[35] P. Ferris Daniel, Gregory S. Sawicki, and Antoinette R. Domingo. Powered lower limb orthoses for gait rehabilitation. *Topics in Spinal Cord Injury Rehabilitation*, 11(2):34–49, September 19, 2005.

[36] Heinz Ulbrich Daniela Förg, Martin Förg. A bipedal robot model with elastic actuation. In *proceedings of the 1st Joint International Conference on Multibody System Dynamics*, May 25-27 2010.

[37] Van-Huan Dau, Chee-Meng Chew, and Aun-Neow Poo. Optimal trajectory generation for bipedal robots. In *Humanoid Robots, 2007 7th IEEE-RAS International Conference on DOI - 10.1109/ICHR.2007.4813933*, pages 603–608, 2007.

[38] Tlalolini Romero David. *Génération de Mouvements Optimaux de Marche pour des Robots Bipèdes 3D*. PhD thesis, Université de Nantes, 2008.

[39] K. Erbatur and O. Kurt. Natural zmp trajectories for biped robot reference generation. *IEEE Transactions on Industrial Electronics*, 56(3):835–845, 2009.

[40] K. Erbatur, A. Okazaki, K. Obiya, T. Takahashi, and A. Kawamura. A study on the zero moment point measurement for biped walking robots. In *Advanced Motion Control, 2002. 7th International Workshop on*, pages 431–436, 2002.

[41] Marc Lebel Matt Peppel Erik Burns, Kelsi Krier. Skeletal muscle tissue engineering, January 2013.

[42] K.D. Farrell, C. Chevallereau, and E.R. Westervelt. Energetic effects of adding springs at the passive ankles of a walking biped robot. In *proceedings of the IEEE International Conference on Robotics and Automation (ICRA 2007)*, pages 3591–3596, 2007.

[43] J.P. Ferreira, M. Crisostomo, and A.P. Coimbra. Zmp trajectory reference for the sagittal plane control of a biped robot based on a human cop and gait. In *Intelligent Robots and Systems, 2009. IROS 2009. IEEE/RSJ International Conference on DOI - 10.1109/IROS.2009.5354408*, pages 1588–1593, 2009.

[44] Y. Fujimoto. Minimum energy biped running gait and development of energy regeneration leg. In *proceedings of the 8th IEEE International Workshop on Advanced Motion Control (AMC '04)*, pages 415–420, 2004.

[45] Chatterjee A. Ruina A. Garcia, M. Efficiency, speed, and scaling of two-dimensional passive-dynamic walking. *Dynamics and Stability of Systems*, 15(2):75–99, 2000.

[46] F.W. Gembicki. *Vector Optimization for Control with Performance and Parameter Sensitivity Indices*. PhD thesis, Case Western Reserve Univ., Cleveland, OH„ 1974.

[47] Hartmut Geyer, Andre Seyfarth, and Reinhard Blickhan. Compliant leg behaviour explains basic dynamics of walking and running. In *proceedings of the Royal Society B*, 2006.

[48] G. Gini, U. Scarfogliero, and M. Folgheraiter. Human-oriented biped robot design: Insights into the development of a truly anthropomorphic leg. In *proceedings of the IEEE International Conference on Robotics and Automation (ICRA '07)*, pages 2910–2915, 2007.

[49] Oriol Gomis-Bellmunt, Flavio Campanile, Samuel Galceran-Arellano, Daniel Montesinos-Miracle, and Joan Rull-Duran. Hydraulic actuator modeling for optimization of mechatronic and adaptronic systems. *Mechatronics*, 18(10):634–640, December 2008.

[50] Keith E. Gordon, Gregory S. Sawicki, and Daniel P. Ferris. Mechanical performance of artificial pneumatic muscles to power an ankle-foot orthosis. *Journal of Biomechanics*, 39(10):1832–1841, 2006.

[51] David Gouaillier, Vincent Hugel, Pierre Blazevic, Chris Kilner, Jerome Monceaux, Pascal Lafourcade, Brice Marnier, Julien Serre, and Bruno Maisonnier. Mechatronic design of nao humanoid. In *Robotics and Automation, 2009. ICRA '09. IEEE International Conference on*, pages 769–774, 2009.

[52] Timothy M. Griffin, Thomas J. Roberts, and Rodger Kram. Metabolic cost of generating muscular force in human walking: insights from load-carrying and speed experiments. *Journal of Applied Physiology*, 95(1):172–183, 2003.

[53] A. Hamon and Y. Aoustin. Study of different structures of the knee joint for a planar bipedal robot. In *proceedings of the 9th IEEE-RAS International Conference on Humanoid Robots (Humanoids 2009)*, pages 113–120, 2009.

[54] A. Hamon and Y. Aoustin. Cross four-bar linkage for the knees of a planar bipedal robot. In *Humanoid Robots (Humanoids), 2010 10th IEEE-RAS International Conference on*, pages 379–384, 2010.

[55] A. Hamon and Y. Aoustin. Walking trajectory optimization with rotation of the feet for a planar bipedal robot with four-bar knees. In *Proceedings of the ASME 2012 11th Biennial Conference On Engineering Systems Design And Analysis (ESDA2012)*, Nantes, France, July 2-4 2012.

[56] S.P. Han. A globally convergent method for nonlinear programming. *Journal of Optimization Theory and Applications*, 22:292, 1977.

[57] E. P. Hanavan. A mathematical model of the human body, amrl-tr-64-102, ad-608-463. Master's thesis, Aerospace Medical Research Laboratories, Wright-Patterson Air Force Base, Ohio., 1964.

[58] K. Hirai, M. Hirose, Y. Haikawa, and T. Takenaka. The development of honda humanoid robot. In *Robotics and Automation, 1998. Proceedings. 1998 IEEE International Conference on*, volume 2, pages 1321–1326 vol.2, 1998.

[59] Neville Hogan. Impedance control: An approach to manipulation. In *American Control Conference, 1984*, pages 304–313, 1984.

[60] Y. Hurmuzlu. Dynamics of bipedal gait; part 1: Objective functions and the contact event of a planar five-link biped. *ASME Journal of Applied Mechanics*, 60(2):331–336, 1993.

[61] J.W. Hurst, J.E. Chestnutt, and A.A. Rizzi. Design and philosophy of the bimasc, a highly dynamic biped. In *proceedings of the 2007 IEEE International Conference on Robotics and Automation (ICRA '07),* pages 1863–1868, 2007.

[62] F. Iida, J. Rummel, and A. Seyfarth. Bipedal walking and running with compliant legs. In *proceedings of the 2007 IEEE International Conference on Robotics and Automation (ICRA '07),* pages 3970–3975, 2007.

[63] S.E. Irby, K.R. Kaufman, R.W. Wirta, and D.H. Sutherland. Optimization and application of a wrap-spring clutch to a dynamic knee-ankle-foot orthosis. *IEEE Transactions on Rehabilitation Engineering*, 7(2):130–134, 1999.

[64] Amir Jafari, Nikos G. Tsagarakis, and Darwin G. Caldwell. Awas-ii: A new actuator with adjustable stiffness based on the novel principle of adaptable pivot point and variable lever ratio. In *proceedings of the 2011 IEEE International Conference on Robotics and Automation (ICRA)*, pages 4638–4643, 2011.

[65] James G. Gamble Jessica Rose. *Human Walking*. 3rd edition, 2005.

[66] S. Kajita, K. Kaneko, M. Morisawa, S. Nakaoka, and H. Hirukawa. Zmp-based biped running enhanced by toe springs. In *proceedings of the 2007 IEEE International Conference on Robotics and Automation (ICRA '07)*, pages 3963–3969, 2007.

[67] H. Kaminaga, J. Ono, Y. Nakashima, and Y. Nakamura. Development of backdrivable hydraulic joint mechanism for knee joint of humanoid robots. In *Robotics and Automation, 2009. ICRA '09. IEEE International Conference on*, pages 1577–1582, 2009.

[68] K. Kaneko, F. Kanehiro, S. Kajita, H. Hirukawa, T. Kawasaki, M. Hirata, K. Akachi, and T. Isozumi. Humanoid robot hrp-2. In *proceedings of the 2004 IEEE International Conference on Robotics and Automation (ICRA '04)*, volume 2, pages 1083–1090, 2004.

[69] K. Kaneko, F. Kanehiro, M. Morisawa, K. Akachi, G. Miyamori, A. Hayashi, and N. Kanehira. Humanoid robot hrp-4 - humanoid robotics platform with lightweight and slim body. In *Intelligent Robots and Systems (IROS), 2011 IEEE/RSJ International Conference on*, pages 4400–4407, 2011.

[70] A.L. Kemurdjian. Planet rover as an object of the engineering design work. In *Robotics and Automation, 1998. Proceedings. 1998 IEEE International Conference on*, volume 1, pages 140–145 vol.1, 1998.

[71] Wisama Khalil and Etienne Dombre. *Modeling, Identification and Control of Robots*. Taylor & Francis, Inc., 2002.

[72] Richard Knoblauch, Martin Pietrucha, and Marsha Nitzburg. Field studies of pedestrian walking speed and Start-Up time. *Transportation Research Record*, 1538(-1):27–38, 1996.

[73] Arthur D. Kuo. Energetics of actively powered locomotion using the simplest walking model. *Journal of Biomechanical Engineering*, 124(1):113–120, 2002.

[74] O. Kurt and K. Erbatur. Biped robot reference generation with natural zmp trajectories. In *proceedings of the 9th IEEE International Workshop on Advanced Motion Control*, pages 403–410, 2006.

[75] T.-T. Lee and Y.-C. Chen. Minimum-fuel path planning of a 5-link biped robot. In *System Theory, 1988., Proceedings of the Twentieth Southeastern Symposium on*, pages 459–463, 1988.

[76] Cara L. Lewis and Daniel P. Ferris. Walking with increased ankle pushoff decreases hip muscle moments. *Journal of Biomechanics*, 41(10):2082–2089, 2008.

[77] Zhibin Li, N.G. Tsagarikis, D.G. Caldwell, and B. Vanderborght. Trajectory generation of straightened knee walking for humanoid robot icub. In *Control Automation Robotics & Vision (ICARCV), 2010 11th International Conference on DOI - 10.1109/ICARCV.2010.5707828*, pages 2355–2360, 2010.

[78] Garcia M., Chatterjee A., Ruina A., and Coleman M. The simplest walking model: stability, complexity, and scaling. *ASME Journal of Biomechanical Engineering*, 120(2):281–289, April 1998.

[79] HOBON Mathieu. *Modélisation et optimisation de la marche d'un robot bipède avec genoux anthropomorphiques*. PhD thesis, ParisTech, l'École Nationale Supérieure d'Arts et Métiers, Metz, 2012.

[80] Tad McGeer. Passive dynamic walking. *The International Journal of Robotics Research*, 9(2):62–82, 1990.

[81] Shane Migliore, Lena Ting, and Stephen DeWeerth. Passive joint stiffness in the hip and knee increases the energy efficiency of leg swinging. *Autonomous Robots*, 29:119–135, 2010.

[82] K. Miura, S. Nakaoka, S. Kajita, K. Kaneko, F. Kanehiro, M. Morisawa, and K. Yokoi. Trials of cybernetic human hrp-4c toward humanoid business. In *Advanced Robotics and its Social Impacts (ARSO), 2010 IEEE Workshop on*, pages 165–169, 2010.

[83] MobileRobotics. Mobile robots powerbot. Online available: http://www.mobilerobots.com/ResearchRobots/PowerBot.aspx. Accessed: 23/01/2013.

[84] Xiuping Mu and Qiong Wu. A complete dynamic model of five-link bipedal walking. In *American Control Conference, 2003. Proceedings of the 2003*, volume 6, pages 4926–4931 vol.6, 2003.

[85] A. Muraro. *Génération de mouvements optimaux pour un robot quadrupède*. PhD thesis, Ecole Centrale de Nantes et Université de Nantes, 2002.

[86] Y. Nakano, K. Chono, K. Yoneda, and H. Kameishi. A dynamic biped walking robot based on the momentum mechanism with flexible beams. In *proceedings of the IEEE/RSJ/GI International Conference on Intelligent Robots and Systems '94. 'Advanced Robotic Systems and the Real World', IROS '94*, volume 2, pages 1318–1323, 1994.

[87] T. Narukawa, K. Yokoyama, M. Takahashi, and K. Yoshida. A simple 3D straight-legged passive walker with flat feet and ankle springs. In *proceedings of the IEEE/RSJ International Conference on Intelligent Robots and Systems (IROS 2008)*, pages 2952–2957, 2008.

[88] Xiuhua Ni, Weishan Chen, and Junkao Liu. A comparison between human walking and passive dynamic walking. In *proceedings of the 4th IEEE Conference on Industrial Electronics and Applications (ICIEA 2009)*, pages 2552–2555, 2009.

[89] Y. Ogura, H. Aikawa, K. Shimomura, A. Morishima, Hun ok Lim, and A. Takanishi. Development of a new humanoid robot wabian-2. In *Robotics and Automation, 2006. ICRA 2006. Proceedings 2006 IEEE International Conference on*, pages 76–81, 2006.

[90] Jose Luis Peralta, Tomi Ylikorpi, Khurram Gulzar, Peter Jakubik, and Aarne Halme. Novel design of biped robot based on linear induction motors. In *proceedings of the international conference on humanoid robots*, 2009. The international conference on humanoid robots, Paris, Dec 7-10, 2009.

[91] M.J.D. Powell. A fast algorithm for nonlineary constrained optimization calculations. *Numerical Analysis, ed. G.A. Watson, Lecture Notes in Mathematics,*, 630, 1978.

[92] G.A. Pratt and M.M. Williamson. Series elastic actuators. In *proceedings of the 1995 IEEE/RSJ International Conference on Intelligent Robots and Systems "Human Robot Interaction and Cooperative Robots"*, volume 1, pages 399–406, 1995.

[93] Jerry E. Pratt and Benjamin T. Krupp. Series elastic actuators for legged robots. In *proceedings of the SPIE*, volume 5422, pages 135–144, Orlando, FL, USA, September 2004. SPIE.

[94] S. D. Prior and A. S. White. Measurements and simulation of a pneumatic muscle actuator for a rehabilitation robot. *Simulation Practice and Theory*, 3(2):81–117, September 1995.

[95] Lei Ren, Richard K. Jones, and David Howard. Predictive modelling of human walking over a complete gait cycle. *Journal of Biomechanics*, 40(7):1567–1574, 2007.

[96] N. Saga, T. Nakamura, J. Uehara, and T. Iwade. Development of artificial muscle actuator reinforced by kevlar fiber. In *proceedings of the 2002 IEEE International Conference on Industrial Technology (IEEE ICIT '02)*, volume 2, pages 950–954, 2002.

[97] Y. Sakagami, R. Watanabe, C. Aoyama, S. Matsunaga, N. Higaki, and K. Fujimura. The intelligent asimo: system overview and integration. In *proceedings of the IEEE/RSJ International Conference on Intelligent Robots and Systems*, volume 3, pages 2478–2483, 2002.

[98] P. Sardain and G. Bessonnet. Forces acting on a biped robot. center of pressure-zero moment point. *Systems, Man and Cybernetics, Part A: Systems and Humans, IEEE Transactions on*, 34(5):630–637, 2004.

[99] T. Schauss, M. Scheint, M. Sobotka, W. Seiberl, and M. Buss. Effects of compliant ankles on bipedal locomotion. In *proceedings of the IEEE International Conference on Robotics and Automation (ICRA '09)*, pages 2761–2766, 2009.

[100] M. Scheint, M. Sobotka, and M. Buss. Compliance in gait synthesis: Effects on energy and gait. In *proceedings of the 8th IEEE-RAS International Conference on Humanoid Robots, Humanoids 2008*, pages 259–264, 2008.

[101] Larry L. Schumaker. *Spline Functions: Basic Theory*. Cambridge University Press, third edition, Aug 16 2007.

[102] R. Sellaouti and F.B. Ouezdou. Design and control of a 3dofs parallel actuated mechanism for biped application. *Mechanism and Machine Theory*, 40(12):1367–1393, December 2005.

[103] Jonathon W. Sensinger and Richard F.ff. Weir. Unconstrained impedance control using a compact series elastic actuator. In *Mechatronic and Embedded Systems and Applications, Proceedings of the 2nd IEEE/ASME International Conference on*, pages 1–6, 2006.

[104] A. Serbencu, D.C. Cernega, A.E. Serbencu, and I. Susnea. Path following problem for patrolbot solved with fuzzy control. In *Automation and Logistics, 2009. ICAL '09. IEEE International Conference on*, pages 2005–2010, 2009.

[105] H. Serhan, C. Nasr, P. Henaff, and F. Ouezdou. A new control strategy for robian biped robot inspired from human walking. In *Intelligent Robots and Systems, 2008. IROS 2008. IEEE/RSJ International Conference on*, pages 2479–2485, 2008.

[106] C.-L. Shih, Y. Zhu, and W.A. Gruver. Optimization of the biped robot trajectory. In *Systems, Man, and Cybernetics, 1991. 'Decision Aiding for Complex Systems, Conference Proceedings., 1991 IEEE International Conference on*, pages 899–903 vol.2, 1991.

[107] F.M. Silva and J.A. Tenreiro Machado. Energy analysis during biped walking. In *proceedings of the 1999 IEEE International Conference on Robotics and Automation (ICRA '09)*, volume 1, pages 59–64, 1999.

[108] C. P. Simon and L. E. Blume. *Mathematics for Economists*. W. W. Norton, 1994.

[109] E. Taskiran, M. Yilmaz, O. Koca, U. Seven, and K. Erbatur. Trajectory generation with natural zmp references for the biped walking robot suralp. In *Robotics and Automation (ICRA), 2010 IEEE International Conference on DOI - 10.1109/ROBOT.2010.5509792*, pages 4237–4242, 2010.

[110] Ali Tehrani Safa, Mohammad Ghaffari Saadat, and Mahyar Naraghi. Passive dynamic of the simplest walking model: Replacing ramps with stairs. *Mechanism and Machine Theory*, 42(10):1314–1325, October 2007.

[111] D. Tlalolini, C. Chevallereau, and Y. Aoustin. Optimal reference walking with rotation of the stance feet in single support for a 3d biped. In *Intelligent Robots and Systems, 2008. IROS 2008. IEEE/RSJ International Conference on*, pages 1091–1096, 2008.

[112] D. Tlalolini, C. Chevallereau, and Y. Aoustin. Comparison of different gaits with rotation of the feet for a planar biped. *Robotics and Autonomous Systems*, 57(4):371–383, April 2009.

[113] D. Tlalolini, C. Chevallereau, and Y. Aoustin. Human-like walking: Optimal motion of a bipedal robot with toe-rotation motion. *Mechatronics, IEEE/ASME Transactions on*, 16(2):310–320, 2011.

[114] K. Trifonov and S. Hashimoto. Active knee-lock release for passive-dynamic walking machines. In *proceedings of the IEEE International Conference on Robotics and Biomimetics (ROBIO 2007)*, pages 958–963, 2007.

[115] B. Ugurlu and A. Kawamura. Bipedal walking trajectory generation based on zmp and euler's equations of motion. In *Humanoid Robots (Humanoids), 2010 10^{th} IEEE-RAS International Conference on DOI - 10.1109/ICHR.2010.5686831*, pages 468–473, 2010.

[116] Brian R. Umberger. Stance and swing phase costs in human walking. *Journal of The Royal Society Interface*, 7(50):1329–1340, 2010.

[117] B. Vanderborght, M. Van Damme, R. Van Ham, P. Beyl, and D. Lefeber. A strategy to combine active trajectory control with the exploitation of the natural dynamics to reduce energy consumption for bipedal robots. In *Humanoid Robots, 2007 7th IEEE-RAS International Conference on*, pages 7–12, 2007.

[118] B. Vanderborght, B. Verrelst, R. Van Ham, J. Vermeulen, and D. Lefeber. Dynamic control of a bipedal walking robot actuated with pneumatic artificial muscles. In *Robotics and Automation, 2005. ICRA 2005. Proceedings of the 2005 IEEE International Conference on*, pages 1–6, 2005.

[119] Bram Vanderborght, Bjorn Verrelst, Ronald Van Ham, Michael Van Damme, Pieter Beyl, and Dirk Lefeber. Development of a compliance controller to reduce energy consumption for bipedal robots. *Autonomous Robots*, 24(4):419–434, May 2008.

[120] M. Vukobratovic and J. Stepanenko. On the stability of anthropomorphic systems. *Mathematical Biosciences*, 15(1-2):1–37, October 1972.

[121] M.W. Whittle. *Gait analysis: an introduction*. 2003.

[122] SN Whittlesey, RE van Emmerik, and Hamill J. The swing phase of human walking is not a passive movement. *Motor Control*, 4(3):273–292, July 2000.

[123] Kanchana Crishan Wickramatunge and Thananchai Leephakpreeda. Study on mechanical behaviors of pneumatic artificial muscle. *International Journal of Engineering Science*, In Press, Corrected Proof:–, 2009.

[124] M. Wisse, D.G.E. Hobbelen, R.J.J. Rotteveel, S.O. Anderson, and G.J. Zeglin. Ankle springs instead of arc-shaped feet for passive dynamic walkers. In *proceedings of the 6th IEEE-RAS International Conference on Humanoid Robots*, pages 110–116, 2006.

[125] Ge Wu and Peter R. Cavanagh. Isb recommendations for standardization in the reporting of kinematic data. *Journal of Biomechanics*, 28(10):1257–1261, October 1995.

[126] Ge Wu, Frans C.T. van der Helm, H.E.J. (DirkJan) Veeger, Mohsen Makhsous, Peter Van Roy, Carolyn Anglin, Jochem Nagels, Andrew R. Karduna, Kevin McQuade, Xuguang Wang, Frederick W. Werner, and Bryan Buchholz. Isb recommendation on definitions of joint coordinate systems of various joints for the reporting of human joint motion part ii: shoulder, elbow, wrist and hand. *Journal of Biomechanics*, 38(5):981–992, May 2005.

[127] Yujiang Xiang, Jasbir S. Arora, Salam Rahmatalla, and Karim Abdel-Malek. Optimization-based dynamic human walking prediction: One step formulation. *Int. J. Numer. Meth. Engng.*, 79(6):667–695, 2009.

[128] J. Yamaguchi, D. Nishino, and A. Takanishi. Realization of dynamic biped walking varying joint stiffness using antagonistic driven joints. In *Proceedings of the IEEE 1998 IEEE International Conference on Robotics and Automation*, volume 3, pages 2022–2029, 1998.

l'université nantes angers le mans
PÔLE DE RECHERCHE ET D'ENSEIGNEMENT SUPÉRIEUR

UNIVERSITÉ DE NANTES

Thèse de Doctorat

Abdul HAQ

Stratégies pour le stockage de l'énergie d'un robot bipède durant une allure de marche

Strategies for Energy Storage during a Walking Step of a Bipedal Robot

Résumé

Ce travail est dédié à l'étude de différentes stratégies pour améliorer l'efficacité énergétique de la marche d'un bipède planaire. Les stratégies proposées comprennent, le blocage de l'articulation du genou de la jambe d'appui, l'ajout des ressorts de torsion en parallèle aux actionneurs existants, et l'utilisation d'actionneurs hydrauliques pour stocker de l'énergie lorsque l'actionneur est bloqué et puis la réutiliser en cas de besoin.

Afin de comparer l'efficacité énergétique de différentes méthodes proposées, un problème d'optimisation paramétrique sous contraintes est posé pour générer un ensemble de trajectoires optimales de marche pour différents types d'allures avec ou sans phases de double appui et d'impact. Les équations de Lagrange sont utilisées pour définir le modèle dynamique et le modèle d'impact du bipède. Ce modèle dynamique tient compte des effets de blocage du genou et de l'ajout des ressorts en parallèle aux actionneurs. Dans la première approche, les trajectoires optimales de marche sont générées en ajoutant des ressorts aux différentes articulations du bipède. Et pour la deuxième approche, le genou de la jambe d'appui est bloqué pendant toute la phase de simple appui. La troisième méthode est fondée sur l'utilisation des actionneurs hydrauliques. Quand l'articulation du genou est bloquée, l'énergie sous forme de pression hydraulique est stockée dans un réservoir, puis est utilisée dès lors que le besoin s'en fait sentir.

Le coût énergétique de la marche est alors calculé pour les différentes vitesses de marche en utilisant stratégies proposées pour chaque allure de marche et puis les performances obtenues sont comparées à celles initiales du bipède sans ressorts et sans stockage d'énergie. Nous avons montré q'une réduction significative de la consommation d'énergie peut être obtenue en utilisant les approches proposées en fonction du type d'allure étudié.

Mots clés

Robot bipède, modélisation dynamique, mouvement optimal, optimisation paramétrique, ressorts en torsion, blocage du genou, stockage d'énergie, actionneur hydraulique.

Abstract

The scope of this work is to propose different strategies to improve energetic efficiency of walking of a planar biped. The proposed strategies include, locking of the support knee joint, addition of torsional springs in parallel to existing actuators, and use of hydraulic actuators to store energy while the actuator is locked and then re-use the stored energy when needed.

To compare energetic efficiency of different methods proposed, a parametric optimization problem under constraints is purposed to generate a set of optimal walking gait trajectories for different types of gaits with or without double support and impulsive impact phases. Lagrange's formulation is used to define the dynamic and impact model of the biped, and taking into account the effects of knee locking and spring addition in parallel to existing actuators. In the first approach, optimal gait trajectories are generated by adding springs to different joints of the biped and in the second approach support knee is locked during entire single support phase. The third approach is related to hydraulic actuators in which a joint is locked and energy is stored in the form of hydraulic pressure in a reservoir and then reused when needed.

The walking cost of generated optimal trajectories is thus calculated for all studied gaits using the proposed strategies. This cost is then compared to that of the respective gait of the basic robot to study the effectiveness of the applied strategy. It is shown that significant reduction in energy consumption can be obtained by using all proposed approaches depending on the type of gait studied.

Key Words

Bipedal robots, dynamic modeling, optimal motion, parametric optimization, torsional springs, knee locking, energy storage, hydraulic actuator.